CRANFIELD INSTITUTE OF TECHNOLOGY

SCHOOL OF MECHANICAL ENGINEERING

PhD Thesis

Academic Year 1989-1990

Arkan Khilkhal Husain Al-taie

Experimental Study of Radiation From Coated Turbine blades

Supervisor : Professor Riti Singh

March 1990

VOLUME CONTAINS CLEAR OVERLAYS

OVERLAYS SCANNED SEPERATELY AND OVER THE RELEVANT PAGE.

SUMMARY

The specific power (or specific thrust) of modern gas turbines is much influenced by the gas temperature at turbine inlet. Even with the use of the best superalloy available and the most advanced cooling configurations, there are competitive pressures to operate engines at even higher gas temperatures.

Ceramic coatings operate as thermal barriers and can allow the gas temperature to be increased by 50 to 220 K over the operating gas temperature for an uncoated turbine .

It is important that the surface temperature of the blade be determined as accurately as possible. Large uncertainties as to the surface temperature require significant margins for safe operation .

Blade surface temperatures can be determined with an accuracy of 10 K using radiation pyrometry and about 30 to 40 K by calculating the blade temperature based on gas temperature measurement of the exhaust gas plane. This makes pyrometry an attractive option for advanced high temperature gas turbines .

However, there is little experience in measuring surface temperatures of blades coated with ceramic coatings. There is evidence that the radiation signal picked up by the pyrometer will not only depend on the surface temperature but also on a number of optical properties of the coating. Important among these are the emissivity of the coating and whether the coating is translucent. Parameters affecting this are the coating material, coating surface finish, coating thickness and whether or not a bond coat is used .

This work explores these variables in a rig that simulates the conditions within a turbine stage of a gas turbine engine. In which six thermal barrier coating systems were tested. These systems are of current interest to gas turbine manufacturers and users. They include the latest advances in coating technology. Four stabilized zirconia systems and two alumina based systems were tested.

It was found experimentally that the surface emissivity of these coating systems was invariant over the range 873 to 1023 K surface temperature. It was found that the use of different stabilizers did not affect the surface spectral emissivity.

In further experiments six turbine wheels were coated with these systems and tested at turbine entry temperatures of 973, 1073, and 1173 K. It was found that the blade surface temperature was function of the coating material, coating thickness and turbine entry temperature. The blade surface temperature was also function of the blade height being maximum at the blade tip and minimum at the blade root .

It was found that the C-YPSZ was better insulator than the rest of the systems. Whilst the blades coated with zirconia based systems suffered minor loss near the edges, the two alumina based systems were lost from more than a blade during the test. This coating loss was picked up by the pyrometer .

Analysis shows that the measured blade surface temperature was within 10 K of that calculated. The use of 0.3 mm of C-YPSZ on air cooled turbine blades caused 250 K surface temperature increase and 270 K metal temperature decrease for turbine entry temperature of 1673 K. The metal temperature reduction was as high as 310 K for coating thickness of 0.5 mm.

ACKNOWLEDGEMENTS

I would like to express my sincere gratitude to my supervisor Professor Riti Singh for his continuous guidance and support.

Sincere thanks are due to the staff of the School of Mechanical Engineering test area, and the staff of the main library.

Thanks are also due to Dr. D. Russell of the Electronic System Design Department and to Mr Martin Roskilly of the Auto Group.

Thanks are due to the staff of Negretti Aviation Ltd, Holset Engineering Co. Ltd. and to Metco Ltd. for their support in making this work possible. Special thanks to Mr Jan Zuidhof of Metco Ltd.

I am grateful to my wife Resala for her patience, understanding and support and to my children Ali (born 17/8/1987), Fatima (born 3/9/1988) and Marium (born 25/12/1989) who all helped me in their own ways to complete this study.

My sincere thanks and gratitude are due to the Iraqi Government for the financial support and for making it possible to further my studies in the field of "jet propulsion".

One should never forget those "who were more generous than all of us" who sacrificed their lives to protect our beloved country. Among whom was my brother "Munthir" born 1962, who died while defending our country on the 17th of May 1987 on the eastern border of Basrah, whose death broke my backbone and left a deep and incurable injury into my heart and to whose remembrance this thesis is dictated.

Arkan Khilkhal Husain Al-tai
CIT, SME, 30 March 1990

NOMENCLATURE

A	Constant	
B	Constant	
C_1	Constant = 3.7413×10^8	$W\ m^{-2}\mu^4$
C_2	Constant = 14388	$\mu\ K$
C-YPSZ	Ceria yttria partially stabilized zirconia	
D	Diameter	mm
dc	Direct current	
E	radiation energy	$W\ m^{-2}$
EGT	Exhaust gas temperature	K
F	Optical factor	mm^2
h	Heat transfer convection coefficient	$W\ m^{-2}K^{-1}$
K	Constant	
k	Thermal conductivity	$W\ m^{-1}\ K^{-1}$
L	Thickness	m
LCD	Liquid crystal display	
MPSZ	Magnesia partially stabilized zirconia	
N	Rotational speed	RPM
n	Temperature exponent	
NGV	Nozzle guide vanes	
NDT	Non distractive testing	
p	Pressure, Larson Miller parameter	$KN\ m^{-2}$
q	Heat transfer	$W\ m^{-2}$
r	Radius	m
RIT	Radial inflow turbine	
SFC	Specific fuel consumption	
T	Temperature	K

t	Creep life	hrs
TBC	Thermal barrier coating	
TBT	Turbine blade temperature	K
TET	Turbine entry temperature	K
U	Blade linear velocity	$m\ s^{-1}$
VDU	Visual display unit	
W	Gas relative velocity	$m\ s^{-1}$
YPSZ	Yttria partially stabilized zirconia	

Greek letters

ε	Emissivity	
ρ	Reflectivity	
γ	Isentropic exponent	
σ	Stefan Boltzmann constant = 5.669×10^{-8}	$W\ m^{-2}\ K^{-4}$
μ	Micrometer = 10^{-6} meter	
λ	Wave length	μm

Subscripts

b	Black body , Bond coat , Blade
c	Coolant
cc	Ceramic coating
f	Flame
g	Gas
in	At inlet
l	Lens
T	Target
T ,t	Total
t	Transmittance

s	Surface , Static
v	Vane
x	Arbitrary station
λ	Spectral
1	station one
2	station two

LIST OF FIGURES

LIST OF TABLES

CHAPTER ONE

1 GENERAL INTRODUCTION

1.1 Blade Temperature Measurements

1.1.1 The Importance of Blade Temperature Measurement

The increase in gas turbine inlet temperatures combined with higher pressure ratios, offer the greatest potential for improvements in the performance of advanced engines .

The performance of the engine is basically limited by the need to operate the hot section at temperatures that allow for long and reliable life. A few minutes of operation at higher temperatures can result in a dramatic reduction in engine life . This may lead to a catastrophic failure of the engine .

Modern gas turbine blades are analogous to extremely high response heat exchangers operating with one fluid above the melting temperature of the metal. Turbine blade wall temperatures are a delicate balance between the extremely high heat flux input resulting from the high velocities, pressures and temperatures downstream and the cooling air flow within the blade .

It is important that the surface temperature of the blade be determined as accurately as possible. Large uncertainties as to the surface temperature require significant design margins for safe operation .

Only a minimum of cooling air is used, since engine performance drops dramatically as cooling flow (compressor bleed) increases.

The use of the best superalloys available and the most advanced cooling configurations are features of modern turbine blades. However, there are still competitive pressures to operate the engine at higher gas temperatures [Gell (1)].

One of the methods for doing so, is to use ceramic coatings. The use of ceramic coatings as thermal barriers allow the gas temperature to be increased by 50 to 220 K, depending on the local heat flux. This is without endangering the blades by over heating them, [Bratton(2),Liebert(3) and Stepka(18)]. Figure 1.1 shows the benefits of employing TBCs and the progress in turbine blade metal temperatures .

These consideration necessitated the knowledge of blade surface temperatures as accurately as possible. Blade surface temperatures can be determined with an accuracy of 10 K employing radiation pyrometry, and about 30 to 40 K by calculating them from exhaust gas temperature measurements , [Curwen(5),Ref.(6) and (7)] .

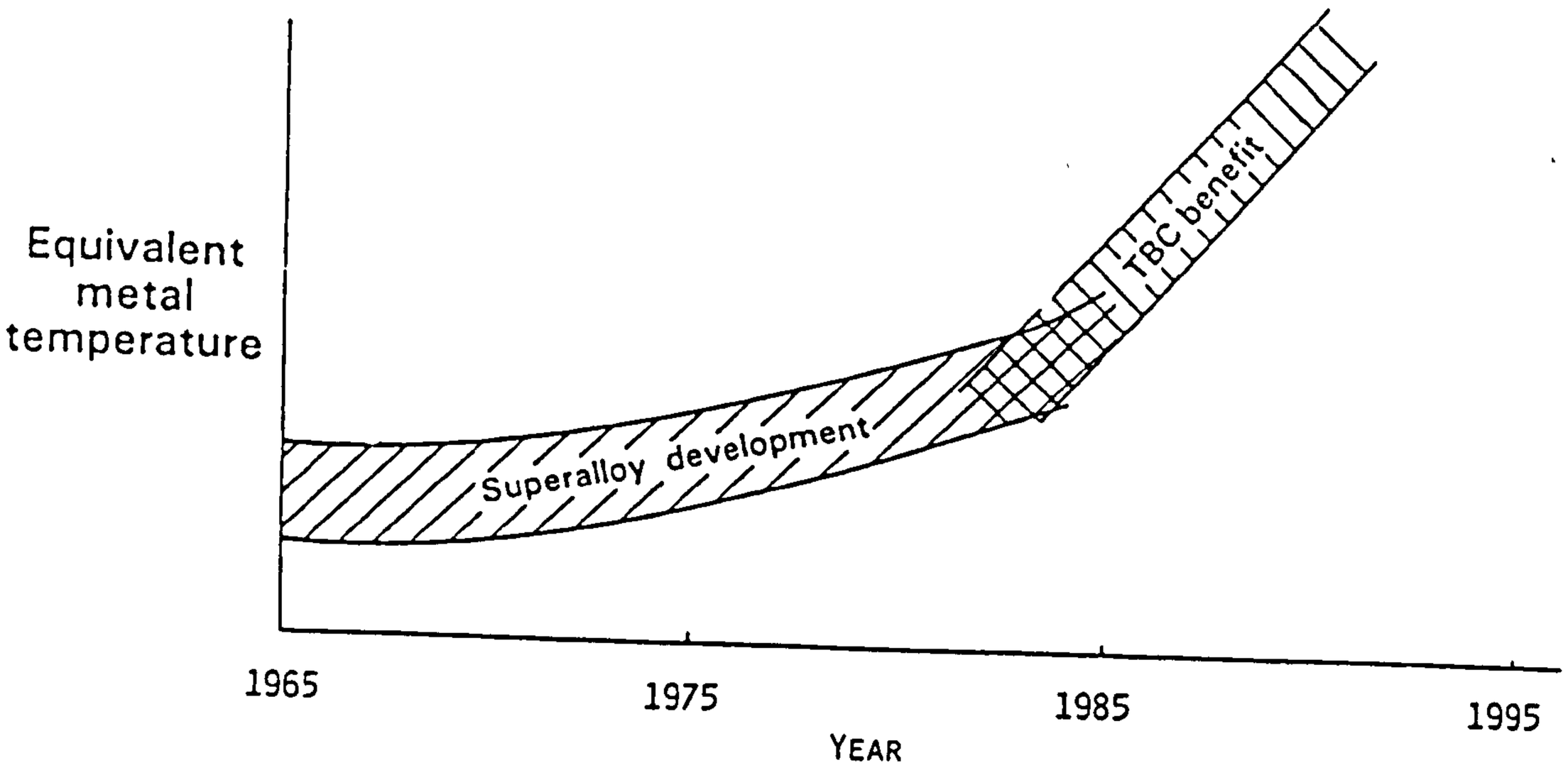

Figure 1.1 The potential benefits offered by TBC compared with the increase in metal temperature capabilities [Ref. 4]

1.1.2 Blade temperature Prediction

In trying to calculate the turbine blade temperature, an iterative method is used. In this method, exhaust gas temperature is measured employing thermocouples. Normally, sets of thermocouples are fitted around the exhaust pipe .

The gas temperature is then calculated upstream through the turbine stages. This requires the knowledge of stage efficiency and expansion ratios. From gas temperatures calculated upstream and downstream the turbine wheel, the blade temperature is then calculated .

Thermocouple harness of exhaust gas and the procedure to calculate blade temperatures may have many uncertainties. These uncertainties are summarized in the following [Rohy(8)] :

1- Even in the exhaust, large point to point variation in gas temperature is observed .

2- Thermocouple temperatures as a result of drift, radiation losses and conduction errors are not equal to gas temperatures but, only proportional .

3- Thermocouple response is poor. Since the type that can have reasonable long life must be relatively massive .

4- Turbine performance must be assumed constant and known to factor the exhaust or downstream temperatures into the turbine blade temperature .

When these shortcomings are considered, the computed turbine blade temperature must have a large safety margin . This safety margin is as high as 40 K .

1.1.3 The Use of Radiation Pyrometry

When the blade temperature is measured directly, small safety margin can be used. The reduced margins allow engine operation at higher turbine entry temperatures (TET) and hence result in improved engine specific power.

Radiation detectors correlate the radiation emitted by the blades and display surface temperatures.

Thermal radiation detectors can be of three types, thermal element , semiconductor and photocell detectors. These types are presented in chapter three.

1.2 The Concept of TBC Systems

Modern gas turbine engines utilize turbine aerofoil alloys with melting points in the order of 1,500 to 1,588 K . These aerofoils are required to operate in the combustion exhaust gas environment which is in excess of 1,643 K , [Sheffler(4)] .

In modern gas turbines upto 20% of the compressor delivery is used to cool these aerofoils. Air bleed from the latter stages of the compressor is flown through complex cooling configurations inside the aerofoils [Meetham(9)].

This air helps to prevent structural failure due to high temperatures. The failure could be due to melting, or some other degradation modes such as creep, high temperature oxidation, thermal fatigue, etc.

Reducing the air flow rate of the compressor bleed increases cycle efficiency. This can be achieved through several ways. One of these ways is to increase cooling efficiency through improvement of the design of the internal cooling configurations. The other possible way is to use superalloys with high melting temperatures. The third way is to isolate these aerofoils from the main gas stream employing low thermal conductivity materials. The use of a thin ceramic layer on the external surface of a cooled turbine blade can provide a quantum increase in cooling efficiency.

Figure 1.1 shows that, the amount of metal temperature reduction due to the use of TBCs is greater than the cumulative gains made in temperature capabilities of aerofoils over the last twenty years, [Sheffler(4)] .

1.3 Description of The Problem

Thermal barrier coatings have been used in jet engine combustors for over 15 years. However, it is only recently that they have been actively used in the harsh environment on nozzle guide vane platforms. It is likely that TBCs will be used on vane aerofoils and on rotating blades where the resulting advantages are maximum.

A careful search of published literature shows that much work has been done within the last five years towards realising this goal. Much of this work is either done for or by large establishments such as Rolls Royce, NASA and others. Such work is very rarely undertaken at a university level due to the very high costs associated with such research. There is therefore very little work in this area in the published domain.

The difficulty of studying TBCs within a gas turbine is that this proves to be a very expensive undertaken. The use of stationary experiments are of limited value and do not produce instrument and or experimental techniques of relevance to engine application.

One of the major challenges for the work undertaken for this thesis was then to devise an experiment which closely approximated the thermal performance of relevant TBCs in a gas turbine, Whilst using a relatively cheap rig.

1.4 Programme Objectives

The specific power or (specific thrust) of modern gas turbines depends considerably on the gas temperature at turbine inlet. This temperature can be increased by 50 to 220 K by employing ceramic TBC systems . And can be increased further by employing radiation pyrometry to measure blade temperatures . The latter when used reduces the safety margin required otherwise .

However, there is little experience in measuring the surface temperatures of turbine blades coated with ceramic thermal barrier coatings employing a radiation pyrometer.

There is evidence that the radiation signal picked up by the pyrometer depends not only on surface temperature. It also depends on a number of optical properties of the coating . Important among these are the emissivity of the coating and whether the coating is translucent.

Parameters affecting this are :

- the coating material ,
- coating surface finish ,
- coating thickness ,
- and whether or not a bond coat is used .

The intention of the present programme is to explore these variables in a rig that simulates the conditions within a turbine stage of a typical gas turbine engines. The use of a radiation pyrometer for blade surface temperature measurement and the application of the results to a typical gas turbine. The operation at turbine entry temperatures currently prevalent in gas turbines. And the testing of ceramic coatings that are of current interest combined with the use of a modern application method.

1.5 Thesis Layout

Chapter one (General Introduction) addresses the area of turbine blade temperature measurement. It discusses the importance of accurate prediction of blade surface temperatures and its consequences on blade cooling design and TET limitations. The use of radiation pyrometry is also introduced in this chapter.

This chapter also presents the concepts of TBCs and their influence on TET. The objectives of the programme are also presented .

Chapter two (Blade Temperature Determination and Its Effect on Performance and Lifing) outlines the benefits of employing a radiation pyrometer instead of thermocouples for the TBT determination. It shows the effect of reducing the error associated with the use of thermocouples on the design safety margin and on the TBT. It then shows the effect of it on blade lifing and on engine performance.

Chapter three (Radiation Pyrometry) Introduces the radiation pyrometer, its development and its principles of operation. It then discusses the use of radiation pyrometers for turbine blade temperature measurement, their types, construction and performance .

It then discusses the signal and the possible sources for it. The pyrometer installation and signal processing are also presented.

This chapter is then concluded by choosing a radiation pyrometer that is of current use in gas turbines and a suitable signal processing to be used in this investigation.

Chapter four (Experimental Rig Selection) introduces the options available for building an experimental rig. A rig that can fulfil the objectives of the programme. This chapter then discusses the choice of the rig and the reasons behind it .

Chapter five (Experimental Rig Design) presents the layout of a typical gas turbine rig . It then presents the design of the rig , its main components and systems .

It also presents the design of a flow meter for air mass flow measurement .

Chapter six (Instrumentation and Control) lists the instruments required for the rig. It also discusses the design of a synchronizing system. This system is to be used for speed measurements and for triggering the data acquisition system. Rig safety and control are also discussed .

Chapter seven (Rig Commission) describes the procedure for rig checking both when cold and when hot. It discusses the problems with getting the sighting window contaminated. Design, manufacture and testing of a purge system are also discussed . This chapter is then concluded by getting an experimental rig that is fully operational and that can simulate a gas turbine rig very closely.

Chapter eight (TBC and coating application methods) presents different types of TBCs. It presents the requirements of TBCs for gas turbine application and the processes used for applying them. It then lists the TBC systems to be tested in this investigation and the method and the equipments used for their application .

Chapter nine (Emissivity Measurement) introduces the emissivity as an important surface property. Its measurement and its relation with other influencing parameters like, temperature, wave length, surface roughness and reflectivity are also presented. This chapter is then concluded by carrying out emissivity measurements of specimens coated with TBC systems.

Chapter ten (Blade Surface Temperature Prediction) presents an application for the TBC system on an air cooled blades. It also presents a theoretical approach for calculating surface temperatures for coated and uncoated blades. The effect of flame radiation and lens contamination on pyrometer indication are also presented .

Chapter eleven (Pyrometer Analysis) presents the possible error sources and their effect on the indicated temperature .

Chapter twelve (Discussion and Observations) presents the results obtained for the six TBC systems employed in this investigation. Then discussion of the results is presented. It then presents a comparison of the six types. This chapter then presents an interesting observation when one of the coatings was lost while testing was still in progress.

The results are then summarized in chapter thirteen (Conclusions and Recommendations), and some recommendations are made for future work .

CHAPTER TWO

2 BLADE TEMPERATURE DETERMINATION AND ITS EFFECT ON PERFORMANCE AND LIFING

2.1 Introduction

The specific power (or specific thrust) of gas turbines is very much influenced by the TET and the turbine blade temperature is in turn dependant on the TET. There are competitive pressures to operate the engine at very high TETs. These TETs are determined by the allowable metal temperature of the first stages of the turbine at the prevailing stress and for the desired life for the turbine alloy chosen. One or a combination, of these factors (metal temperature, stress level, life) will often limit the capability of the engine and hence influence its competitive position. So, there is competitive pressures to increase the blade metal capability to operate at higher TETs and hence produce more thrust without reducing the blade lifing. Operation at 15 K higher blade temperature reduces the creep life by a factor of 2 [Douglas(10) and Berenblut(16)].

Superalloys are used in order to increase the turbine blade temperature capability and hence to increase the TET. Complex cooling configurations are introduced to reduce the blade metal temperature further and hence increase the allowable TET. Research in this area and during the 1960s and 1970s resulted in about 5 to 10 K increase in TBT per year [Bennet(40)]. This implies that in order to increase the TET by 100 K the industry would have to wait for about 10 years.

It is important that the blade temperature, which is the limiting factor of the TET, be determined as accurately as possible. Any large uncertainty in the determination of the blade temperature means that large safety margins have to be employed, and hence the allowable TET has to be reduced. The accurate determination of TBT reduces the uncertainty and allows the designer to design for higher TET without sacrificing the safety margin.

Following are two methods that are available for the turbine blade temperature determination for engines in service:

2.2 The use of Thermocouples for TET Measurement

At the turbine entry plane (combustor exit plane) gas temperatures are often very high and in addition there are very large temperature gradients in the radial and circumferential directions. If an attempt were made to measure TETs using thermocouples at this plane these thermocouples would have to be

relatively robust and well cooled to survive in this environment. In addition a fairly large number of thermocouples are required to get the metal temperature because of the large temperature gradients.

Whilst a few gas turbines do use thermocouples at the turbine entry plane, this is not generally favoured for modern advanced gas turbines because of the aerodynamic disturbance the probe would create and the risk of mechanical failure of the probe which could result in major secondary damage within the engine.

Since the measurement of the TET is impractical, in most gas turbines, the gas temperature is measured downstream either at a turbine interstage or at the turbine exit plane. However, the EGT varies radially and circumferentially across the exhaust plane, and multiple probes are required to find an average EGT to minimize measurement errors. Probes with multiple thermocouples are sometimes employed to minimize radial errors.

After the EGT is measured, the TET can then be derived by applying algorithms. The turbine blade metal temperature calculated from the gas temperature measured by thermocouples has large error. This large error results from the following error sources:

a. averaging errors;

b. sensor errors;

c. gas stream uncertainties and algorithm errors (in order to get the turbine blade metal temperature a number of calculations have to be made which involve the knowledge of turbine efficiencies, heat fluxes to turbine blades,cooling effectiveness, etc).

Each of these error sources consists of more than one source. The overall accumulated uncertainty in this method is about 30 to 40 K in the blade temperature [Curwen(5)]. However, this uncertainty does not consider any degradation the engine may have suffered. Hence, what is true in the first operating hours might not be true later, and this again has to be considered for safe operation.

2.3 The Use of Radiation Pyrometry for Turbine Blade Temperature Measurement

A radiation pyrometer can directly view the blade surface and from the knowledge of the blade emissivity and the pyrometer signal, the blade temperature can be determined. As long as the blade surface emissivity is known (from prior measurements) the blade temperature can be accurately determined.

Most modern gas turbine blades are made from high nickel superalloys. Fortunately this type of material once in operation it has a stable surface emissivity of 0.8-0.85 [Kirby(79) and Harman(80)]. The other advantage is that most radiation pyrometers are made from silicon detectors which, as presented in chapter three, are not very sensitive to the blade emissivity error.

The overall uncertainty in blade temperature is then about 3K which is associated with the pyrometer electronics. So, by employing a radiation pyrometer instead of thermocouples, the safety margin is reduced by more than 35 K. This reduction is equivalent to 4 to 7 years of research. It means that the customer has to wait for this long time in order to be able to get this extra thrust from his engine while it already exists.

One other advance in blade metal technology is the use of ceramic coatings as thermal barriers. These thermal barrier coatings provide thermal insulation to the blade and hence, in one way, can allow the TET to be increased by 50 to 220 K [Bratton(2) and Liebert(3)]. This advance if it were to be covered by improvement in metallurgy would take 5 to 20 years of research.

Because coatings allow the turbine to operate at much higher surface temperatures than is possible for uncoated turbine blades, it follows that the loss of the coating could result in an early failure of a blade and hence the engine, if the loss of coatings were not detected. Coating loss can have large implications for the user both in terms of safety and cost. High temperature coatings are difficult and expensive to develop and, as will be shown later in this thesis, radiation pyrometry offers an important opportunity in this context.

The use of thermocouples for EGT measurement and hence blade temperature via the TET measurement provides no informations about the coating degradation. This is an added uncertainty to this method and hence an added limitation. The use of radiation pyrometry, on the other hand, can provide informations on these coatings during engine operation. This has a great assistance for choosing the right type of coating and for monitoring it. As the pyrometer views the coated blades, it provides a temperature profile. Any change to the radiation signal picked is translated as change in blade surface temperature . So, any coating

degradation changes the surface emissivity of the blade and hence changes the pyrometer output profile for the blade under view. By constantly monitoring these blades any change in signal can easily be identified to be checked. Not only it provides accurate informations about the blade temperature, it also acts as an early warning system for coating loss to avoid sudden turbine failure.

2.4 The Effect of TBT on Lifing and Performance

The TET and TBT of an engine are critical to the engine performance and life. The maximum allowable TET depends on the maximum allowable TBT. So, If the error in the determination of the TBT can be reduced, the design safety margin can also be reduced and hence, the TET can be increased.

Figure no.(2.1) shows the effect of using radiation pyrometry instead of thermocouples on engine thrust for different pyrometer and thermocouple errors. Figure no.(2.2) shows the effect of the same parameters on the specific fuel consumption (SFC). If a typical error for thermocouples is 50 K and the error for radiation pyrometers is about 10 K, the improvements would be about 5% in thrust and about 1.5% in SFC. There would be an additional benefit from using the radiation pyrometer and as was discussed above it would be used for continuous monitoring of the coatings.

The lifing effects of choice of thermometry system depend on the failure mode for the blades. Turbine blades of high bypass engines are most likely to fail via creep, whereas those of low bypass engines for a fighter or a multimission aircraft are most likely to fail via low cycle fatigue (LCF). The failure is time dependent in the first case and cycle dependent in the second case.

For the high bypass engines were the creep is the dominant failure mode, the Larson-Miller parameter may be used to estimate turbine blade creep life difference between using thermocouples and using radiation pyrometery. The Larson-Miller parameter is as follows:

$$P = T\,(C + \mathrm{Log}\ t) / 1000 \qquad 2.1$$

where: P is the Larson-Miller parameter
T is the blade metal temperature [K]
t is the creep life [hrs]
C is constant [about 20]

For high bypass engines and at constant stress, P and C are constants, Hence the creep life is function of the blade metal temperature only.

Figure no.(2.3) shows the percentage increase in blade creep life for different blade temperature reductions as a result of temperature error reduction. It shows that a 5 K reduction in the TBT, increases the blade creep life by 29.5% . This figure also shows that by using a radiation pyrometer instead of thermocouples for the TBT measurement and assuming 'only' a 5 K reduction in the error results in more than 295 hrs increase in the blade creep life. This calculation was done assuming the blade metal temperature was 1073 K and the creep life was 10,000 hrs. The typical difference in error is of the order of 40 K in which case there will be an improvement in creep life of several hundreds percent.

Low bypass engine lives are limited by low cycle fatigue, thermal fatigue as well as creep. Whereas the creep life depends on time and temperature, the low cycle fatigue (LCF) depends upon the number of engine cycles, type of cycle and the blade stress experienced during each cycle. Thermal fatigue life depends on the number of thermal cycles, type of cycle and the cycle temperature. It was shown by Wheatly [87] that for a blade temperature of 1173 K and a creep life of 1000 hrs, the creep life can be improved by 25% by using a radiation pyrometer in stead of thermocouples for the turbine blade temperature prediction, assuming only a 5 K reduction in the measurement error. And the engine fatigue life can be improved by 6.6% for the same case. While a 15 K reduction in the TBT results in about 96% improvement in the creep life and about 20.8% improvement in the thermal fatigue life or a 29% improvement in the overall lives.

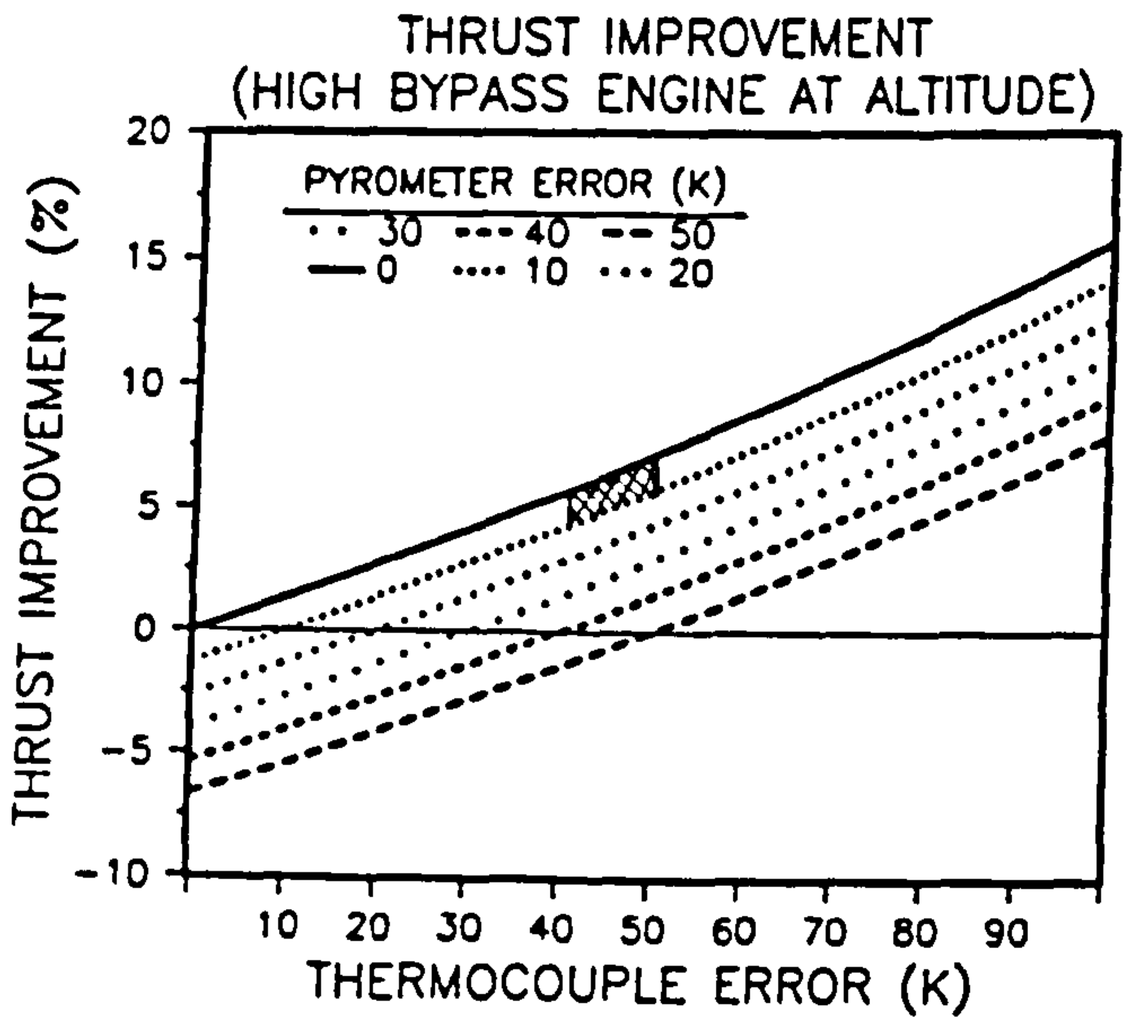

FIG no.(2.1)
Thrust improvement versus thermocouple error for various pyrometer errors (High bypass engine at altitude)

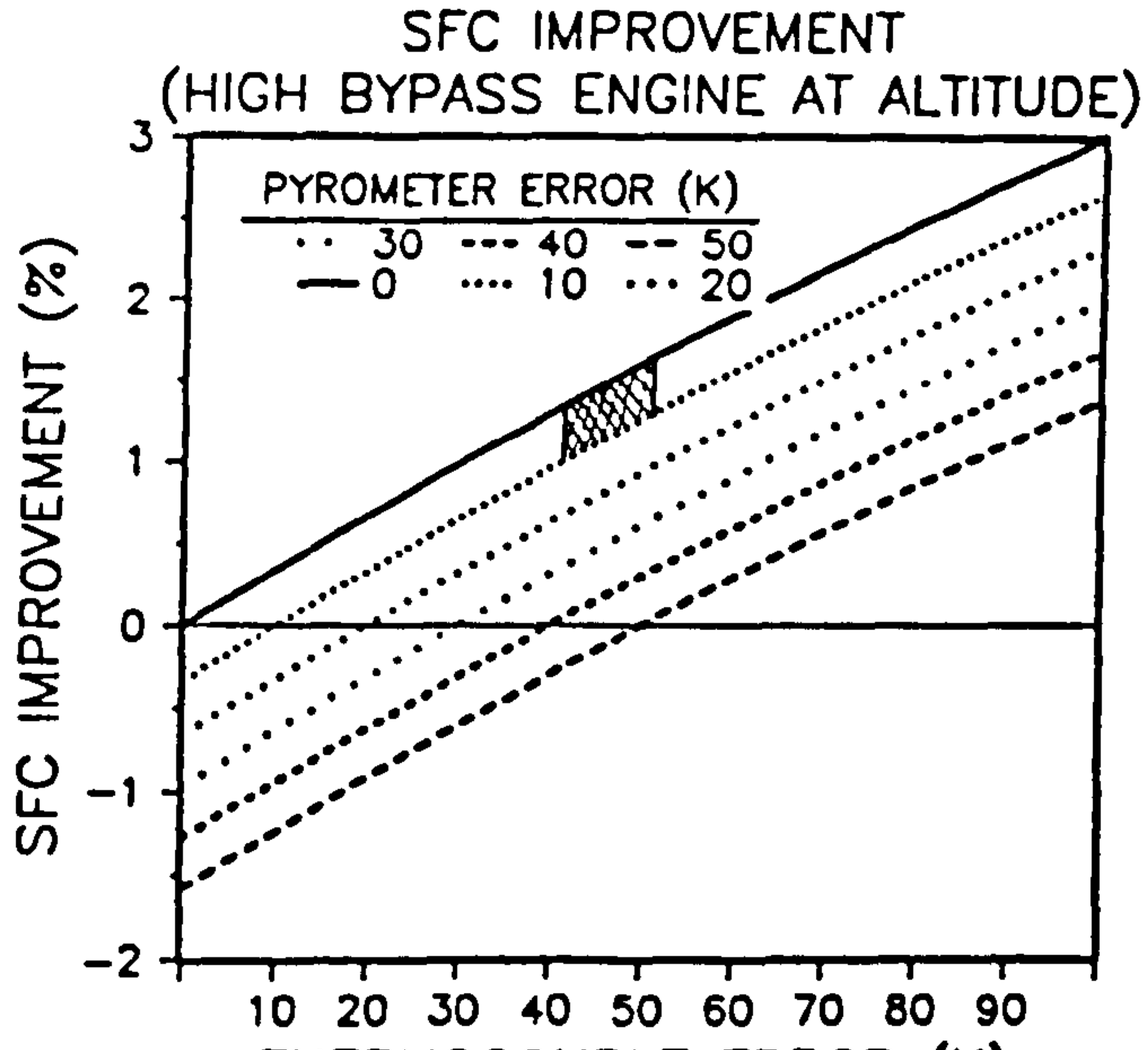

FIG no.(2.2)
Sfc improvement versus thermocouple error for various pyrometer errors (High bypass engine at altitude)

Region of Typical Improvement

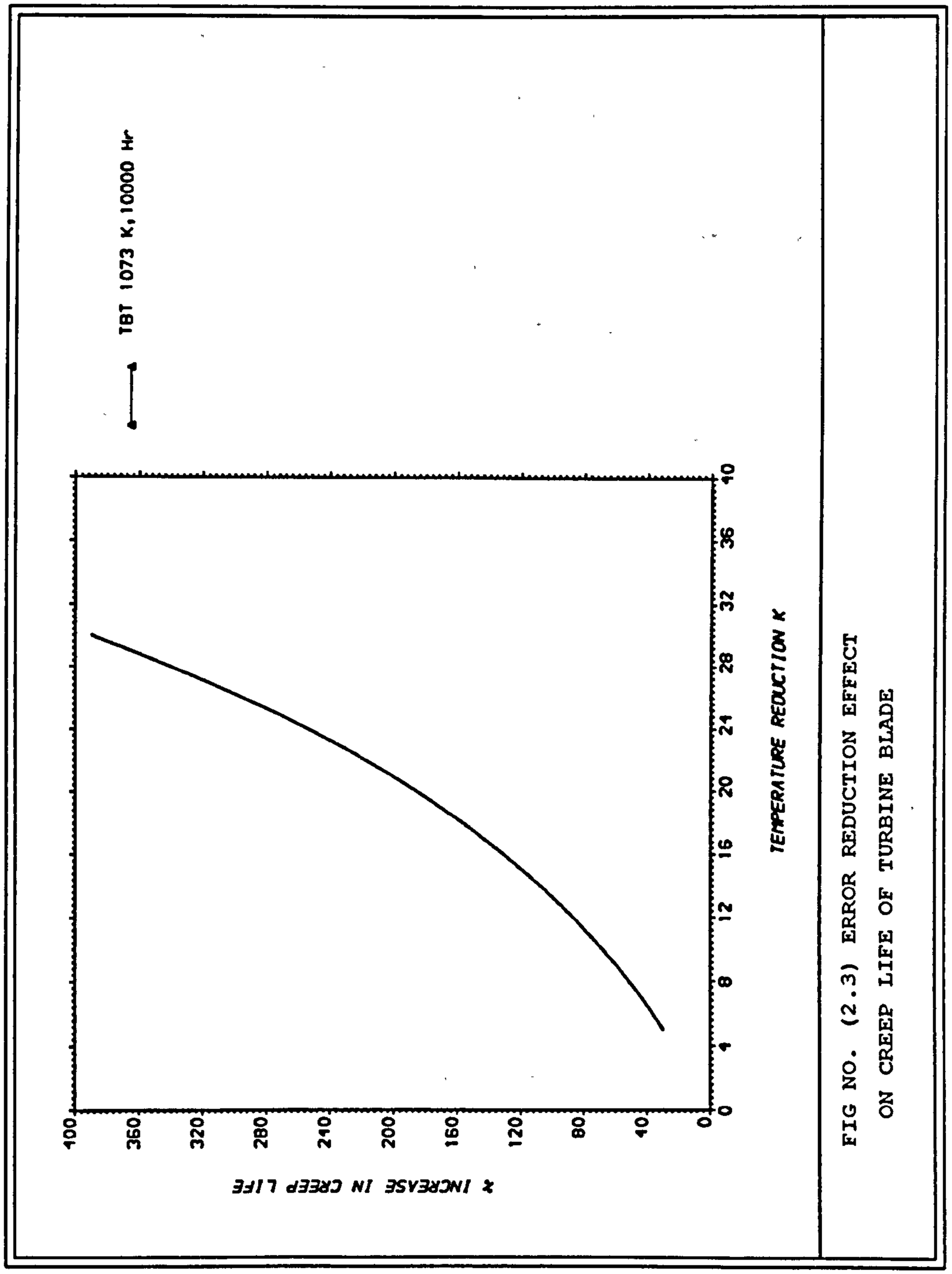

FIG NO. (2.3) ERROR REDUCTION EFFECT
ON CREEP LIFE OF TURBINE BLADE

CHAPTER THREE

3 RADIATION PYROMETRY

3.1 Introduction

For military gas turbines powering the present and next generation for air superiority fighters it is essential to deliver the highest specific power. It is now recognised that both high temperature TBCs and radiation pyrometry have an important role to play in the design, development and operation of high specific power engines .

The increase in the operating gas temperatures is a factor that has been instrumental in the development of the new advanced technology engines . By increasing the combustion temperature , efficiency and thrust can be improved without the need to increase engine's weight or size .

Increasing the operating temperature creates a hostile environment for the hot section components of the engine . This necessitated the use of exotic materials and cooled turbine hardware . The increased operating temperature has introduced a whole new set of problems relative to the measurement of turbine inlet temperature .

The TET should be as high as possible consistent with the lifing requirements, a prevailing stress and maximum allowable surface temperatures. However, the increase of 15 K in the blade metal temperature will reduce the creep life of the blade by a factor of 2 [Meetham(9),Douglas(10) and Berenblut(16)] .

The conventional technique for TET measurement employs thermocouples. These are usually , made from Chromel-Alumel junctions and have the advantage of simplicity. However,it proved to be unsafe to locate these upstream of the turbines of modern gas turbine engines. That is if they break , which is more likely to be the case, they would endanger the engine by causing turbine failure. They are therefore fitted in the exhaust section of the engine . The temperature these thermocouples indicate is of the exhaust gases .

A stage by stage gas temperature calculation is carried out upstream . From the calculation of the temperature upstream and downstream of the blades raw , the blade temperature can be calculated .

However, there are two possible direct methods for blade temperature measurement. One is to embed thermocouples in the blade. The output is to be obtained by transmission techniques such as slip rings. This is expensive and often impractical. The transmission might have a limited life and poor reliability.

The second method, is to use radiation pyrometry. These pyrometers measure the radiation emitted from the blade surface. The radiation signal depends on the blade surface temperature and surface condition. This has the advantages of being contactless, and of being able to measure with a single instrument the temperature of one blade, or a part of the blade (1/10) of a blade. It can also provide information on the mean and the peak temperatures of the entire turbine wheel [Ref.6]. Moreover, radiation methods do not have the inherent thermal inertia of the thermocouple technique, and so can have very rapid response, and by the usage of modern electronic circuitry, they can be of great sensitivity, and accuracy.

3.2 Historical Aspects

The development of radiation pyrometry was started during the late 1960's. The time where thermocouple techniques proved to be unsatisfactory and can not match the requirements of the newly developed engines, and the new materials incorporated. That initial development has defined the basic system that has been used. This system consists of the pyrometer head, and the signal processor. The pyrometer head is fitted to the turbine casing. Due to the harsh environment the pyrometer head is usually cooled. Figures 3.1 and 3.2 are air and fuel cooled pyrometers respectively.

To avoid complexity an alternative design was introduced by employing fibre optics to isolate the pyrometer from the turbine casing. In such design, high temperatures and vibrations are to a certain extent eliminated.

The advanced engines that were developed during the early 1970's have introduced new problems in turbine pyrometry. The indicated metal temperatures were found to be biased high under certain conditions. This was due to the reflected energy from the flame, superimposed on the signal. To minimize this various techniques were approached. One approach has led to the development of the dual spectral area pyrometer [Atkinson(12)].

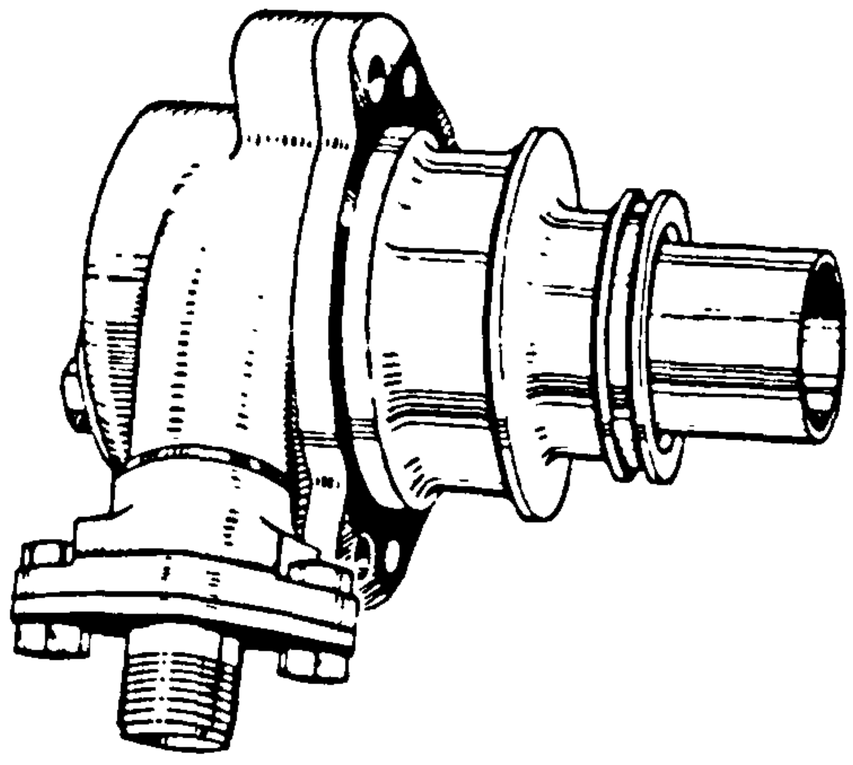

FIG no. (3.1) Early Air-Cooled Pyrometer

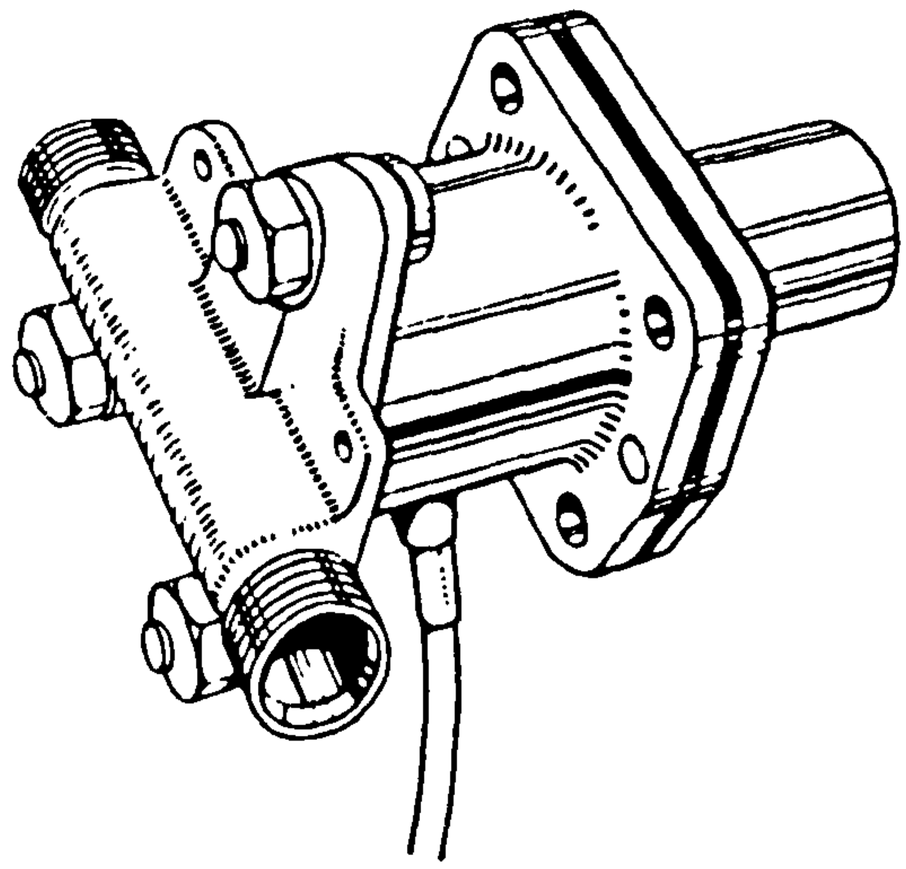

FIG no.(3.2) Fuel Cooled Pyrometer

This has been used for more than ten years and has proved to be useful in situations were the reflected energy is less than 50% of the total signal [Atkinson(13)].

In the mid 1970's, the interest was focused on temperature mapping of turbine blades. Which was achieved by traversing the pyrometer optical probe, driven under computer control, across the blade surface. This produces a profile when combined with the three dimensional blade geometry, produces surface temperature mapping.

The 1980's have experienced the development of new and more advanced engines. These engines are characterised with short combustion chambers, more open turbine IGVs, higher TETs and pressures, alternative fuel capabilities, the introduction of nonmetallic components and TBCs. All these affect in one way or another the performance of the pyrometer by increasing the reflected radiation signal to more than (75%) of the signal.

These and others have led to the many types of pyrometers being developed. The accurate design and employment of the right type to be used in the right position and the right way, reduces the reflected radiation to minimum [Douglas(14) and Curewn(15)].

3.3 Principles of Operation

3.3.1 Turbine Blade Temperature Measurement System

The turbine blade temperature measurement system is fitted on the turbine casing, in a way, it can view the turbine blades. Then, by measuring the electromagnetic radiation emitted from the blade (s), it produces a signal dependant on the temperature of the blade under view. Figure 3.3 is a schematic representation of the system.

The emitted radiation is guided through a clear path from the blade surface via the pyrometer optics to the sensor. Fibre optics are used to enable the mounting of the sensor in a remote position, with the right operating conditions.

The signal output from the detector is then processed and conditioned to give the required information(s). This information normally, include [Ref. 6] :

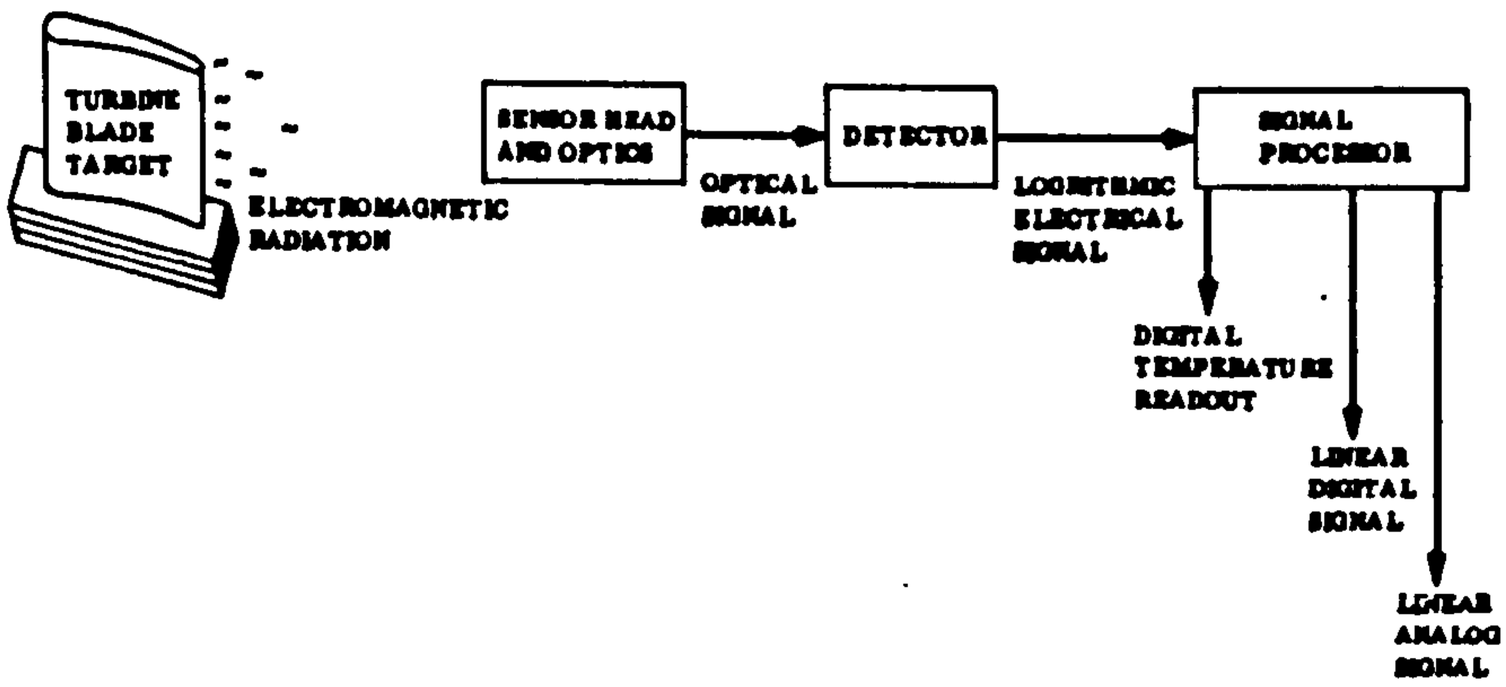

Figure no. (3.3) Schematic Representation of Turbine blade temperature measurement system [Rohy(8)]

- Average blade surface temperature ,
- Maximum blade surface temperature ,
- Individual blade temperature profile ,
- The temperature of (1/10) of the blade surface ,
- The temperature profile of a group of blades under consideration .

3.3.2 Physical Laws

The radiation detected by the pyrometer detector can be expressed in the following exponential form [Sharp(17)]

$$E_\lambda = \varepsilon_\lambda \quad K \quad T^n \qquad \text{.....3.1}$$

Where n is function of both surface temperature and detector wave length and

$$n = 5 \quad \lambda_{MAX} / \lambda \qquad \text{where} \qquad \lambda/\lambda_{MAX} \leq \quad 2.5$$

Most of the detectors used for turbine blade temperature measurements are of silicon or germanium type. These detectors generate a photo current as a result of the incident radiation .

3.4 Radiation detectors

The detection process requires an interaction of the incident optical radiation with the detector material to produce a measurable signal output. This signal is usually and most conveniently electrical. The parameters, properties and characteristics of the detector defines, to a large extent, the performance of the radiation detector .

3.4.1 Types of Radiation Detectors

Two types of interaction between the detector and the incident radiation may take place. This give rise to two different types of detectors. They are the thermal and the photon detectors [Petritz(19)].

In thermal detectors, the incident radiation interacts with, and is absorbed by the detector molecules. This will increase the detector temperature and produce a second measurable effect.

Three different effects are produced in the three types of thermal detectors, namely thermoelectric detector bolometer detector, and golay cell or the penumatic detector, details of these detectors are given by De waard [20].

The second type of radiation detectors is the photon detector [Petritz(19), Klein(21) and Planck(22)]. The interaction between the photons of the incident radiation and the electrons of the detector material produces one of the following effects: photoconductive effect, photovoltaic effect, photoemissive effect, and photoelectromagnetic effect. Details of these types are given by Petritz [19].

Thermal detectors have the advantage of being sensitive to all wavelengths uniformly. Photodetectors are normally wavelength selective. Photodetectors have shorter response times measured in microseconds, compared with milliseconds for thermal detectors. They are more sensitive, since two energy conversions processes are involved in thermal detectors [Petritz(19)].

3.4.2 System Construction

Turbine pyrometer systems are usually composed of four distinct elements, as shown in Figure no. (3.3). These elements can be grouped under two units. The pyrometer transducer and the signal processing unit.

3.4.2.1 Pyrometer Transducer

The pyrometer transducer consists of the fibre optics and the detector .

The purpose of the fibre optics is to guide the energy radiated from the target on to the detector. They also define the field of view of the pyrometer. These optics are purpose designed and vary from one application to an other .

The first types of pyrometer optics were merely a group of lenses to focus the radiation beam on to the detector. This type of optics requires the pyrometer to be mounted on the turbine casing. This has introduced thermal and vibrational problems .

To minimize these problems, the fibre optic cables were introduced to permit the location of the detector in a more benign environment. These systems are applicable to turbine blade temperature measurement systems .

3.4.2.1.1 Lens type optics

The lens type system, Figure 3.4, consists of an objective lens and a field aperture. The lens focuses the beam on the field aperture and the aperture defines the target shape .

The radiation is then transmitted to the detector by a solid light pipe, a flexible fibre optic bundle or a combination of both.

To gather maximum energy from the target, the lens should be as big as possible. for structural reasons, penetration through the engine casing should be as small as possible. Therefore the lens becomes a trade off.

Similarly, the target area, that is the area on the turbine blade from which radiation is gathered by the pyrometer optics, should be as large as possible to provide the maximum energy and hence maximum signal. On the other hand and for better resolution, it should be small .

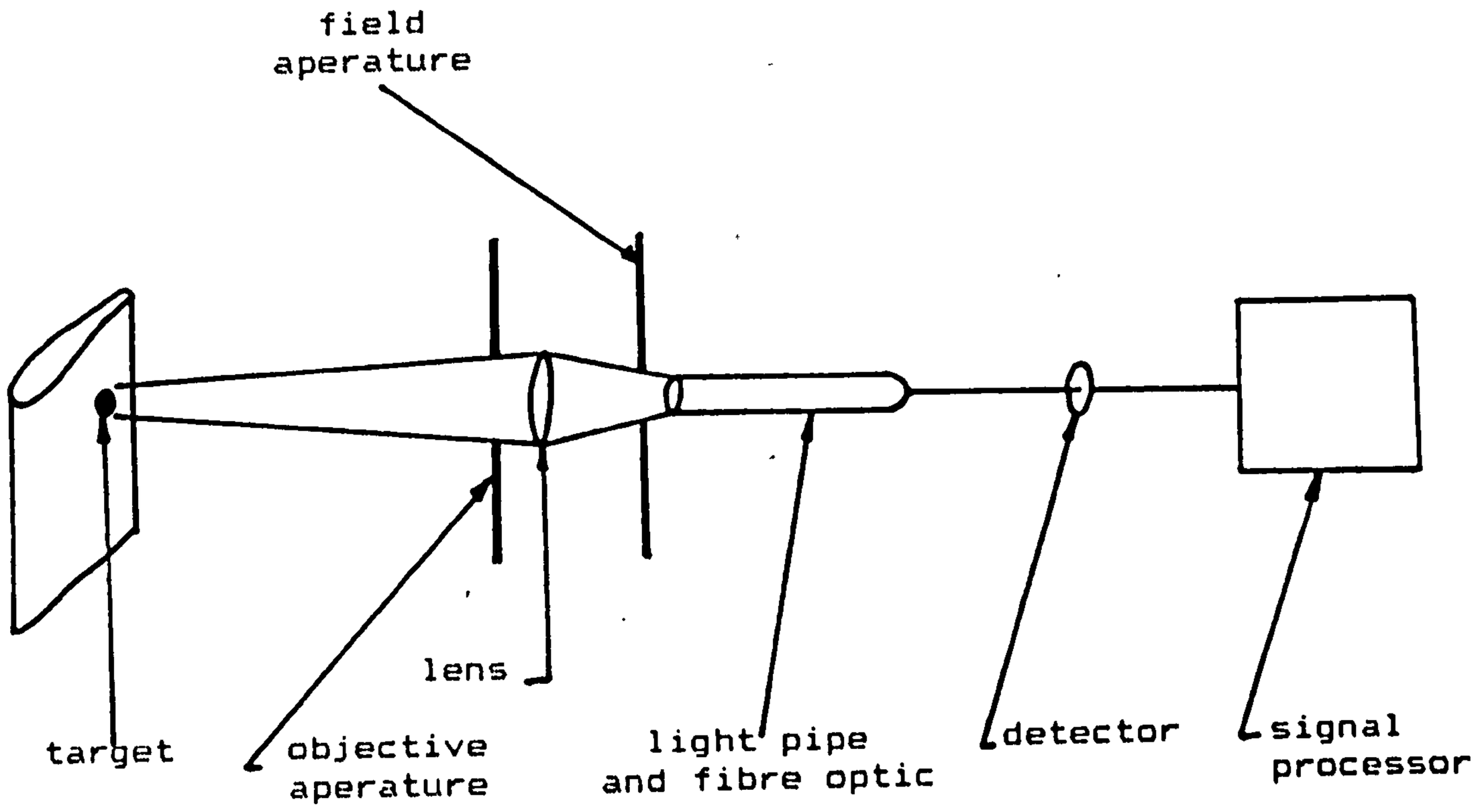

Figure no 3.4 Lens Type Optics

The lens material depends on the wave length range, maximum transmission required and high temperature capabilities. Figure no. (3.5) shows the spectral transmittance of some of the optical materials used for making windows and lenses for pyrometry applications [Ref.23].

3.4.2.1.2 Aperture type optics

In this type of arrangement, Figure 3.6, the radiation falls directly on the light pipe or the flexible fibre optics bundle. This, then guides the beam to the remotely positioned detector.

The radiation is normally accepted from within a cone of 15 to 30 degrees . This cone defines the target area , which is larger than the target area of the lens type system [Rohy(24)] .

Barium Fluoride BaF_2

Caesium Bromide CsBr

Caesium Iodide CsI

Calcium Fluoride CaF_2

Germanium Ge

Lithium Fluoride LIF

Magnesium Fluoride MgF_2

Potassium Bromide KBr

Potassium Chloride KCl

Sapphire Al_2O_3

Silicon Si

Silver Bromide AgBr

Silver Chloride AgCl

Sodium Chloride NaCl

Sodium Fluoride NaF

Strontium Fluoride SrF_2

Thallium Bromide TIBr

Thallium Bromide_
Iodide KRS5

Thallium Chloride TICl

Zinc Selenide ZnSe

Zinc sulphide ZnS

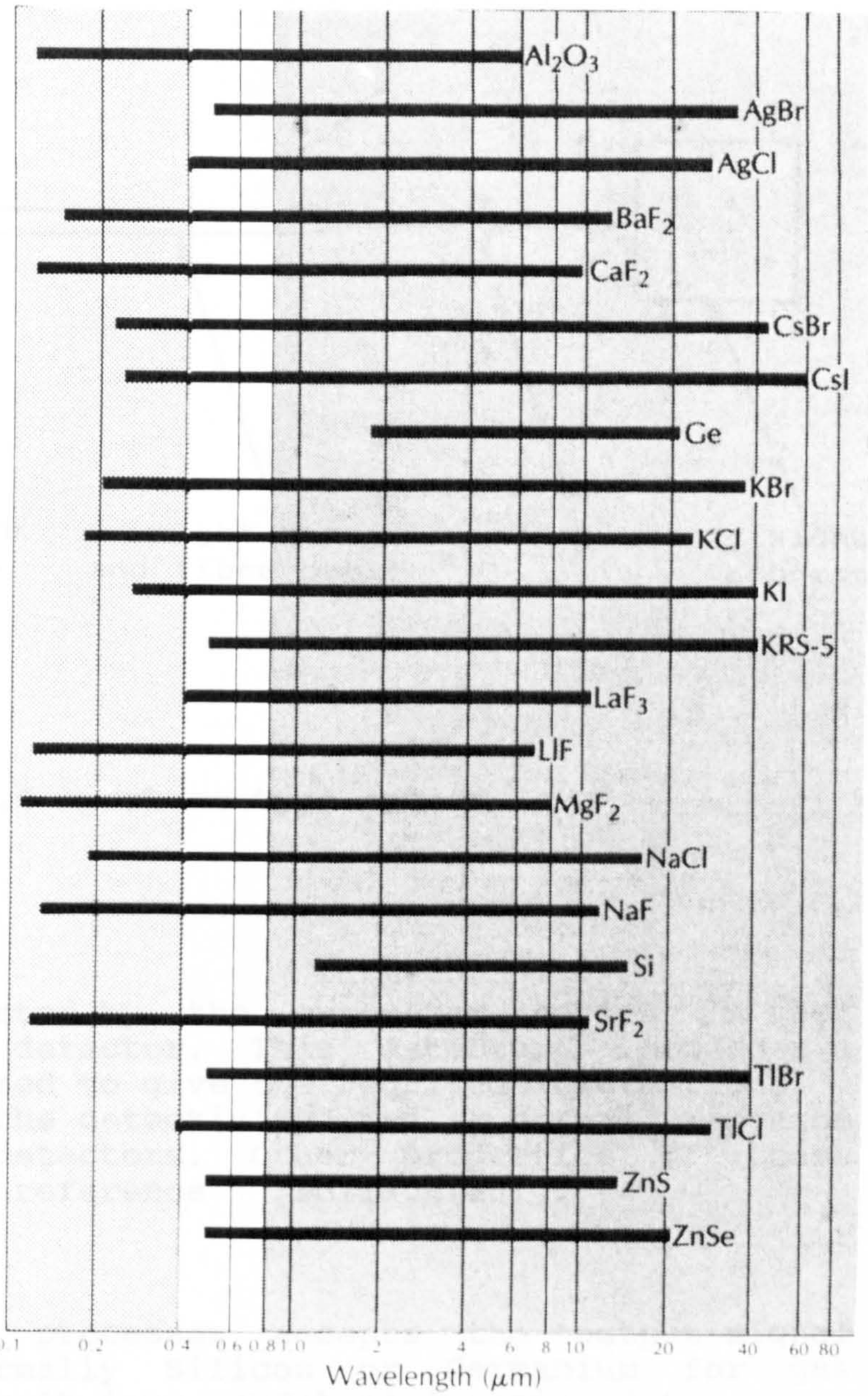

Figure no. (3.5) Transmission range of optical materials
[from Ref. 23]

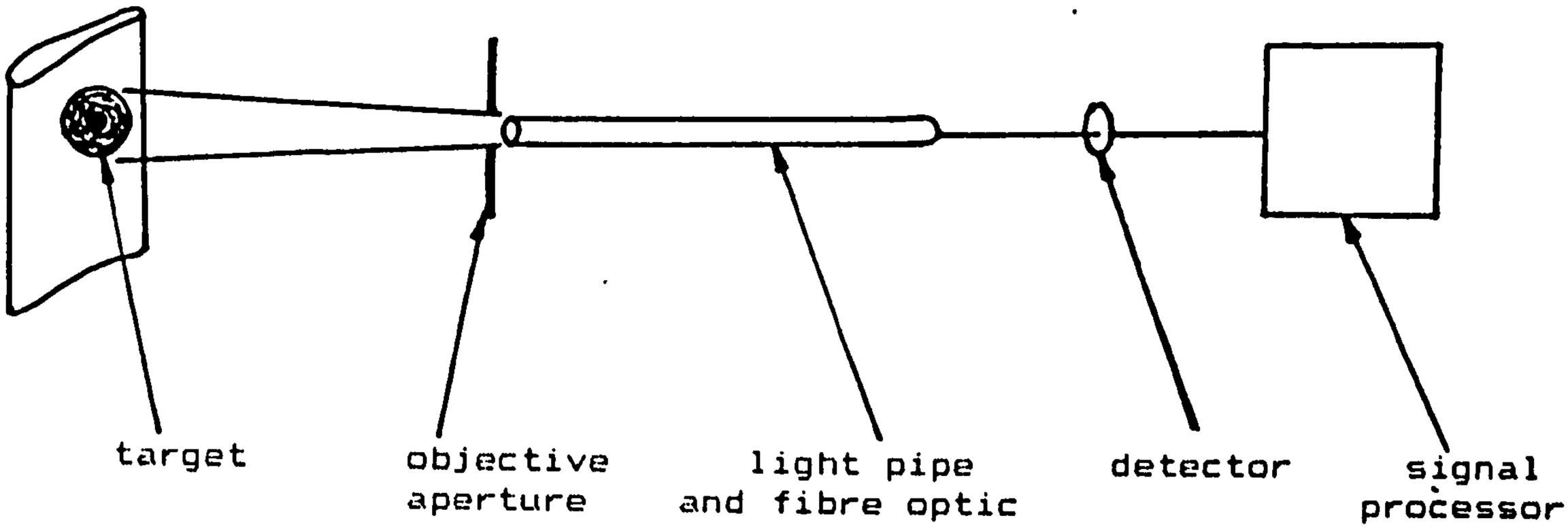

Figure no 3.6 Aperture type optics

3.4.2.2 Detectors

The radiance collected by the pyrometer optics is then focused on the pyrometer detector. This detector produces a signal that can be processed to give the required informations. Figure no. (3.7) shows the detectivity and spectral range of commercially available detectors. Other properties of these detectors are given in reference [Pollack(25)].

3.4.4 Signal processing

The pyrometer signal processor accepts the output signal from the detector, normally Silicon or Germanium for gas turbines. It then converts it into useful engineering data .

The signal processor functions include :

1) Signal modification ,

2) Ambient temperature compensation ,

3) Surface emissivity compensation ,

4) Noise filtration ,

5) Linearization ,

NO.	MATERIAL	MODE	WORKING TEMP. K
1	Si	pv	295
2	Si	pc	295
3	GaAs	pv	295
4	Ge	pv	259
5	PbS	pc	295
6	PbS	pc	195
7	PbS	pc	77
8	InAs	pv	295
9	InAs	pv	195
10	InAs	pv	77
11	PbSe	pc	295
12	PbSe	pc	195
13	PbSe	pc	77
14	InSb	pem	295
15	InSb	pc	295
16	InSb	pc	77
17	InSb	pv	77
18	Ge:Au	pc	60
19	Ge:Hg	pc	27
20	(Hg-Cd)Te	pv	77
21	Ge:Cd	pc	4.2
22	Si:Sb	pc	4.2
23	Ge:Cu	pc	4.2
24	Ge:Zn	pc	4.2

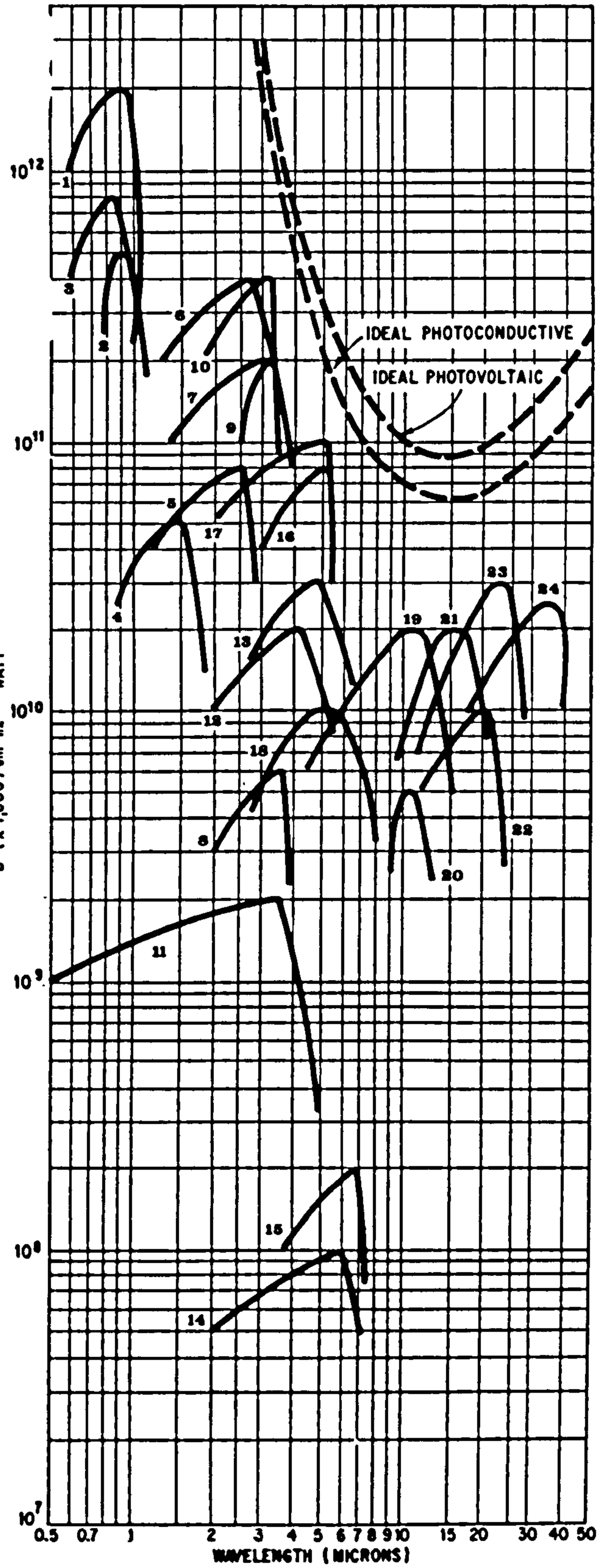

Figure no (3.7) Spectral detectivities of commercial detectors

6) Temperature display ,

7) Provide temperature profile analog signal ,

These are the main functions of most signal processors. However, they differ from one research establishment to an other. Some use buffer memory together with A/D, D/A convertors and computers [Buchele(26)]. Others use one box to perform the main functions coupled to an oscilloscope [Ref.6].

Some of the research establishments and companies employ other equipments to perform certain functions like the blade analysis and selection equipment, BASE, employed by Negretti Aviation [Ref.11]. The BASE enables monitoring of one or (1/10) of a blade. Some use different techniques to overcome the problem areas. Like the use of minimum picking technique to eliminate interference errors [Smith(27)].

3.5 Possible Sources of Signal

The radiation signal reaching the detector can include contributions from the following sources :

3.5.1 Target Radiation

Target radiation is the radiation emitted from the target spot by virtue of its temperature and surface conditions. The strength of the pyrometric method is its exponential response to target temperature which minimizes the effect of the uncertainty in the spectral emissivity of the target surface on the indicated target temperature. Equation 3.1 indicates that, to minimize measurement errors due to the uncertainty in surface emissivity, a detector with the shortest wave length should be used. For most turbine blade materials, equation 3.1 holds for the same values of surface emissivities over a view angle of up to 65 degrees with the normal (chapter seven).

The spectral emissivity of newly machined surfaces is low. It begins to increases as the surface begins to oxidize and stabilizes at a maximum [Beynon(28)].

Based on the above, and to measure a surface temperature, one should :

1) Use the shortest operating wave band detector (silicon) ,

2) Avoid viewing the surface at large angles ,

3) Ensure that the target is fully oxidized ,

For a given detector, the optical signal is determined by the optical factor (F) of the system , where :

$$F = \{(D_\ell \times D_T)/(LT)\}^2 \quad \text{.....3.2}$$

Where LT is lens to target distance

3.5.2 Reflected Radiation

Reflected radiation is the radiation emitted from surfaces other than the target surface, and reflected by the target on to the detector.

Temperature measurement by optical pyrometry is based on the measurement of radiation emitted by the target surface. The pyrometer detects only portion of the total radiated energy. In turbine pyrometry, the detectors used are usually silicon detectors. Silicon detectors are responsive to radiation in the wave length band (0.4 to 1.2) micrometers. In this region, the detected energy is approximately proportional to the tenth power of temperature [Barber(29)].

In some cases the temperature of other engine components is significantly higher than the target temperature. This will have the effect of biasing the indicated temperature high by reflecting radiation from hotter engine components that are in view of the target. Flame radiation can cause high measured temperatures. In these cases the measured temperatures must be adjusted for to consider the reflected radiation. This has led to the development of the dual spectral area pyrometer [Atkinson(12)]. However, These pyrometers are not currently been specified for the present or the next generation engines.

3.5.3 Emission From The Sight Path Gases

In turbine pyrometry, the optics are placed far from the rotating surface. Radiation emitted by the target has to travel through burnt gases to reach the optics. If these gases are not completely transparent at the pyrometer working wave band, they will affect the temperature measurement.

When these gases are cooler than the target, they absorb some of the radiated energy, and cause the pyrometer to read low. While, when they are hotter than the target, the pyrometer indicates higher values due to gases emission.

In the case of silicon detectors, the effect of combustor gases on the pyrometer reading is negligible. This is because, these gases do not have significant emission or absorption in the detector working waveband. Figure 3.8 shows water vapour and Carbon dioxide emission bands .

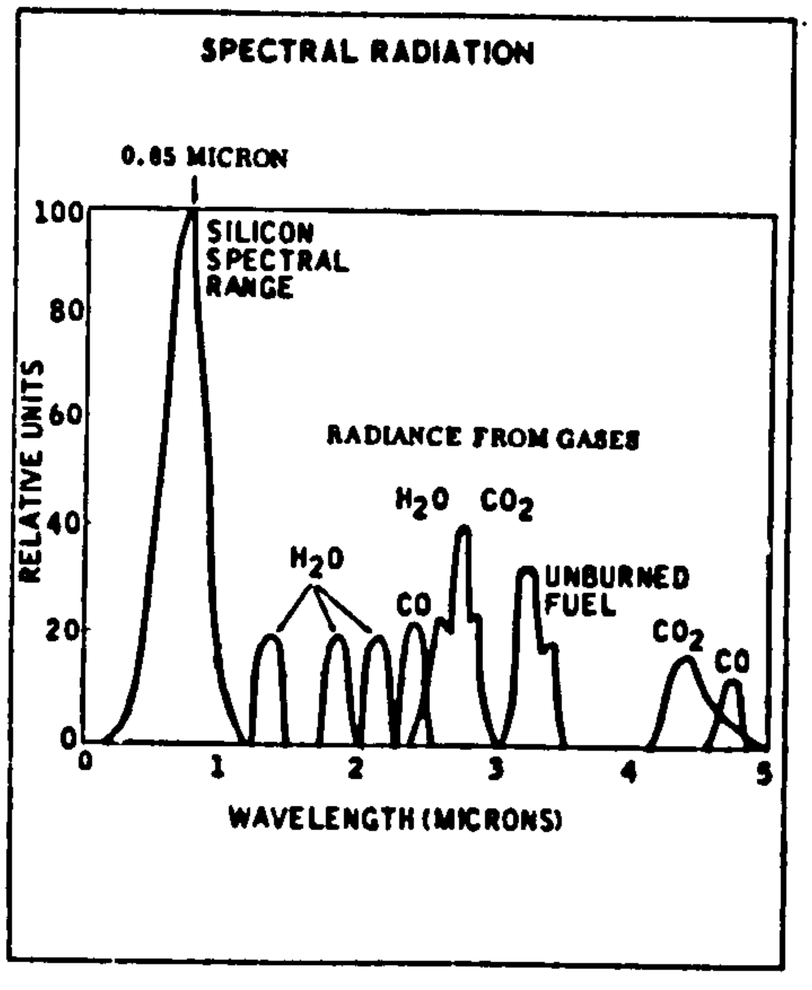

Figure no. (3.8) Spectral response of silicon detectors and radiance from turbine gases [Rohy(24)] .

3.5.4 Transient Interference

This interference arises mainly from two sources. The first is the flame. This is significant in the case of the measurement of the first turbine stage or the NGVs temperature. The right positioning of the optics on the casing helps to minimize this interference .

The second source of interference is from the hot Carbon clouds. These have higher temperatures and cause noise spiking in the signal when they pass through the field of view .

To overcome this type of interference, two techniques may be employed. The first is, the two colour technique. This type eliminates particle spiking without masking an over heated blade. In this technique, the radiation is sensed simultaneously in two different wavebands. One of the channels is used for the

temperature measurement. The second channel is used for continuous comparison of the signal. This comparison is then used for gating the measurement channel to hold the 'last good value' [Beynon(28)] .

The second technique is called the minimum picking technique. In this technique a blade timing / counting system is employed. This system enables the sampling and storing of the target spot radiation. This radiation is compared with the radiation from the same spot in the second revolution. If the value is lower, a (1) is entered in to the measurement validity counter. If the second value is retained, the counter is reset and the validation process starts again. Until the counter reaches a pre-determined value at which point the retained value is transferred to a central store and the evaluation of a second target spot begins. Employing this technique, a complete rotor profile that is free from transient interference may be obtained. More details about this technique are in [Douglas(14)]. However, both these techniques are experimental and are not currently been specified for the present or next generation engines.

3.5.5 Other Sources of Emission

In addition to the proceeding sources, some other sources may prove to be of significant interference. Mirrors can be employed to give optical access to view the target when direct viewing is not possible. These mirrors can contribute to the target emission giving a biased reading by the pyrometer. This is usually insignificant, provided that the mirror temperature is at least (100 K) lower than the target temperature [Beynon(28)].

Dirty mirrors and lenses can produce a significant scattering of the radiation causing the pyrometer to indicate biased temperatures.

3.6 Installation Considerations

The design of the optical probe installation within the engine has a significant effect on the pyrometer performance . It is necessary to identify the main sources of error and how to reduce or overcome their effect . These are :

3.6.1 Lens Obscuration

lenses and windows are usually used in radiation pyrometry for focusing and directing the radiation emitted from the target to the detector through fibre optics. Lenses are also used to

specify the target diameter and lens to target distance [Ref.6]. Their obscuration can have a great effect on the pyrometer performance .

It is normal practice to purge the lens with high pressure air. This is to prevent contaminants in the gas stream from impinging on the lens surface. Purge air is normally bled off the final stages of the compressor. However, at start up and shut down, the purge air might be absent. But With air velocity nearly sonic, it has the effect of removing contamination deposited in the absence of purge air. This high velocity air should not reach the target spot and to some extent not to disturb the main flow [Ref.6].

One of the important features of the probe installation is that the siting of the optical probe should not contribute to the obscuration problem. When the pyrometer lens is placed directly below the turbine, debris is liable to gravitate towards its surface. On the other hand when it is placed at the top of the turbine, it is more likely to suffer contamination from hot engine vapours .

3.6.2 Optical Probe Working Temperature

The operating temperature of some optical probes can be as high as 973 K, while that of the fibre optic bundles are much lower, 623 K. Detectors and head amplifiers can not work at temperatures higher than 400 K. Above which they might drift giving biased readings [Ref.6].

In gas turbine applications, the detector, head amplifier and fibre optics are usually in an environmental temperatures below those stated above. While the optical probe can be working in an environmental temperature much in excess of 973 K.

Cooling of the optical probe is essential to prevent degradation of its material. Cooling is normally provided by the purge air. To economize on high pressure bleed, a separate air supply is sometimes used. The survival temperature of the lens is normally greater than that of the hot end fibre bundle termination. Splitting the purge system allows the use of hot high pressure air at the lens and a cooler low pressure air for the fibre bundle termination. Relatively unclean air can be used for purging all but the lens [Pointer(31 and 33)].

3.6.3 Reflected radiation

The radiation emitted by a target surface consists of the radiation due to the target temperature, and for grey bodies ,with emissivity less than one, a reflected component from the surroundings .

The typical blade surface emissivity is(0.8) [Smith(27)]. So the blade surface reflectivity is 0.2. This means 20% of incident radiation on the blade surface is reflected .

Due to the exponential response of the pyrometer detector to temperature, Surfaces that are more than 100 K hotter than the blade surface can have a very significant reflected component of the target radiation when they are in view of the target blade surface. Two of the possible ways to eliminate the effect of the reflected radiation are :

1) To position the pyrometer, where no hotter components are in direct line of sight from the blade under consideration .

2) Detailed radiation calculations can be performed on the whole turbine wheel. This is to be used as a correction method for the measurement. This is extremely complex to perform. However, simplified calculations can provide a significant improvements [Atkinson(12)] .

3.7 Negretti Aviation Radiation Pyrometer

3.7.1 Introduction

As a conclusion to this chapter, a pyrometer has to be chosen. This pyrometer should have the characteristics that allow it to be mounted on an aerogas turbine engine .

The Negretti aviation pyrometer has features that made it very suitable for this work. It is of the type that is designed for aerogas turbine engines. It is accurate, simple to use and easy to handle. It does not need a special coolant and can operate at normal atmospheric conditions. It provides an analog signal and a digital display of turbine blade temperature when connected to the pyrometer processing unit .

3.7.2 Transducer Elements

The Negretti pyrometer transducer collects thermal radiation from a well defined target area on the turbine blades. This optical signal is routed via an optical fibre link to a detector and a signal conditioning unit. The output of the pyrometer transducer may then be processed within this unit to provide a signal that is function of the turbine blade temperature. The main elements of the pyrometer transducer are shown in Figure no.(3.9).

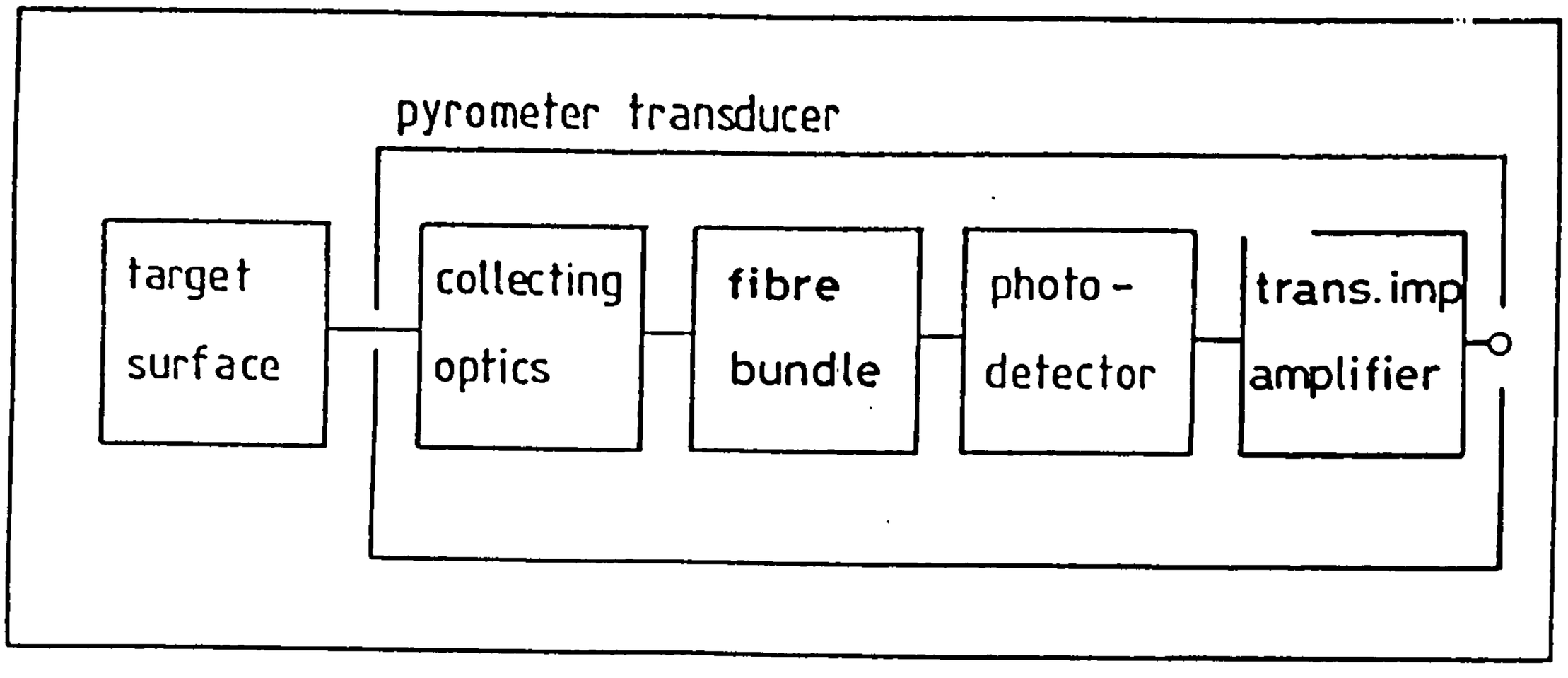

Figure no. (3.9) Transducer elements [Ref.6]

3.7.2.1 Collecting Optics

The collecting optics of this pyrometer consists of a sapphire lens brazed into a metal holder. The image of the target area is focused onto the field stop placed at a set distance behind the lens .

The radiation collected from the target area is transmitted via a fibre bundle placed behind the field stop and routed to the detector .

The collecting power of the optics is characterized by the optical factor, Eq.3.4. And the values for it are :-

The optical factor F = 0.08 mm2

The lens diameter D_l = 5.3 mm

The target diameter D_T = 4.0 mm

The lens to target distance LT = 75 mm

3.7.2.2 Optical fibres

The harsh environment of the turbine casing necessitates the remote location of the pyrometer detector. Fibre optic bundles are used to guide the radiation beam from the target to the detector.

Fibre optic technology is based on the phenomenon of total internal reflections. Each bundle is made from many fibres . Each fibre is made from a glass core and coated with a second layer of glass. The diameter of each of the fibres is 0.003 Inch. The flexible fibres which compose the cable are not attached to each other over the entire length. They are only attached to each other at both ends. It is at the ends where they are collected into a metal ferrule and cemented together .

The cementing process of the fibres is what determines the good packing densities and the long life of the cables [Rohy(24)]

The absolute transmission of the bundle is dependant upon many factors. These factors are the transmission area, reflection at fibre ends, the end surface finish and the absorption and scattering of both ends .

The total transmission loss of 2 to 3 Feet long fibre bundle, is nearly 60% of the incident energy. This loss is compensated for in the initial calibration of the fibre bundle [Rohy(24)].

The optical fibres bundle is connected to the collecting optics from one end and to the amplifier from the other end. This flexible fibre optic light guide, along which energy is transmitted from the optic head to the head amplifier module has a protective armoured sheath. The optical fibres are terminated at the receiving end of the fibre bundle by a 'hot_formed' process. This is to minimize losses due to non_transmitting areas. The termination of the fibre bundle at the photo_detector coupling is by a conventional adhesive process. This meets the requirements of survivability quoted for the electronics assembly.

3.7.2.3 Silicon Photo-Detector

Silicon radiation detectors have been used almost exclusively for turbine blade temperature measurements. The significant properties of the silicon detector that make it uniquely suitable for the measurement are [Barber(29)]:

1) Robustness. The sensitive chip of the silicon can withstand high levels of shock and vibration. Gas turbine engines are normally prone to high levels of shock and vibration. This makes silicon detector a better choice .

2) High working temperatures. The silicon can withstand very high temperatures without suffering permanent damage. It can have a working range of 200 to 400 K. This makes it suitable for turbine blade temperature measurements without the need for special coolants, when used with fibre optics .

3) Suitable wave band . Carbon dioxide and water vapour are two dominants of a combustor out put. FIG. 3.8 shows no major absorption or emission of air or combustion gases in the wave length range, to which silicon is sensitive. This reduces the interference of these gases on the radiation signal detected by the pyrometer.

There are three types of silicon detectors. They are the surface barrier, diffusion junction, and the Lithium drifted. In the surface barrier type detector, the active junction is formed by depositing a thin film of gold on the surface of an N-type silicon. The diffused diode is produced by diffusion of an impurity into an N or P type silicon to produce an N-P junction.

The active area of the Lithium drifted detector, is produced by the diffusion of Lithium in an N type silicon. The diffused junction detectors are the most suitable and reliable detectors for turbine blade temperature measurements [Rohy(24)].

The radiation collected by the optics is detected by the silicon photo diode operated in a zero voltage bias mode. This voltage is necessary to minimize errors due to leakage currents at high ambient temperatures.

3.7.2.4 Head Amplifier

The current from the photodiode is converted to a proportional voltage by the head amplifier which also amplifies the signal.

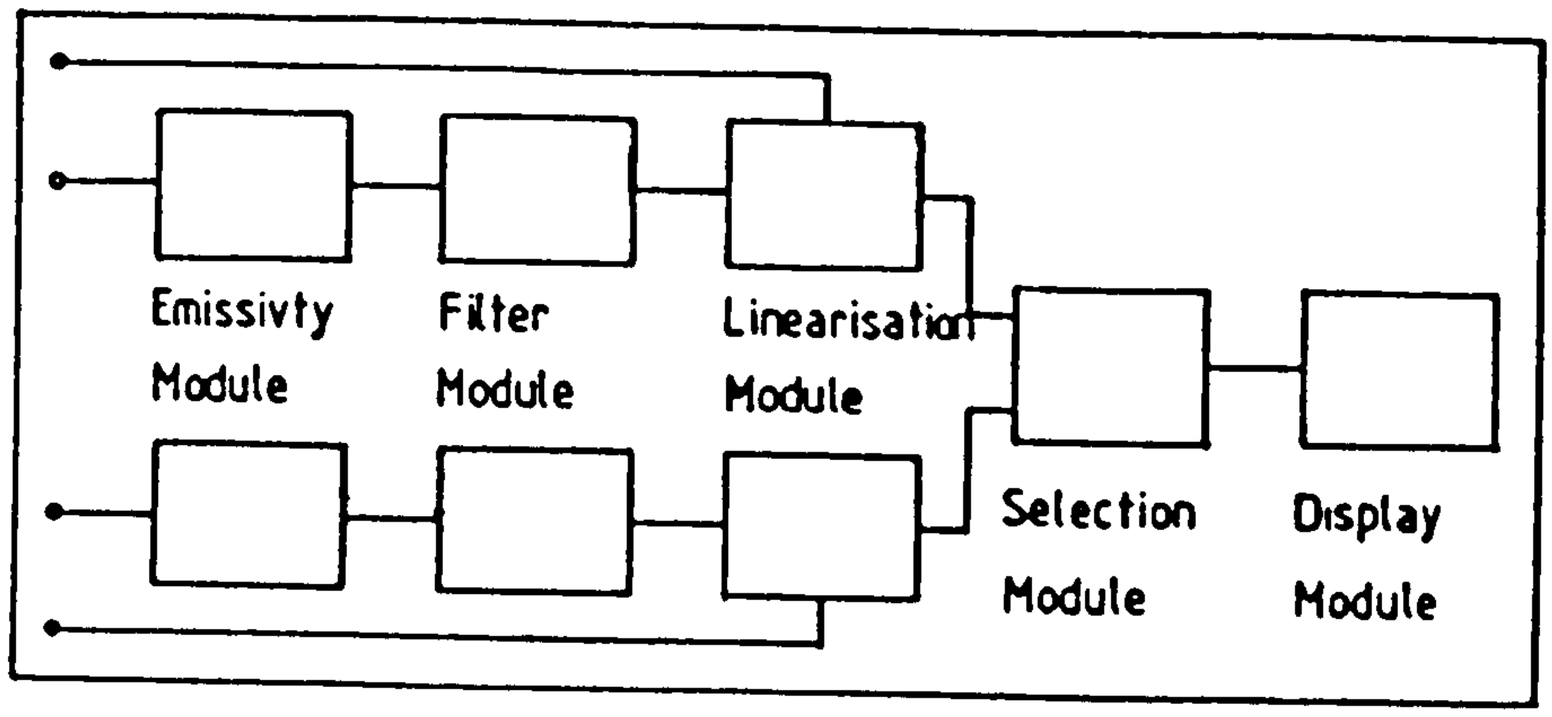

Figure no. (3.10) Pyrometer signal processing modules

3.7.3 Signal Processing

3.7.3.1 MK2 Pyrometer Signal Processor (PSP)

The (PSP) is designed to accept the signals from one or two pyrometer transducers. The output signal from either one of the two transducers is processed by the PSP and an indication of peak and mean temperature is provided .

The PSP is of modular construction. It is made of six modules, providing a stabilised power supply and transducer channel selection. The other modules are as follows, Figure no.(3.10):

- Interface module. The transducers are connected to the PSP via this module. This module also provides emissivity compensation and a self test facility. Unprocessed blade radiance signals are available from the interface module.

- Filter module. Two four pole low pass filters, one for each channel, with a pre-set cutoff frequency are incorporated in this module. These filters remove excess high frequency noise from the transducer output signal. Filtered blade radiance signals are also available from this module .

- Linearising module. The transducer output signal is non_linear in relation to blade temperature. The linearising module linearises the blade radiance signal and also compensates for ambient temperature fluctuations of the detector within the head amplifier. Linearised blade radiance signals are available from this module. Figure 3.11 shows the pyrometer signal before and after linearization.

- Output display module. This module has an LCD providing mean or peak blade temperature readings in degrees centigrade. Both the peak and the mean temperature signals are available from this module .

3.7.3.2 Blade Analysis and Selection Equipment (BASE)

This equipment, is used in conjunction with the PSP to select individual, or part of individual turbine rotor blades in order to measure their temperature profiles.

When one pulse signal per turbine revolution is available from the engine, any blade can be selected from any total number of blades, on the turbine rotor. Individual blade temperature is indicated on the PSP allowing the hottest blade on the rotor to be identified. Each blade can also be divided into ten equal widths to obtain the blade temperature profile .

3.7.4 Pyrometer Assessments

3.7.4.1 Pyrometer Calibration Check

The pyrometer was checked against the Negretti Aviation black body furnace type 12143. This furnace is a reference furnace used for the calibration of pyrometers [Ref.34].

The pyrometer was checked for furnace temperature settings between 600 to 1200 C. The results of this check are shown plotted in Figure 3.12.

3.7.4.2 Pyrometer Check Against "Land" Research Pyrometer

The aim of this test was to check the "Negretti Aviation" pyrometer against "Land" research pyrometer, (Appendix A). Both of the pyrometers were made to look at the black body furnace for the same temperature settings .

Figure no. (3.13) shows a comparison of the readings of the two pyrometers and black body readings .

3.7.4.3 Stainless Steel Emissivity Measurements

The pyrometer was then used for measuring the emissivity of a stainless steel plate. A sample furnace ,see chapter nine, was used to heat up the plate .

3.7.4.4 Black and White Paint Tests

The above test was repeated twice. The first was by employing a white painted stainless steel plate. The second was for a black painted stainless steel plate. The results of the three tests are shown in Figure 3.14.

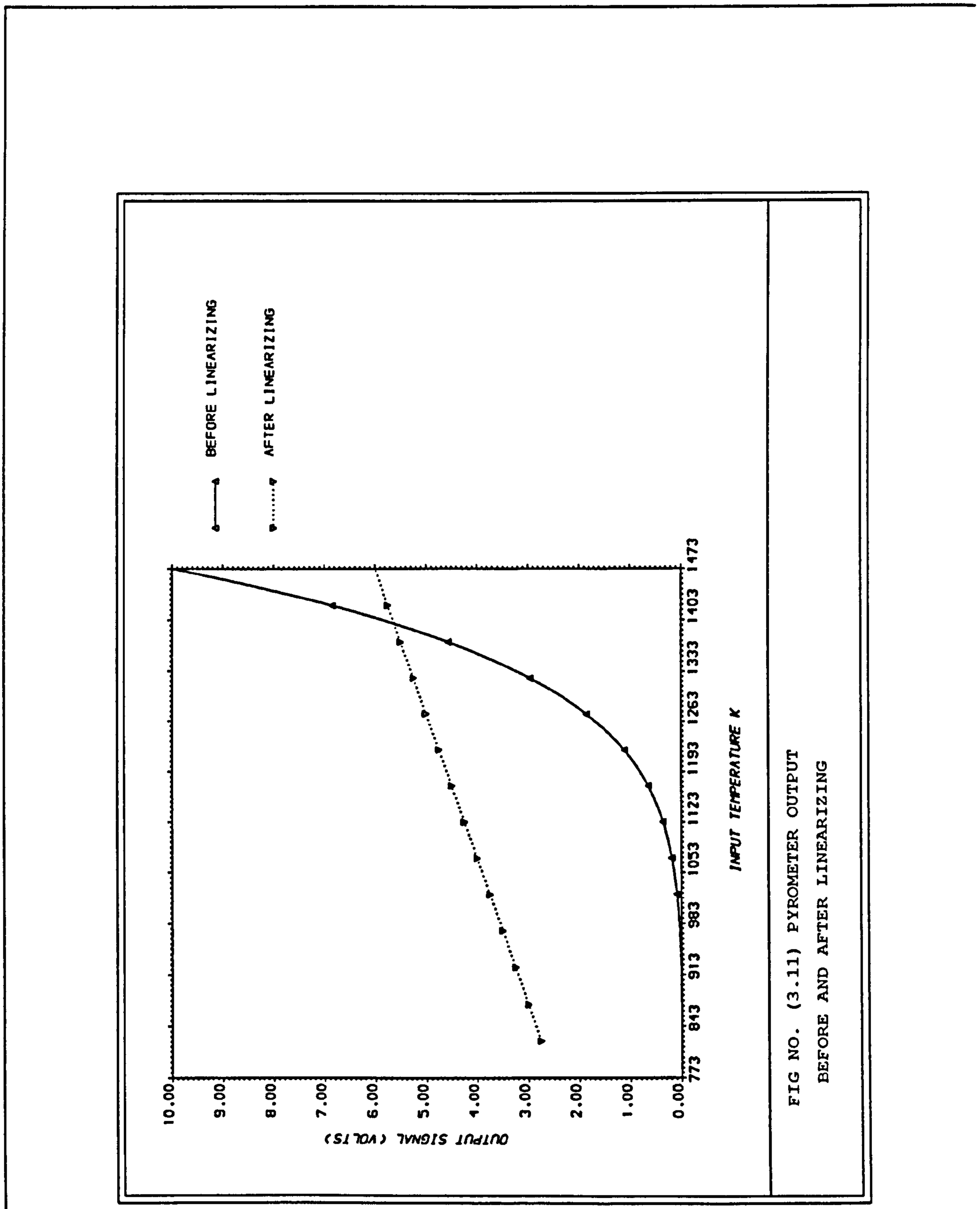

FIG NO. (3.11) PYROMETER OUTPUT
BEFORE AND AFTER LINEARIZING

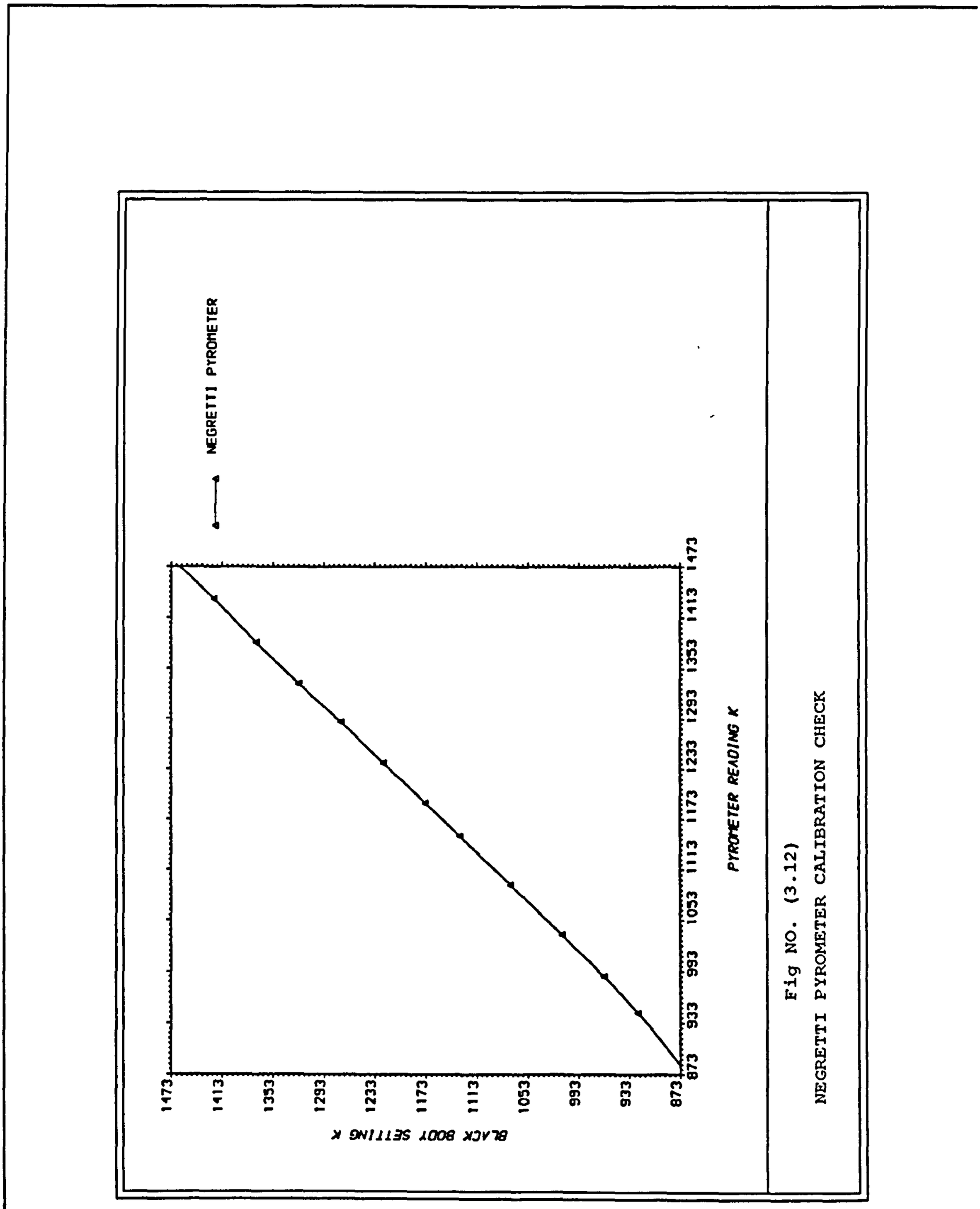

Fig NO. (3.12)

NEGRETTI PYROMETER CALIBRATION CHECK

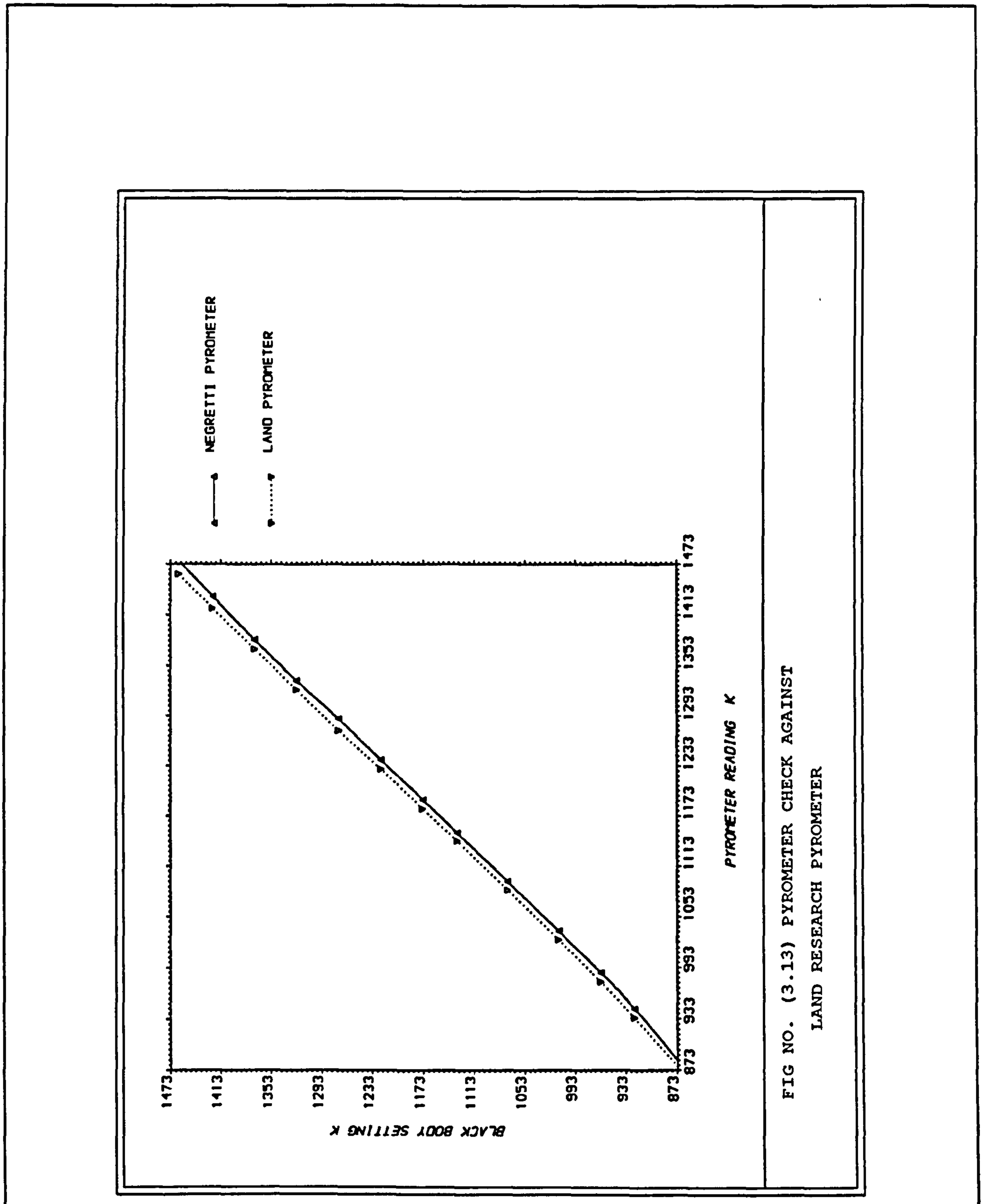

FIG NO. (3.13) PYROMETER CHECK AGAINST
LAND RESEARCH PYROMETER

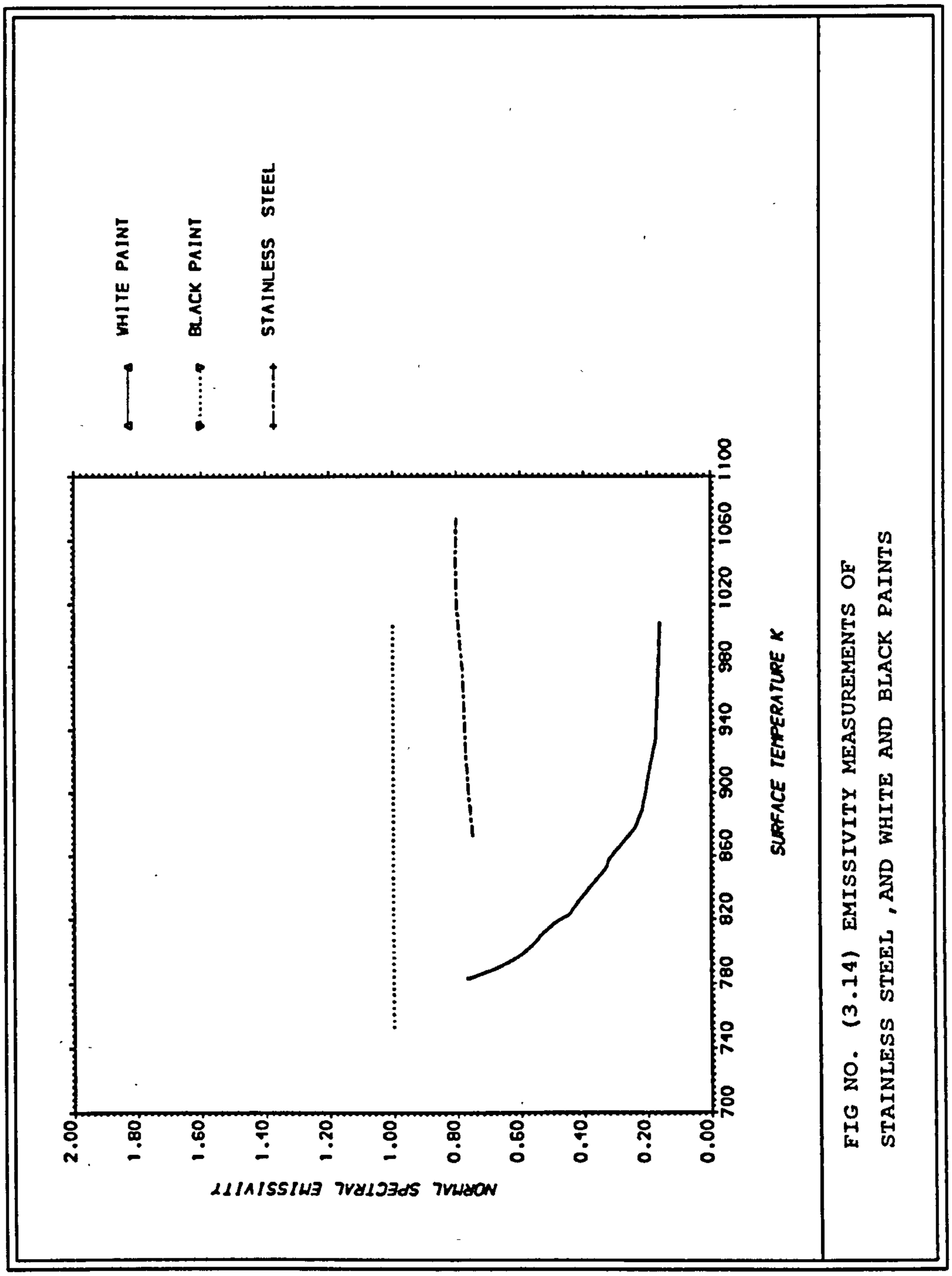

FIG NO. (3.14) EMISSIVITY MEASUREMENTS OF STAINLESS STEEL , AND WHITE AND BLACK PAINTS

CHAPTER FOUR

4 EXPERIMENTAL RIG SELECTION

4.1 Introduction

Unless gas turbine blade coatings are reliable, the designer is unable to take due credit for potential improvement to the engine as in the absence of reliable operation the improvements could not be guaranteed .

During the development of a gas turbine, blade coatings are qualified for the particular engine application and environment by extensive and expensive engine test. The usual method involves introducing several different coatings to different blades on the same NGVs and turbine stages. As the different coating types experienced the same operating conditions and environment, the coating that performs "best" during such a qualifying test is chosen.

Such tests are very costly and time consuming. They have an added disadvantage that only the final result of the total operation is known. The test is unable to identify coatings that were better during parts of the test, for example start up, rapid acceleration, high temperature operation and operation in a corrosive environment. Thus the coating chosen may prove to be unacceptable for the same engine when used under different conditions of operation and environment. There is clearly a need to identify and develop a better way of assessing coatings suitability .

This chapter outlines the selection of a suitable experimental rig to study the behaviour of coatings during engine operation. This rig was used for the study of coatings and blade metal temperature measurements with a rotating turbine wheel .

4.2 Gas Turbine Rig

The obvious route to do this work is to use a gas turbine based test rig. Preliminary design and cost study for gas turbine test rig was performed . The assumption was made that the gas turbine could be got free of charge, but in spite of this modification to the gas turbine, cost of installation and test were so large as to make this impractical. Therefore a different route was necessary .

4.3 Gas Turbine Simulator

In order to measure the metal temperature for rotating blades a non intrusive technique was essential. The technique chosen was radiation pyrometry.

The requirements for a gas turbine simulator rig were then that the blade passing frequency, passed a fixed radiation pyrometer was approximately that of a typical gas turbine, that the metal/coating temperature was typically in the same range as experienced by a modern gas turbine and that high temperature coatings of interest could be applied to the simulator.

Early investigation established that the use of even a small gas turbine would be prohibitively expensive. However, it was considered crucially important that if an alternative experiment was carried out that the results from this experiment should be applicable to gas turbines. It was therefore essential that the metal temperature be measured in an equivalent environment with rotating blades passing a fixed pyrometer at approximately the correct blade passing frequency, operating at the metal temperatures currently prevalent in gas turbine blading.

These constraints along with the requirement to achieve the test within a modest budget and the requirement that the test include ceramic coatings of current interest to gas turbines was initially a difficult impasse. The progress of the task was critically dependent upon an acceptable solution to these constraints.

Discussed below briefly is the approach that was eventually adopted. There was early attempts to design the experiment based on an axial turbine stage. This proved to be very expensive in spite of assuming that the turbine could be obtained free of charge.

The attention was then focused on radial inflow turbines. Turbocharger turbines are of radial inflow types and looked very attractive alternative for the following reasons:-

Turbochargers are small in size so they are economical to run.

Turbocharger turbine and compressor are connected to one shaft. This saves a great deal on the time spent for developing the experiment.

The turbocharger has 12 blades compared with 80-100 for a typical gas turbine. However, The turbocharger turbine runs to 110,000 rpm compared with 9,000-13,000 rpm for a typical gas turbine. Thus the blade passing frequency of the turbocharger is of the same order as that of a typical gas turbine.

Radial inflow turbines have one important, and in this context a useful, difference from axial turbines. The gas temperature reduces progressively from the tip as the gases are expanded within the radial inflow turbine, the lowest temperatures resulting at the outlet of the radial inflow turbine that is near the root section. The consequence of this is that the tip of the turbine is operating in a region of high gas temperatures and therefore high metal temperatures whilst the root is at much lower temperatures, that is those that result from the lower gas temperatures of the expanded gases.

Additionally it needs to be recognized that the stresses at the tip are very low because of the small mass that has been rotated at the tip radius. The stresses at the root are much larger now but then these are combined with lower gas temperatures.

It is therefore possible to operate radial inflow machines at much higher tip temperatures than axial machines where the temperature at the tip and the root is approximately the same and it is the combination of temperature and stress in the root that limits the maximum operating gas temperature for an axial turbine.

This meant that it was possible to design an experiment with a relatively cheap rotor, without advanced cooling techniques, where the resulting metal temperatures would be in the same region as that for modern axial gas turbines whilst using a cheap simple rotor.

The life of the turbine blade is a combination of stress metal temperature and material properties. For an experiment, the total life required from the blade was modest to be measured in tens of hours rather than tens of thousands of hours. It was therefore possible to run the radial inflow turbine at even hotter temperatures than would normally be acceptable given the fact that the tip stresses were low.

These unique features of radial inflow turbine allow the possibility of an elegant solution to be adopted by a design which trades stress for temperature. Figure no. (4.1) shows the stress distribution for a typical radial turbine as function of the radius ratio for various expansion ratios (solid line).

Using the material properties of a typical high temperature material , e.g., IN-100 identified in Figure no.(4.2) by a plot of allowable stresses against temperature for 1000-hr stress rupture life and converting these data to allowable stress factor for an assumed turbine entry temperature of 1473 K, the dashed lines in Figure no. (4.1) results.

Figure no.(4.3) shows the maximum temperature potential for a radial turbine as a function of the expansion ratio for different blade designs assuming IN-100 material, operation

at the optimum turbine velocity ratio, and stress rupture life of 1000 hr. Comparing Figures 4.3 with 4.4 for the axial type turbine, it can be seen that the maximum allowable gas inlet temperature for a 50% reaction axial turbine is significantly lower than those for radial turbines (100 K or more at expansion ratio of 1.5).

Another advantage, in this context, for the radial inflow machine is its transient response to sudden changes in gas temperature. When the gas temperature is suddenly increased, the tips of the radial inflow machine are rapidly heated and quickly follow the sudden temperature increase. Axial turbines, unlike radial inflow turbines, are unable to grow rapidly following a step change in gas temperature because they are physically attached to the turbine disk which is not in the hot gas stream and does not heat up at the same rate. This causes additional stress in axial rotors. Thus a certain derating factor depending on the nature of the transient operation will have to be applied to all rotor types. This factor, however, is expected to be more significant for axial turbine designs than for radial turbines [30].

Another important constraint for this programme was the ability to apply plasma sprayed ceramic coatings to the blade surface. Whilst plasma sprayed ceramic coatings can be readily applied to axial turbines, this is an expensive process, because the coatings have to be applied with some considerable precision. The coating is applied to the blading by a robot that has to be programmed to carefully follow the shape of the blade as the coating is applied. For a limited experiment with a tight budget constraint, it was not practical to get such coatings applied with sufficient accuracy on axial turbines. Radial inflow turbines had the advantage that as the coatings were to be applied essentially to the flat part of the blade surface the programming of the robot was relatively straight forward and it was therefore possible to persuade the supplier of the current aerogas turbine coatings to use the expensive production machinery which involve the robot for this exercise. An important aspect of being able to persuade the vender to do this was the fact that the programming of the robot and the time of application was short.

Because of the number of coatings were investigated a number of turbine wheels were required. The use of turbocharger turbine wheels in this context is a major advantage because the cost of purchasing several sets of axial blades would be prohibitive.

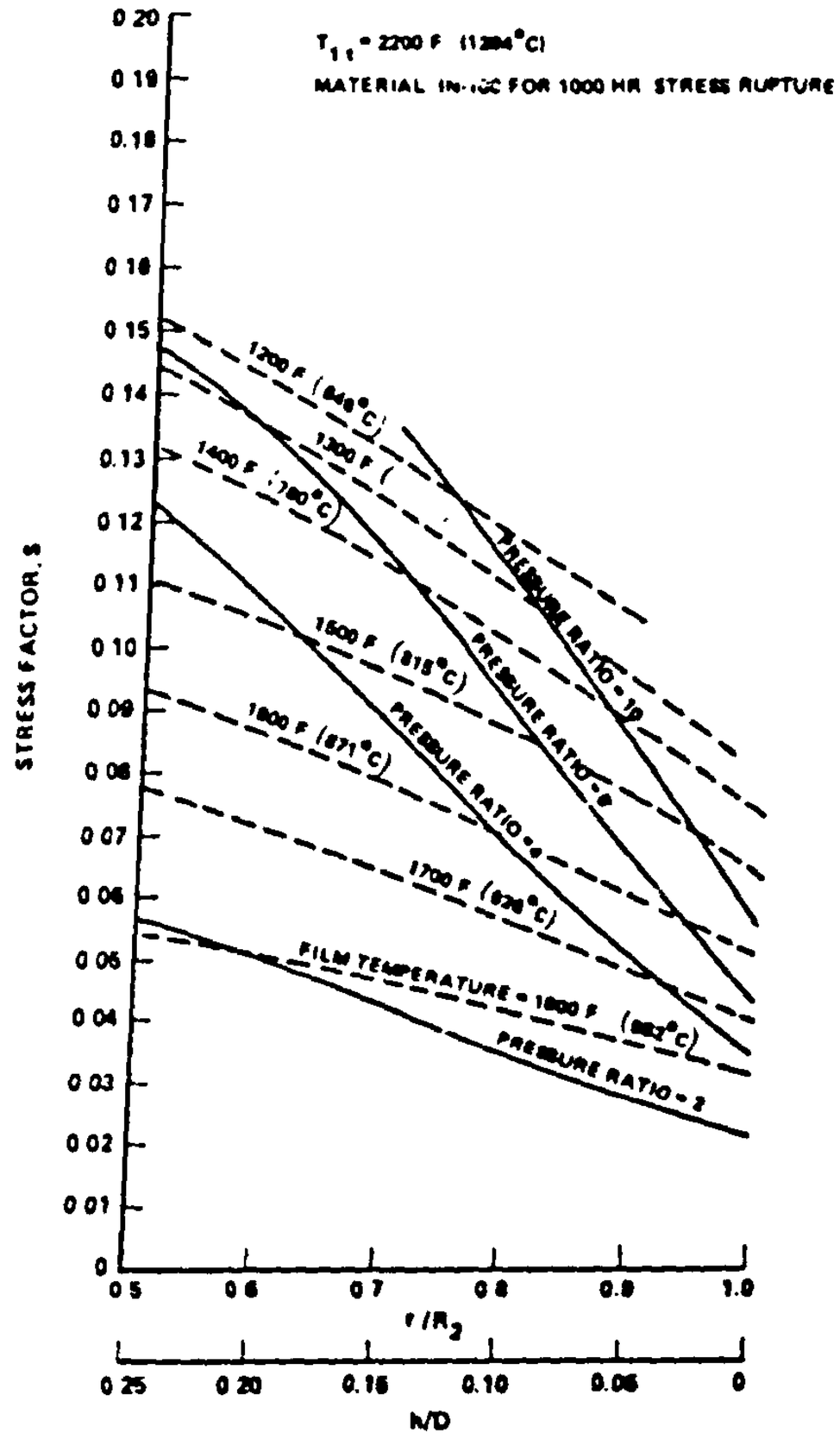

FIG no.(4.1) Effect of Pressure Ratio on The Gas Film Temperature and Strength Available for Radial Turbines [from Ref.30]

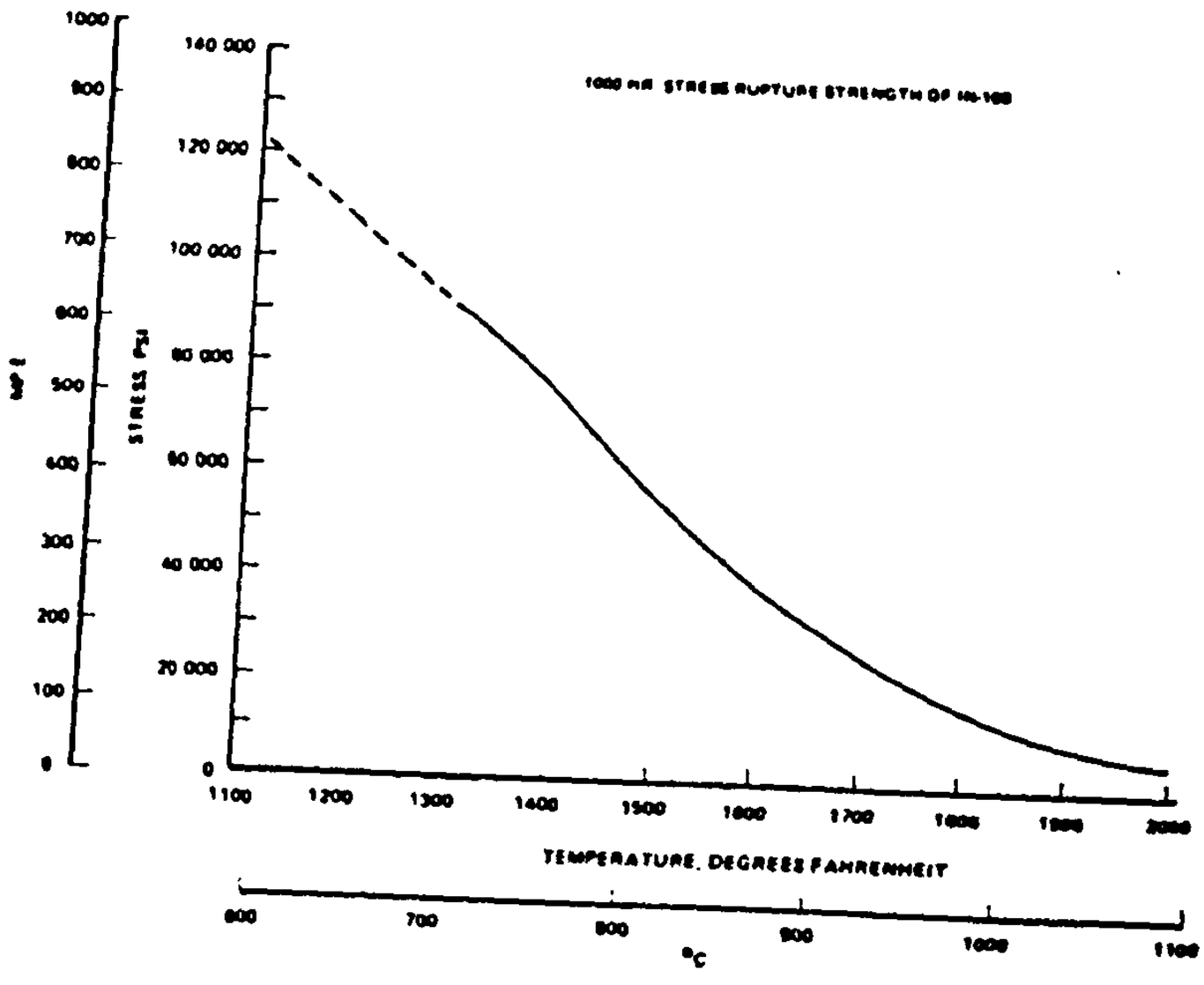

FIG no.(4.2) 1000-hr Stress Rupture Strength of IN-100 [from Ref.30]

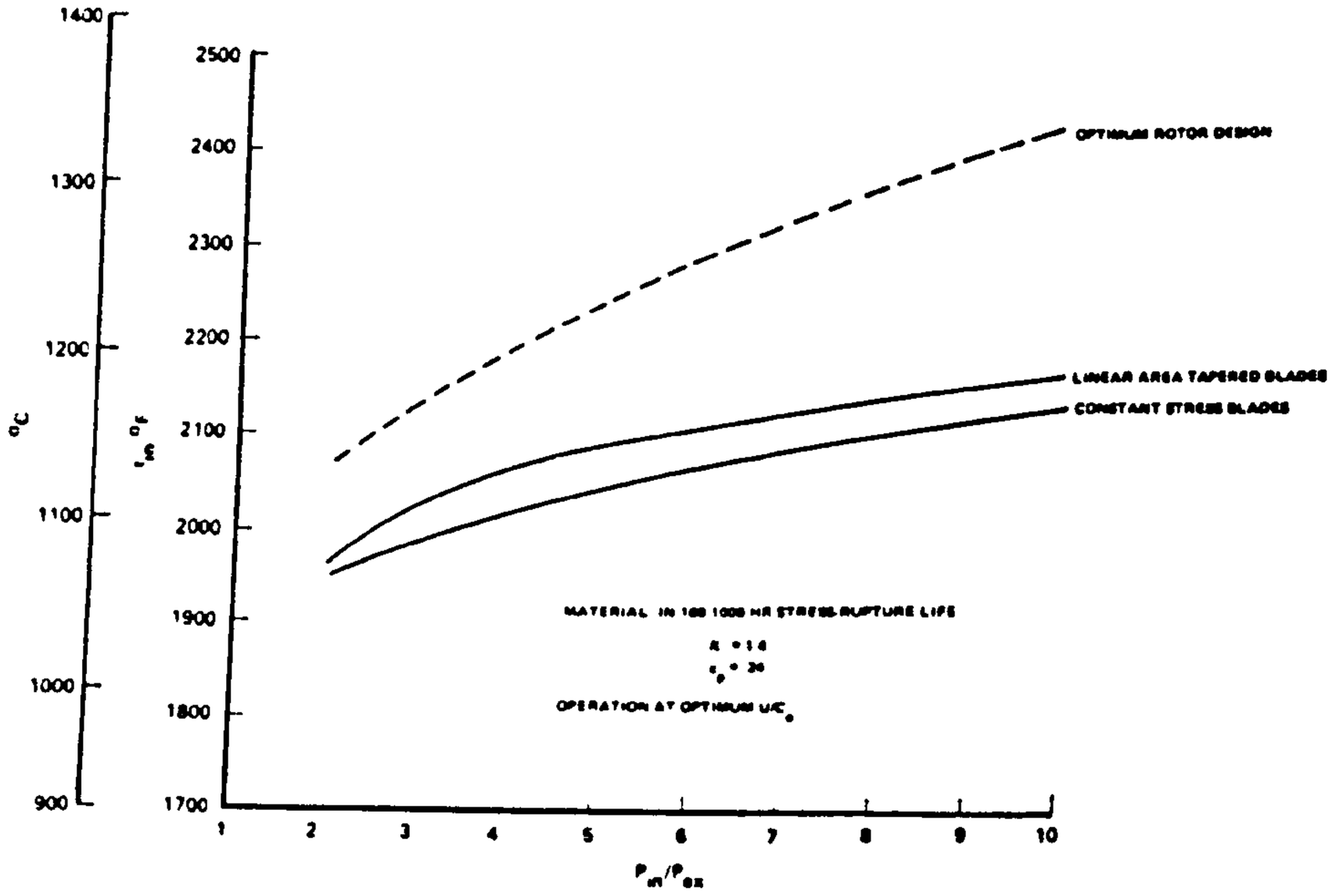

FIG no.(4.3) Temperature Potential of Radial Rotor as Function of Expansion Ratio [from Ref.30]

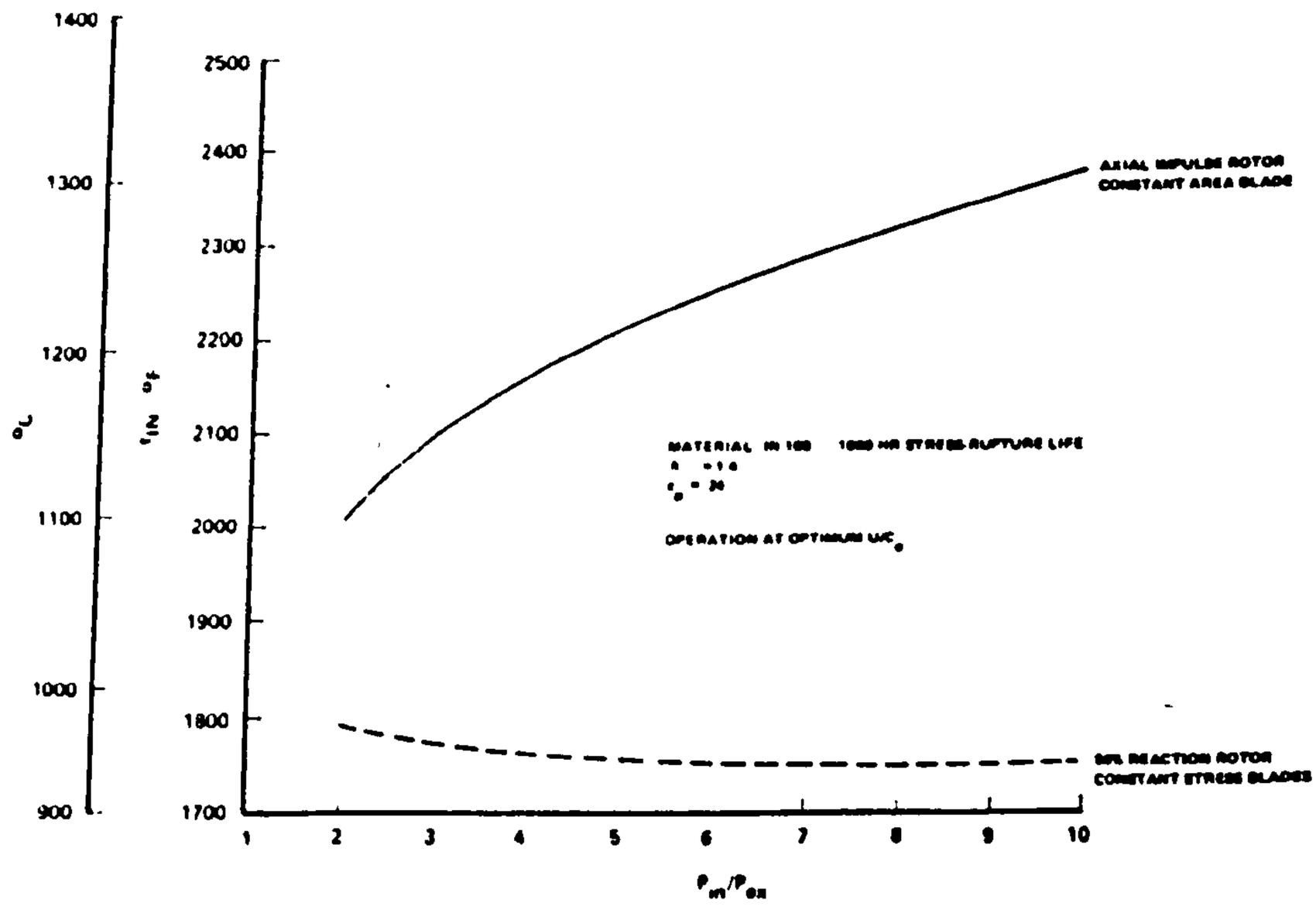

FIG no.(4.4) Temperature Potential of Axial Rotor as Function of Expansion Ratio [from Ref.30]

CHAPTER FIVE

5 THE EXPERIMENTAL RIG DESIGN

5.1 Introduction

The reasons for using a turbocharger rig have already been identified in chapter four. The turbocharger rig chosen allows experiments to be conducted at the same metal temperatures and the same blade passing frequency as is typical in a modern aero gas turbine engine. The flat sided blades of the radial inflow turbine makes it easier to apply high temperature coatings than would be the case for an axial turbine.

The main elements of the rig are the compressor , the combustion system and the turbine. Each of these elements are discussed below. The instrumentation, development and commissioning of the experimental rig are discussed in the following chapters, (chapter 6 and chapter 7 respectively).

5.2 Compressor

The compressed air was delivered from an existing School of Mechanical Engineering compressed air facility. This facility consists mainly of five "Howden" multi-stage compressors . Each of these compressors is capable of compressing 1.6 Kg/sec to 345 KN/m2 gauge pressure. These compressors are interconnected by a network of ducts , in such a way as to allow the operation of one or more combination of the compressors . Spill valves are used to control the output of each of the compressors .

One of the above compressors was used to supply compressed air for this rig. The spill valve of this compressor is controlled by an electrical switch positioned in the control panel of the rig. This switch activates a hydraulic system which controls the opening of the spill valve .

Between the compressor and the rig there is a shut-off valve which ensures that the rig is isolated from the compressed air system to protect the rig when it is not in operation but where the compressor plant is being used for other rigs. This valve is manually operated, and it was a normal practice to ensure that this valve was fully closed before and after each test.

5.3 Air Flow Meter Design

The air mass-flow rate to the compressor needs to be measured. The air flow meter was designed and manufactured in accordance with the British Standard "BS1042" [35].

The air flow meter is a standard pressure difference type and consists of an orifice plate with pressure tappings on either side.

5.3.1 Orifice Plate

The orifice plate chosen has an accuracy of 1.1% [BS1042 Ref.35]. It consists of a circular plate mounted between flanges in the centre of which a circular aperture was machined.

Figure no. (5.1) shows a cross section of the orifice plate. The part of the plate inside the pipe was circular and concentric with the pipe centre line. Both faces of the plate were flat and parallel [Ref.37,38]. The plate was machined from stainless steel (321). This was to give it the required oxidation resistance .

5.3.2 Pressure Measurement

In order to measure the air-mass flow rate into the combustion chamber it was required that at least one upstream pressure tapping and one downstream pressure tapping were provided for the orifice plate. The distance to the upstream pressure tapping from the orifice equals 154 mm, which was the diameter of the pipe through which the compressed air was flowing. The distance to the downstream pressure tapping 77 mm, which was one half the pipe diameter. Both the upstream and the downstream pressure tappings were measured from the plate up stream face. The size of these tappings equals 5 mm or (t/2.5), where t is the pipe wall thickness.

5.3.3 Temperature Measurement

It was required to measure the air temperature in order to compute the air mass-flow rate. A chromel_alumel thermocouple was fitted in a 6 mm diameter boss to measure the air temperature. This thermocouple was fitted at a distance of 800 mm or 5 pipe diameters downstream of the orifice plate upstream face.

DRAWING No PD 20401

ISSUE	MODIFICATION
A	—

ALL DIMENSIONS IN MILLIMETRES UNLESS OTHERWISE STATED.

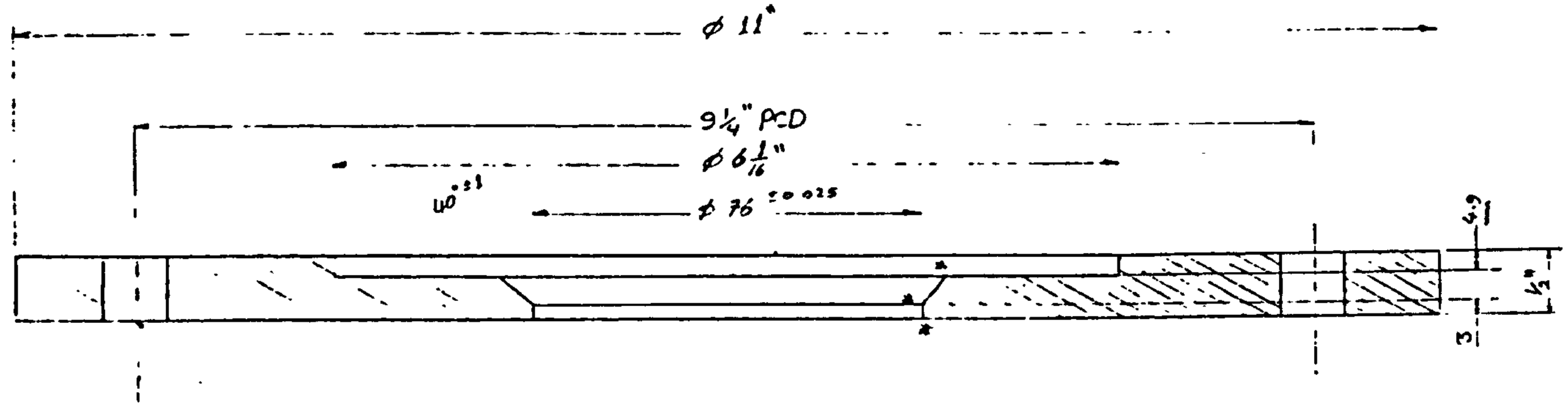

— 2 CLEARANCE HOLES FOR ø ½" BOLTS

NOTES

1. AT POSITIONS * SHARP EDGES NO BURRS
2. MACHINE ALL OVER
3. REMOVE SHARP EDGES (UOS)
4. ALL DIAS TO BE CONCENTRIC AND SQUARE TO ALL FACES.

FIG no.(5.1) Cross-Sectional View of The Orifice Plate

THIRD ANGLE PROJECTION			SHEET SIZE A3	1	PD20401	ORIFICE PLATE	1	S.S	321	
				ITEM	PART No.	DESCRIPTION	No. OFF	MAT!	SPEC.	REMARKS
GENERAL TOLERANCE ON DIMENSIONS MACHINED ±0.25 (±0.010") UNMACHINED OTHER DIMENSIONS AS STATED	JOB No	No OF SETS REQ'D	SCALE 1:1	DRAWN	CHK'D	APPV'D	STRESS APPVD	TITLE:- Orifice Plate		
	PPAE	—		A.K.H 15-1-1989	RHD 18/1/89					
WELD WHERE SHOWN THUS			FINISH SELF	ISSUED BY SME				DRAWING No PD20401		
MACHINE WHERE SHOWN THUS ✓	USED ON DRG.	—		CRANFIELD INSTITUTE OF TECHNOLOGY CRANFIELD.				SHT 1 OF 1 SHEETS		

5.4 Combustion System

A Spey combustion system was used to supply combustion gases at the required temperature to the turbine inlet. The combustion system consists of the following :

5.4.1 The Combustion Chamber

The "Spey" combustion system was chosen because, the components were readily available and the combustor would meet the requirements in terms of coping with the mass flow to be put through the radial inflow turbine and the inlet temperature required. The "Spey" combustor is a tubo-annular combustion chamber but in this application only one combustor, in a cylindrical pressure casing, was used. The end part of the Spey combustion chamber was removed. A convergent nozzle was designed and fitted at the rear end of the combustor. The sizes and positions of the secondary air flow passages were developed in separate experiments aimed at providing a clean and stable combustor outlet.

Figure no. (5.2) shows the combustion system used . The Combustor includes an igniter and a fuel injector. Exhaust gases from the combustor outlet feed into the turbine casing leading to the volute from which the gases are then fed into the radial inflow turbine.

The Spey gas turbine combustion system consists of 10 combustors. It has a pressure ratio of 19:1, and an air mass-flow rate of 57 Kg/sec. The air mass-flow rate through every combustor is 5.7 Kg/sec. In order to calculate the compressor delivery temperature the following procedure was followed:

From an isentropic compression process through the compressor, the compressor delivery temperature can be calculated as follows:

$$T_{is} / t = (\Delta P)^{\frac{\gamma-1}{\gamma}} \qquad \text{.....5.1}$$

where: T_{is} is the compressor outlet isentropic temperature [K],

t is the compressor inlet temperature [K],

ΔP is the compressor pressure ratio,

let t equal 288 K, then from equation 5.1, T_{is} equals 668 K. The isentropic temperature rise across the compressor is:

$$\Delta T_{is} = T_{is} - t = 668-288= 380 \text{ K} \quad \text{.....5.2}$$

Let the compressor isentropic efficiency equals 0.86, then the actual temperature rise across the compressor equals:

$$\Delta T_{ac} = \Delta T_{is} / \eta_{is} = 380/0.86 = 442 \text{ K} \quad \text{.....5.3}$$

The actual compressor delivery temperature equals:

$$T_{ac} = \Delta T_{ac} + t = 442 + 288 = 730 \text{ K} \quad \text{.....5.4}$$

The combustor cross sectional area was 7.8 E-3 m2 and the compressor delivery pressure was 1926 KN/m2

Table 5.1 shows a comparison between the characteristics of the experimental rig to that of the Spey gas turbine. These values suggest that this combustor was operating well within its capability.

Figure no. 5.2 shows the experimental rig layout. It also shows the combustor outlet pressure and temperature measurements. The combustor was housed in a steel pipe of 150 mm inner diameter.

5.4.2 The Fuel System

Figure no. (5.3) shows a layout of the fuel system. This system was used to supply and control the fuel to the rig. It consists of :

1- Fuel tank ,

2- Fuel filter ,

3- Fuel pump ,

4- Fuel injector ,

Table 5.1 : Comparison between typical Spey combustor parameters with the test parameters

Parameter	Typical Spey	Test	comments
M [Kg/sec]	5.7	0.2	Within the Spey capability
T [K]	730	299	Within the range
T [K]	1261	1173	Within the range
P [KN/m2]	1926.6	139.321	Within the range
A [m2] x10E-3	7.8539	7.8539	The same combustor
V [m/sec]	79	15	Within the Spey capability
$M x \sqrt{T} / A x P$	0.01	0.003	Within the range
$V/\sqrt{T}$	2.92	0.867	Within the range

5- Servo valve ,

6- Isolation valve ,

7- Control valve ,

8- Solenoid valve ,

9- Piping

The fuel pump was a multi piston type. The output stroke of each and every individual piston was controlled by a "swash" plate. This plate rests on a spring which is controlled by the servo valve.

An isolation valve and a solenoid valve were used to isolate the combustor from the fuel system. The fuel-flow rate was controlled via a "fine" control valve.

AVTUR (kerosene) was used as fuel. This is because it is a gas turbine fuel and relatively clean combustion products would result from it.

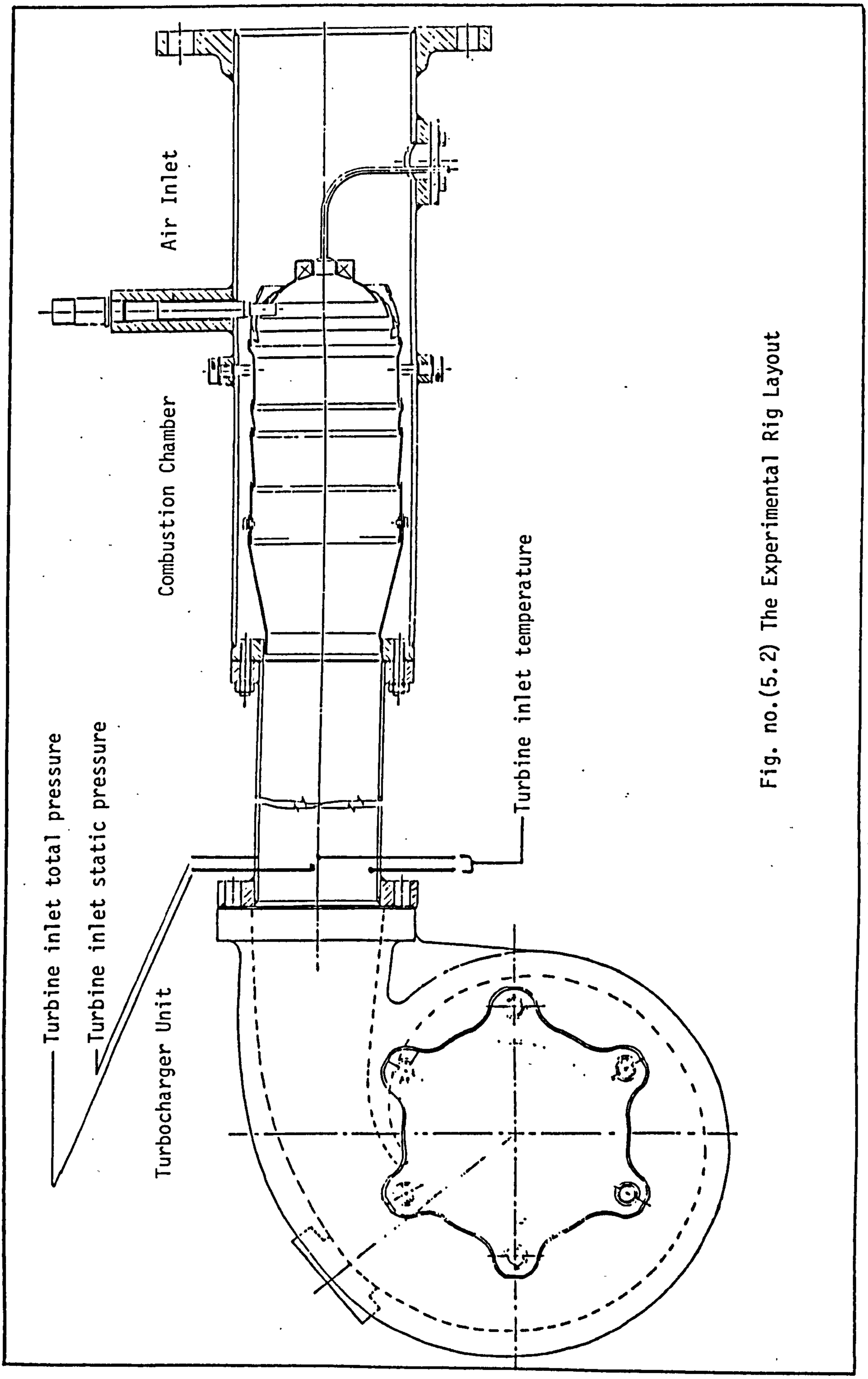

Fig. no.(5.2) The Experimental Rig Layout

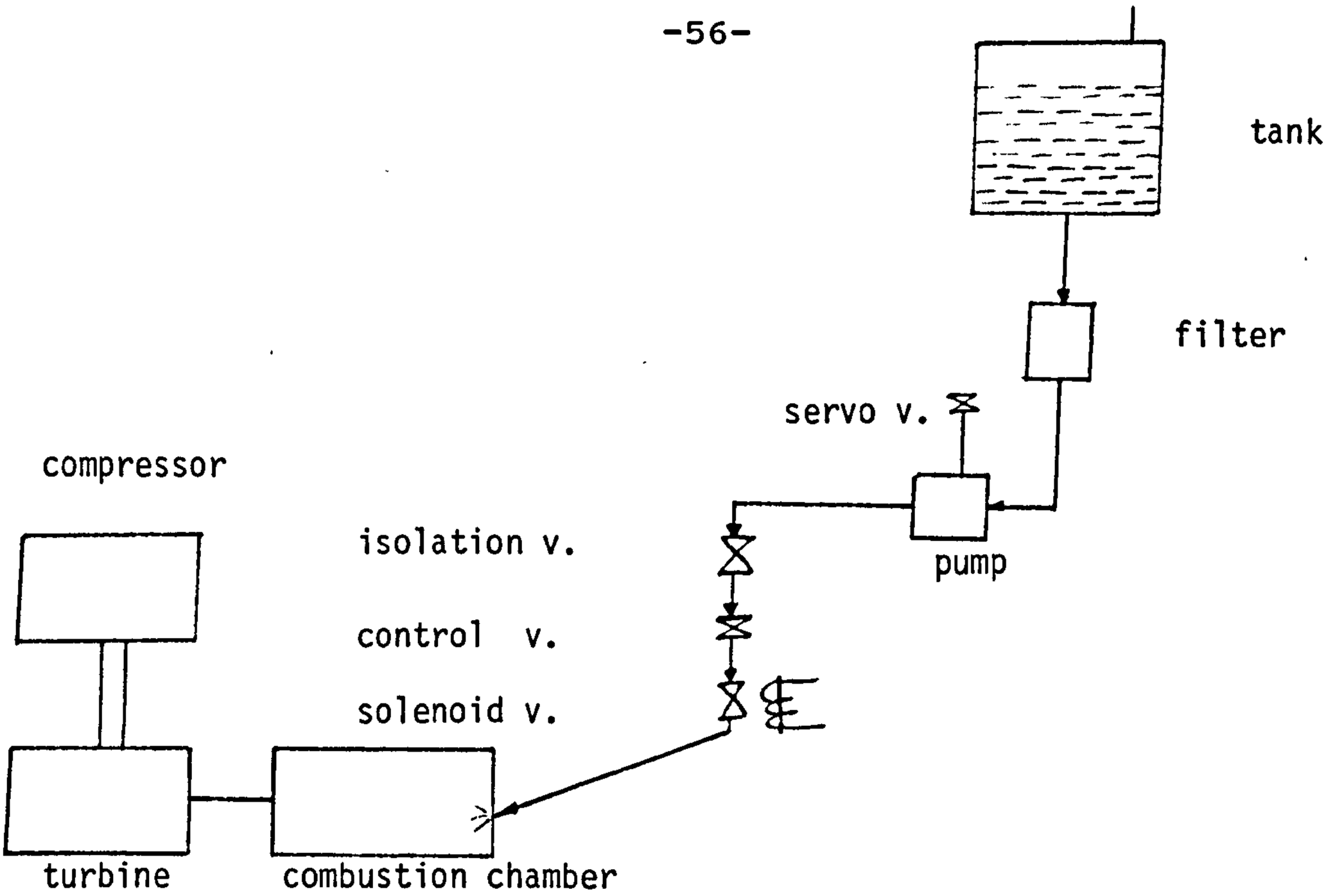

Figure no. (5.3) The Experimental Rig Fuel System

5.4.3 Ignition System

The ignition system used consists of a high-energy unit and surface discharge igniter plug. This high-energy ignition system employs a capacitative unit giving a lower voltage spark of much higher energy. The unit output energy was 12 Joules whilst the dissipated energy in the spark was 3 Joules. The repetition rate is about 2 sparks per second. The igniter was a standard high energy surface discharge semiconductor type igniter.

5.5 Turbocharger Unit

The combustor is followed by a straight pipe of 100 mm inner diameter and 220 mm length. Instrumentation to measure the gas static and total pressure and temperature were placed in this pipe, Figure no. (5.2).

The turbocharger unit is connected to the rear of this tube. The turbocharger consists mainly of a compressor and a turbine coupled on a common shaft. The gases from the combustor were directed by the turbine inlet casing on to the blades of the

turbine and subsequently discharged to atmosphere through the turbine outlet casing. The exhaust gases are utilized in the turbine to drive the compressor, which compresses the air and directs it through the compressor outlet. The combination of a single stage centrifugal compressor and a single stage radial turbine is almost universally used in turbochargers.

The complete compressor impeller, shaft and turbine rotor assembly must form a well balanced unit as the rotational speed can be very high and may reach 110,000 rpm. To achieve free interchangeability of parts, on assembly the compressor impeller and the turbine rotor were balanced separately. This was necessary as many turbine rotors needed to be in balance with one compressor. Metal was removed from the front of the hub and the back face of the impeller or from the periphery of the impeller between blades. By separate balancing, the impeller may be assembled on the shaft at any angular position relative to the turbine wheel. However, and for the coated rotors, it was necessary to fix that position as each blade of every rotor carried different extra weight.

The turbocharger unit was the main focus of this programme, as most of the research was done on the turbine blades. This unit, figure no. (5.4) , comprises the following :

5.5.1 The Turbine Casing

The gases enter the volute through a circular section then they are directed into the radial inflow turbine through a vaneless scroll. The volute is cast from mild steel. The turbine casing includes the exhaust outlet from the turbine. It also has the turbine bearing housing.

In order to obtain a uniform inlet flow, the cross-sectional area of the housing is reduced around the circumference of the turbine rotor. This geometrical layout of the housing is so arranged to feed the gas into the rotor as if there is a vortex with its centre at the rotor centre, the aim being to give the gas a constant inlet angle and velocity around the periphery of the turbine rotor.

5.5.2 Turbine Wheel

Figure no. (5.5) shows a photograph of the turbine wheel. It is of radial inflow type. The radial inflow turbine has 12 blades and is of one casting. The tip diameter of the wheel is 100 mm.

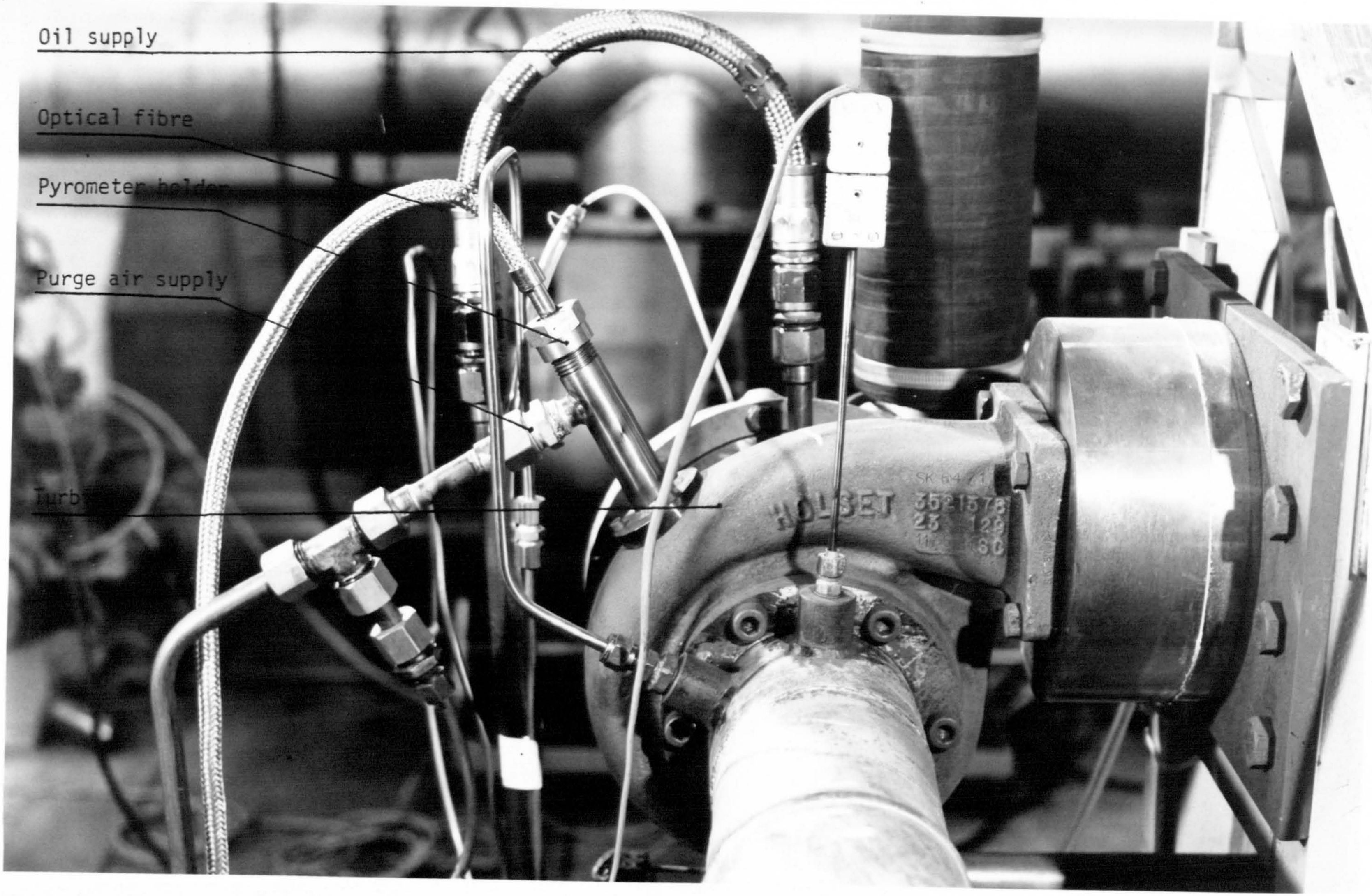

FIG no.(5.4) The Turbocharger Unit

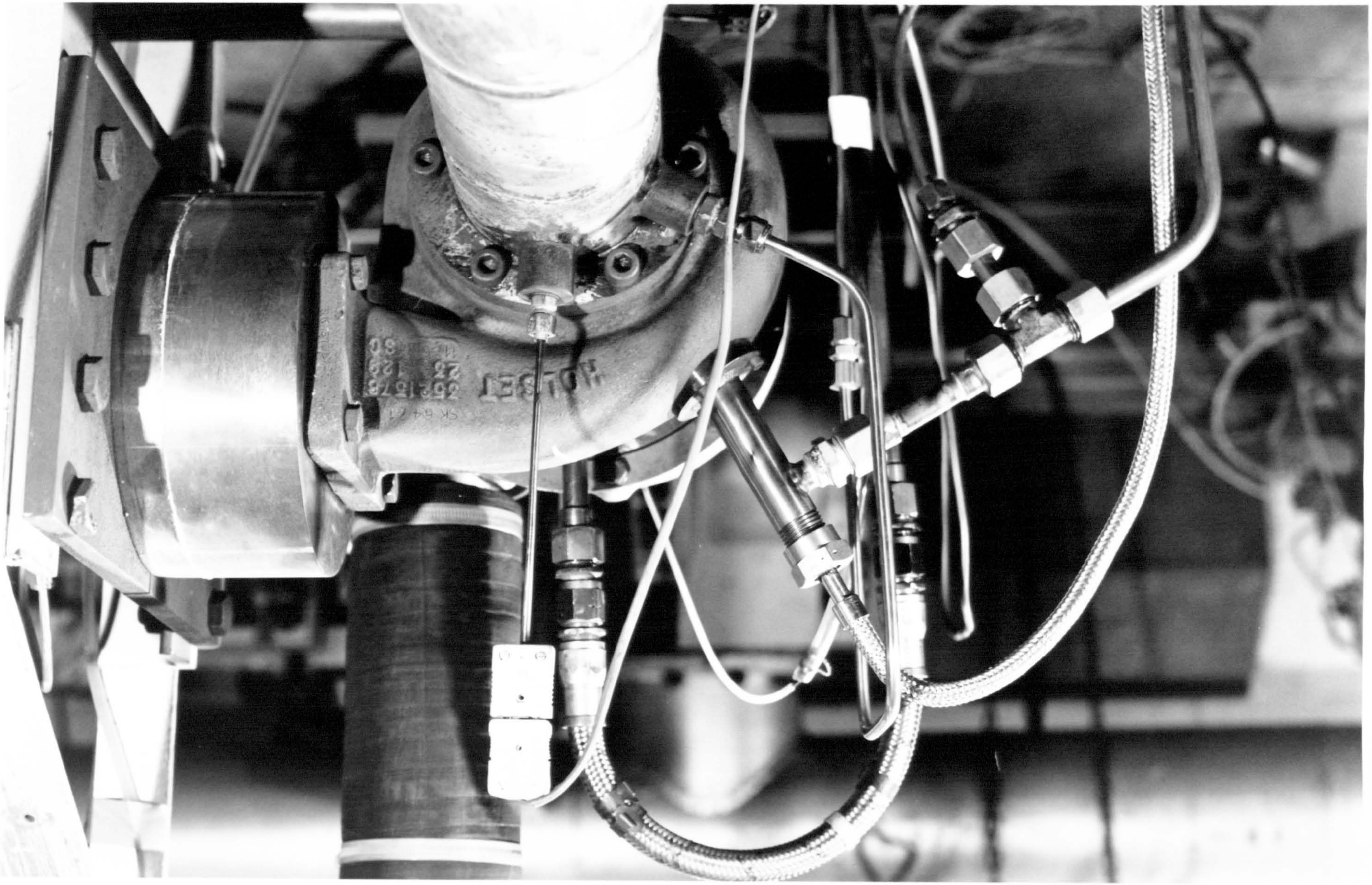

For continuous operation the maximum temperature is 873 K and the maximum rotational speed is 110,000 rpm (tip speed of 576 m/sec). The turbine wheel is cast in 713C Inconel (high nickel alloy). It was then electron beam welded to the shaft. Although it is possible to cast the turbine wheel and shaft in one, machining may then be awkward. The shaft was made of high carbon steel and was induction hardened. For limited tests the turbine wheel was run in an environmental temperatures of up to 1173 K at a reduced speed of 55,000 rpm (tip speed of 288 m/sec).

5.5.3 Radial Compressor

The compressor of the turbocharger, which is usually connected to the turbine shaft, was retained because, it acts as a load and makes control of the rig easier. Using the whole rotor removes the problems of balancing. The radial compressor has eight blades cast from aluminium alloy and then machined. This compressor was housed in a casing that has both inlet and outlet.

The compressor impeller was interface fitted on the other end of the shaft. A self-locking nut holds the impeller tight against an abutment on the shaft. No splines or keys were provided as the friction force created was adequate to transmit the torque.

5.5.4 Throttle Valve

The compressor outlet was connected to a pipe of 120 mm inner diameter. Mounted on this pipe was the throttle valve which was controlled electrically by a stepper motor. The stepper motor movement was controlled by a switch located on the control panel of the rig. For a given power output from the radial inflow turbine the operating speed can be adjusted by adjusting the blockage downstream of the compressor.

This valve was closed slowly until a near surge condition was established. The position of the stepper motor was then fixed at this condition. This was necessary so as to produce the highest compressor efficiency.

Fig. no.(5.5) Turbine Wheel

5.5.5 Bearing System

The shaft connecting the compressor and the turbine is supported on two sets of sleeve-bearings. These and the shaft are housed inside a casing. This casing has inlet and outlet passages for the oil feed. Figure no. (5.6) is an assembly drawing of the turbocharger unit.

The demand and search for a simple, light and cheap turbocharger led to the adoption of the inboard mounted bearing arrangement (bearings located towards the centre of the shaft with the compressor impeller and turbine wheel overhanging at each end of the shaft). This arrangement as shown in figure 5.6 permits the direct entry of gases to the turbine wheel and the air to the compressor impeller. It also provides a convenient turbine exhaust layout.

This bearing system is a fully floating sleeve bearing made of leaded bronze with an added tin flashing which is free to rotate at an intermediate speed. This speed is normally lower than that of the shaft and is dependent on the bearing clearances, sleeve lengths, diameters and oil viscosities. The bearing tolerance was 0.0075 mm on shaft and bearing sleeve bore, and 0.013 mm on inter diameter and housing bore.

The bearings run directly in the bore of the centre casing. This casing also contains the oil drain and holds the compressor and turbine casings. The compressor and turbine casings are designed so that they can be freely rotated into a convenient angular position relative to the centre casing on the assembly.

The oil is fed to the bearing system for lubrication and cooling of the rotating parts. Figure no. (5.7) shows the oil system which consists of the following :

1- Oil tank ,

2- Oil pump ,

3- Filter ,

4- Pressure relief valve ,

5- Drainage and pipping .

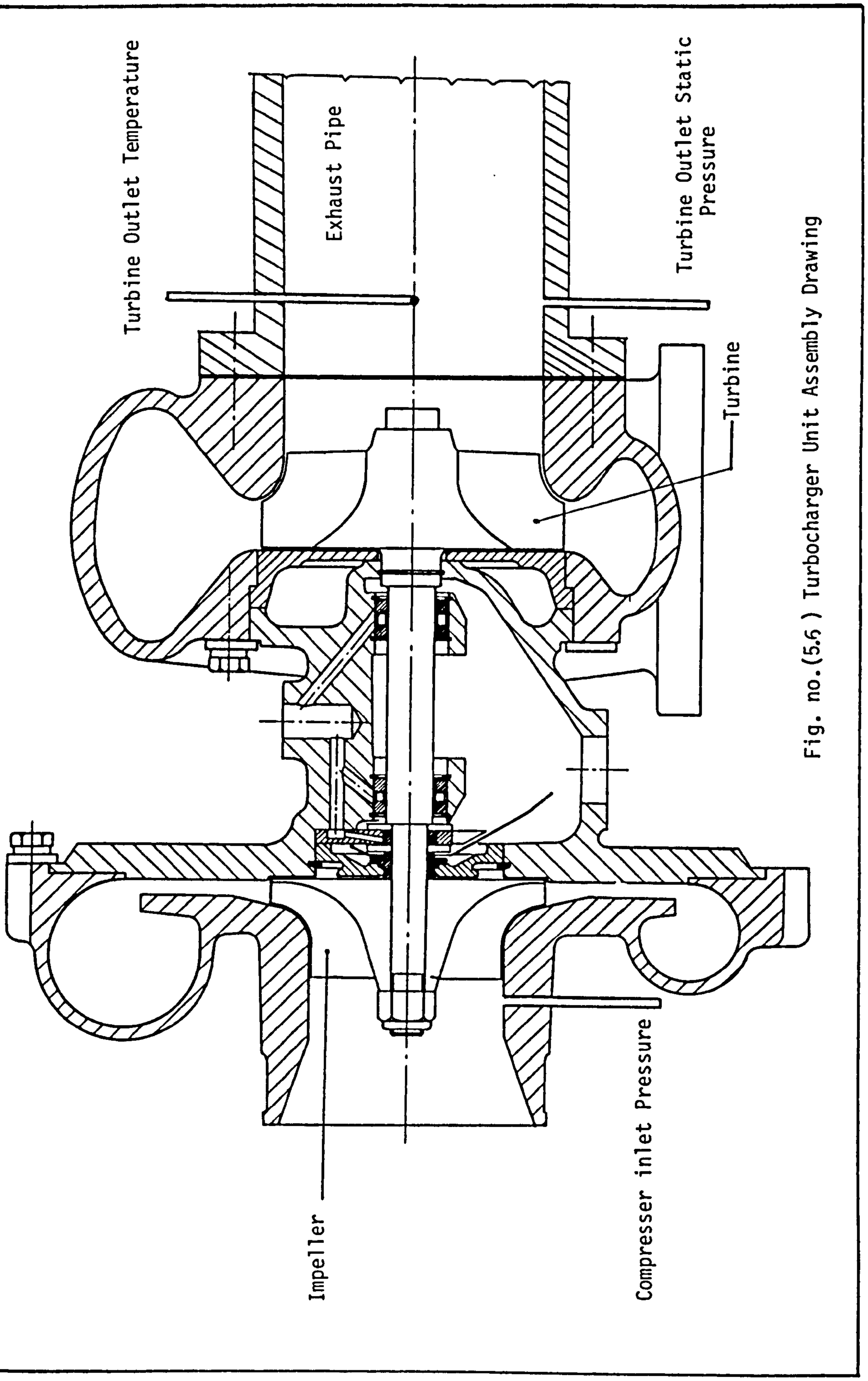

Fig. no.(5.6) Turbocharger Unit Assembly Drawing

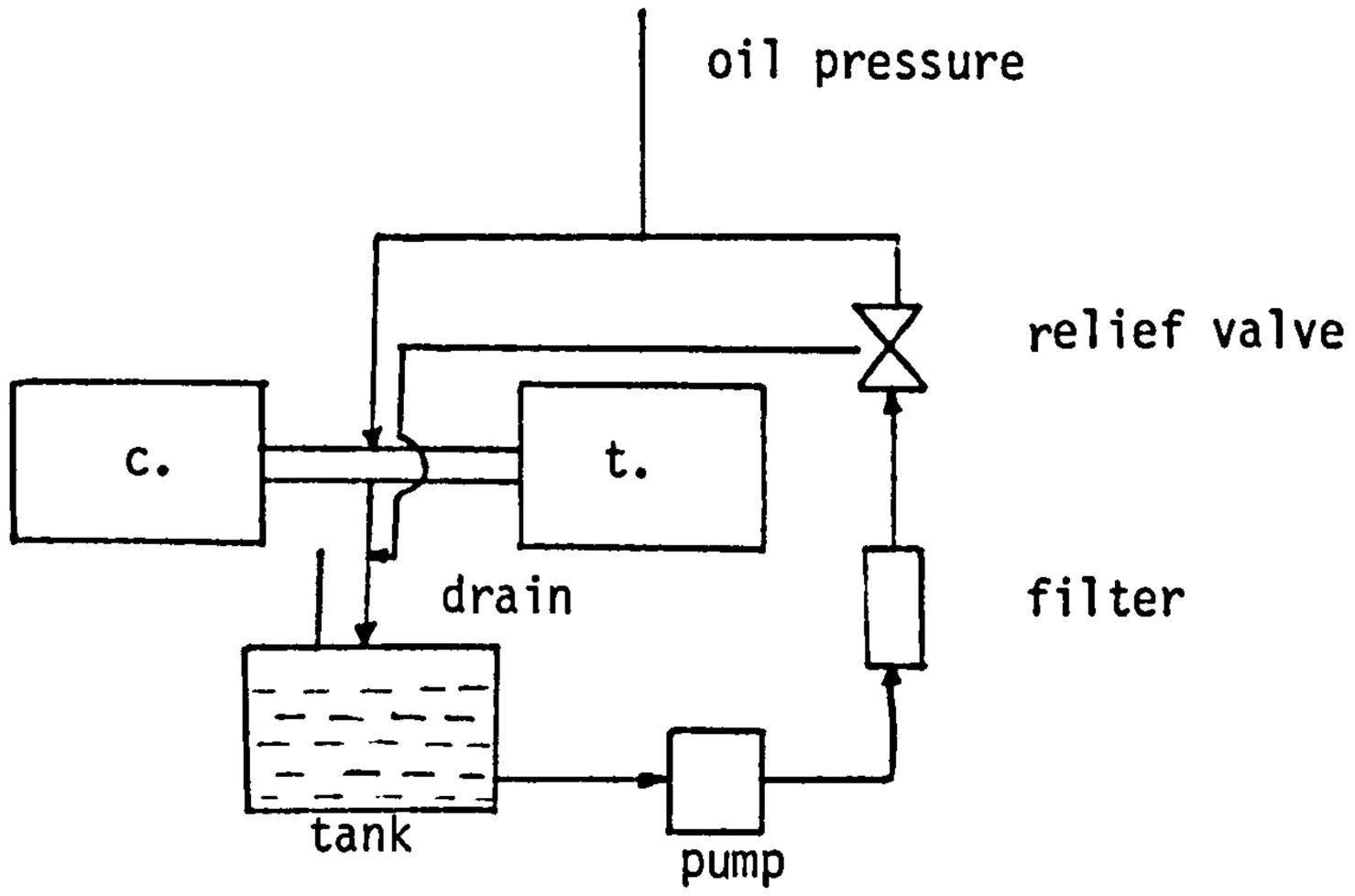

Figure no. (5.7) The oil system

5.6 Exhaust System

The exhaust from the turbine is ducted away by an exhaust pipe which turns the direction of the exhaust by 90 degrees for safety reasons and to allow easy access to the rig. The exhaust pipe is fitted to the turbine casing via bolted flange. Turbine outlet pressure and temperature were monitored at the entry of the exhaust pipe as shown in figure 5.6.

5.7 Preliminary Testing of The Experimental Rig

5.7.1 Cold Run

After the experimental rig was built and assembled and before the modification of the turbine casing the rig was run to check the normal functioning of its individual components. This

run was also to check rig safety. Functioning of the flow meter and the throttle valve were also to be checked. The following is the procedure adopted:

The rig and all systems were checked visually;

The oil pump was started, the oil system was checked for any leaks or unexpected noises;

The main compressor was started; the spill-valve was fully opened to atmosphere;

The shut-off valve was opened, and the rotor was rotating;

Functioning of the air-flow meter was checked;

The spinning speed was increased by partially closing the spill valve, the valve was functioning properly;

The throttle valve was closed slowly until a near surge condition was established;

The speed was then set to minimum by opening the spill valve completely;

The shut-off valve was closed;

The oil pump was switched off;

The main compressor was closed down;

The rig was then checked visually.

5.7.2 Hot Run

The aim of this run was to check rig safety at high speeds and high temperatures, the functioning of the fuel and ignition systems were also to be checked. The following is the procedure adopted:

The rig was inspected visually;

The oil pump was started;

The shut-off valve was opened;

The rig was rotated;

The ignition was switched on;

The fuel pump was started;

The fuel isolation and solenoid valves were opened, and the fuel control valve was opened slowly;

Ignition took place, the spinning speed was increased as the gas temperature was increased;

The spill-valve opening and the fuel control valves were varied to establish the required conditions;

Fuel flow and speed were then reduced to a minimum;

The solenoid valve was closed;

The shut-off valve was closed;

The main compressor was stopped;

The oil pump was switched off, and the rig was checked visually and left to cool.

CHAPTER SIX

6 INSTRUMENTATION AND CONTROL

6.1 Instrumentation

After the rig was manufactured and assembled as in Figure no.(6.1) a number of instrumentations were required for operating and monitoring the rig. Most of these instruments are for pressure and temperature measurement of the air , gas , fuel and oil. These instrumentations are shown in Figure 5.1 and 5.5, they include :

1- Air pressure upstream and down stream of the orifice plate ,

2- Air temperature downstream of the orifice plate ,

3- Gas total and static pressures downstream of the combustion chamber ,

4- Gas temperature measurement downstream of the combustion chamber

5- Exhaust gas temperature ,

6- Fuel pressure ,

7- Fuel flow rate,

8- Oil pressure ,

9- Oil inlet and outlet temperatures and,

10- Turbine casing metal temperature .

6.2 Pyrometer Sighting Tube

The sighting tube was designed for housing the pyrometer probe and mounting it on the turbine casing. In order to get the required lens to target distance (75 mm), the pyrometer had to be positioned outside the turbine casing [Ref.7,39] .

In so doing, the turbine casing had to be modified to accept the sighting window. This window is to allow the radiation beam to travel from the blade surface to the collecting optics. It was made from quartz and mounted in a stainless steel frame. Quartz was chosen for its high

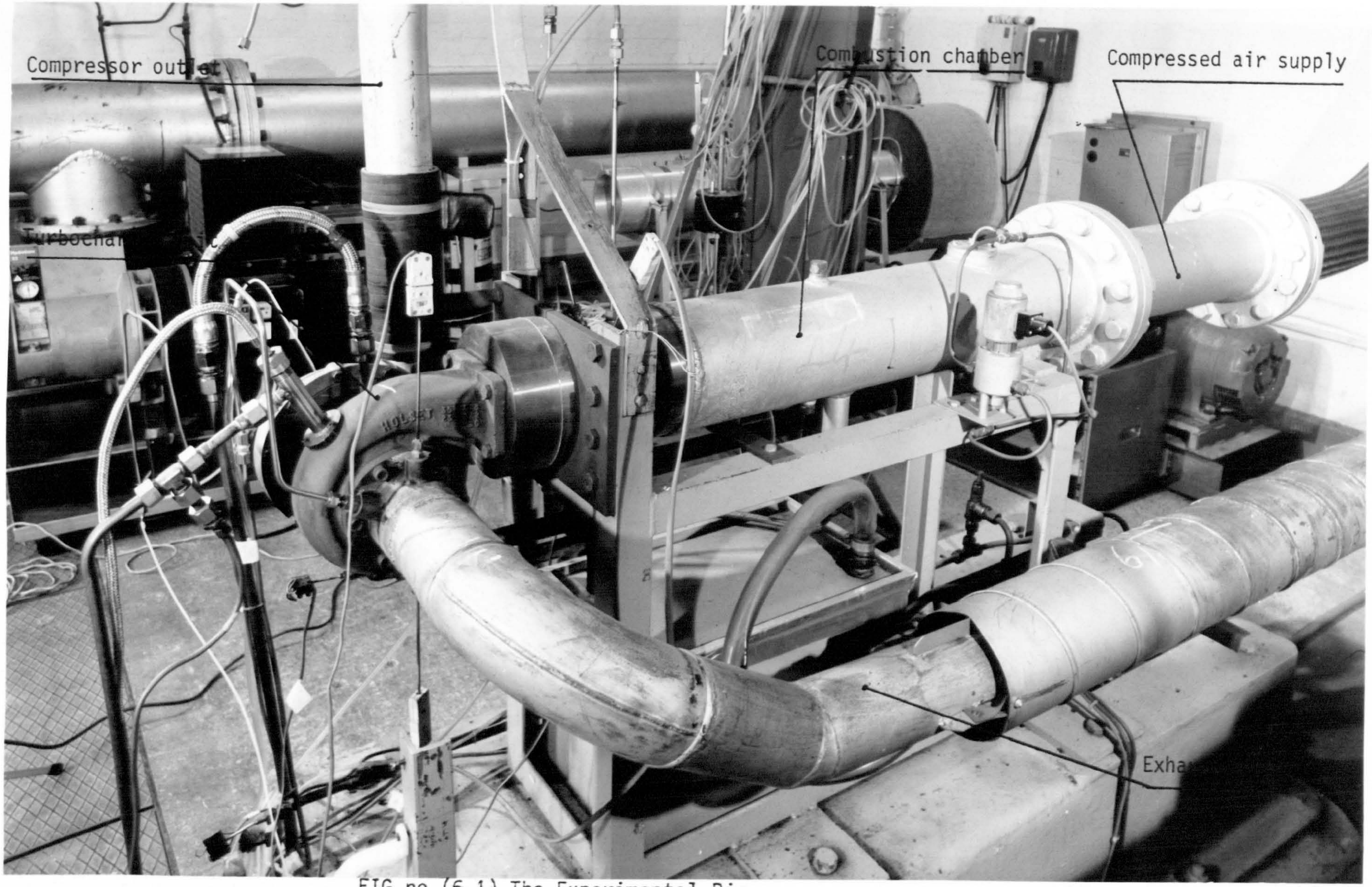

FIG no.(6.1) The Experimental Rig

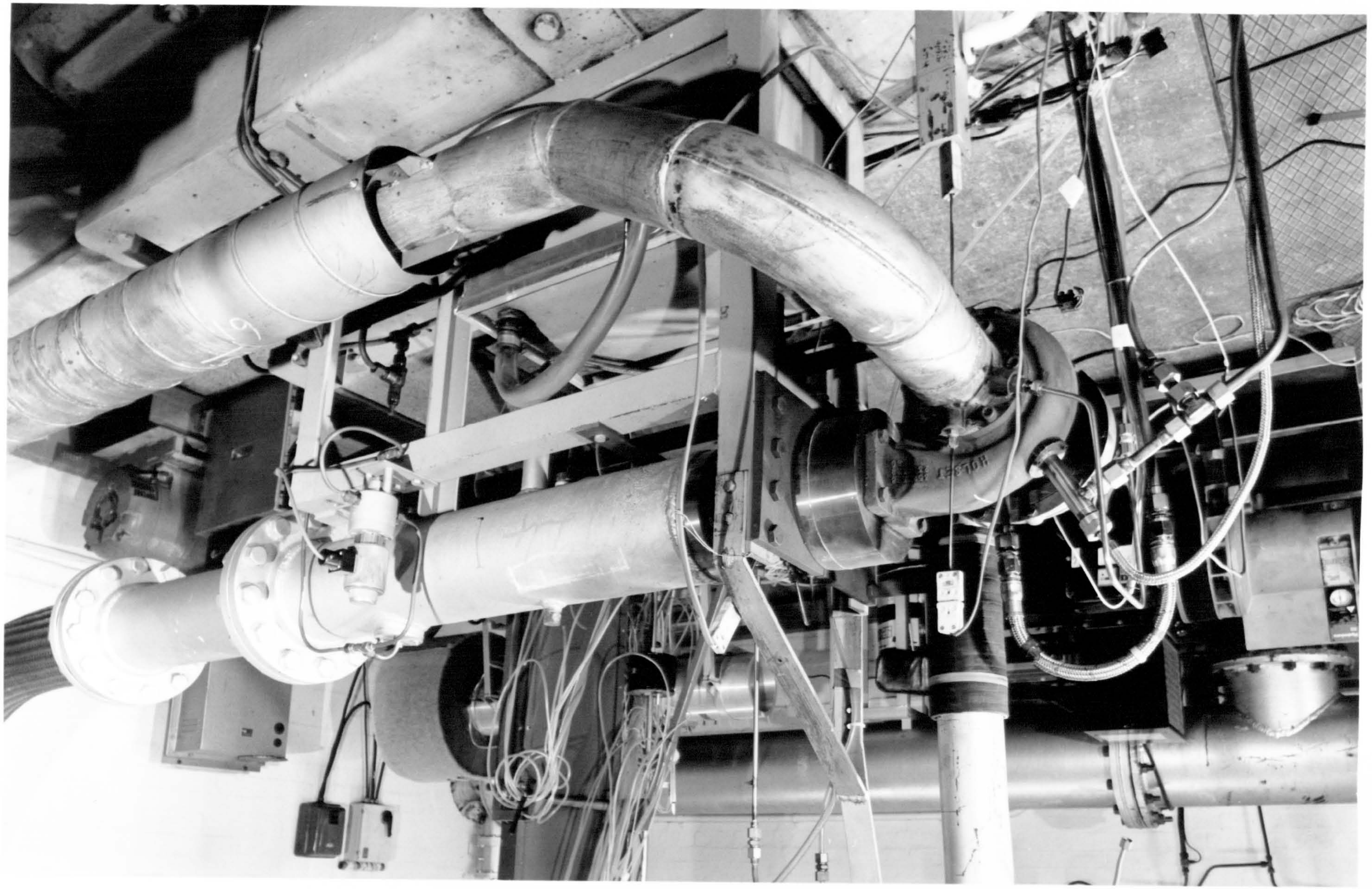

temperature capability and good transmittance in the range of interest. It has a melting point of 1300 K, thermal expansion coefficient of 0.5 x 10E-6/C, and good transmittance within the range 0.13 to 10 microns [Ref.23]. Stainless steel (316) was used for making the window frame for its high thermal shock resistance, high temperature capabilities. Figure no. (6.2) shows the position of the window on the turbine casing .

A viewing angle of 39 Degs. from the vertical was decided upon to give no direct radiation from the flame. By avoiding the top and the bottom of the casing the angle chosen also minimizes the number of particles gravitating towards the quartz window and reduces the risk of hot gases condensing on it. This position also enables the monitoring of the blades close to the nozzle exit .

The arrangement enables scanning of the entire blade height. It also makes an angle of 59 Degs. with the normal to the blade surface under view as shown if Figure 6.3. This was to avoid sharp decrease or increase in surface emissivity when the surface is metal or ceramic, respectively (chapter nine) .

6.3 The Synchronizing System

6.3.1 Construction

This system was designed to produce a once per turbine revolution signal. This signal was used to measure the turbine rotational speed and for synchronizing the pyrometer signal .

Figure no. (6.4) is a block diagram of the system. It consists of a head amplifier, transmission and reception channels and a rectifying circuitry .

6.3.2 Principles of Operation

The tip of one of the compressor blades was polished, to increase its reflectivity relative to other blades. The end of the transmitting and receiving channels was fitted on top of the compressor inlet such that the top of the blades could be viewed directly through window in the compressor casing .

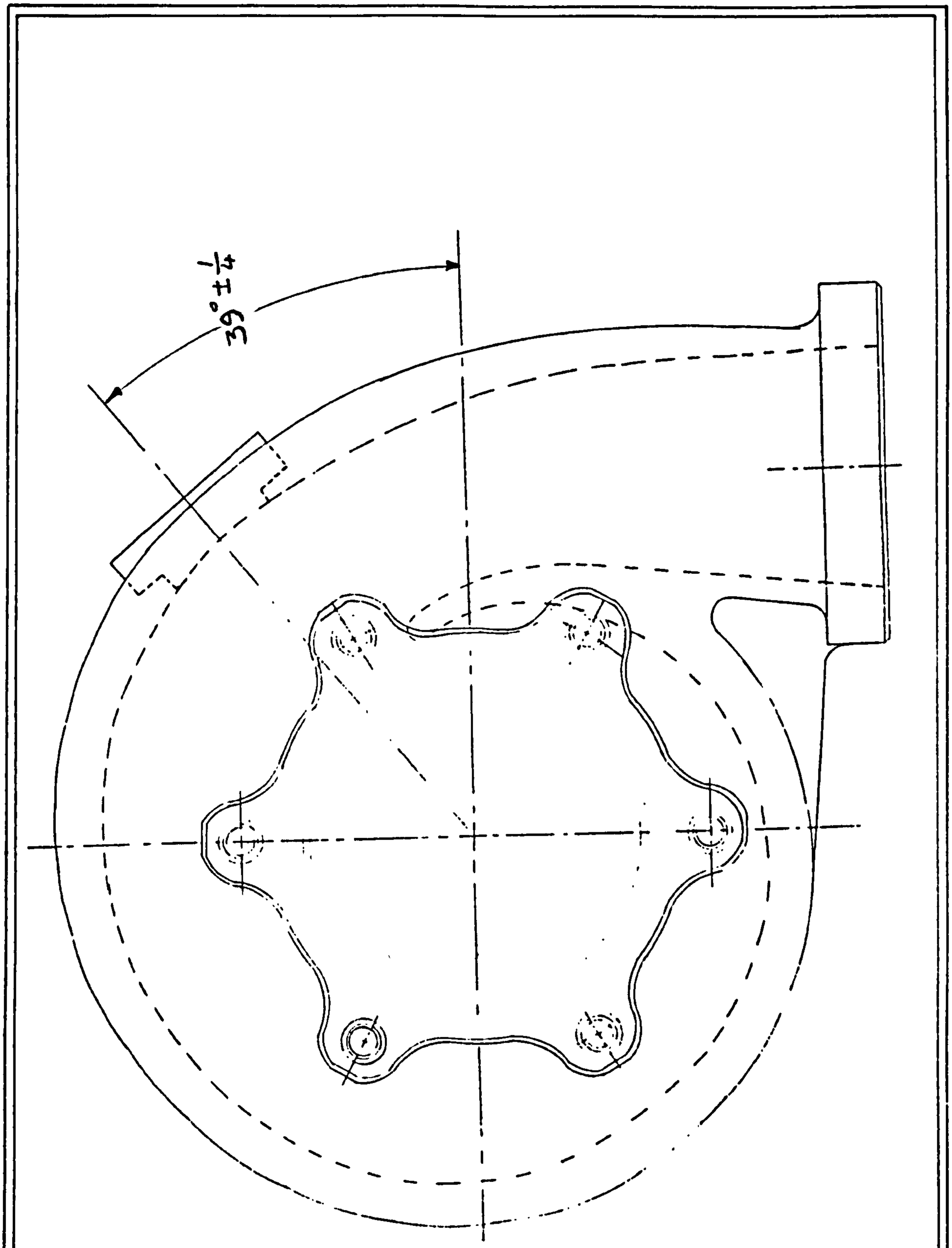

FIG no.(6.2) The Position of The Sighting Window
on The Turbine Casing

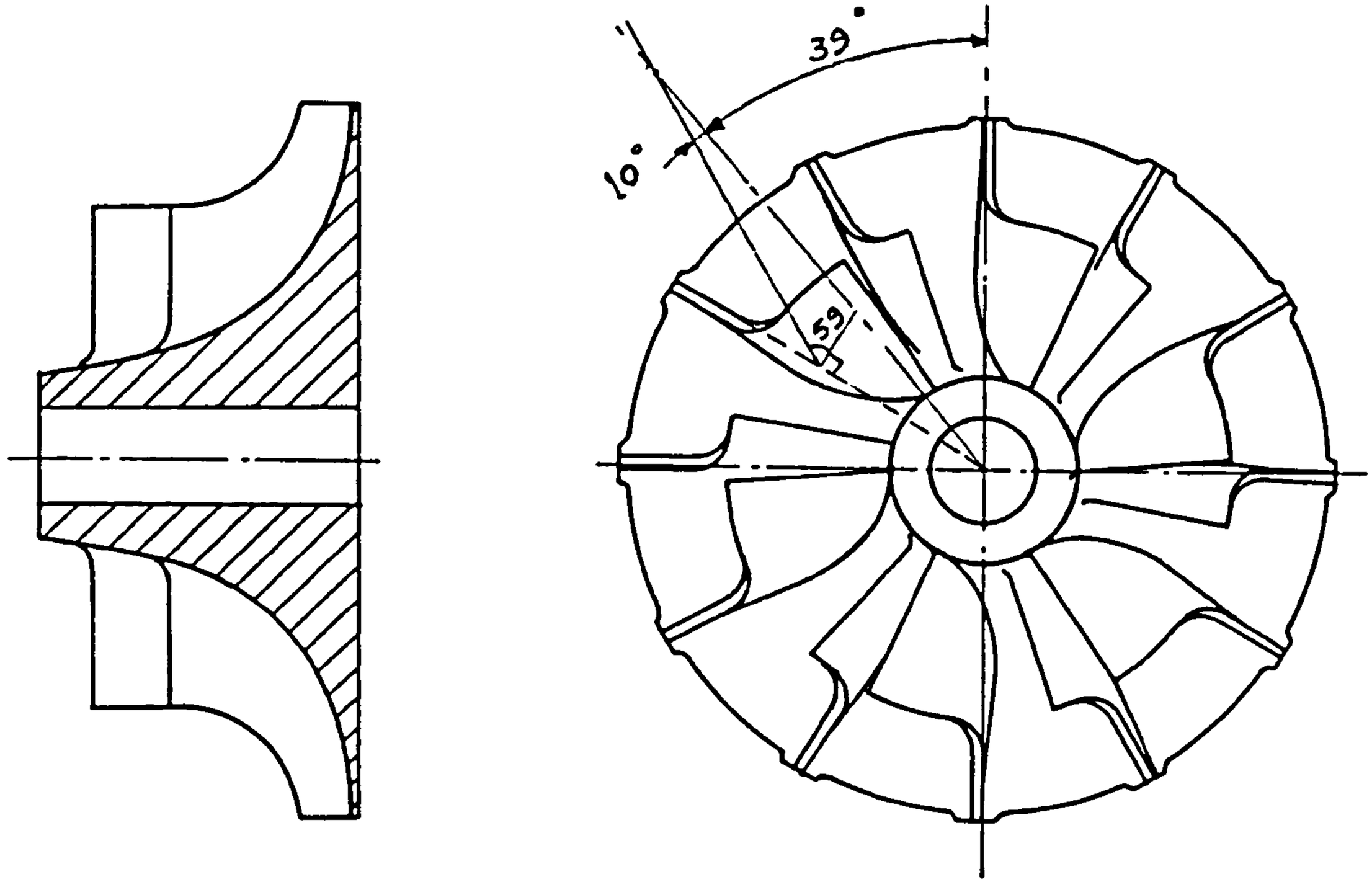

Fig. no.(6.3) Pyrometer Viewing Angle

The light emitting diode (LED) sends a beam of light through the transmitting channel. This beam is then reflected by the blades and picked up by the receiving channel. The received signal is function of the blade reflectance , so a complete trace of the eight compressor blades was picked up. The signal reflected by the polished blade is the maximum , as this is the blade with the highest reflectivity .

The signal was then amplified. The signals of all but the polished blade were eliminated in a threshold. The resulting signal was then rectified to the required shape by the monostable. This signal was then fed to the speed counter and to the storage oscilloscope .

The synchronization of the pyrometer signal allows the identification of individual turbine blade temperature profiles.

6.4 Rig Control

The turbine rig was run at high temperatures and high speeds. Safe operation of the rig required that instruments read out and control of the rig was undertaken remotely in the control room. The layout of the rig was chosen such as to minimize risk to personal in the event of danger.

Operation of the experimental rig was controlled by the following :

1- Main compressor spill valve opening ,

2- Fuel flow rate ,

3- Turbocharger compressor throttle valve .

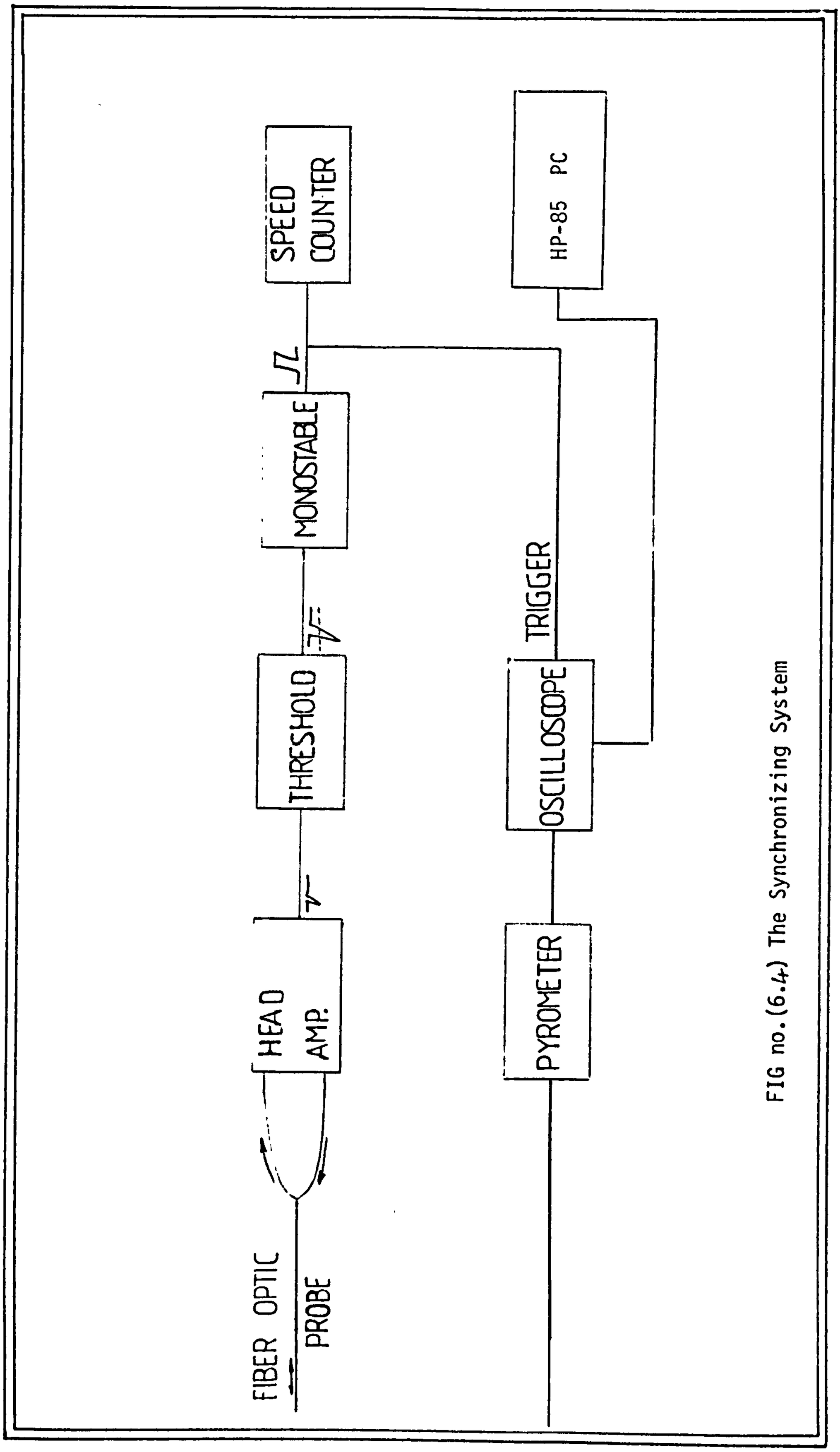

FIG no.(6.4) The Synchronizing System

CHAPTER SEVEN

7 EXPERIMENTAL RIG DEVELOPMENT AND COMMISSIONING

7.1 Introduction

After it was manufactured the rig was assembled and all instrumentations were connected. Fuel and oil systems were assembled and connected to the rig. Ignition and synchronizing systems were also connected. Figure no. (7.1) shows another view of the experimental rig.

7.2 Rig Testing

Prior to a hot run a cold run was undertaken. Before the cold run was undertaken the rig was checked to ensure that all the instrumentation was operational and the relevant valves closed, that the fuel and oil systems were in functioning order.

During the cold run, functioning of the spill valve, flow meter and throttle valve were checked. In this run the rotational speed was varied by varying the spill valve opening. Then a hot run was undertaken. In this run functioning of the fuel and ignition systems were checked. The rotational speed was raised by closing the spill valve and the gas temperature was increased by increasing the fuel flow. Both of these runs were undertaken with uncoated turbine wheel.

7.3 Pyrometer Purge System

The first hot run was performed employing the quartz window. This was employed to allow radiation to pass through it to the pyrometer and to prevent the gases from escaping .

At the end of that run there was no useful pyrometer signal. When the rig was cold the pyrometer and the window were disassembled .

It was found that the window was contaminated and had a crack into it. Figure no. (7.2) is a photograph of the cracked window. Cleaning of the window was found impractical .

In order to overcome this problem a new pyrometer holder was designed. This new holder houses the pyrometer and has a connection for supplying compressed air. The compressed air is used to ensure that carbon particles do not reach the pyrometer lens and to ensure that the pyrometer probe does not get hot. The pyrometer holder then accelerates the air leaving passed the pyrometer lens into the turbine gas stream.

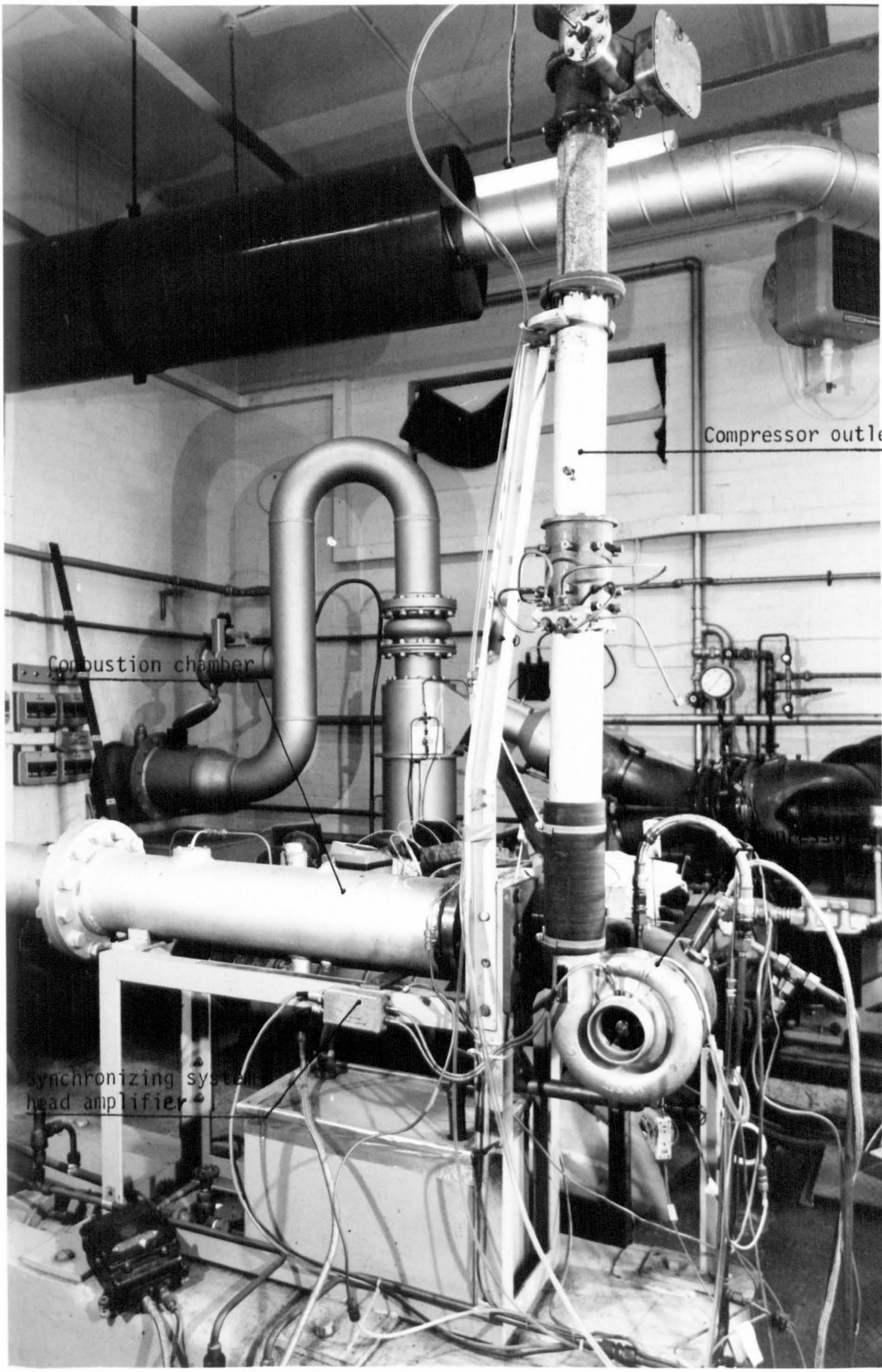

FIG no.(7.1) The Experimental Rig

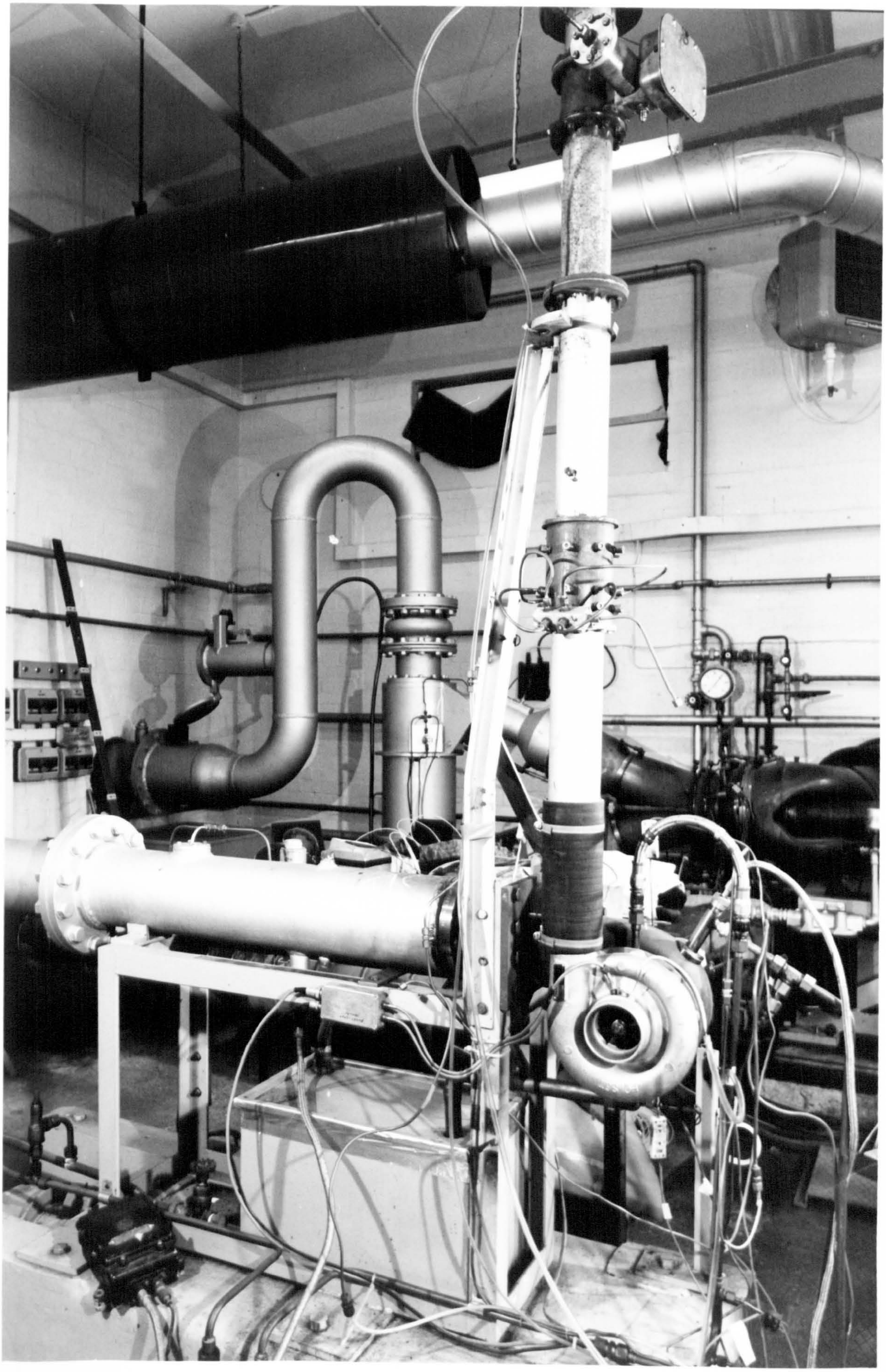

Fig. (7.2) The Quartz Window
After The Test

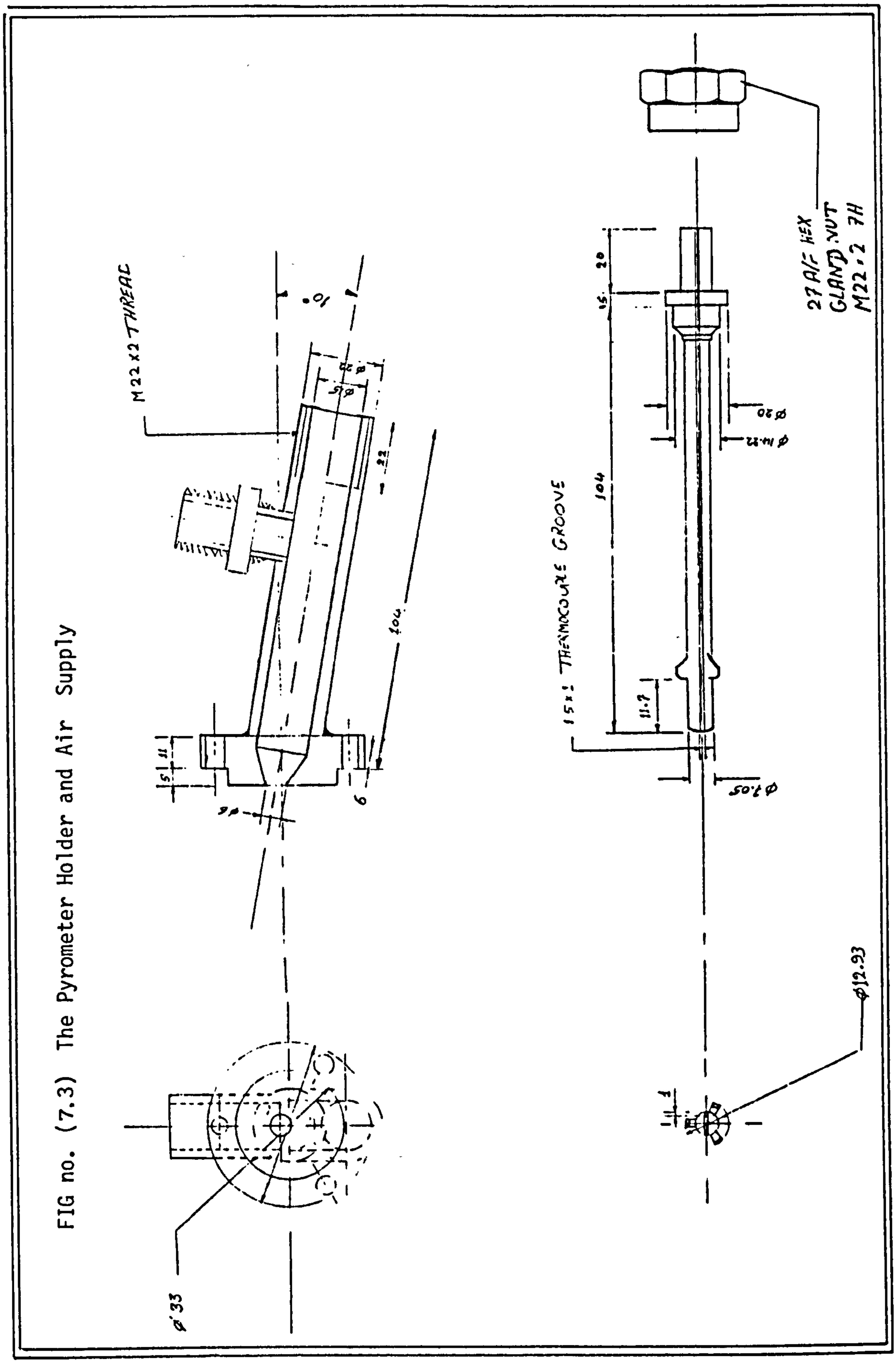
ALL DIMENSIONS IN MILLIMETRES UNLESS OTHERWISE STATED
FIG no. (7.3) The Pyrometer Holder and Air Supply
M22x2 THREAD
104
THERMOCOUPLE GROOVE
27 A/F HEX
GLAND NUT
M22 x 2 THREAD
ø12.93
ø33

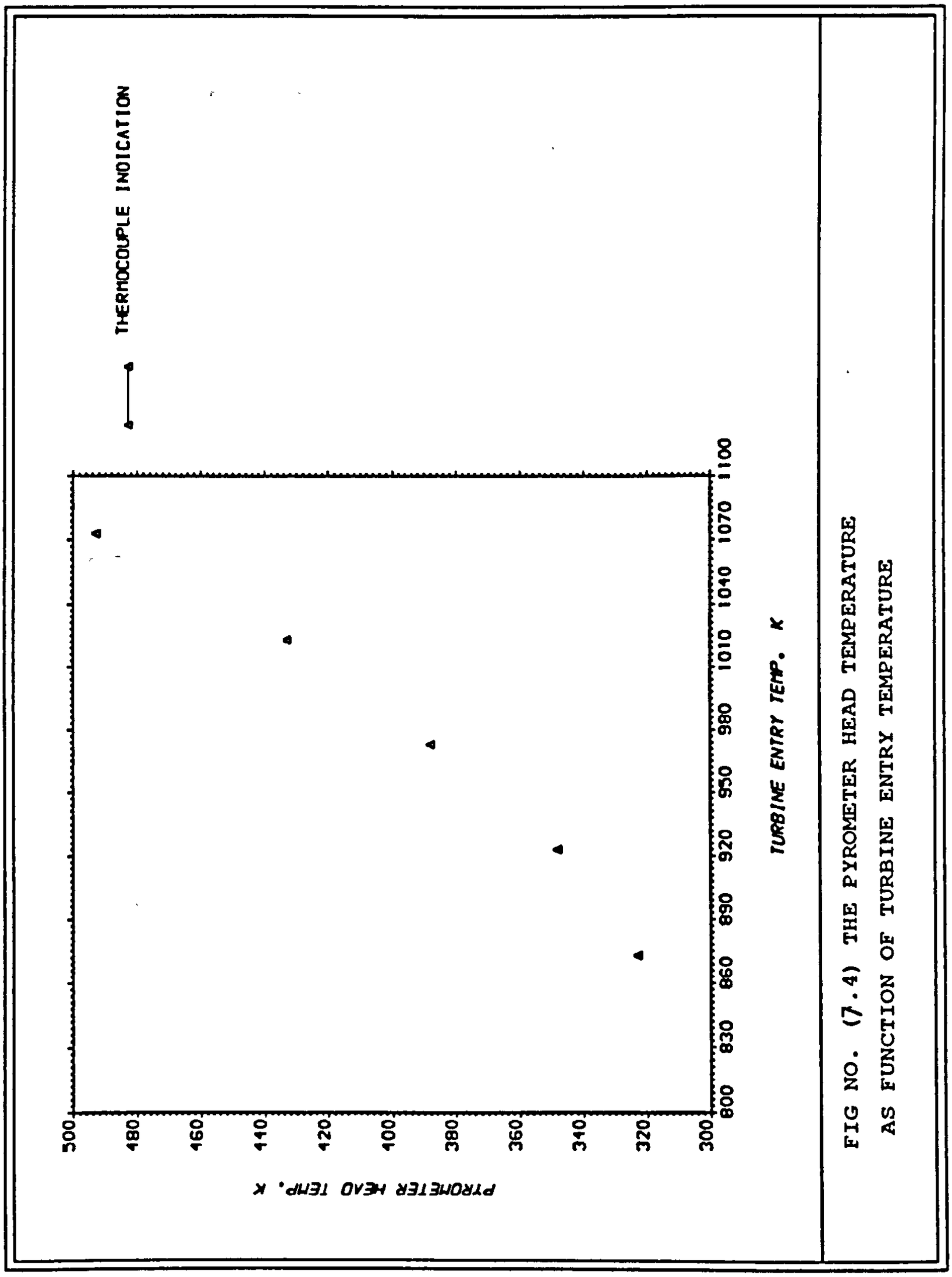

FIG NO. (7.4) THE PYROMETER HEAD TEMPERATURE AS FUNCTION OF TURBINE ENTRY TEMPERATURE

7.6 Data Storage

The PSP was connected to a storage scope, each stored signal contains "4000" points for the surface temperature profiles of the "twelve" blades. This had made it necessary to digitize the signal and then analyse it.

In order to do this a "Hewlett Packard HP-85" personal computer was employed. This PC was used to save the digitized signal. An "RS232" interface was employed to transfer the data from the scope to the HP-85 and from HP-85 to the main frame computer .

These measurements were taken as follows:

It took about 10 minutes to establish the first running condition including the starting period;

It took about 6 minutes to store, digitize and save the first signal;

It took about 11 minuted to establish the second running condition, store, digitize and save the signal;

It took about 11 minutes to establish, store, digitize and save the signal at the third running condition;

It took about 15 minutes to cool down, and shut the rig.

7.7 Data Acquisition System (DAS)

7.7.1 Introduction

The pyrometer head amplifier provides a voltage signal that is function of the target radiation. This signal is then fed to the "PSP" unit. The output of the "PSP" is an analog signal that varies linearly with target temperature .

This signal is then fed to the "Nicolet" oscilloscope together with a once per turbine revolution signal. This trigger signal is useful to identify each blade.

Figure no. (7.5) shows the rig monitoring equipment. The "Nicolet" is interfaced with the "HP-85" personal computer via an RS232 interface .

7.7.2 The "DAS" Units

The data acquisition system used for saving, digitizing storing and analysing the pyrometer signal consists of the following units :

1) The pyrometer signal processing unit "PSP". This unit was employed to perform the following on the pyrometer signal :

a- emissivity compensation ,

b- noise filtration ,

c- signal linearisation ,

d- mean and peak temperature display ,

e- The "PSP" also provides analog output from each module .

2) "Nicolet" oscilloscope . This unit serves to :

a- display the pyrometer signal fed from the "PSP" .

b- display the signal fed from the synchronizing system .

c- store the pyrometer signal .

3) "RS232" interface . This unit serves to transfer the data from the "Nicolet" to the "HP-85" PC. And from the "HP-85" to the main frame computer .

4) HP-85 personal computer. This unit was employed to :

a- display the transferred signal ,

b- save the transferred signal ,

c- transfer the saved signal to the main frame computer .

5) Software employed to transfer the data to and from the "HP-85"

6) Software employed for the data analysis on the main frame computer .

Figure no. (7.6) shows the signal stored on the "Nicolet" and plotted on the (VDU) of the "HP-85". The effect of plotting every 5th point which was done to save time is evident on the VDU displayed signal.

7.7.3 Data Storage, Transfer and Analysis

Following is the procedure used for data transfer and analysis :

1) Step one :

a- The "DAS" units were interconnected and powered .

b- The rig was run at the set condition .

c- The pyrometer signal was fed to the "PSP" and displayed with the trigger signal on the "Nicolet" .

d- The signal was then stored on the "Nicolet" .

e- The programme "NICSAV" was executed on the "HP-85". This programme replots the transferred signal before saving it on a magnetic tape .

2) Step two :

a- The "HP-85" was connected to the main frame computer line via the "RS232" interface and the "RS232" switch box. This box either allows the main frame computer to receive and acknowledge data from the "HP-85" position "D" or disconnect them from each other position "A" .

b- The switch box was on position "A" .

c- The programme "VBSAV" was executed. This programme reads the data file and replots it. It then asks the user to log into the main frame computer , edit a data file and issue the insert command .

d) "VBSAV" then asks the user to put the switch box on position "D" and to press <continue> on the PC.

e- The data was then transferred to the main frame computer .

f- At the end of data transfer the user will be asked to reposition the switch box on "A". The data are now written on the main frame computer in a "20I5" format .

3) Step three :

Three methods were used for analysing the transferred data on the main frame computer .

First method :

In this method the programme "NICPLT" was executed. The output of this programme is a graph of the transferred signal in terms of voltage and time .

Second method :

In this method the following programmes were executed:

1) "TRANS" this programme rewrite the data in terms of temperature and distance .

2) "DISFILT" this programme filters any high frequency noise from the signal (chapter eleven).

3) "ZONE" this programme rewrites each blade profile in a separate data file .

4) "PLOT" this programme plots the data files written by "ZONE" .

Third method :

In this method the same programmes mentioned in the second method were executed but without the programme "DISFILT" .

Figure no. (7.7) is a flow chart of these three methods .

FIG no.(7.5) Data Analysis Units

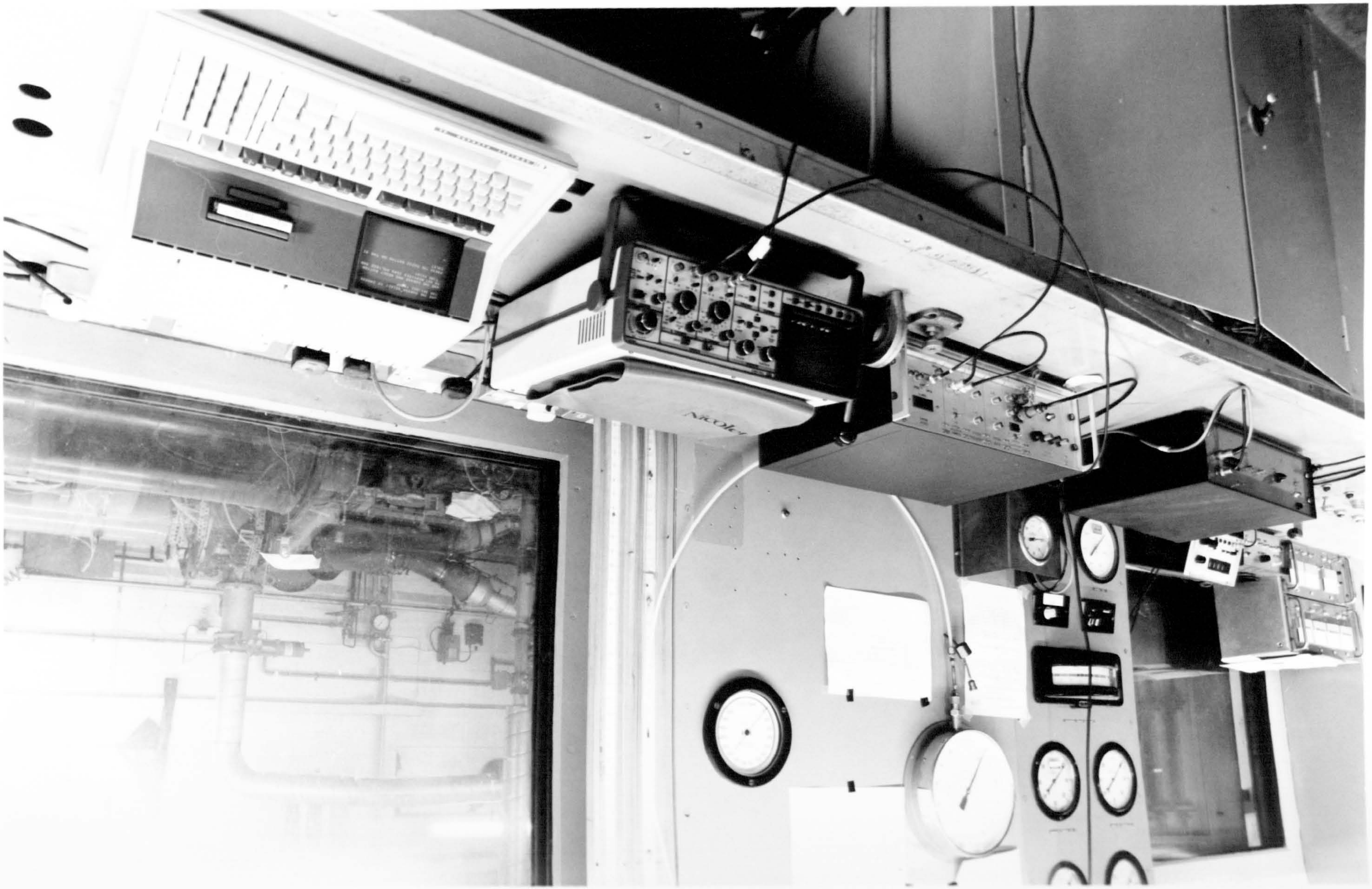

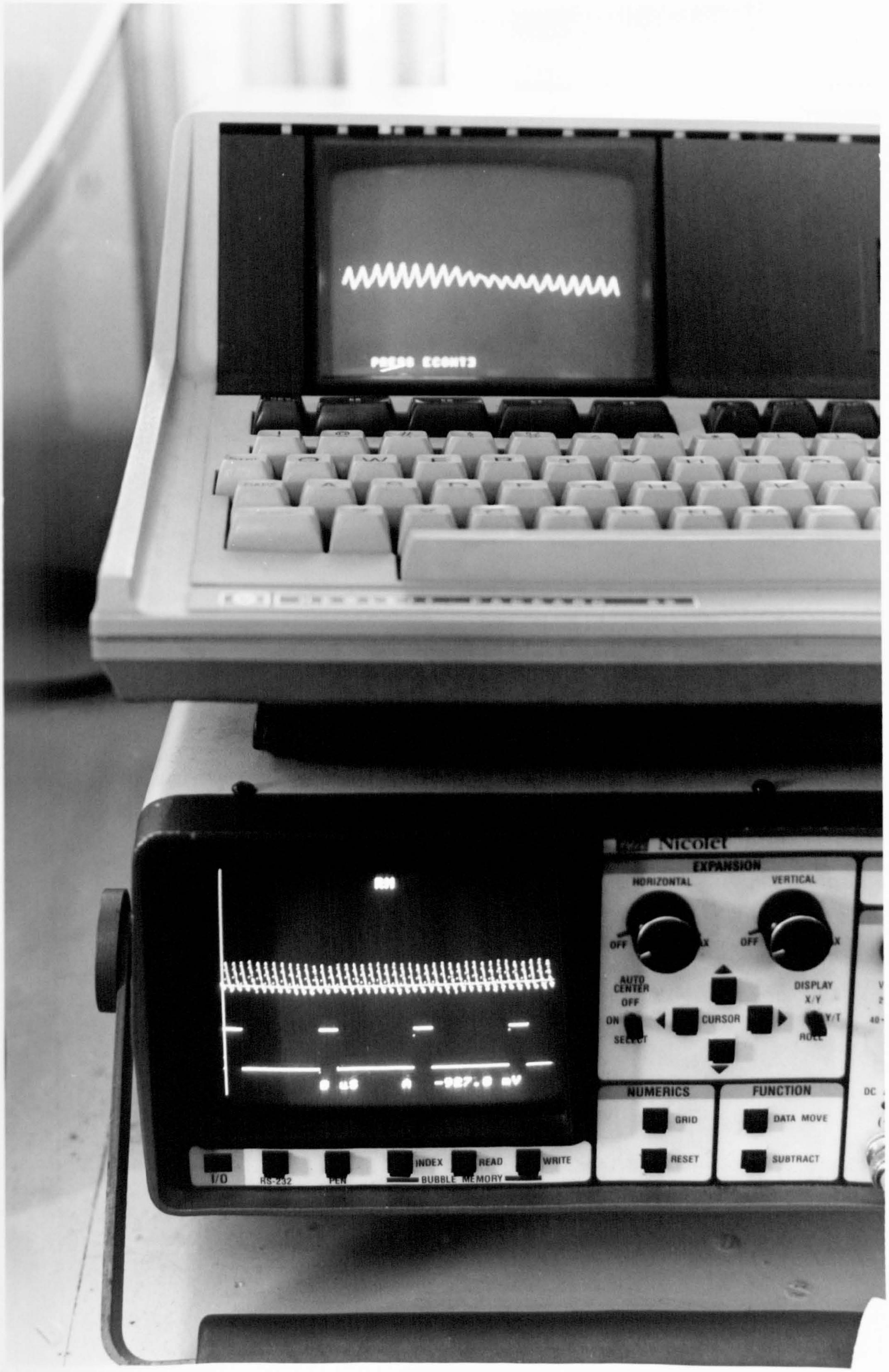

FIG no.(7.6) Pyrometer Signal

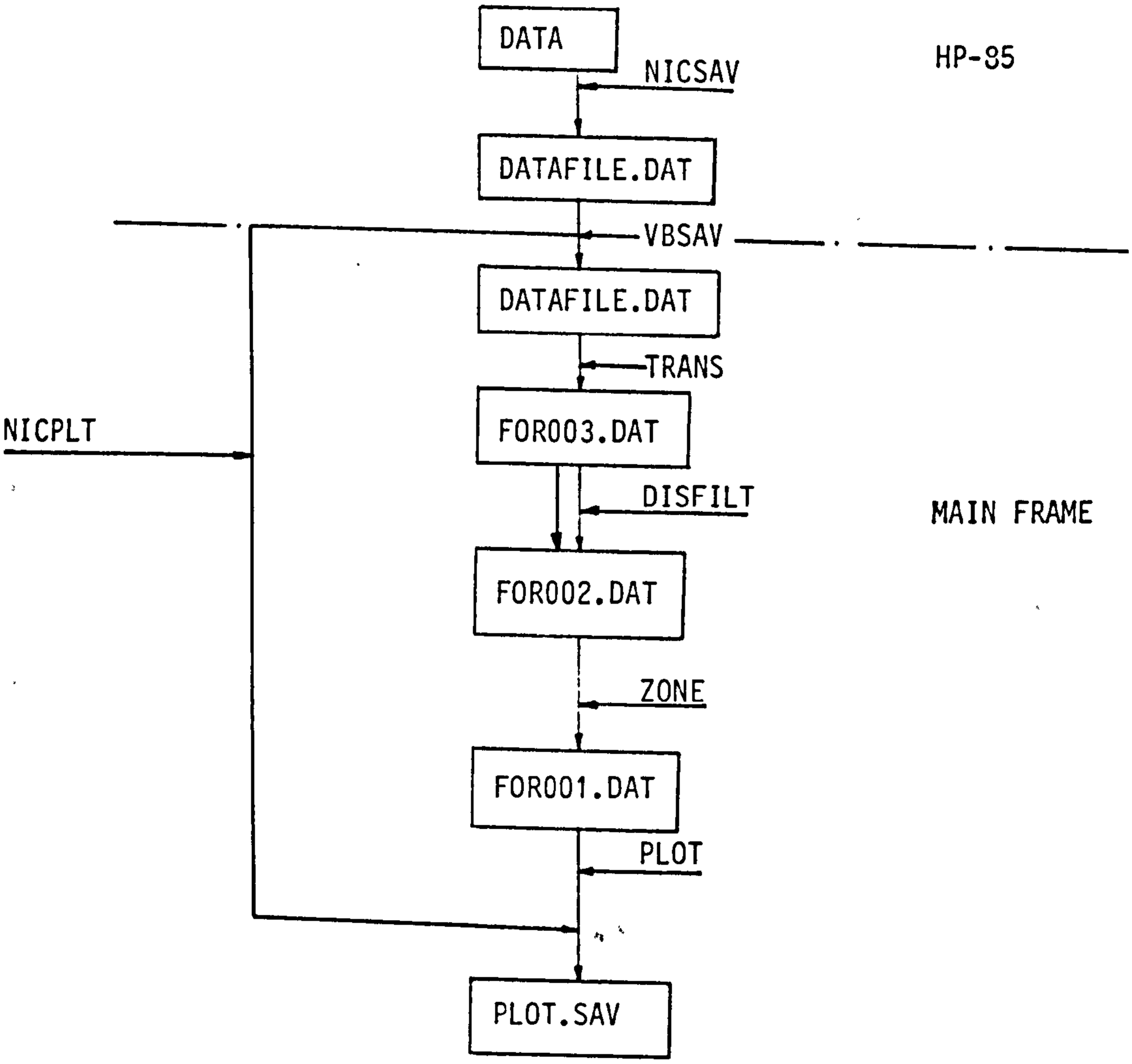

FIG no.(7.7) Data Analysis Flow Chart

CHAPTER EIGHT

8 THERMAL BARRIER COATINGS AND COATING APPLICATION METHODS

8.1 Introduction

Turbine blades are required to operate at gas temperatures higher than the melting point of their materials. Superalloys are employed because of their capability to work at high temperatures but additionally complex cooling configurations are also used so that the blade metal temperature is within the operating range of the superalloys because of the very high gas temperature used. The results of the research in this area in the 1960s and 1970s achieved 5-10 degrees increase per year in the turbine blade capability [Bennet(40)]. However, thermal barrier coatings can be used to lower blade metal temperatures by providing thermal insulation to the coated blades.

There are several advantages in using ceramic thermal barrier coatings. For example, an increase in engine reliability is possible by reducing metal temperatures by 50 to 220 K [Bratton(2)], increase engine efficiency and power by increasing gas temperatures and maintaining current metal temperatures. Reduced fabrication costs by eliminating elaborate cooling schemes. Fuel flexibility can also be achieved by the use of thermal barrier coatings as these protect the superalloy .

These coatings can be of thin or thick layers depending mainly on their material and the task required . Application techniques also differ from one type to an other depending on the required task .

8.2 The Concept Of High Temperature TBC

8.2.1 General Coating Concepts

Coatings are used in high temperature environment to perform one or more of the following [Pentecost(41)] .

1) Chemically , to control oxidation , corrosion or diffusion of the substrate material .

2) Electrically , as an insulator or conductor depending on it's electrical properties .

3) Physically , as a resistance to erosion or abrasion .

4) Thermally , to influence conductive heat transfer .

5) Emittance control , to control radiative heat transfer .

The overall suitability for a given task of coatings is a compromise of one or more of the above functions . In the case of TBC for gas turbine application , the over all performance of the coating is usually a compromise of the coating thermal conductivity , emissivity , and corrosion and erosion resistance, provided that the coating has a satisfactory endurance. Usually , the coating used are of low thermal conductivity and low emissivity.

8.2.2 TBC Requirements

The generally required properties of a particular TBC are [Wilkins(42)] :

1) A close match of thermal expansion characteristics of the ceramic and metallic components of the coating and the substrate, to prevent spalling .

2) Resistance to concentrated mechanical stresses , which might result in cracking and hence promote loss of coating .

3) High reflectivity and hence low emissivity and absorptivity .

4) Maximum resistance to oxidation and hot corrosion of the metallic constituents of the coating .

5) Low thermal conductivity .

6) Reparability during manufacturing and at overhaul after field service operation .

7) Good adherence to resist thermal stress spalling , which is function of good inter-particle bonding and bonding of the coating system to the substrate alloy .

8) Stabilization of the ceramic crystal structure is necessary to minimize the effects of non-linear thermal expansion caused by structural transmission of the ceramic during engine operation .

8.3 Types Of Coatings

TBCs can be classified according to their structure, into duplex and multi layer systems. Duplex (two layer) systems which as the name indicates are made of two layers. These two layers are normally a thin under coat bond layer which is usually from metallic material, and a thicker overcoat layer usually from pure oxide.

Multi layer systems are sometimes called continuous graded coatings. This type is usually constructed from more than two layers. It usually begins with metallic layer, a mixed layer, and a pure oxide layer. The mixed layer begins rich with metallic fraction and ends rich with oxide fraction close to the oxide layer.

The multi layer system often outperforms their counter parts and are better with regard to adherence properties [Wilkins(42)].

8.4 TBCs for Gas Turbine Aerofoils

Due to the harsh environment under which the turbine blades are operating and due to the growing demand to operate them under even harsher environment, superalloys and complex cooling configurations have been introduced. These are not only very expensive but they reached their optimum. However, the use of ceramic coatings on turbine hardware as thermal barriers can achieve even greater results.

There are three main objectives of employing TBCs on gas turbine aerofoils [Boch ,1989, Ref.85]:

1) an increase in the operating temperature and thereby an increase in the thermal efficiency;

2) the replacement of "expensive" superalloys by ceramics assumed to be producible at an acceptable cost;

3) a weight reduction due to the low density of ceramics compared with metals;

8.4.1 Degradation Modes

The modes by which the thermal barrier coatings employed within a gas turbine is degraded or damaged are important because it is from a study of the degradation modes experienced in service that the proper coating system can be chosen and developed. However, the harsh environment of the turbine hot section cause different modes of degradation. These degradation modes involve the following :

8.4.1.1 Erosion

The high velocity particulate carried by the hot gases can greatly accelerate turbine blades degradation when impinged on them, especially when the environment is corrosive .

Erosion processes can be classified into, [Stephenson(44)],

i) Erosion due to solid particle impingement ;

ii) Erosion due to liquid drop impingement ;

iii) Erosion-corrosion ;

8.4.1.1.1 Solid Particle Impingement

This is one of the main and common causes of engine degradation. There are a number of factors influencing this process, such as :

- Angle of Impingement ,
- Particle impact velocity ,
- Particle size ,
- Gas temperature , and
- Properties of the target surface .

All of these factors and others, [Stephenson(44)], can influence in a way or an other the erosion process caused by solid particles impingement. Velocity, and size of the impinging particles, and temperature of the target surface are usually the most important factors influencing gas turbine blade erosion .

Solid particles can range from carbon particles produced within the gas turbine combustor to ingested sand or other material either ingested to the engine or produced within the engine.

8.4.1.1.2 Liquid Drop Impingement

Liquid drops, in a similar manner to that of solid particle impingement can cause severe surface erosion when the impingement velocity is sufficiently high.

The problem of liquid droplet erosion in gas turbines is mainly due to the un evaporated fuel or water droplets (water injection), and liquid phases of compounds formed in the combustor of material ingested into the engine (salt for example).

8.4.1.1.3 Erosion-Corrosion

In systems operating at high temperatures such as gas turbines, erosion and corrosion processes may interact simultaneously, resulting in a very short component life time .

Turbine blades are often exposed to corrosive environments. Operation in the corrosive environment results in corrosion resistance films been formed on the blades surfaces, typically metal oxide layers. Any process that disrupt this protective film will accelerate the degradation process by enabling the ingress of corrosive species to the substrate and hence increasing the rate of film formation. Under these conditions the properties of both the substrate and the surface scale are important in defining the erosion behaviour of the material [Stephenson(45)] .

8.4.1.2 High Temperature Oxidation

Turbine blade materials usually work at temperatures in access of 900 K, all materials form a surface oxide film when operated at high temperatures in an oxygen rich environment. For successful operation in such environments, it is essential that the formed oxide film is thin, continuous, slow growing and adherent.

Formation of such oxides is possible, but the maintenance of these films on the surface of the blades under severe conditions is difficult. After these films are formed, they act as an effective barriers separating the blade material from the environment. Further oxidation can then occur only by metal ions diffusion through the oxide film. If oxide failure occurs or indeed if non-protective oxides are formed such that the metal is still in direct contact with the environment, then the oxidation process is considerably accelerated, limiting the life and on occasion causing catastrophic failure [Teer(46)] .

8.4.1.3 Hot Corrosion

Gas turbine hot corrosion is normally exhibited in the marine environment, it occurs in direct response to the operating environment to which the corroded parts have been exposed. Hot corrosion takes place due to the high salt content of the marine environment.

Hot metal corrosion in gas turbines may also occur due to the impurities contained in the fuel, especially Sulphur, Vanadium, Sodium, Potassium and Chlorine [Hart(48)]. These elements may form deposits on the structural parts which frequently contain small amounts of compounds that melt at modest temperatures (880 C for sodium solphate, 675 C for vanadium pentoxide and 625 C for sodium vanadyl vanadate) [Singh(47)].

Combustor design influences the amount of carbon formed within the combustor primary zone. The amount of carbon formed can, in many cases, be reduced by a detailed attention to the fuel injection process, the mixing of fuel with the air, by detail attention to the aerodynamics associated with the primary zone and secondary combustion zone, and by designing the primary zone for a weak equivalence ratio [Tamaru(49)]. Blade cooling technology controls the blade surface temperature distribution which plays an important part in the corrosion process. The use of coatings as thermal barriers reduces metal temperatures and provides protective oxide layers by ensuring that the blade material is not in direct contact with the environment and hence protected from it.

8.4.2 Ceramic Thermal Barrier Coating systems

Thermal barrier coatings are now often applied to the combustion chamber liner and are increasingly been considered for the early stages of the turbine. They must therefore function in an extremely hostile environment. They can be subjected to chemical and physical attacks by gas streams, at high temperatures and pressures, moving at very high speeds .

Thermal barrier coatings must be insulating (have low thermal conductivity). They must withstand thermal shock and remain adherent to the substrate. Their cost, availability, ease of processing, and interactions with the substrate material must also be taken into consideration.

Research and development in thermal barrier coatings has resulted in a wealth of literature published by various interested concerns around the world [Refs. 50-68].

One of the most successful developments in thermal barrier coatings is a zirconia based system. Zirconia (ZrO2), is chemically inert. It has a melting point of about 2960 K and low conductivity of less than 2 W/mK with thermal expansion coefficient of 10E-6/K. Zirconia is widely available, the production of its minerals is (1/2) million tons per annum. This has made it reasonably cheep and plentiful [Bratton(2)].

The greatest drawback in zirconia is the increase of its density when cooling from high temperatures. This large change in density signifies a large volume change which is generally destructive as it cause the coating to spall and fall off.

This major drawback can be overcome by the addition of magnesia, calcia and oxides of yttrium as stabilizers. Zirconia has thus become the base for a range of thermal barrier coating systems .

The experimental development of coatings has concentrated on the effect of differing levels and types of the stabilizing oxides. This has yielded significant improvements in coating behaviour particularly with materials containing around (8%) by weight yttria (Y2O3). This system is known as yttria partially stabilized zirconia (ZrO2-8Y2O3) .

One other conclusion of the experimental research in coatings is the use of bond coatings. The NiCrAlY coatings, (NiCrCoAl-Y2O3), has been developed specifically for their oxidation resistance. When these are used as bond coatings, they offer substantial increase in the life of coatings subjected to high temperature exposure [Bratton(2)] .

Six TBC systems were investigated in this programme . They included an 0.16 mm of bond coat (NiCrCoAl-Y2O3), and different thicknesses of [Ref.69] :

a) 8% Yttria Partially Stabilized Zirconia (8%YPSZ);

b) 24% Ceria Yttria Partially Stabilized Zirconia (24%CYPSZ);

C) 20% Yttria Partially Stabilized Zirconia (20%YPSZ);

d) 24% Magnesia Partially Stabilized Zirconia (24%MPSZ);

e) Grey Alumina , and

f) White Alumina .

8.5 Coating Application Methods

There are numerous methods available for applying coating materials on a given substrate material to form a coating system.

For any coating system, each method of application has its advantages and disadvantages. Detailed discussions are presented in [Withers(67) and Johner(68)] .

Following is a list of the methods used for high temperature applications of the coatings .

1) Electrodeposition method ,

2) Spraying method ,

3) Cladding method ,

4) Vapour (gas) deposition method ,

5) Enamelling method ,

6) Vacuum metallizing method ,

7) Hot dipping method ,

8) Slurry method ,

9) Exothermic reaction method ,

Each of these methods can be implemented in many different techniques. The spraying method for applying coatings is considered in more detail here partly because of its importance in applying coatings to the hot section of the gas turbine and partly because this was the process which was used for applying the coatings studied in this work.

Two basic techniques can be used for spraying materials to form high temperature coatings, these are the flame and the plasma techniques. Generally, three stages can be defined in a spraying method. These stages are :

1) Heating of the coating material to form molten or semimolten droplets in flame or plasma .

2) Projecting these hot droplets at a high velocity on to the base metal surface .

3) The collision of these droplets with the substrate , where they adhere to it to form the final coating .

Coating materials may be supplied to the hot zone in wire , rod or powder form .

Flame guns use Oxygen as oxidizer and usually Acetylene, hydrogen, or Propane as fuel.

Plasma spray guns employ a controlled arc between two electrodes to ionize a flowing gas, such as Argon or Nitrogen to liberate heat [Withers(67)] .

8.5.1 Flame Spraying

There are two types of equipment used in this technique, wire type and powder type equipment. In the wire type, the wire or rod is fed by the feeding mechanism into the cone of the flame where its tip is melted at a controlled rate. These molten droplets are atomised and propelled by the gases onto the substrate. The parameters having influence on this process are, the air and gas flow rate and pressure, the wire diameter and the wire feed rate.

The powder type has the same principles as the wire type, except that the powder is fed into a cone of Oxygen-gas flame.

One advantage of the wire type, is that, the propelled material must become molten before it can be released from the wire to be projected on the substrate.

The limitation of it, on the other hand, is that the coating material must be capable of being drawn into wires or made into rods and large droplets may melt off the tip without being completely atomized [Withers(67)] .

The outstanding advantage of the powder type is that more than one coating material powder can be used in the process of forming a coating system. This system when formed from several coating materials will for example, produce a better thermal expansion match to the substrate material. The other advantage is that, single or multi feeder can be employed in this technique depending on the required end properties and application.

Heating of the coating material can be achieved through different methods [Withers(67)]. The use of laser beams as the source of heat looks promising even it is still in the development phase [Sheffler et al (4)].

8.5.2 Plasma Spraying

In this technique, a direct electric current is struck between the nozzle and the electrode, whilst a stream of mixed gases is passed through this arc. This results in dissociation

and ionization of the gases. The plasma arc spraying utilizes the very high temperatures, normally greater than 10,000 K. The heated and expanded gas is used to melt and propel the injected powder particles of the coating material at a particle velocity of up to 3,000 m/sec onto the substrate to form a dense and well bonded coating .

This is a continuous coating process and high melting point materials can be applied.

There are many different practical designs of torches to cater for different coating requirements. However, they are all based on the same principles .

The electrical connectors are made of positive Copper anode nozzle and negative tungsten electrode. These connectors are generally made with water cooled electrical cables which also serve to carry cooling water to the torch .

The gas used to form the plasma flame is usually Argon, Nitrogen, Hydrogen or Helium. Mixtures of two or more of these gases are sometimes used .

Accurate control of the gases, water, powder, and electric current flowing through the torch is essential for producing a reproducible physical and metallurgical properties in the applied coatings, that is to maintain a consistent coating quality [Johner(68)] .

For the following reasons, plasma sprayed coatings are preferred over flame sprayed ones :

1) Higher particle velocities result in higher bond strength and coating density .

2) More efficient heat source .

3) Minimum oxidation .

4) And the higher plasma temperatures permit the spraying of materials with higher melting points .

8.5.3 The Application Method Used in This Investigation

8.5.3.1 Introduction

As was stated before, six coating systems were used in this investigation. Each system was applied to a turbine wheel. Every other blade of each turbine carried a different coating thickness. This arrangement was necessary to give a wide range of coatings and coating thicknesses for a minimum number of turbine wheels .

8.5.3.2 "Metco" EG88 Computer Aided Plasma Spraying System

All the parameters of the application method used were monitored and controlled by a fully computerized system.

The EG88 CAPS system has been developed by "Metco" to monitor all parameters that influence the deposited layer. This should maintain the high quality and consistency of the coated product .

The EG88 CAPS system consists of :

1) Main unit type EG88-B, this unit incorporates the metering hardware for the electrical current, gases and compressed air. The powder feed system is fully integrated into the main unit.

2) Distribution unit type EG88-D, this unit incorporates the cooling water control and the high frequency ignition system. The cooling water and the electric current are then connected to the plasma gun through water cooled cables .

3) Computer control unit type EG88-C, this unit houses the microprocessor, visual display unit and printer. The microcomputer random access memory has the capacity to store 255 sets of coating data. Each set of coating data comprises two sets of spraying parameters, bonding and main coat. The system parameters of plasma and carrier gas flow, dc current, powder feed rate, cooling air pressure, etc., are entered via the keyboard following prompting messages on the VDU, which also displays the entered data.

4) Powder feed unit type EG88-P, either two or four individual patented powder hoppers can be used. Feeding of the powder is accomplished without an electric motor. There are no moving parts in contact with the powder and the main unit controls the carrier gas flow .

5) High performance rectifier type 2 OG, this unit is developed specifically for the plasma system. It is an efficient high performance DC-power source. Closed loop regulation ensures constant current output. The value of the ignition current, and the overload protection are controlled from the computer controlled unit .

6) High energy production plasma spraying gun type 10MB, this is a robust, high performance machine mounted gun. It employs two separate cooling water circuits for the nozzle and for the electrode to ensure optimum cooling flow for each part .

8.5.3.3 "Metco" AR1000 Thermal Spraying Robot

To further develop the mechanization of coating application, the AR1000 robot is employed. This thermal spraying robot system is an all electric, computer controlled, six axis articulated arm robot .

The robot body's highly efficient waist, shoulder and wrist design enables it to accurately maintain spray distance and precisely control traverse speed over an almost infinite number of geometric part configurations .

All the spraying processes including spray gun start up, part pre-heating, spray coating application and spray gun shut down can be co-ordinated with the movements of the AR1000 robot and the tilting of the turntable unit.

Figure no. (8.1) shows the robot body with the six axis of movements .

8.5.3.4 Turntable Unit Type LR500-5

This microprocessor controlled 5-axis turntable, Figure no. (8.2), was developed for joint operation with the robot. It consists of a manipulator unit, a power supply, a control unit, a programming module and a control module .

Programs are entered into the work-piece manipulator and control module by an input keyboard. These programs may be run by the turntable control module or by the AR1000 robot .

Combination of the EG88 CAPS system, the AR1000 robot and the LR500-5 turntable made coating application process fully automated. This has permitted the coating of very complicated geometries. It has also provided the facility for producing different coating systems.

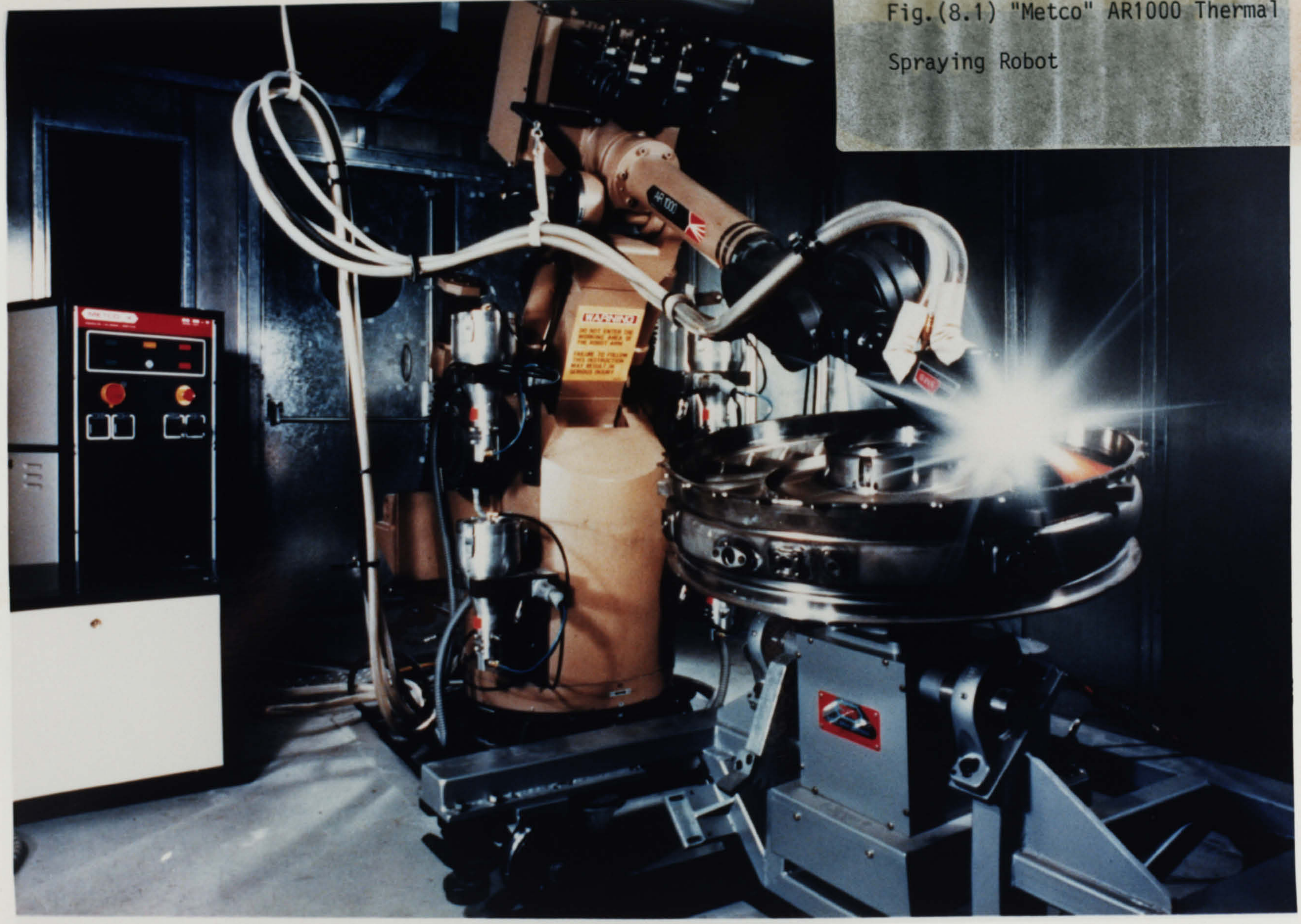

Fig.(8.1) "Metco" AR1000 Thermal Spraying Robot

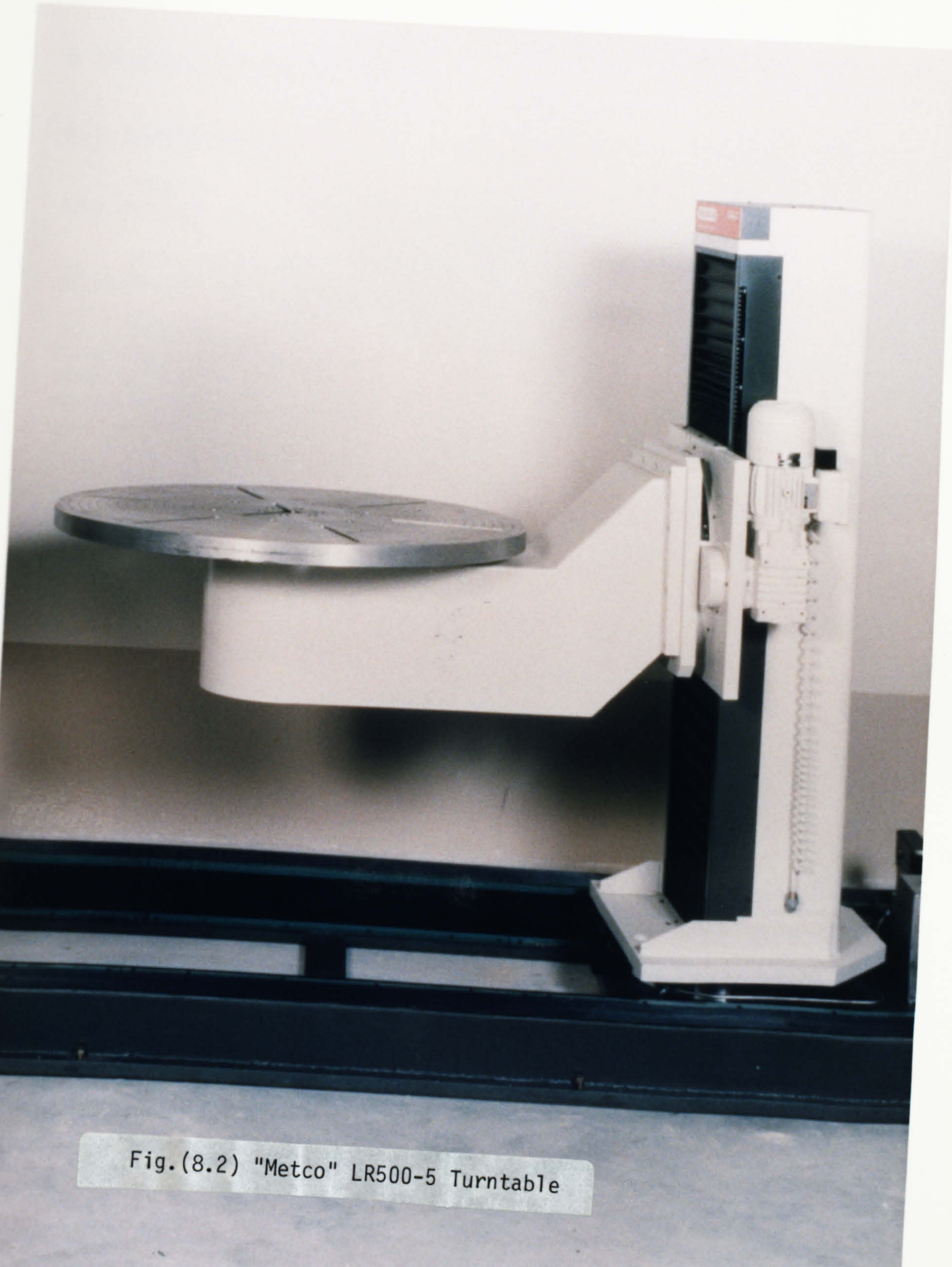

Fig.(8.2) "Metco" LR500-5 Turntable

CHAPTER NINE

9 EMISSIVITY MEASUREMENTS

9.1 Definition

The energy radiated from a non- black body is a fraction of the energy radiated from a black body at the same temperature .

The ratio between radiance emitted from a material to that of a black body at the same temperature is termed the emissivity.

Emissivity values are dependent upon various factors. These factors include material composition, size, shape, surface conditions, temperature of the body and wavelength at which the emissivity is measured. The value of emissivity is between zero and one .

Radiators can be divided into three groups :

9.1.1 Black Body Radiator

The value of emissivity for this type of radiators is unity by definition and its total emissivity is equal to its spectral emissivity which is also equal to unity .

$$\varepsilon_T = \varepsilon_\lambda = 1 \qquad \text{.....9.1}$$

Black body radiators are also called ideal radiators.

9.1.2 Grey Body Radiator

For grey radiators, the total emissivity is equal to the spectral emissivity and is equal to a constant. This constant is less than unity.

$$\varepsilon_T = \varepsilon_\lambda \leq 1 \qquad \text{.....9.2}$$

9.1.3 Selective Radiators

The total emissivity of selective radiators is not equal to its spectral emissivity and is less than unity .

$$\varepsilon_T \neq \varepsilon_\lambda \quad < \quad 1 \qquad \text{.....9.3}$$

Figure no. (9.1) is a comparison between the three radiator types.

9.2 Emissivity and Other Parameters

9.2.1 Kirchhoff's Law

When radiant energy falls upon a surface, part of it is reflected, part is transmitted and part is absorbed. The absorbed part is converted to heat. The transmitted part passes through without having its original electromagnetic form changed. The rest of the incident energy is reflected by the surface .

There is a close relationship between absorption and emission of any surface. If we consider an absorbing and emitting body located in an isothermal enclosure than if this body is not black it will be characterized by an emissivity that is less than unity. The absorptivity of this body is defined as the ratio between the energy absorbed to the energy incident on the surface.

For a non-black body enclosed in a cavity, the emitted and the absorbed radiation must be equal at all wavelength and in each direction, similar to that of a black body, otherwise there would be no thermal equilibrium.

As the radiation incident on the body in the isothermal cavity is black body radiation, then

$$\varepsilon_{\lambda T} \; E_{bT} = \alpha_{\lambda T} \; E_{bT} \qquad \text{.....9.4}$$

This leads to :

$$\varepsilon_{\lambda T} = \alpha_{\lambda T} \qquad \text{.....9.5}$$

This fundamental relation is known as the Kirchhoff's law. This is true at all wavelengths and in all directions .

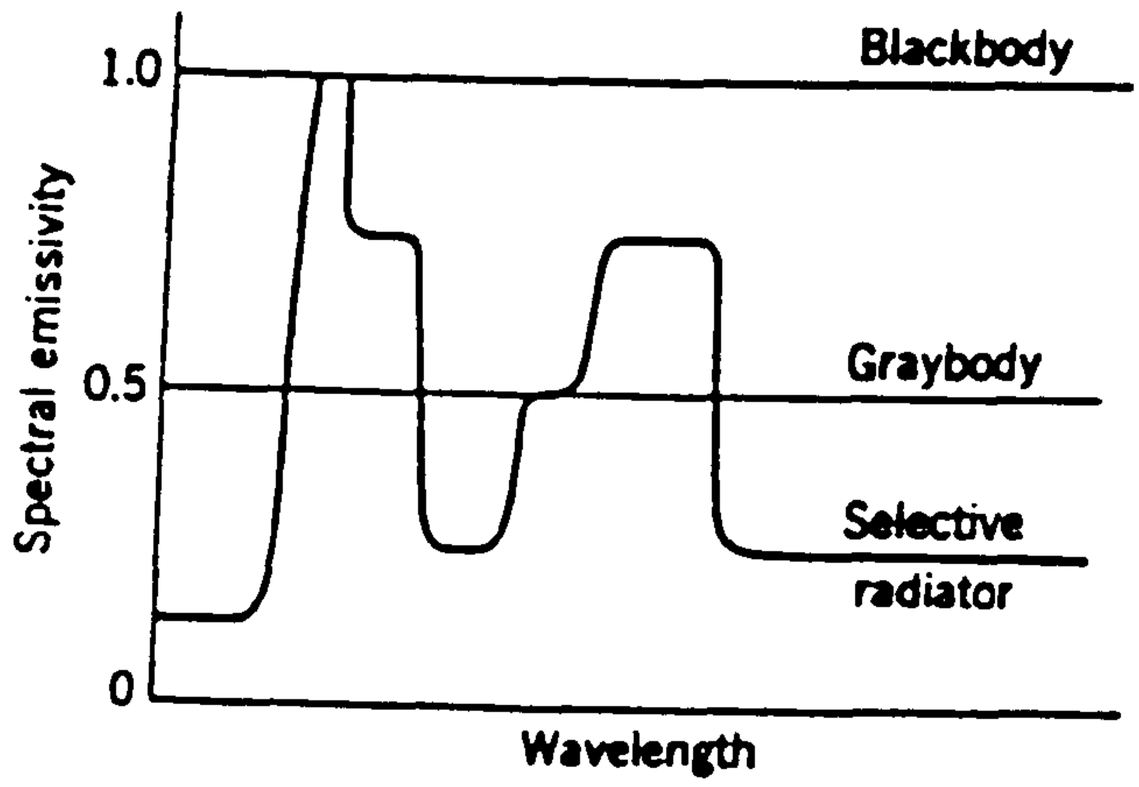

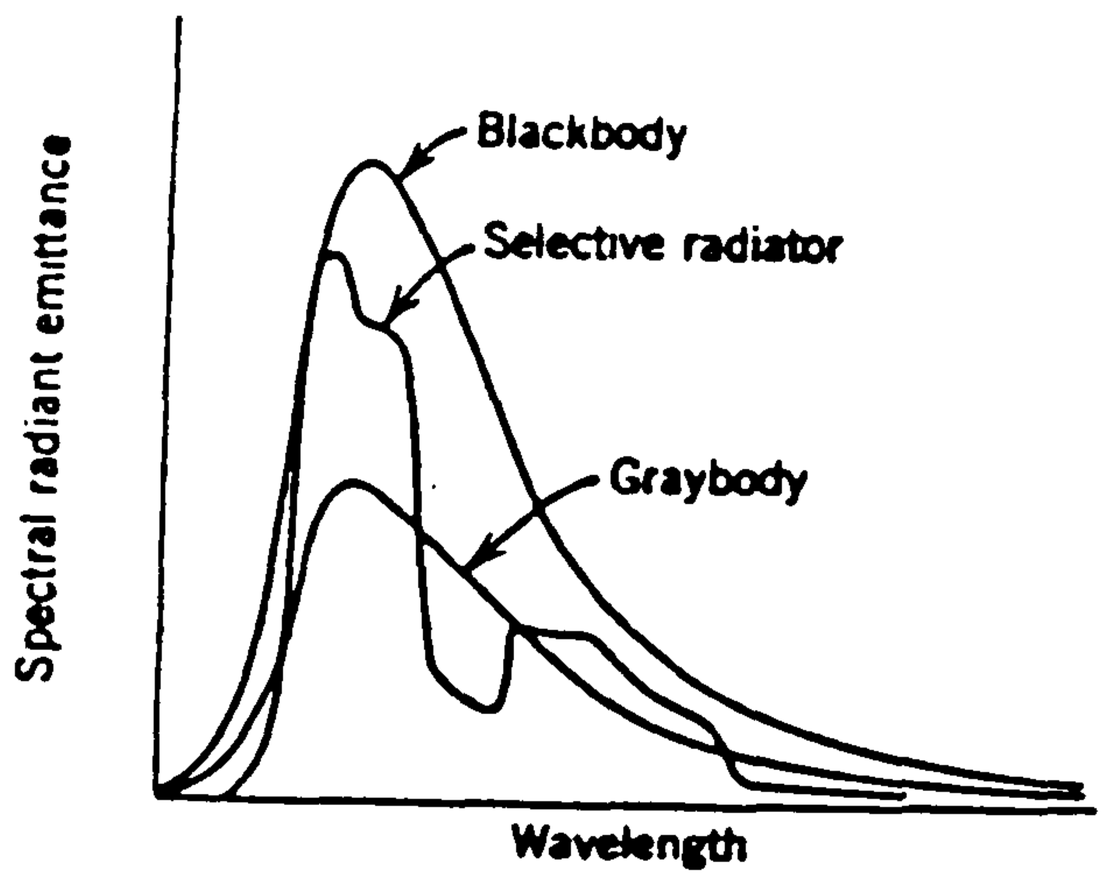

FIG no.(9.1) Spectral Emissivity and Spectral Emittance of Black, Gray and Selective Body Radiator

9.2.2 Emissivity and Temperature

In studying the relation between emissivity and temperature materials are divided into electrical conductors and non conductors. The total emittance of metallic surfaces or the electrical conductors increases considerably with temperature at short wavelengths (0.4 to 1.2 micrometers). This is the region of interest because the pyrometer used works within this wavelength band.

This increase is due to two factors, the first is that at higher temperatures a great proportion of the emitted radiation is concentrated in the short wave length region. In this region metals display their largest spectral emittance at any temperature as shown in Figure no. (9.2). The second factor is that the general level of spectral emittance increases with increasing temperature [Ubhi(86), Blair(71), Snyder(73) and Clark(74)].

For electrical non-conductors, it is expected that materials that appear light to the eye experience decrease in total emittance with increasing temperature. Whilst surfaces that appear dark to the eye may experience either an increase or a slight decrease in total emittance with temperature, the reasons for this are not well understood [Sparrow(75)]

Ubhi [Ref.(86)] gives many experimental results on the relation between spectral emissivity and temperature .

9.2.3 Emissivity and Wavelength

The emissivity of interest of a surface can be either total or spectral. The total emissivity is the emissivity measured over the entire spectrum, whilst the spectral emissivity is the emissivity measured at a single wave length. However, the emissivity is often measured over a band of wavelengths and then the emissivity is called band emissivity.

The surface spectral emissivity depends on both the material of the surface and the wavelength of measurement. For metals, the spectral emissivity decreases with increasing wave length. Whilst for electric nonconductors, the spectral emissivity increases as the wave length increases.

Clark [Ref.(74)], gives many experimental results of the relation between emissivity and wave length .

9.2.4 Emissivity and Angle of View

The emissivity can be angular or hemispherical. Angular emissivity is the emissivity in a particular direction that makes an angle with the normal to the surface under view. This angular emissivity can be total or spectral.

Normal emissivity is the emissivity measured normal to the surface. Hemispherical emissivity is the emissivity to the hemisphere.

Sparrow and Cess [Ref.(75)] summarize the behaviour of directional emissivities of real surfaces in that for non-metals, Figure 9.3, the directional emissivity remains uniform over angles between zero and 50 to 60 degrees with the normal to the surface. The emissivity then drops sharply beyond 60 degrees to reach zero at 90 degrees .

These angles of uniform emissivity were found by Ubhi [Ref.(86)] to be 70 and 80 degrees for zirconia and alumina, respectively .

The directional emissivity for metallic surfaces is different from that for nonmetals. For metallic surfaces, Figure 9.4, the emissivity stays uniform over angles between zero and 30 to 40 degrees. It then increases sharply beyond 40 degrees before dropping to zero at 90 degrees. The level to which it increases is higher the lower is the emissivity [Refs.35, 71 and 76].

9.2.5 Emissivity and Surface Roughness

The emissivity is a property of the surface under consideration. It is a normal practice to assume this surface as a smooth one. However, the emissivity of rough surfaces differ from that for smooth ones .

The emissivity tends to increase with surface roughness increase. This is true for both metals and non-metals. The rate of increase of spectral emissivity of metals is larger than that for non-metals. Edwards and Catton [Ref.(84)] relates this to the variation in surface reflectivity between metals and non-metals.

9.3 Emissivity Measurements

Two methods can basically be employed for determining the emissivities of materials. They are the "radiometric" and "caliometric" methods .

The radiometric method is based on comparison of radiation emitted from the surface whose emissivity is required to that from a black body at the same temperature .

While the caliometric method is based on comparison of heat lost or gained by the material, to that calculated theoretically for a black body at the same temperature .

An other method is based on the calculation of the emissivity from the measurement of the reflectivity then subtracting that from unity. This is possible only when the transmissivity can be neglected .

Appendix A, gives details of the experimental arrangement for the "radiometric" method. It also shows the results of emissivity measurements for aluminium enamel coated surfaces .

These measurements were taken employing the "Land" research pyrometer. The detector is made from a semiconductor of p-n construction of indium antimonide material.

The working temperature of this semiconductor is 77 K, which was accomplished by employing liquid nitrogen. To prevent the chip from 'frosting up' because of this low temperature, the entire chip was suspended within vacuum .

The use of "Negretti Aviation" pyrometer for surface emissivity measurement is easy and straight forward practice. In this pyrometer the indicated surface temperature should be matched with the measured one. This is achieved by changing the "dial" emissivity value, once the indicated temperature equals the measured then the "dial" emissivity is the surface emissivity at that temperature. Details of surface temperature measurements are presented in Appendix A.

The emissivities of the TBC systems employed in this investigation were measured employing the "Negretti Aviation" pyrometer. Figure no. (9.5) shows the results for the partially stabilized zirconia coatings. This figure shows that the emissivity was invariant with temperature in the range of measurements 873 to 1023 K. This range was limited by the sensitivity of the pyrometer and by the maximum temperature the sample furnace can withstand. It also shows that the emissivity did not change with the use of different stabilizers .

Figure no. (9.5) also shows a comparison between these measurements and similar measurements taken by Liebert for the "NASA" TBC systems, [Ref.77]. A curve fitting technique is employed to correlate these measurements with the coating thickness , which is also plotted on the same figure .

Figure no. (9.6) shows the measurements for the two alumina coatings. This figure shows a similar variation of emissivity with coating thickness .

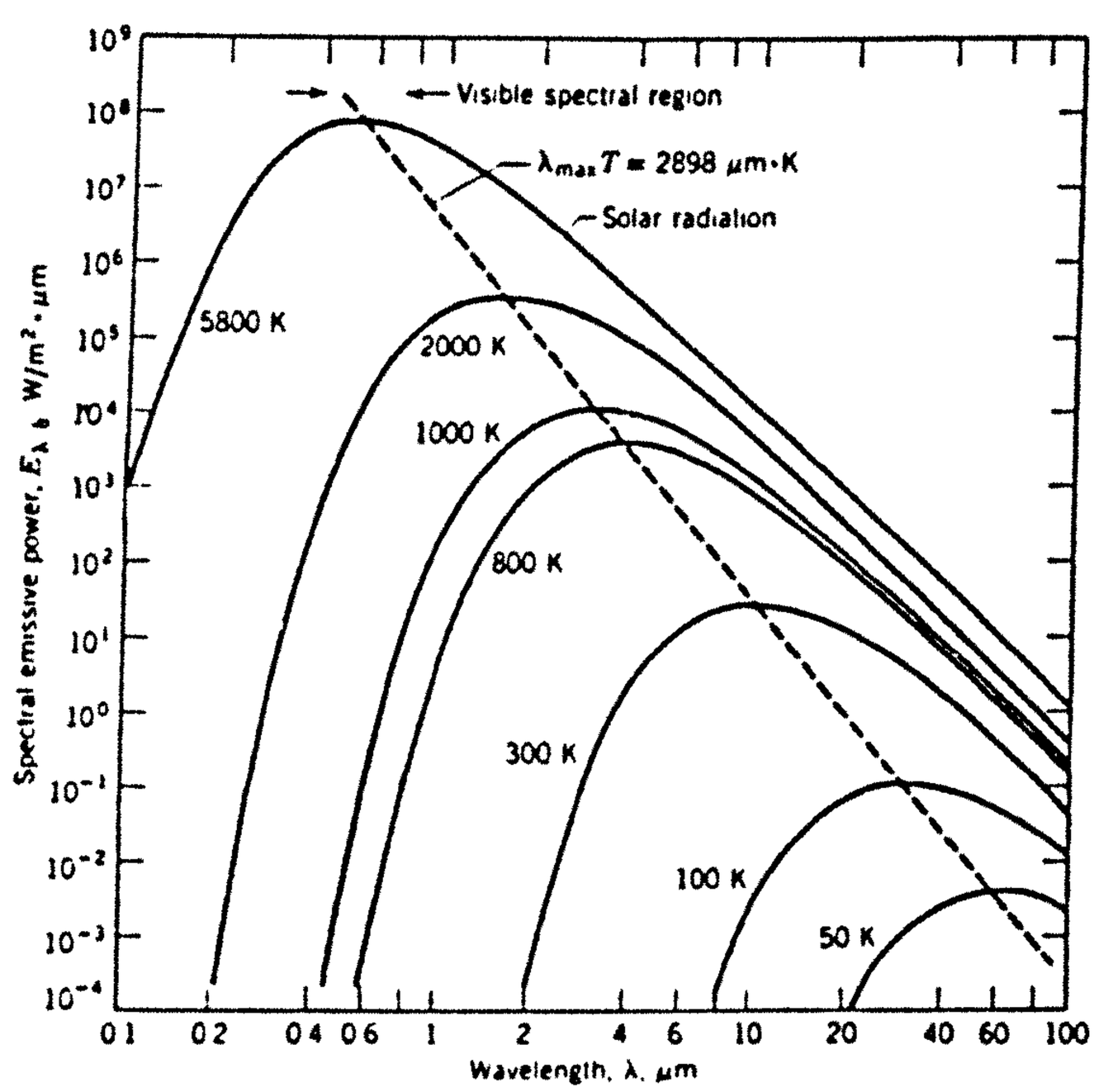

FIG no.(9.2) Spectral Radiant Emittance of a Blackbody at Different Temperatures

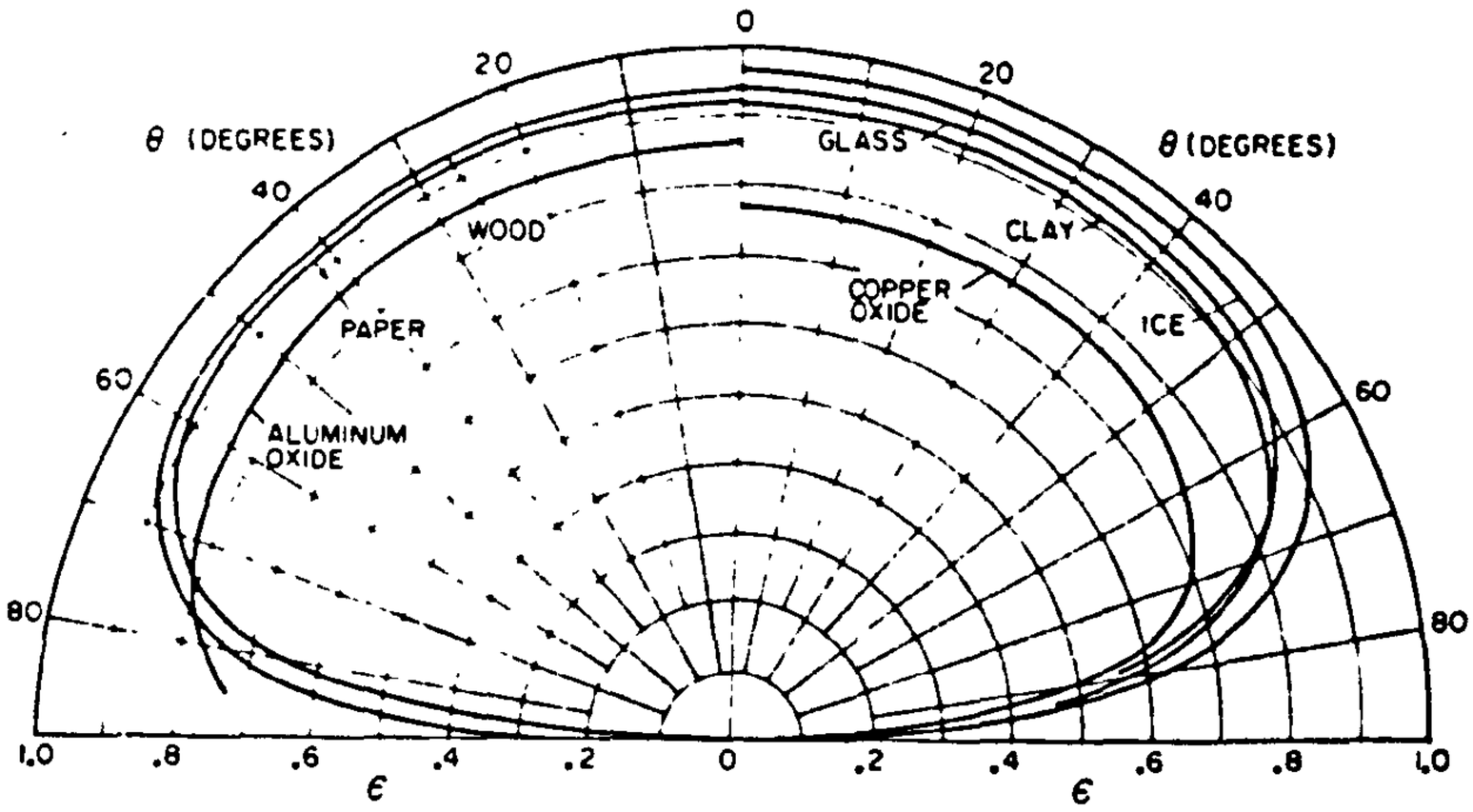

FIG no.(9.3) Distribution of The Total Directional Emittance for Several Electric Non-Conductors [from Ref.75]

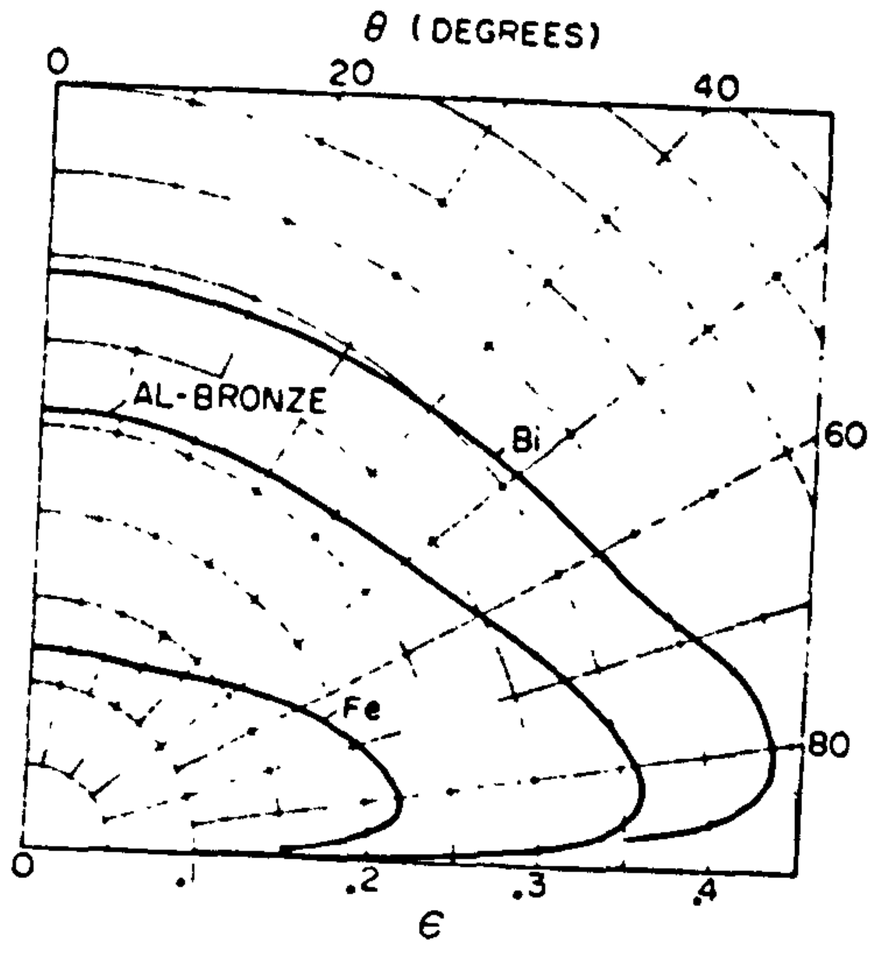

FIG no.(9.4) Distribution of The Total Directional Emittance of Several Metals [from Ref.75]

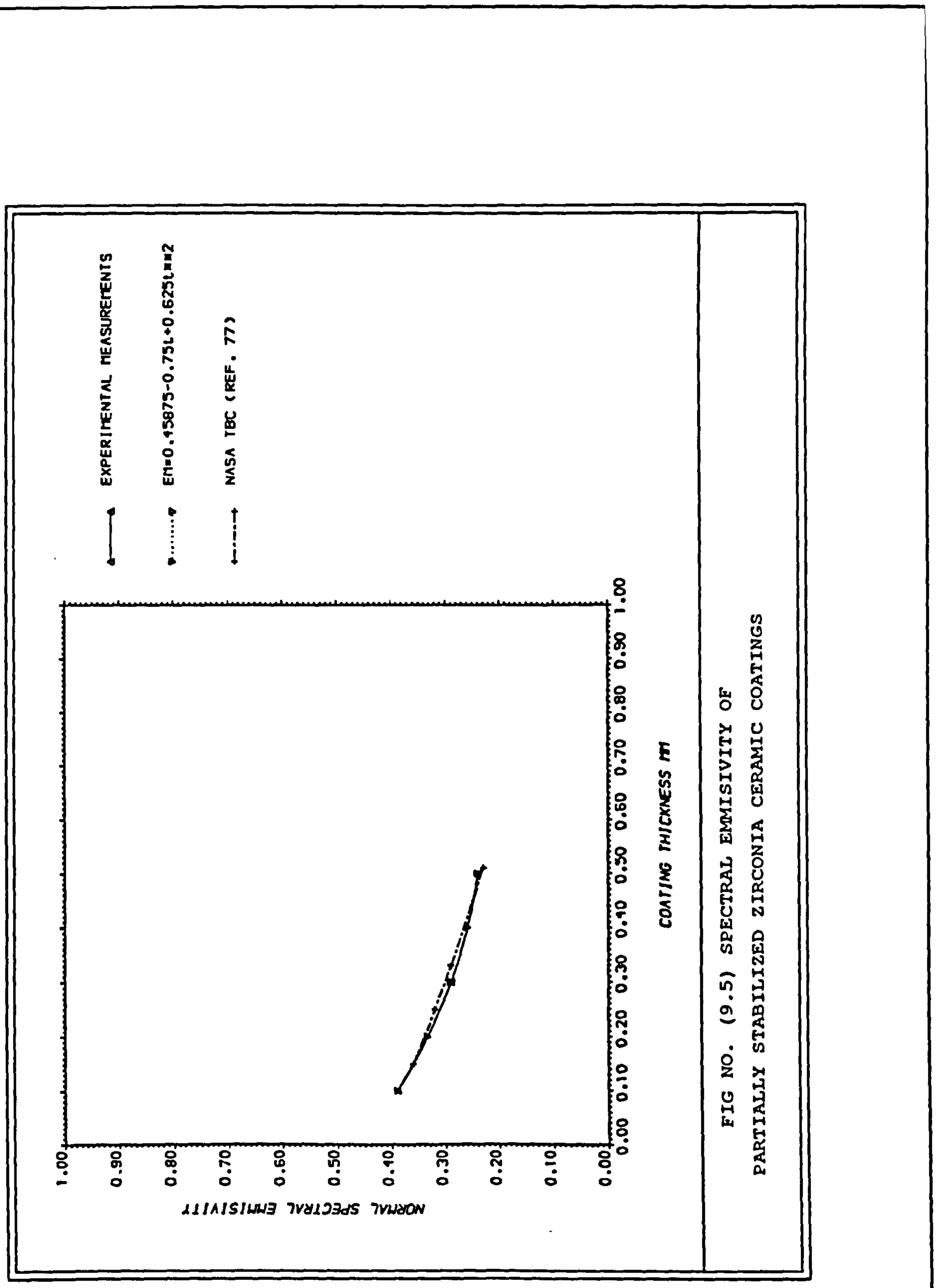

FIG NO. (9.5) SPECTRAL EMMISIVITY OF
PARTIALLY STABILIZED ZIRCONIA CERAMIC COATINGS

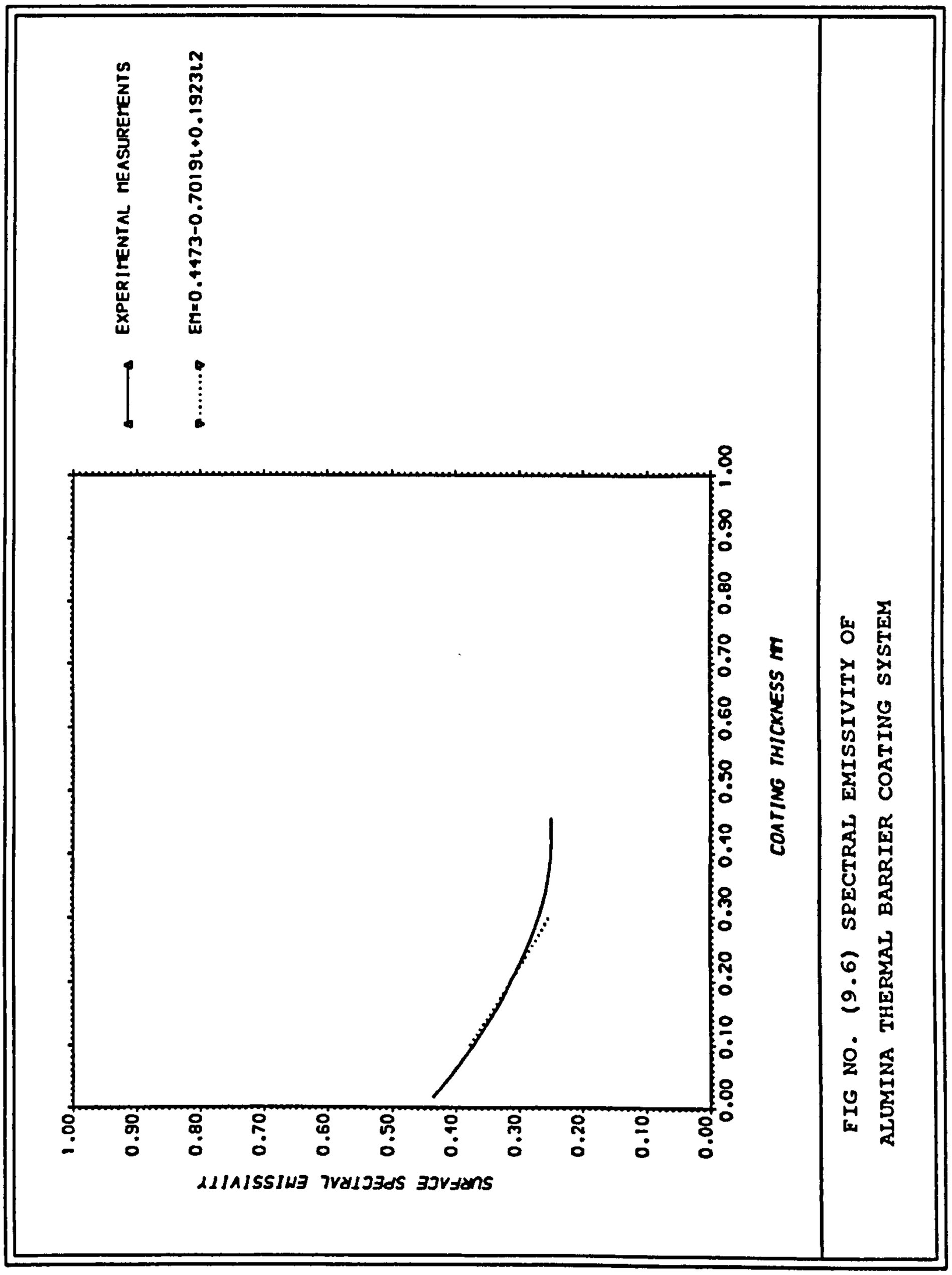

FIG NO. (9.6) SPECTRAL EMISSIVITY OF
ALUMINA THERMAL BARRIER COATING SYSTEM

CHAPTER TEN

10 BLADE SURFACE TEMPERATURE PREDICTION

10.1 Uncoated Blade

10.1.1 Theory

This section presents an approximate method for predicting uncoated blade surface temperatures of radial inflow turbines. The analytical relations used are based on the assumption that the static gas temperature follows the relation :

$$T_g = T_{1t} - C_2^2 / (2\,Cp) \qquad 10.1$$

The metal temperature differs from the static gas temperature by the temperature recovery factor (tr) meaning that :

$$T_m = T_g + tr\, W_2^2 / (2\,Cp) \qquad 10.2$$

For laminar flow with Prandtl number (Pr) smaller than 10, it holds for a flat plate that [Arnold(30)] :

$$tr = \{Pr\}^{1/2} \qquad 10.3$$

For turbulent flow the recovery factor is higher. The recovery factor increases with Reynolds number to about (6%) higher value. Balje [Ref. 78] assumes an average value of (0.85) for tr .

For the calculation of the blade metal temperature through the flow passage, the effect of the radius ratio between any position (x) and the tip position (2) i.e.(r_x/r_2) has to be considered. The expansion of the gas through the rotor channels by flowing from tip to root causes an additional temperature drop $(\Delta u^2/2\,Cp)$.

Restricting the calculations to a radial inflow rotor with an inlet angle of (90) degrees , it results that :

$$T_m/T_{in} = 1-Y\{0.15(C_2/C_0)^2(W_x/W_2)^2 + (U_2/C_0)^2[2-(r_x/r_2)^2-0.15(W_x/W_2)^2]\} \qquad 10.4$$

Where $Y = 1-(P_3/P_2)^{(\gamma-1/\gamma)}$

C_0 is called the spouting velocity

10.1.2 Results

Figure no.(10.1) shows the pyrometer scan line along which the experimental measurements were taken.

Figure no. (10.2,10.3,10.4,10.5) show the blade temperatures as predicted employing Balje equation. These figures also show the experimental results obtained for the same conditions. They show that the procedure is within (± 10) K of the experimental measurements .

In order to calculate the blade metal temperature a number of parameters need to be known. These parameters are measured. Following is a list of the measured parameters that were used in the calculation.

T_{1t} turbine entry total temperature

P_1 turbine entry total pressure

P_{s1} turbine entry static pressure

P_{s3} turbine exit static pressure

N rotational speed , and

r_x and r_2 arbitrary and blade tip radius , respectively .

Attempts were made to measure the surface temperature by using thermal paints. Figure no.(10.6) shows a calibration sample of metal temperature measurement of the paint used. Figure no.(10.7) shows the thermal paint colours before and after testing. Whilst the thermal paint exercise was successful showing that these thermal paints can be used in radial inflow machines the colour changes occur in relatively large bands and it was not possible therefore to get detail comparison although the results do not contradict the measured temperature by the radiation pyrometer or the calculated metal temperature.

10.2 Application

10.2.1 Heat Transfer Model

A simple heat transfer model is used in this section to demonstrate some of the benefits of employing TBC systems for air cooled turbine blades . This model is based on a simple one dimensional steady state heat balance through the coated blade wall . In this analysis and for simplicity it was assumed that heat convection is the dominant heat transfer between the surrounding gas and the blade surface .

Figure no. (10.8) is a schematic representation of the model . The blade wall consists of:

metallic wall ,

bond coating layer, and

ceramic coating layer .

These layers have the thicknesses L_m , L_b , and L_{cc} with the thermal conductivities K_m , K_b , and K_{cc} , respectively .

If the thermal conductivity is assumed to be a linear function of temperature, a heat balance across the composite wall results in

$$q = (T_g - T_c) / \{(1/h_g)+(L/K)_{cc}+(L/K)_b+(L/K)_m+(1/h_c)\} \qquad 10.5$$

where the boundary temperatures are given by :

$$T_1 = T_g - q/h_g$$

$$T_2 = T_1 - q\,(L/K)_{cc}$$

$$T_3 = T_2 - q\,(L/K)_b \qquad 10.6$$

and

h_g is the gas convection coefficient

h_c is the coolant convection coefficient

T_g is the gas temperature ,

T_c is the cooling air temperature ,

T_1 is the ceramic surface temperature ,

T_2 is the ceramic/bond interface temperature ,

T_3 is the bond/metal interface temperature .

In this analysis three TBC systems were compared against each other. These were C-YPSZ, 8%YPSZ and 24%MPSZ systems with thermal conductivities of 0.9, 1.3 and 1.5 W/m.K, respectively. The parameters assumed to be known in this analysis were the coolant temperature T_c; the thickness of the various layers L; and the heat transfer coefficients on the gas and coolant sides h_g and h_c, respectively. The value of these parameters were assumed to be the same as those used by Liebert et al [3]. For the sake of simplicity and to demonstrate the benefits of different TBC systems both h_g and h_c were assumed to be 'constant' (as in Ref.3) and equal to 1186 and 1915 $Wm^{-2}K^{-1}$, respectively and the coolant temperature was also assumed to be constant and equal to 811 K. The blade material thickness and the bond thickness were assumed to be equal to 1.27 mm and 0.102 mm, respectively. The blade metal thermal conductivity was 30.7 W/mK and the bond thermal conductivity was 15 W/mK.

Figure no. (10.9) shows the metal temperature reduction as function of the coating thickness for the three coatings at T_g of 1673 K. Figure no. (10.10) shows the metal temperature reduction as function of turbine entry temperature for 0.5 mm thickness of the three TBC systems. It should be noted that whilst the metal temperature is reduced when a thermal barrier coating is used the surface temperature of the ceramic TBC is actually higher than the metal temperature would have been without the presence of the TBC. Figure no. (10.11) shows both the reduction in the metal temperature and the increase in the ceramic surface temperature with coating thickness at T_g of 1673 K. Figure no. (10.12) shows the surface temperature increase as function of turbine entry temperature for 0.5 mm thickness for the three TBC systems. Whilst Figures 10.10 and 10.12 show a linear relationship between metal temperature reduction and T_g, and between surface temperature increase and T_g, respectively, Figures 10.9 and 10.11 show nonlinear relationship between surface temperature increase and coating thickness and between metal temperature decrease and coating thickness.

So for a typical thickness of 0.30 mm of C-YPSZ TBC system the blade metal temperature can be reduced by about 260 K at TET of 1673 K. For turbine blades that are limited by creep life this metal temperature reduction means a 17 fold increase in the blade creep life.

10.2.2 Optical Model

The radiation recorded by the radiation pyrometer depends on the amount of radiation the blade reflects from the flame, the view factor between the blade and the flame besides the blade metal temperature and emissivity. The analysis below seeks to quantify this.

The intensity of radiation from a black body is given by Wien's approximation as follows:

$$E_\lambda \cong (C_1 / \lambda^5) / EXP\ (C_2 / \lambda\ \ T) \qquad 10.7$$

Where $C_1 = 3.7420 \times 10^8\ W.\mu^4.m^{-2}$

$C_2 = 1.4388 \times 10^4\ \mu.K$

T = black body temperature (K)

λ = wavelength of the measurement (μ)

Equation no. (10.7) can be rewritten as

$$E_\lambda \cong A\ \ EXP\ (-B/T) \qquad 10.8$$

Where $A = C_1 / \lambda^5$

$B = C_2 / \lambda$

If the spectral emissivity of a body is (ε) then the spectral radiation from this body is :

$$E_\lambda \cong \varepsilon\ A\ EXP\ (-B/T) \qquad 10.9$$

Let the subscripts f , v , and b denote the flame , vane and blade respectively . Then the spectral radiation emitted by the flame , vane and blade are :

$$E_\lambda(T_f) \cong \varepsilon_f\ A\ EXP\ (-B/T_f)$$

$$E_\lambda(T_v) \cong \varepsilon_v\ A\ EXP\ (-B/T_v)$$

$$E_\lambda(T_b) \cong \varepsilon_b\ A\ EXP\ (-B/T_b) \qquad 10.10$$

Let V_f be the view factor of the flame by the vane and V_v be the view factor of the vane by the blade .

Then the intensity of radiation from the flame that reaches the vane is :

$$E_\lambda'(T_f) = V_f\ E_\lambda(T_f) \qquad 10.11$$

And the intensity of radiation from the flame that is reflected by the vane is :

$$E_\lambda''(T_f) = (1-\varepsilon_v)\ E_\lambda'(T_f) \qquad 10.12$$

So the total radiation that leaves the vane is :

$$E_\lambda'(T_v) = E_\lambda(T_v) + E_\lambda''(T_f) \qquad 10.13$$

And the total radiation that reaches the blade from the vane is :

$$E_\lambda''(T_v) = V_v\ \ E_\lambda'(T_v) \qquad 10.14$$

And the amount of this that is reflected by the blade is :

$$E_\lambda'''(T_v) = (1-\varepsilon_b)\ E_\lambda''(T_v) \qquad 10.15$$

Thus the total radiation emitted by the blade is :

$$E_\lambda'(T_b) = E_\lambda(T_b) + E_\lambda'''(T_v) \qquad 10.16$$

The radiation that reaches the pyrometer depends on the radiation emitted by the blade ,that reflected by it and on the lens transmittance . that is :

$$E_\lambda''(T_b) = t_l\ E_\lambda'(T_b) \qquad 10.17$$

Where t_l is the lens transmittance .

This is true if the intervening media does not absorb or emit any radiation .

Equation no. (9.17) can be expanded to :

$$E_\lambda''(T_b) = t_\ell \{E_\lambda(T_b) + (1-\varepsilon_b) \quad V_v [E_\lambda(T_v) + (1-\varepsilon_v) V_f E_\lambda(T_f)]\} \qquad 10.18$$

Figure no. (10.13) shows the effect of flame view factor on the observed blade temperature for different vane view factors. And Figure no. (10.14) shows the error introduced in the observed temperature for different lens contamination .

These calculations were made based on an assumed constant parameters to give an indication of the effect on the pyrometer signal. These parameters were:

T_f = 2300 K , ε_f = 0.8;

T_v = 1200 K , ε_v = 0.85; and

T_g = 1673 K , ε_b = 0.85

As a conclusion to this section, if the radiation is measured from the first stage turbine blades and the combustor is short and the flame is highly radiant then the error involved in measuring blade metal temperature using this technique can be large. Under these circumstances it would be then necessary to try to reduce this error by for instance measuring the radiation from first stage turbine blading from the trailing edge of the blading so that the flame view factor is very low at that point and also the view factor from the NGV is very low.

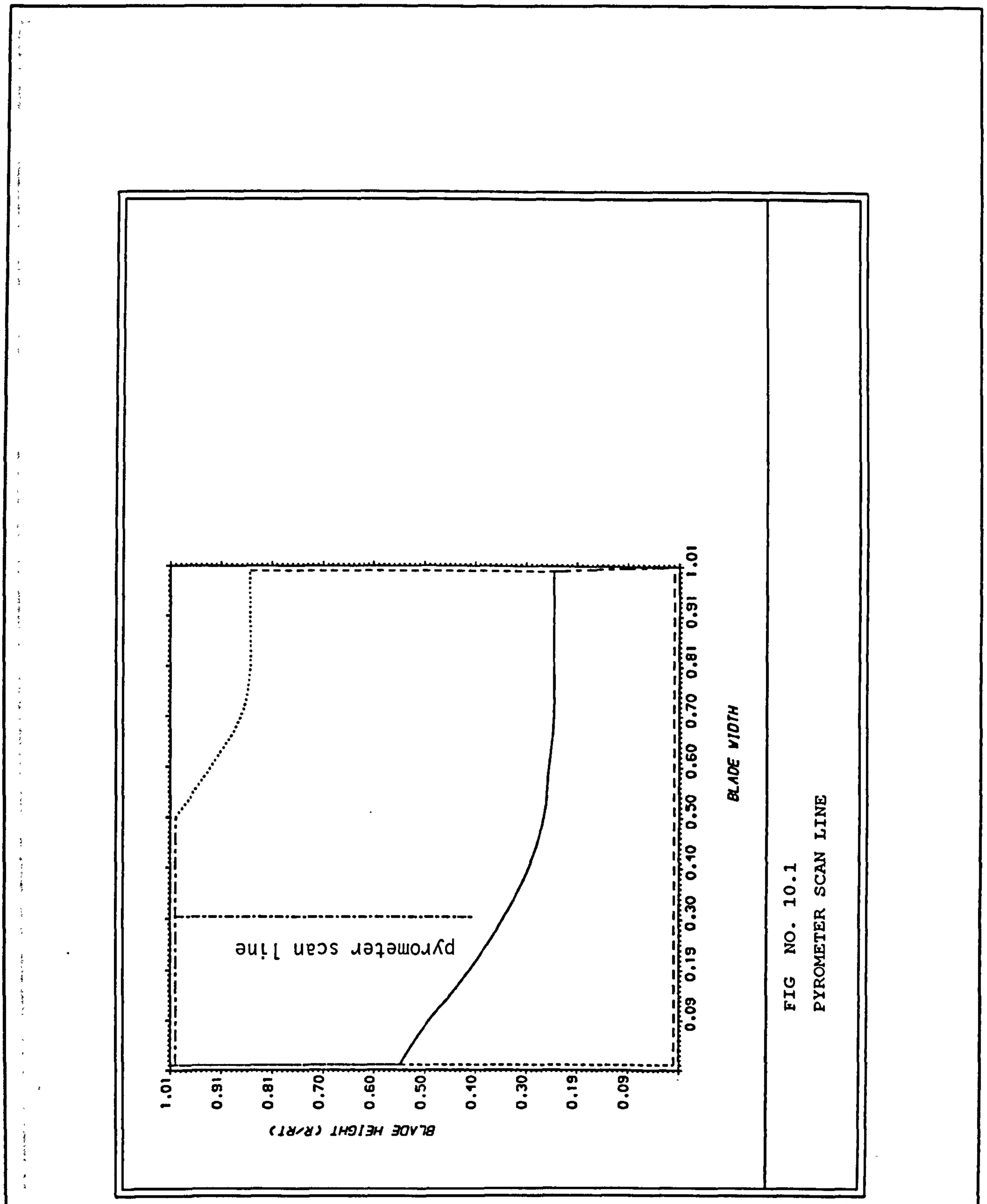

FIG NO. 10.1
PYROMETER SCAN LINE

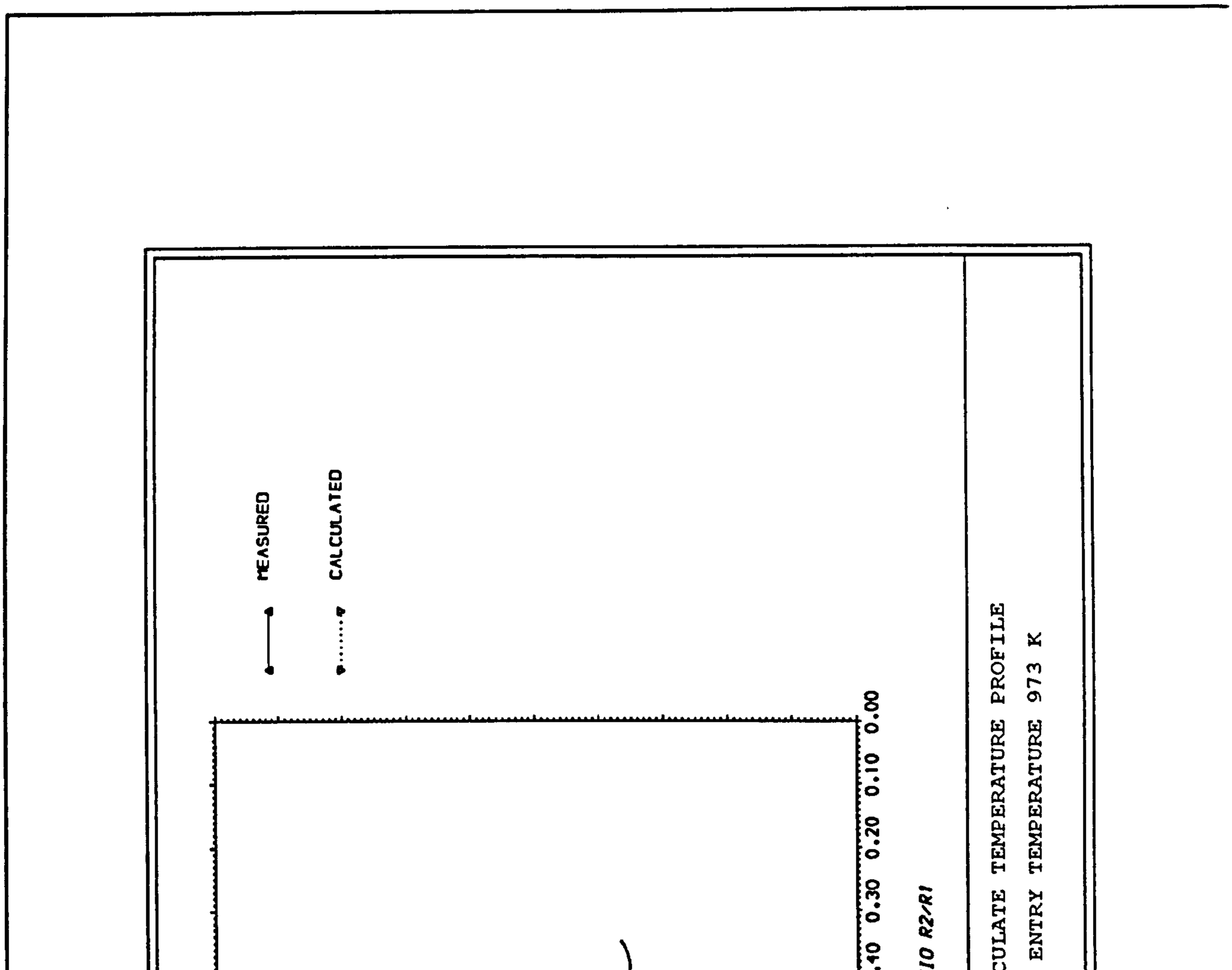

FIG NO. 10.2 MEASURED AND CALCULATE TEMPERATURE PROFILE
OF UNCOATED BLADE AT TURBINE ENTRY TEMPERATURE 973 K

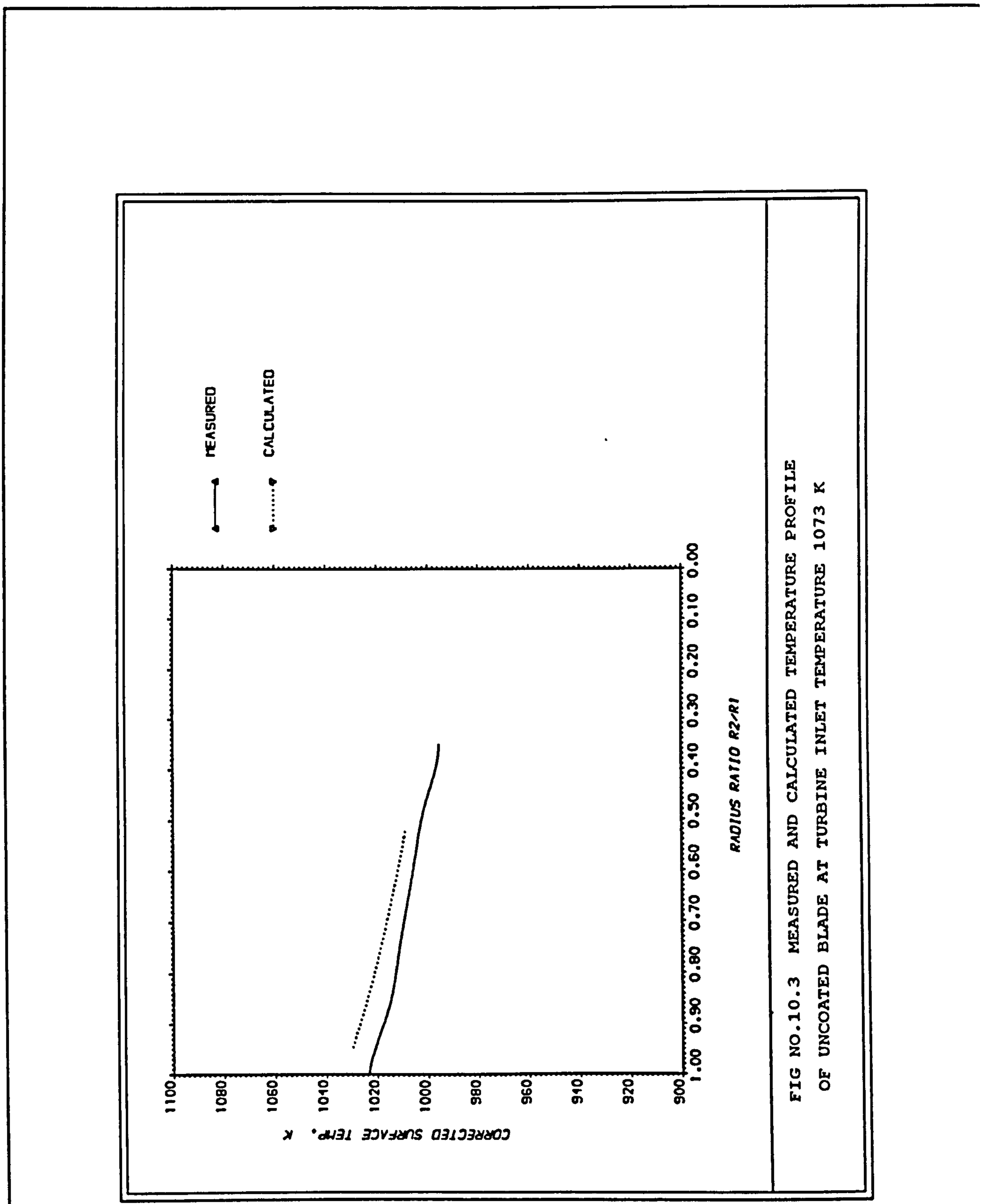

FIG NO.10.3 MEASURED AND CALCULATED TEMPERATURE PROFILE OF UNCOATED BLADE AT TURBINE INLET TEMPERATURE 1073 K

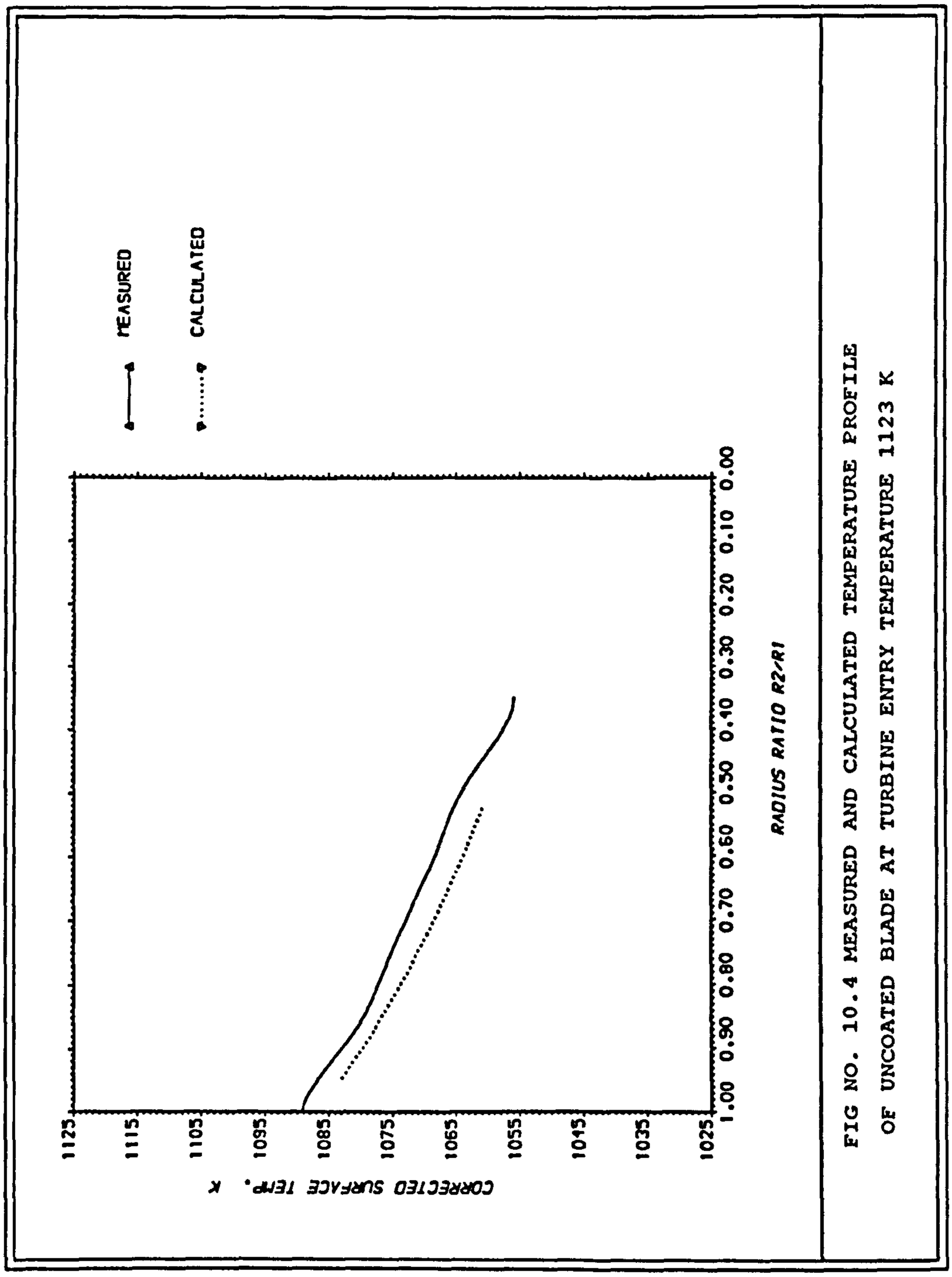

FIG NO. 10.4 MEASURED AND CALCULATED TEMPERATURE PROFILE OF UNCOATED BLADE AT TURBINE ENTRY TEMPERATURE 1123 K

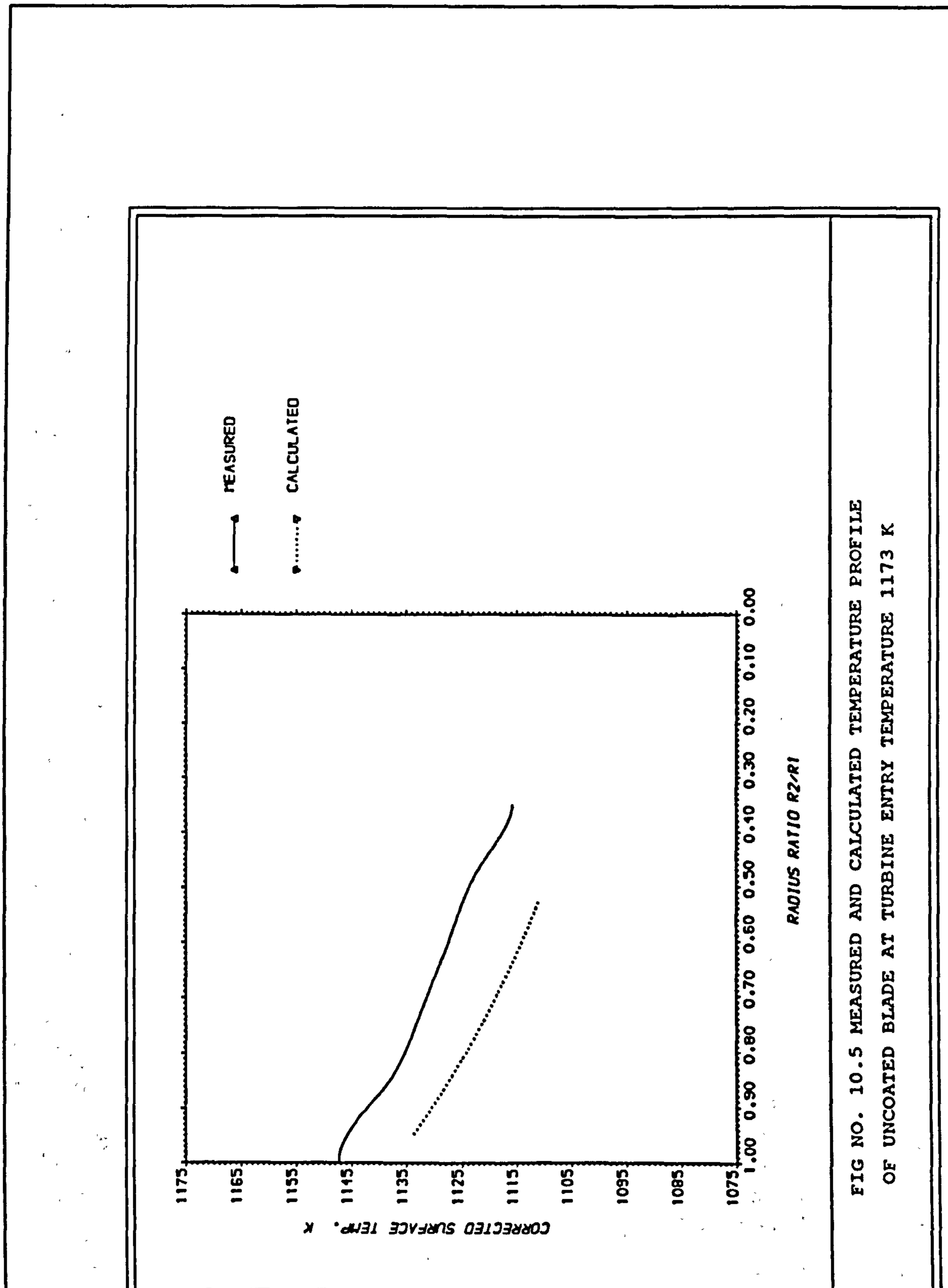

FIG NO. 10.5 MEASURED AND CALCULATED TEMPERATURE PROFILE OF UNCOATED BLADE AT TURBINE ENTRY TEMPERATURE 1173 K

Fig.(10.6) Thermal Paint Sample

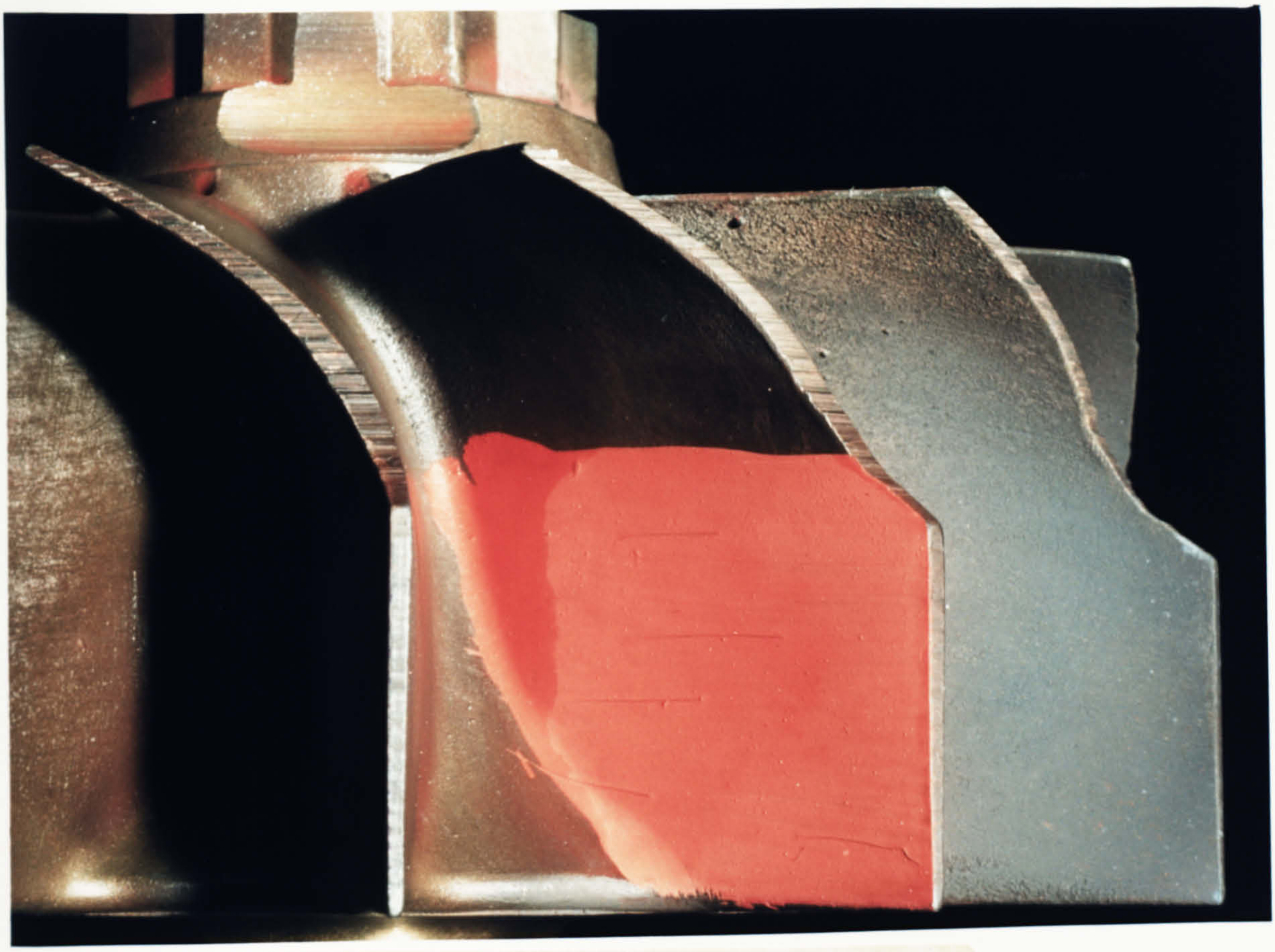

Fig.(10.7) Thermal Paint Before and After Testing at TET of 1073 K

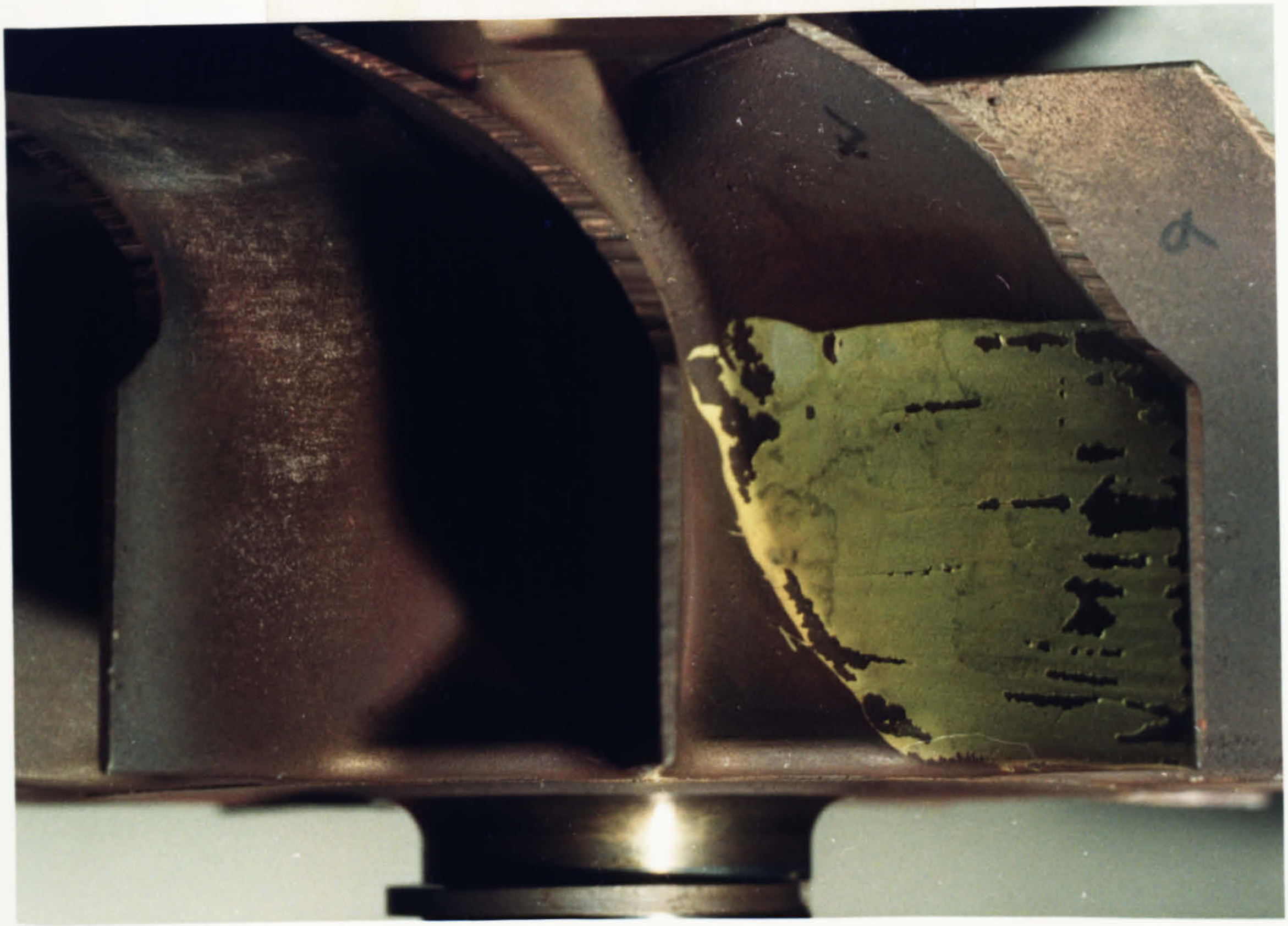

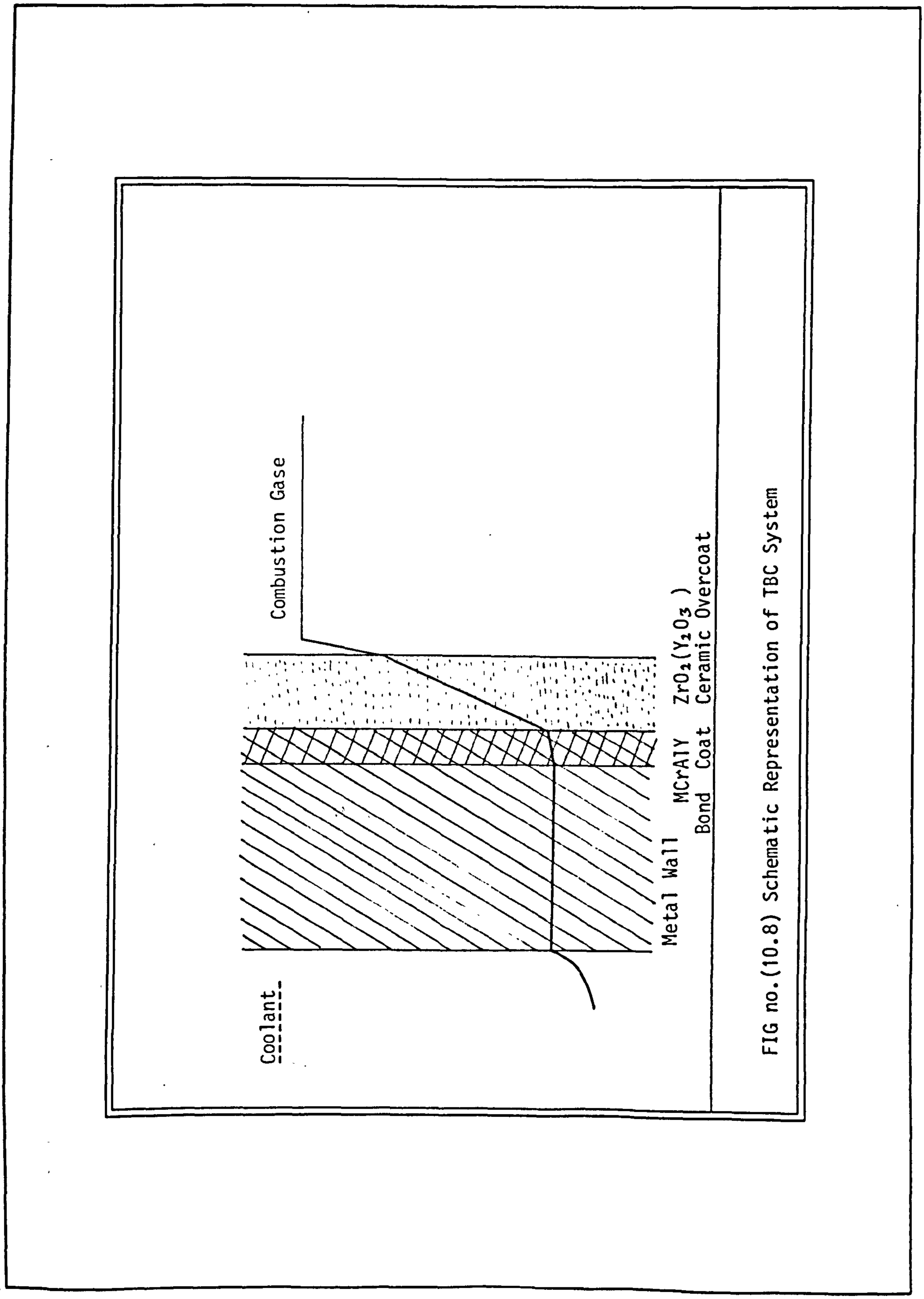

FIG no.(10.8) Schematic Representation of TBC System

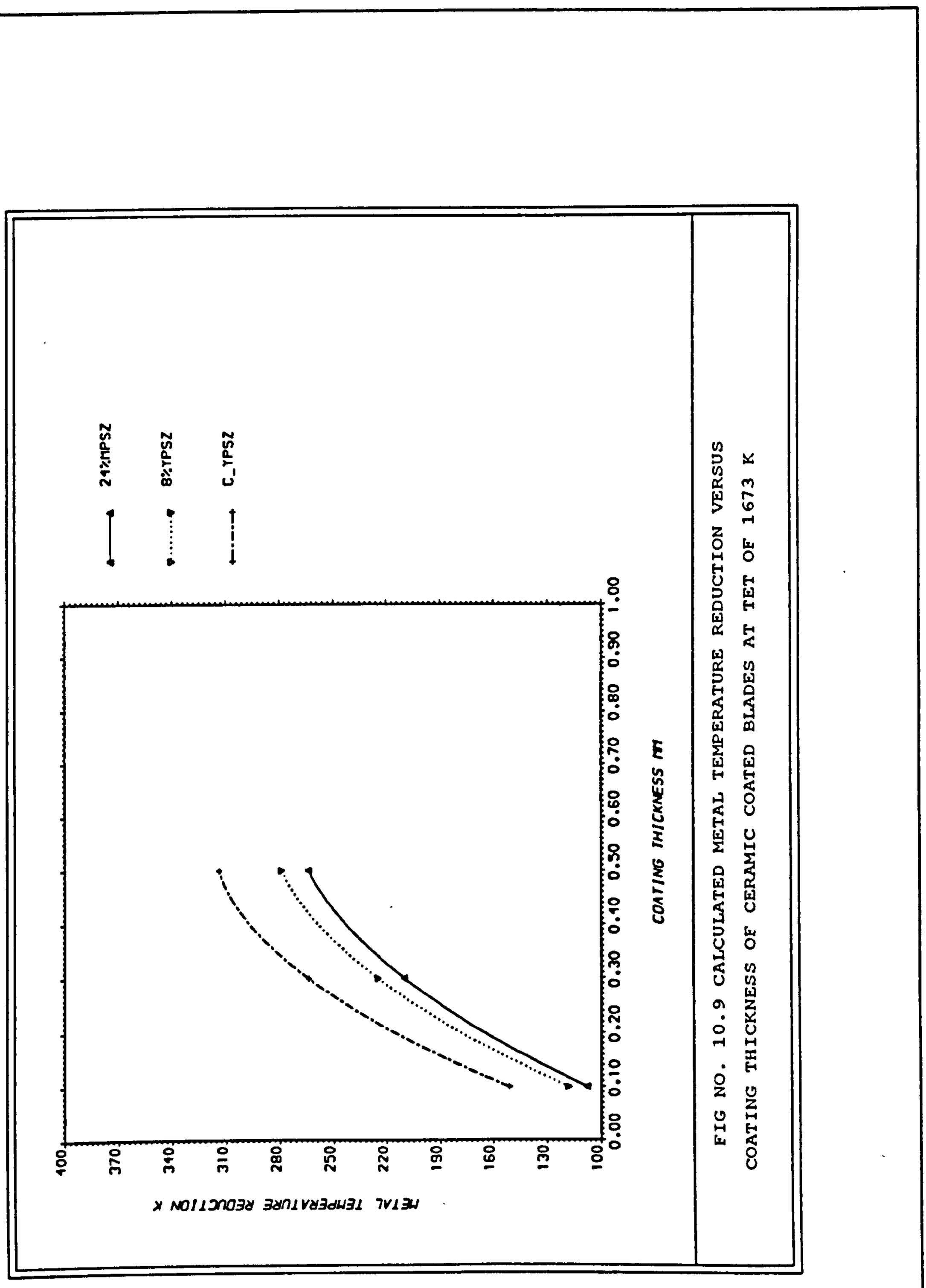

FIG NO. 10.9 CALCULATED METAL TEMPERATURE REDUCTION VERSUS COATING THICKNESS OF CERAMIC COATED BLADES AT TET OF 1673 K

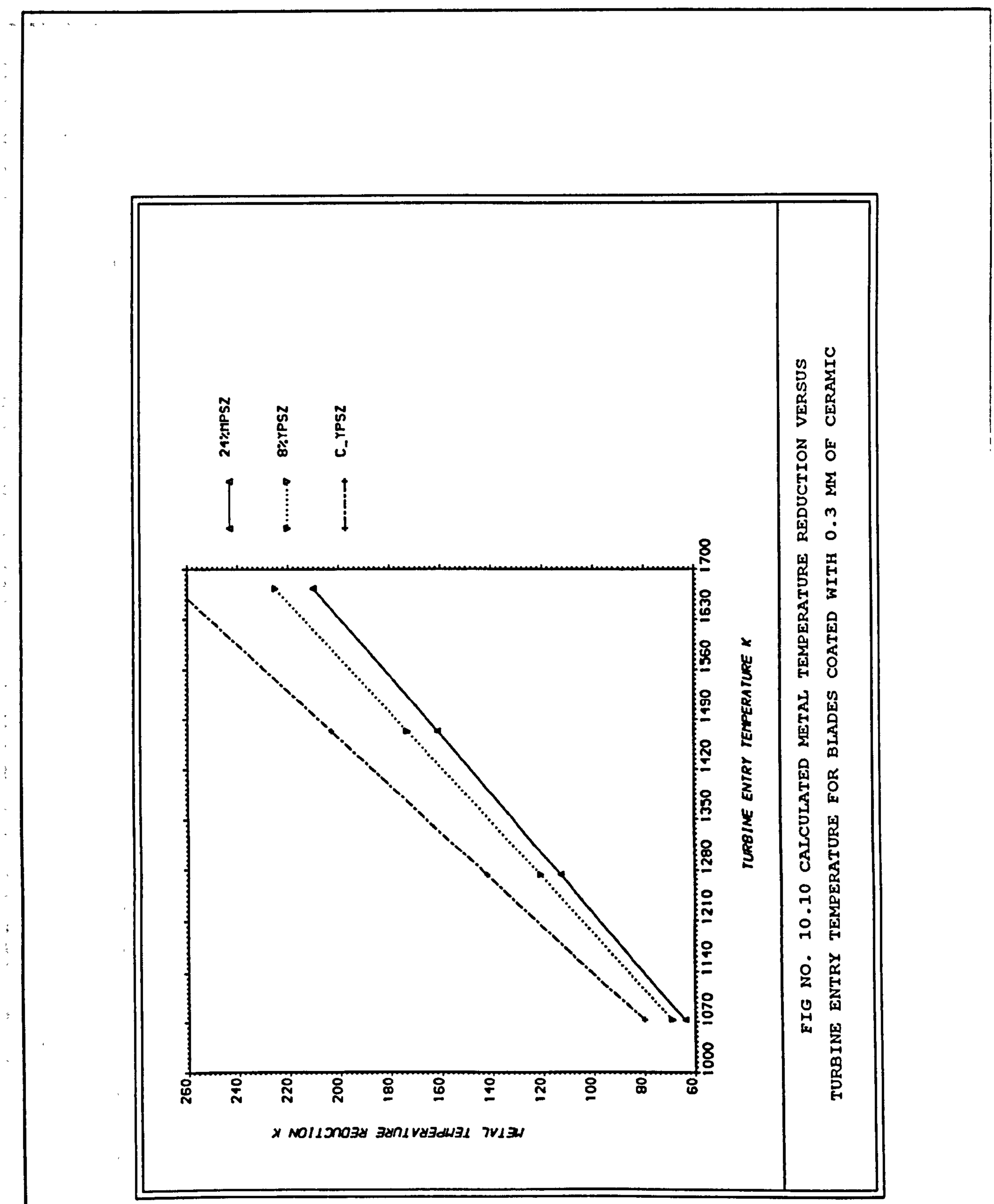

FIG NO. 10.10 CALCULATED METAL TEMPERATURE REDUCTION VERSUS TURBINE ENTRY TEMPERATURE FOR BLADES COATED WITH 0.3 MM OF CERAMIC

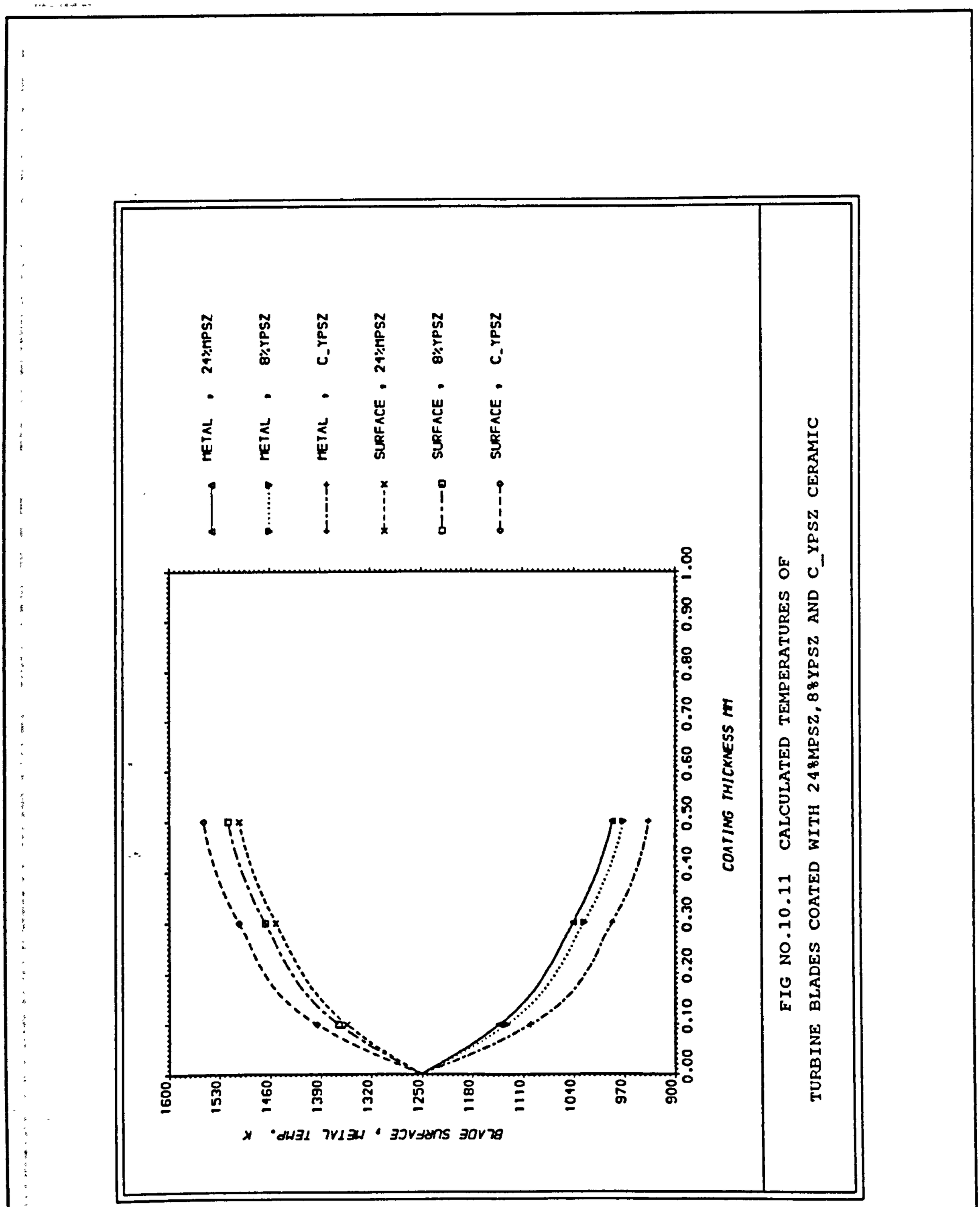

FIG NO. 10.11 CALCULATED TEMPERATURES OF TURBINE BLADES COATED WITH 24%MPSZ, 8%YPSZ AND C_YPSZ CERAMIC

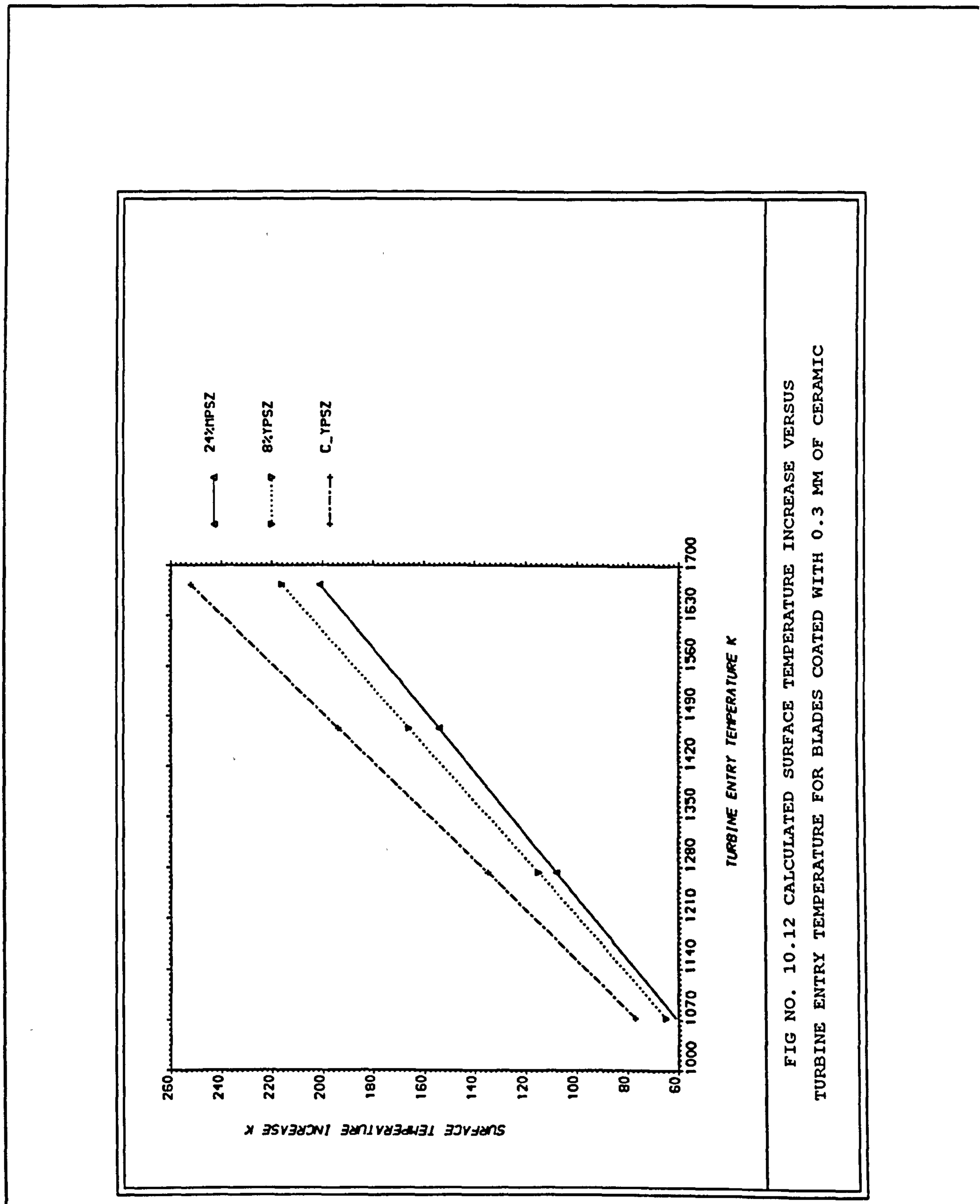

FIG NO. 10.12 CALCULATED SURFACE TEMPERATURE INCREASE VERSUS TURBINE ENTRY TEMPERATURE FOR BLADES COATED WITH 0.3 MM OF CERAMIC

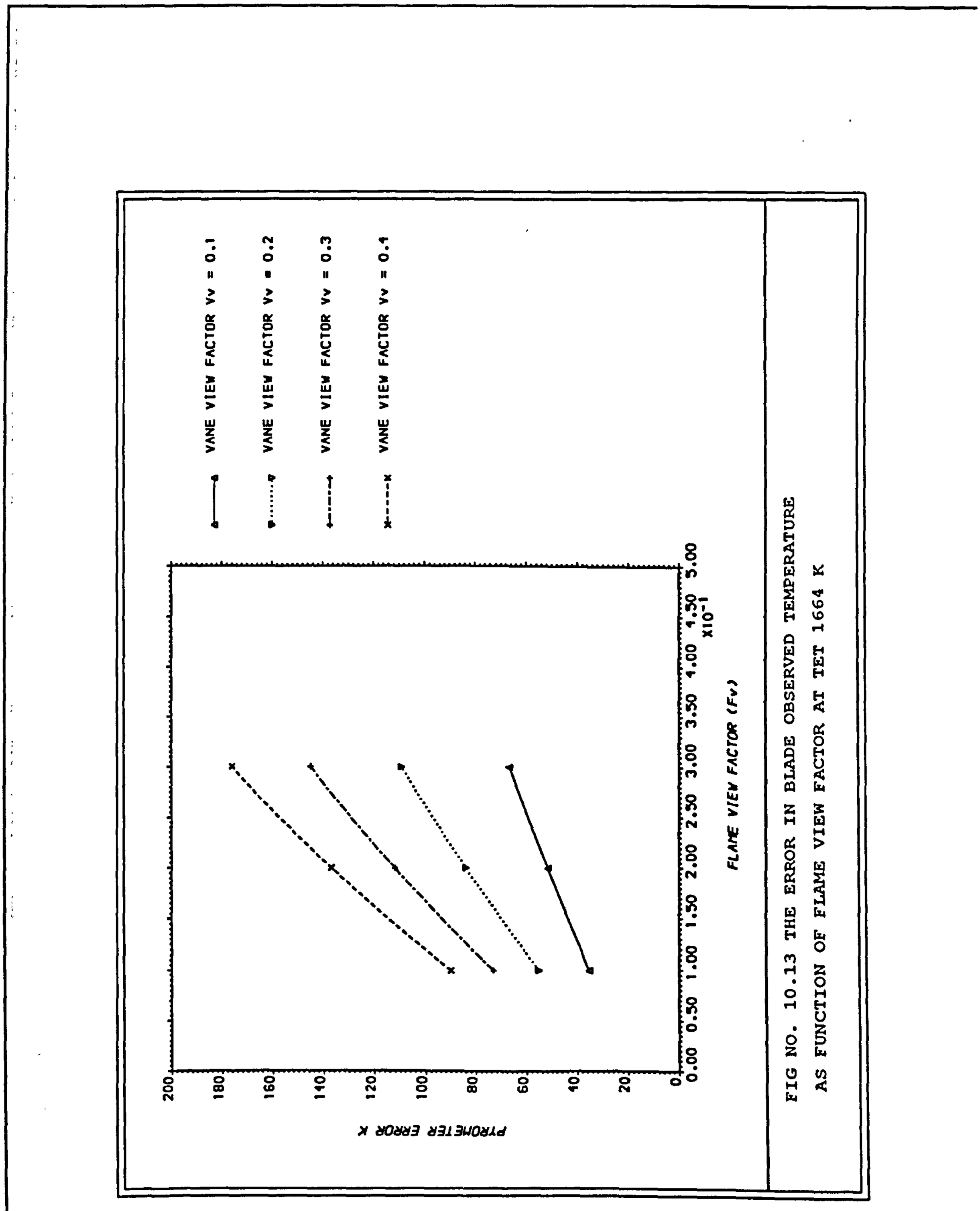

FIG NO. 10.13 THE ERROR IN BLADE OBSERVED TEMPERATURE
AS FUNCTION OF FLAME VIEW FACTOR AT TET 1664 K

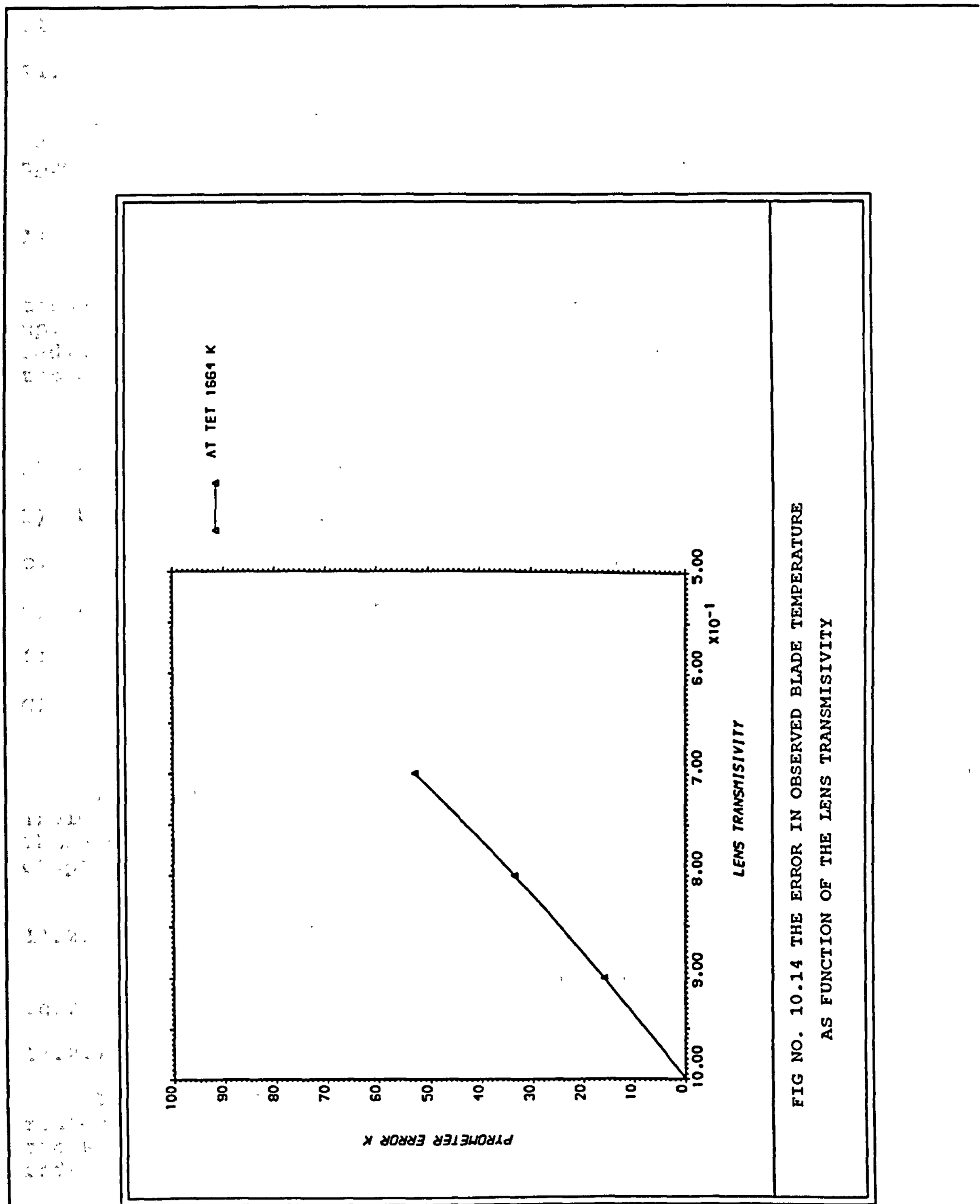

FIG NO. 10.14 THE ERROR IN OBSERVED BLADE TEMPERATURE AS FUNCTION OF THE LENS TRANSMISIVITY

CHAPTER ELEVEN

11 Pyrometer Analysis

11.1 Introduction

Chapter three presents the possible sources of error in radiation pyrometry in general. This chapter presents the specific sources of error experienced in this investigation .

11.2 Pyrometer Specific Errors

The radiation pyrometer picks up the radiation from the target area on the blade surface and from the radiation picked up, it derives the blade surface temperature. Any change in the radiation intensity will be translated as change in surface temperature .

The intensity of radiation is affected by the following :

a) blade surface temperature ,

b) blade emissivity ,

c) absorption and emission by the intervening media ,

d) emission from gas born particles ,

f) reflected radiation , and

g) lens contamination .

The parameters (b) to (g) are sources of error for the indicated blade surface temperature parameter (a). The effect of these parameters on the pyrometer read out is analysed in this chapter.

11.2.1 Blade Emissivity

In the arrangement of the coatings on the turbine wheels, there exist blades with coatings and blades without .

11.2.1.1 Uncoated Blades

It was stated in chapter nine and according to the radiometric method, the surface emissivity is the ratio between the surface emittance at a certain temperature to that of a black body at the same temperature.

The main problem with the emissivity of uncoated turbine blades stems from the uncertainty of the nature of the surface of the blade once it is in operation. The emissivity is then not only function of the blade material but, depends on the operating environment, usage time, operating history, etc .

The turbine blade material is "inconel 713C". This is a high nickel alloy. Fortunately, this type of material once in operation, it has a stabilized emissivity of 0.8-0.85 [Kirby(79) and Harman(80)] .

The use of silicon detectors for turbine pyrometry systems minimizes the effect of uncertainty in blade emissivity . For example, at a metal temperature of 1,000 K, a 10% error in emittance results in less than 1% error in the indicated temperature [Barber(29)].

11.2.1.2 Coated Blades

The emissivity of TBC systems depends on :

a) substrate material ,

b) bond coat material ,

c) bond coat thickness ,

d) coating material ,

e) coating thickness ,

f) coating surface roughness and ,

g) method of application .

Chapter eight presented the TBC systems employed in this investigation, their method of application was also presented .

11.2.1.2.1 Coating Thickness Measurements

The application method used for applying the coatings was completely automated. There was a little control on the coating thickness. The only way to do that was to calibrate the number of passes against the coating thickness. Due to the fact that the turbine blades are complex in geometry and the calibration was done on flat plates, this calibration did not achieve accurate results.

The coating thicknesses were measured employing a micrometer. Each measurement was repeated several times to minimize uncertainty .

11.2.1.2.2 Surface Roughness

For the same reasons mentioned above, the only way to control surface roughness is to change the spraying parameters. Although the same spraying parameters were used for applying all the coatings, the surface roughness of all the blades was relatively in the narrow range 9.03 to 11.10 micrometers.

Figure no. (11.1) shows the computer driven surface analysis laboratory used in this investigation. It was used to measure the surface roughness of :

a) Substrate surface. Before the application of the bond coat, the blades were blasted by chilled iron balls G24 at an air pressure of about 60 psig. This was necessary to produce a rougher surface in order to obtain better adhesion. The mean RMS of the substrate was 13.0 micrometers. Figure no. (11.2) shows a three dimensional and a two dimensional plots of this surface .

b) Bond coat. A 0.16 mm bond coat of NiCrCoAl_Y2O3 was applied. The mean RMS of the bond coat was 11.62 micrometers. Figure no. (11.3) is a three dimensional and a two dimensional plots of this surface .

c) Ceramic coatings. Next the ceramic coatings were applied. The final surfaces of TBC systems had a mean RMS of 9.03 to 11.10 micrometers.

Figures (11.4) and (11.5) are plots of the three dimensional and the two dimensional plots of a 9.03 and an 11.10 micrometers RMS surfaces .

Figures (11.2,11.3,11.4 and 11.5) show the variation in surface roughness of different surfaces. It also shows the distribution of the roughness in each of the surfaces. They also show that the maximum roughness of sprayed coatings is about 11.0 micrometers. These surfaces are considered to be smooth when compared with the surface roughness of turbine blades that have been in service. The mean RMS of a turbine blade being in operation has a value of about 44.0 micrometers. That was nearly four times as rough as the newly coated surfaces [Taylor(81)] .

11.2.2 Emissivity Measurements

The method and the results of the emissivity measurements are presented in chapter nine. Appendix (A) presents the method of surface temperature measurements .

11.3 Intervening Media

One of the advantages of using a silicon detector is its operating waveband. It detects radiation between 0.4 and 1.2 micrometers. This waveband should avoid the emission bands from the CO2 and from water vapour, Figure no. (3.8) chapter three.

11.4 Radiation from Gas Borne Particles

Gas borne particles almost always exist in combustion products. They cause , when caught in the sight path , massive spikes in the radiation profile . These spikes vary in length and size according to the carrier gas velocity and to the size of the particles cloud .

Spikes are normally hotter than the blade surface under view so they cause a positive bias in the radiation signal . This positive bias can be dealt with according to their frequency of occurrence .

a) When the size of the spike is less than the size of one blade profile . This is the dominant type of spikes . In this case , an electronic filter could be used to eliminate them from the main blade signal ,References [48,49,50,51] .

b) When the size of the spike is larger than one blade profile. This type is usually caused by clouds of hot particles. Figure no.11.6 shows the effect of a (hot) cloud on the pyrometer signal. This signal was picked up at a turbine entry temperature of 1173K.

11.5 Lens Contamination

The pyrometer lens is liable to contamination from the gas borne particles impinging on it. This is due to the fact that the pyrometer has to view the target blade. This is one of the main problems that limit the use of radiation pyrometry .

The usual solution to this problem is the design of a purge system to minimize contamination between cleaning periods. References [6,15,31,33] give some of the approaches to the best designs of purge systems .

The amount of contamination experienced by the pyrometer lens depends to a large extent on the following :

1) fuel type ,

2) fuel injector design ,

3) engine mode of operation ,

4) operating time ,

5) the purge system used and ,

6) the position of the lens in the gas stream .

The design of the purge system used in this investigation was outlined in chapter seven. The pyrometer lens was checked after each run, and no contamination was found. Each run normally takes 60 minutes from start up to shut down. The lens was also checked after ten such runs, there was hardly any contamination .

11.6 Reflected Radiation

The system used in this investigation was to coat the pressure surface of every other blade. One of the advantages of this is that the coated blade surface temperature is higher than the facing suction surface temperature of the opposite blade .

The pyrometer was positioned in such a way to avoid radiation from the flame. The casing temperature was much cooler than the blade surface temperature, as can be seen from Figure no. (11.7). This figure shows the casing metal temperature as function of turbine entry temperature .

11.7 Other Sources of Error

11.7.1 Filter Error

The temperature profiles obtained for the blade surface were very "noisy". The maximum noise level was experienced at the lowest detectable surface temperatures. The higher the turbine entry temperature, the lower was the noise level .

This type of noise was related to engine vibration and to electrical noise. The former was due to the sliding movement between the insulation and the core of the connections caused by vibration, Whilst the latter is the electricity mains noise .

A "low pass" filter was used to eliminate this high frequency noise. Figures (11.8 and 11.9) are two plots of one signal before and after applying the filter, respectively .

The effect of this filter is 3 K reduction in the blade tip temperature .

11.7.2 Sensor Errors

This type of error stems from uncertainties associated with the detector electronics. One uncertainty is that the pyrometer output needs to be linearized with the detected temperature. Figure no. (3.11) shows the detector output before and after linearization (chapter three).

The sensor error is taken to be 3 K in the range of 873 to 1473 K [Ref. 6]. Whilst the calibration error is about 10 K in this temperature range (chapter three)

11.8 Error Summary

*sensor error is 3 K

*calibration error is 10 K

*filter error is 3 K

*error due to lens contamination is 1 K

*The emissivity error comes merely from uncertainties in coating thickness measurements. This uncertainty is assumed to be 50 micrometers. This produces about 6% error in surface emissivity, which in turn produce less than 1% error in the indicated temperature.

The root sum square error in the indicated blade surface temperature is about 15 K. This error is calculated for a gas temperature of 1000 K.

Fig. (11.1) Surface Analysis Lab.

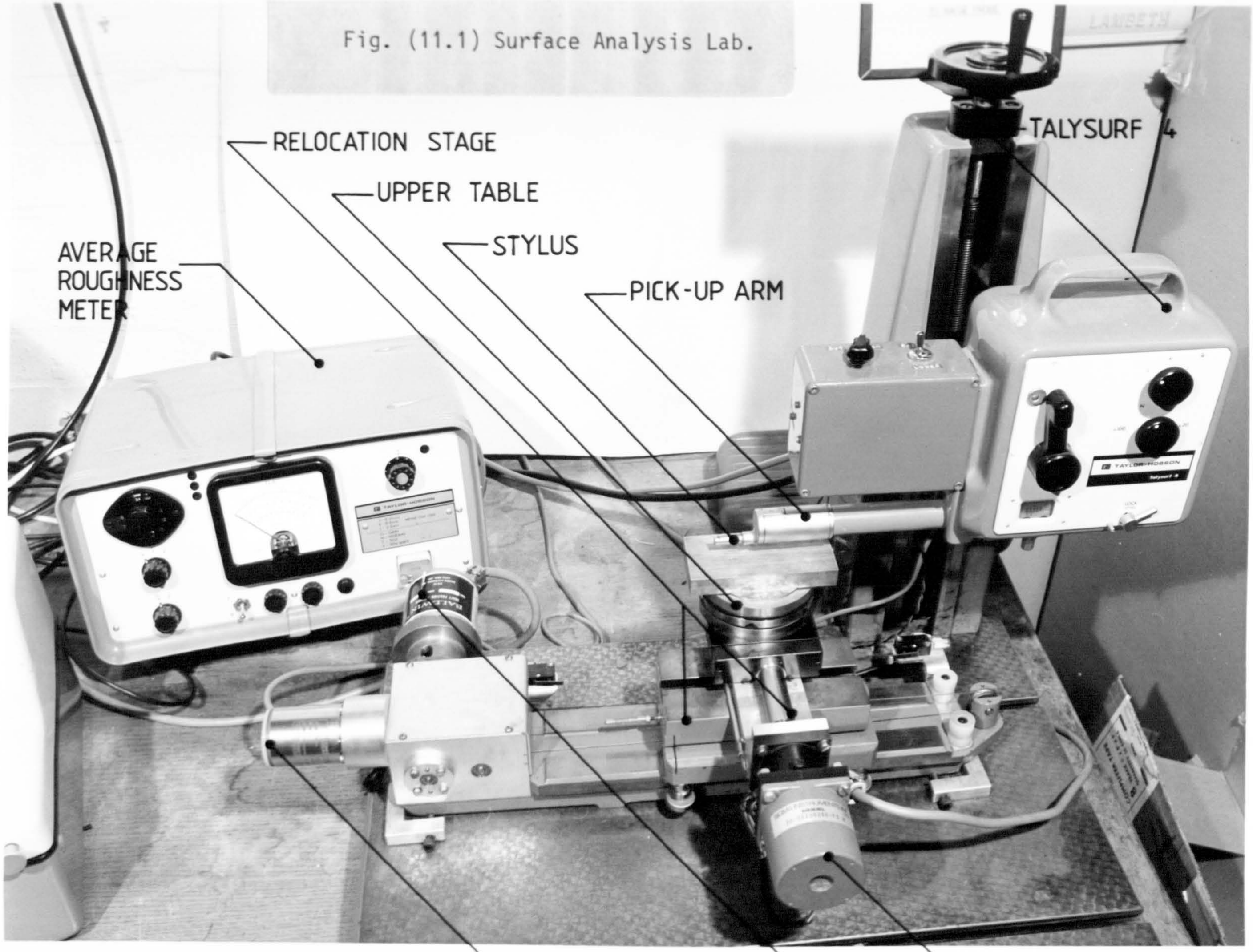

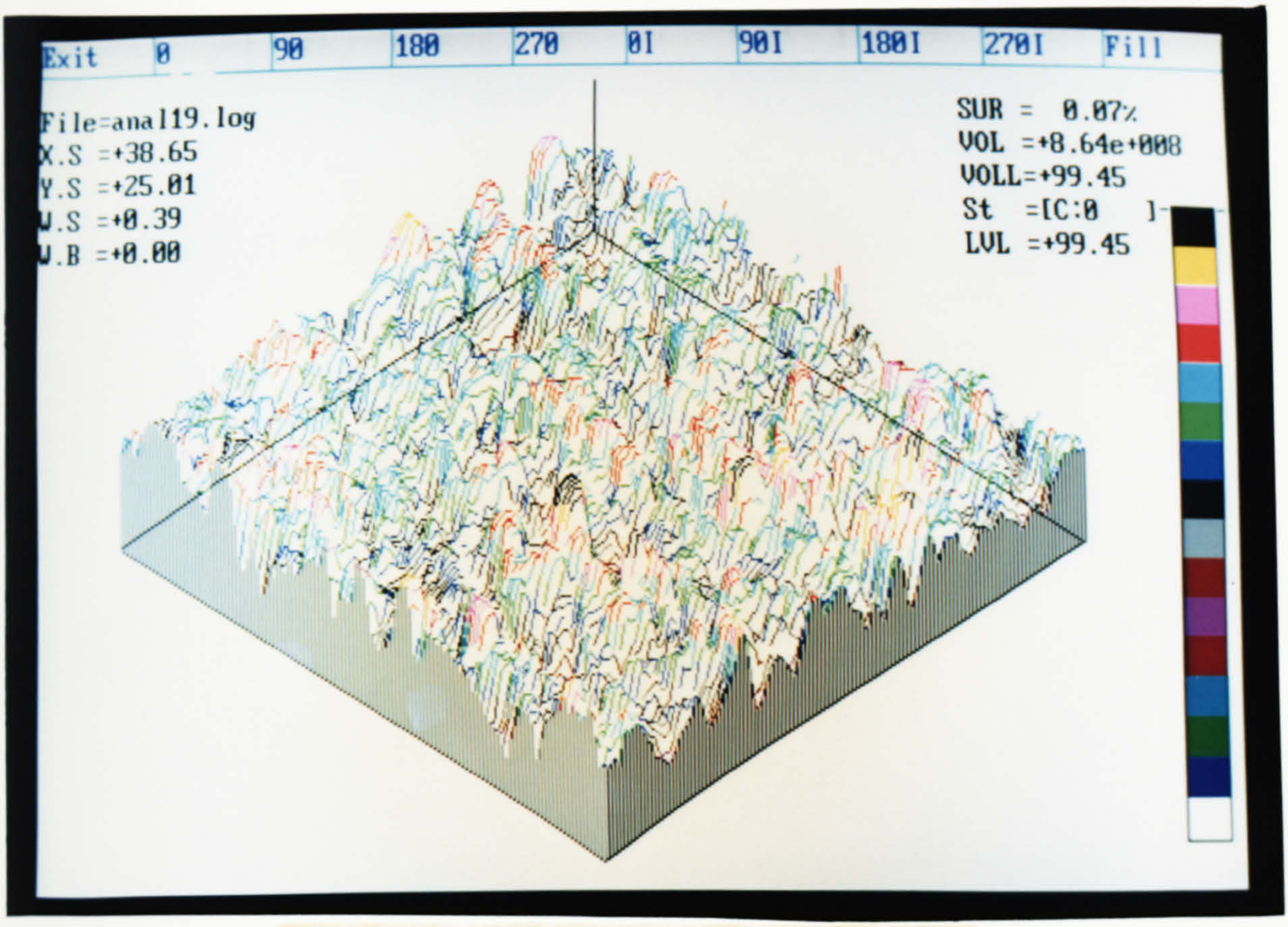

Fig. (11.2) Surface Analysis of Blasted Specimen

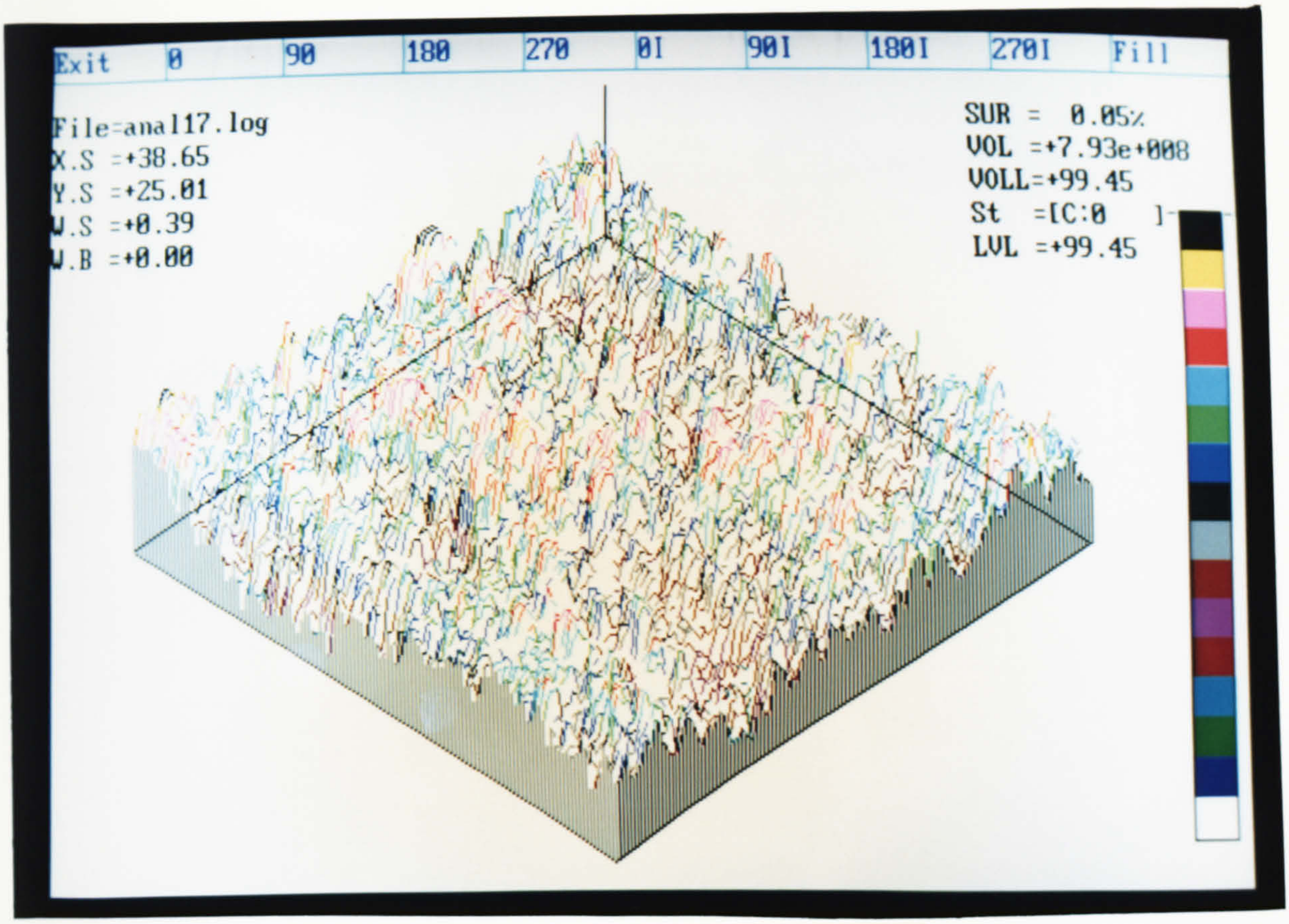

Fig. (11.3) Surface Analysis of
Bond Coated Specimen

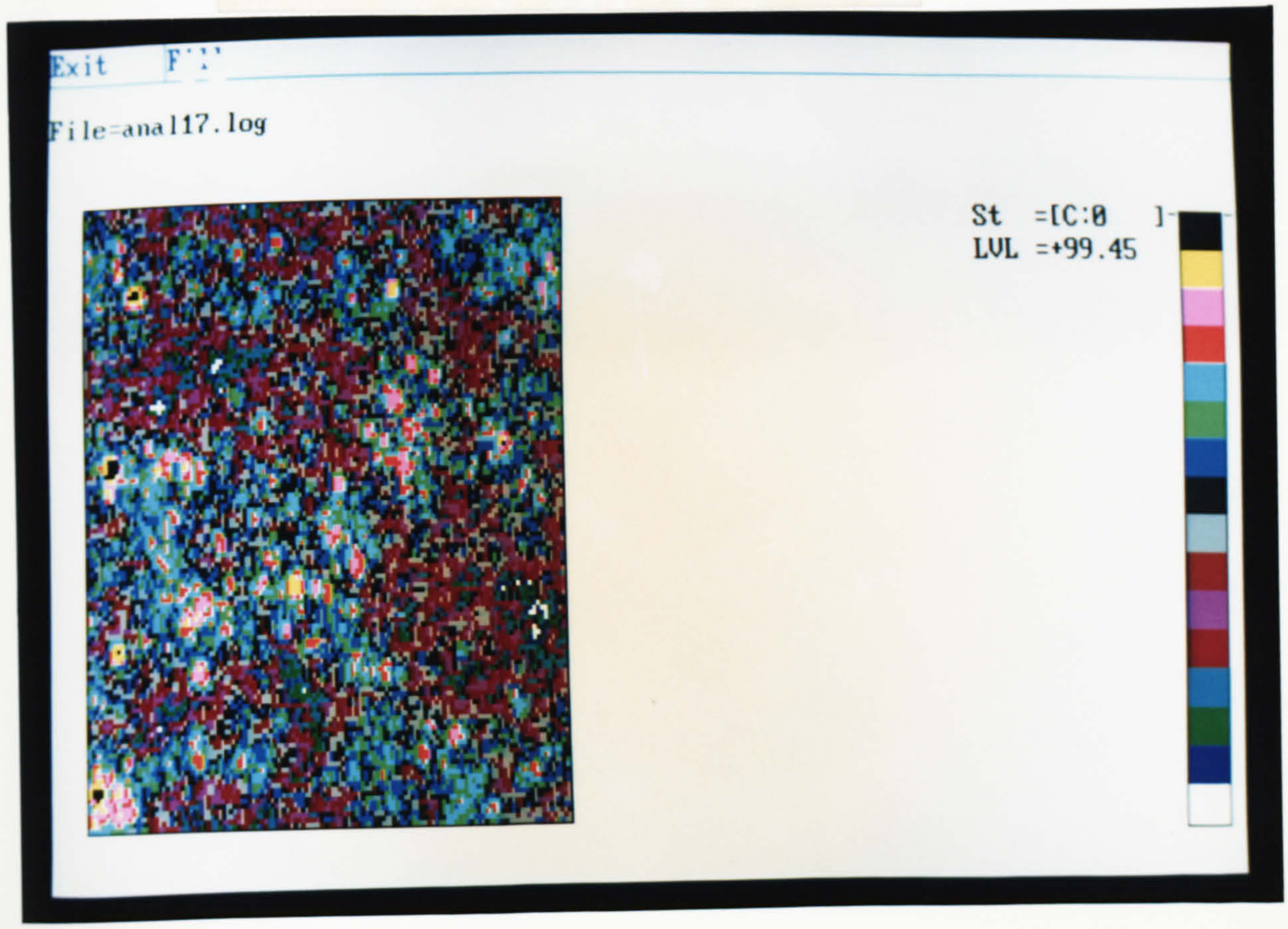

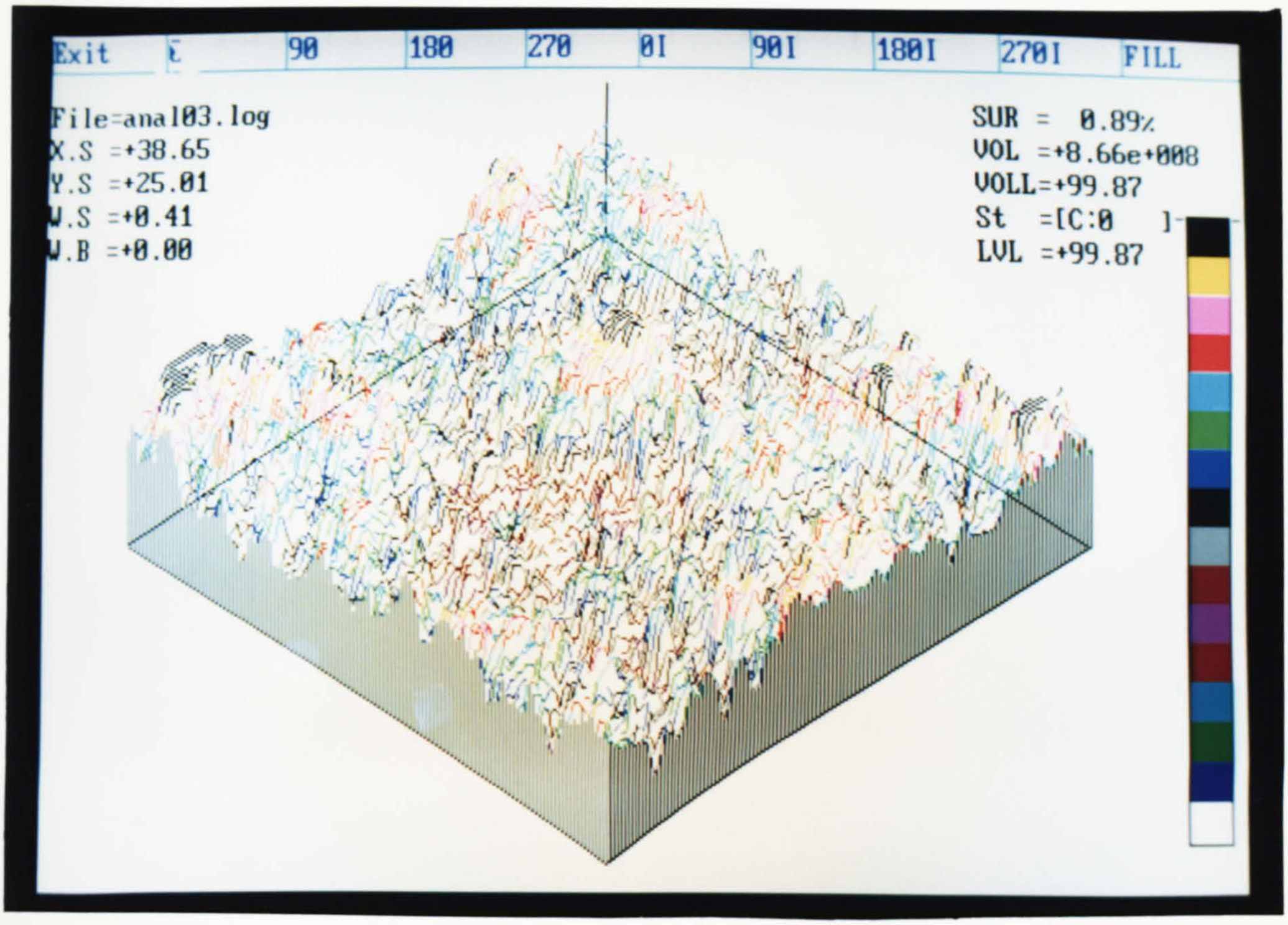

Fig. (11.4) Surface Analysis of TBC Coated Specimen

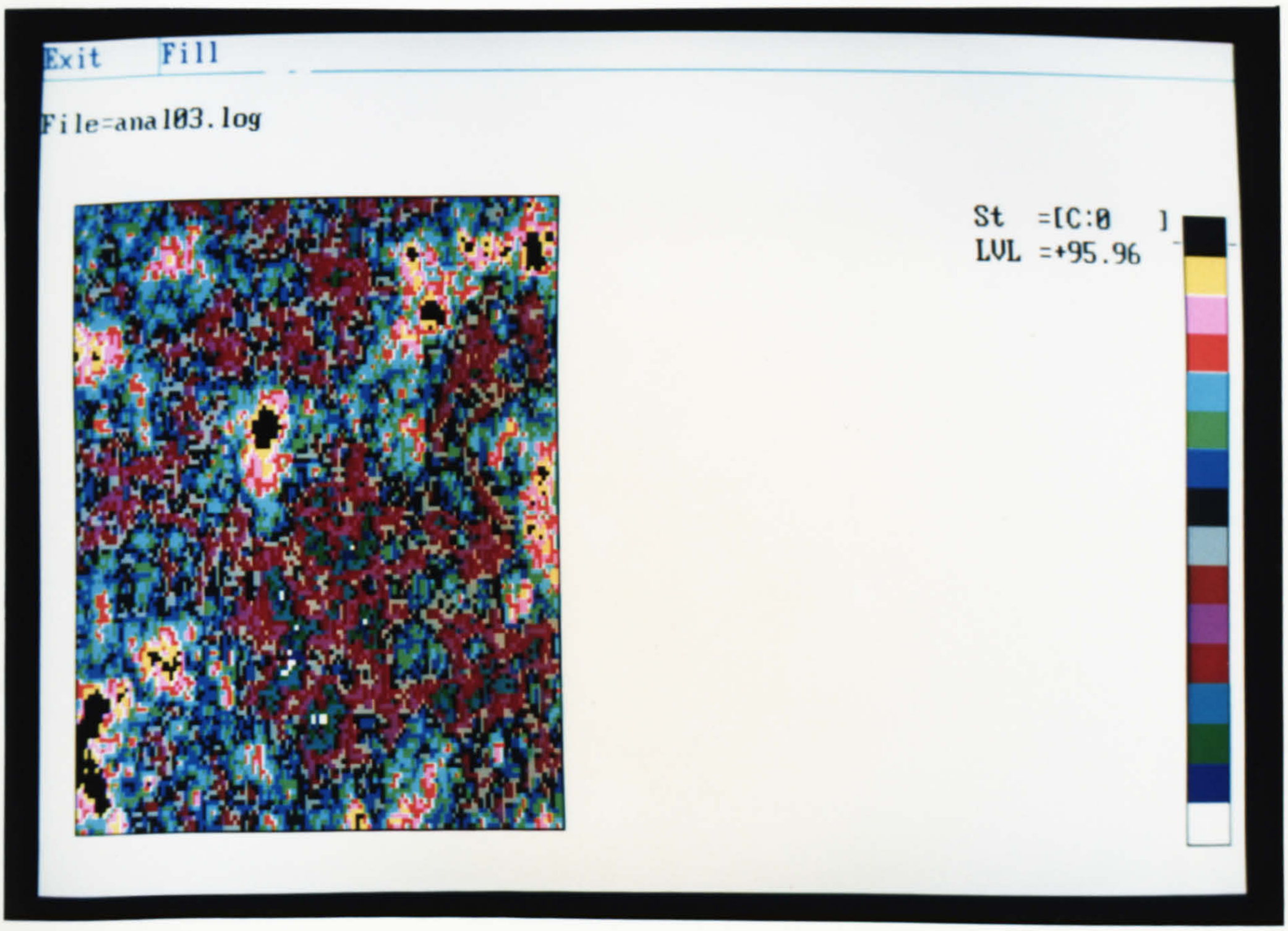

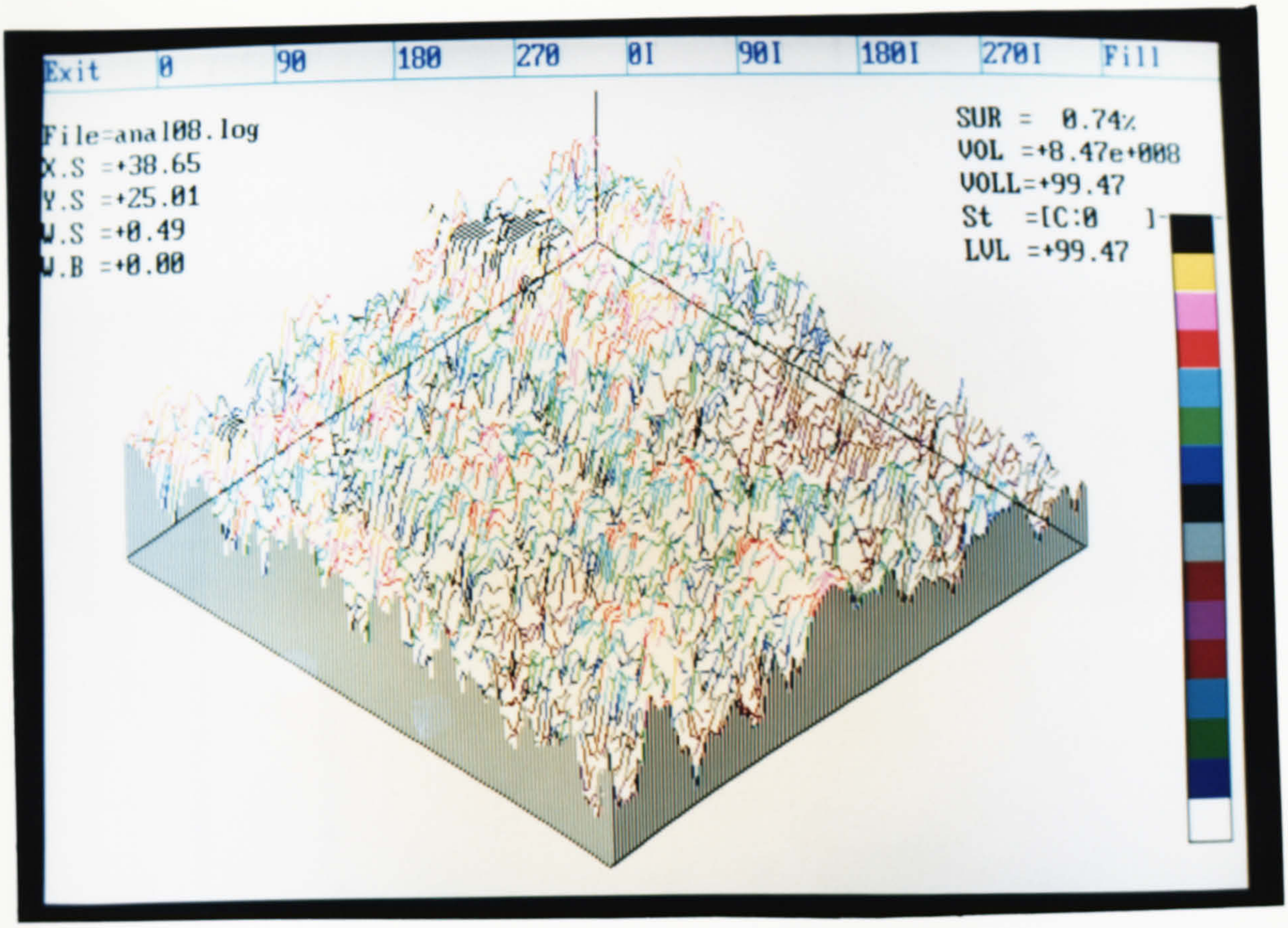

Fig. (11.5) Surface Analysis of TBC Coated Specimen

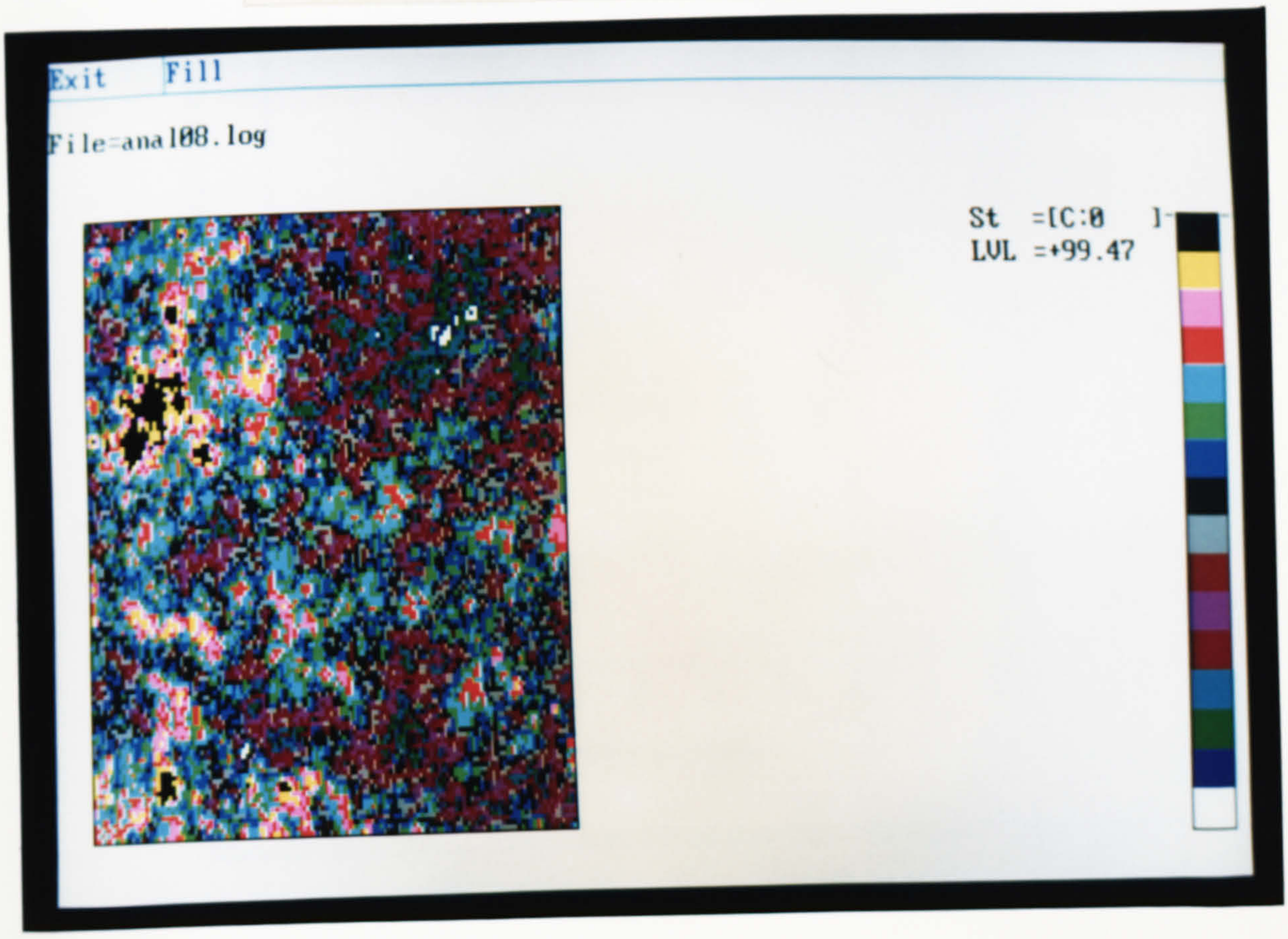

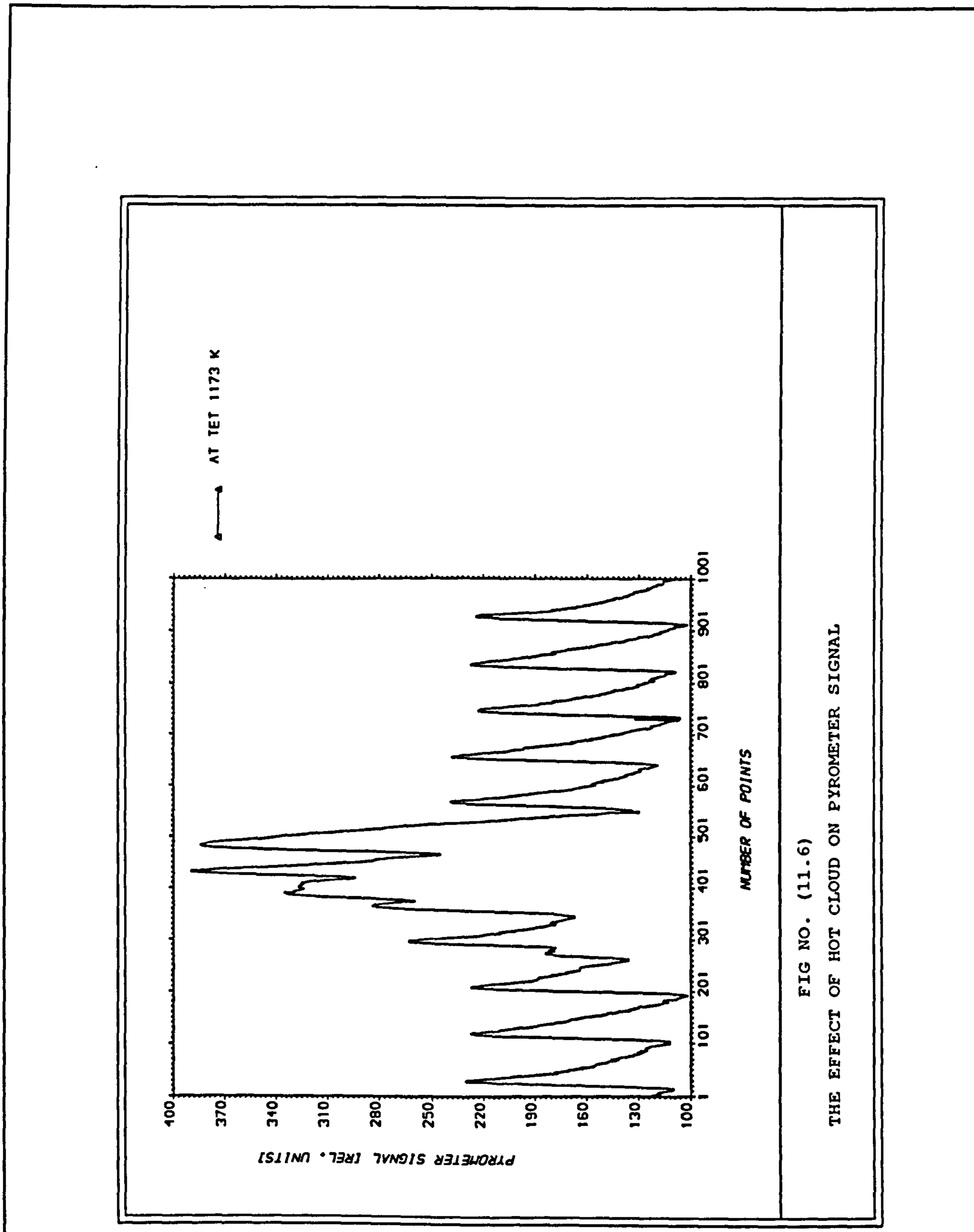

FIG NO. (11.6)

THE EFFECT OF HOT CLOUD ON PYROMETER SIGNAL

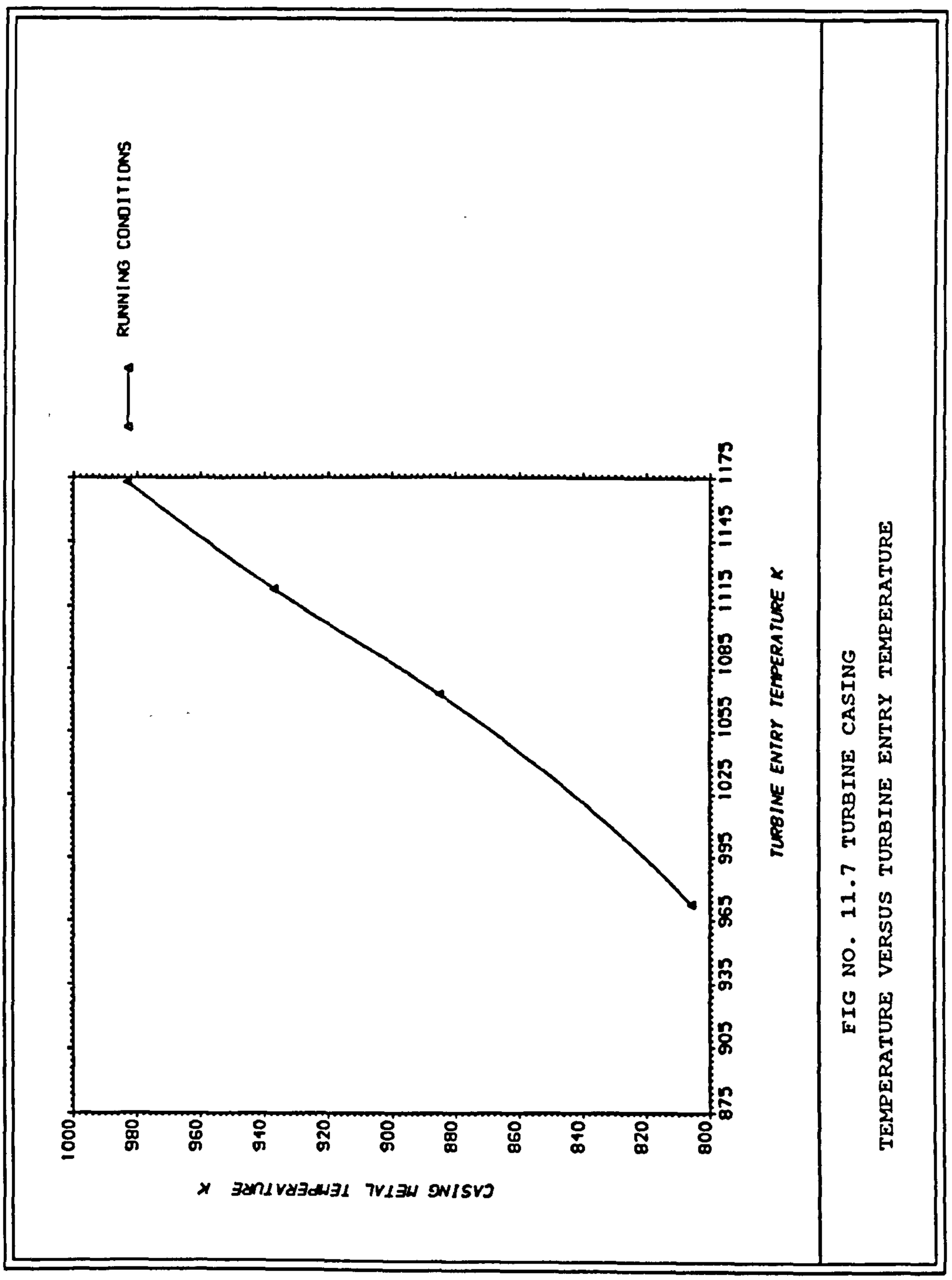

FIG NO. 11.7 TURBINE CASING TEMPERATURE VERSUS TURBINE ENTRY TEMPERATURE

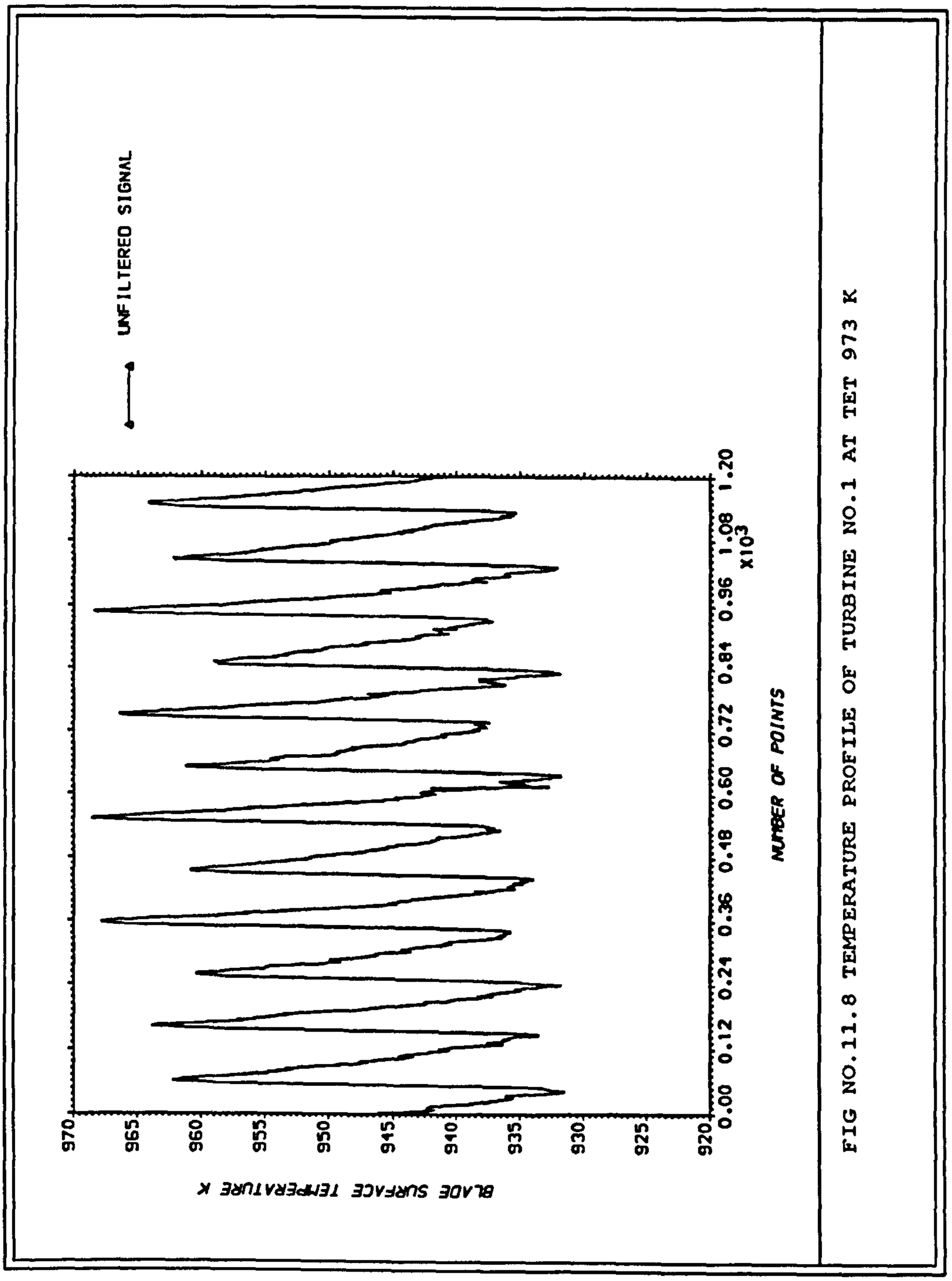

FIG NO.11.8 TEMPERATURE PROFILE OF TURBINE NO.1 AT TET 973 K

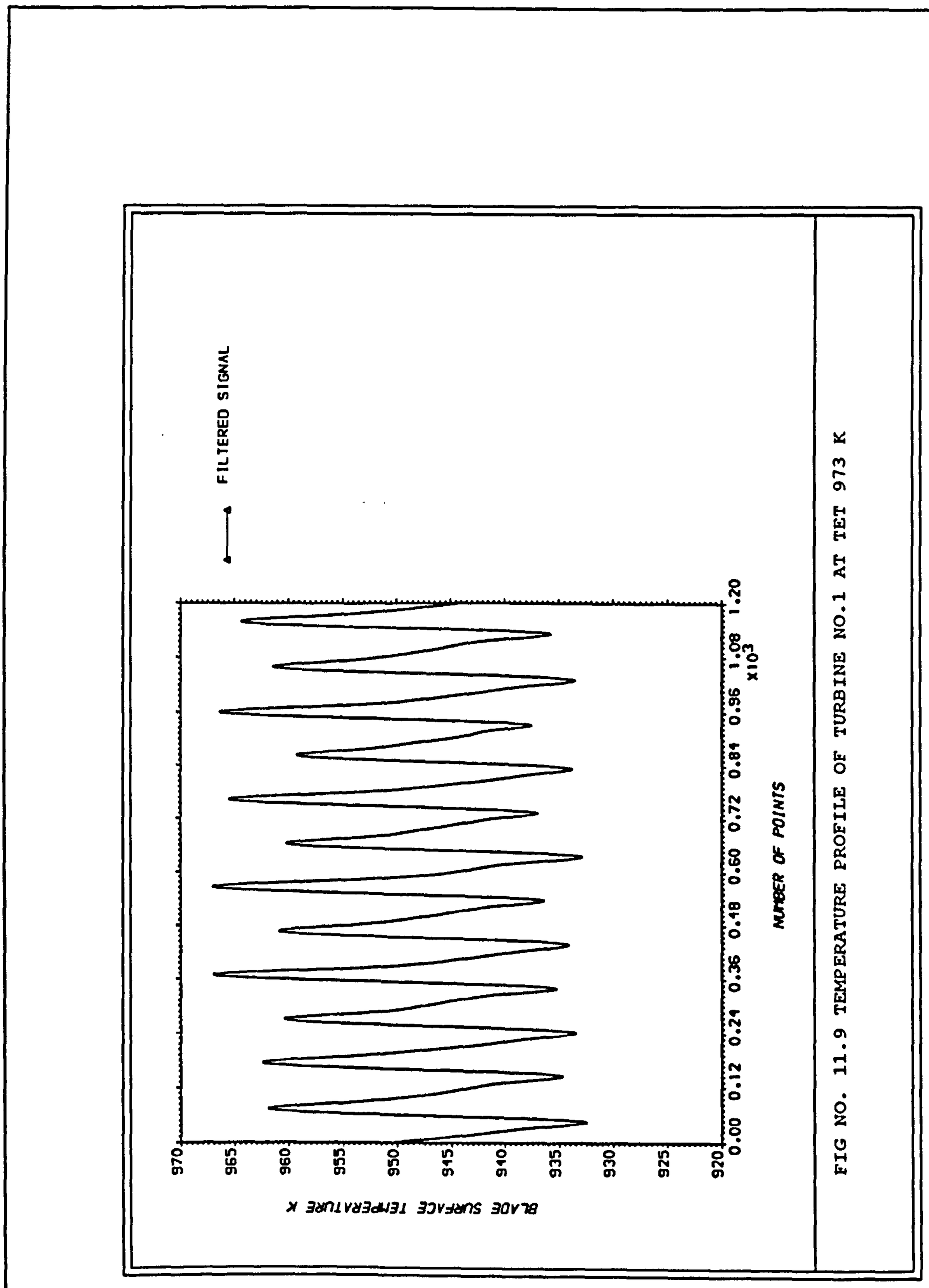

FIG NO. 11.9 TEMPERATURE PROFILE OF TURBINE NO.1 AT TET 973 K

CHAPTER TWELVE

12 DISCUSSION AND OBSERVATIONS

12.1 Introduction

The first part of this chapter presents the discussion of the experimental measurements of the TBC systems emissivities and surface roughness. The second part presents the discussion for the surface temperature measurements performed on the 8%YPSZ TBC system. The results of the measurements of the other systems are then presented for completeness. These systems consist of 0.16 mm bond coat of NiCrCoAl-Y2O3 and : C-YPSZ, 20%YPSZ, 24%MPSZ, grey alumina, and white alumina. These coating systems were applied on six turbine wheels. The turbine wheels are numbered 1 to 6 and carry the TBC systems in the same order mentioned above.

A discussion comparing these systems is also included. This involves similar coating thickness of different coating systems being run under the same conditions.

This chapter is then concluded with the observation that the pyrometer can be used to detect coating degradation. This conclusion potentially has importance in the future developments of gas turbine coatings.

12.2 Discussion of The Experimental Results

12.2.1 Emissivity Analysis

In order to determine the surface temperature from the pyrometer reading a knowledge of the surface emissivity was necessary. The emissivity of each of the different coating types was measured in a separate experiment.

The pyrometer picks up the radiation signal collected by the optics. It then processes that signal, which falls in the wavelength band 0.4 to 1.2 micrometers. As was mentioned in chapter three, this signal is function of the target temperature and of the target surface spectral emissivity. It also include radiation reflected by the target or emitted by hot particles in the sight path.

12.2.1.1 Surface Finish of Test Pieces

For each of the six TBC systems tested, coated specimens were prepared specifically for the measurement of emissivity. These specimens were made by applying the coating to the "nimonic 75" sheet after a bond coat had been first applied to the nimonic sheet. Prior to the application of the bond coat the surface of the nimonic 75 sheet was roughened by impacting it with chilled iron balls so as to give better adherence to the bond coat. The dimensions of the test pieces are given in appendix (A).

The surface roughness was measured in the "Surface Analysis Laboratory" in the "School of Mechanical Engineering" (chapter eleven).

The surface analysis results show that in spite of the different coating materials and the different coating thickness the average surface roughness RMS values were in the narrow range 9.03 to 11.1 micrometers. These surfaces are more than 4 times smoother than uncoated turbine blades in operation. This variation in the surface roughness is small and has very little effect on the emissivity of these surfaces.

12.2.1.2 Emissivity Results

The spectral emissivity of these specimens was then measured. The method used was the "radiometric method", which was outlined in chapter nine and presented in appendix (A) .

These results are shown plotted in Figure no. (9.5). This figure shows that as the coating thickness increases the spectral emissivity decreased. It then levels out at about 0.35 mm coating thickness (chapter nine).

This phenomenon can be understood by considering the following : the bond coat has spectral emissivity of 0.64, [Liebert(77)]. So when the overcoat is "thin" it is translucent. And the system spectral emissivity is influenced by the bond spectral emissivity. The thicker the overcoat is the less it is translucent and the less is the influence. When the overcoat is opaque at a coating thickness of about 0.35 mm, then the system spectral emissivity is the overcoat spectral emissivity. This thickness was found by Liebert [77] to be about 0.33 mm.

It was also found that the spectral emissivity was not function of stabilizer material. This could be related to the microstructure of these systems. These systems apart from the two alumina types are alloys of the same base material. The added stabilizers are only a percentage of the base and they don't have much influence on the microstructure. On the other hand, these

systems are applied by the same technique employing the same gases and following the same procedure. This ensures that the microstructures are similar.

Figures (12.1, 12.2 and 12.3) show some of the microstructures of these systems. Figure no. (12.3) shows the effect of employing hydrogen instead of nitrogen as the driving gas on the microstructure of a C-YPSZ TBC system [from Ref. 82].

The surface spectral emissivity and coating thickness were then correlated by a suitable curve fitting technique. This correlation is shown plotted in Figure no. (9.5).

Figure no. (9.5) also shows a comparison of these results with measurements performed by Liebert [Ref.77] on the "NASA" TBC system. This shows an agreement between the two independent experimental results.

The same exercise was repeated for specimens coated with alumina TBC systems. The results of which are shown plotted in Figure no. (9.6). This figure shows similar relation between spectral emissivity and coating thickness, whilst the absolute values are somewhat higher. This could be due to the microstructures being different. Figures 12.4 and 12.5) shows a cross section of the microstructure of alumina TBC system. A curve fitting technique was then employed to correlate the spectral emissivity with coating thickness .

These emissivity measurements were taken in the temperature range 873 to 1023 K because , :

a) The pyrometer can only detect temperatures beyond 873 K. and

b) The sample furnace could only be used up to a sample surface temperatures of 1023 K .

However, over this range the spectral emissivity was temperature invariant. This result was also noticed by Liebert [Ref.77].

12.2.2 Blade Surface Temperature Profiles

The experiment was designed to allow several coating thickness to be evaluated during the same test run to provide good comparative data of the thermal performance of the coating systems, and to pick up coating degradation. Comparative information of other coating systems was obtained by running tests at the same operating conditions. Whilst the experiment does provide absolute measurements of temperature, it is the comparative performance of the coating systems that is considered important, was studied and is discussed below.

Six TBC systems were applied on six turbines. Each of these turbines has twelve blades. Six of these blades were coated with different coating thickness. It was arranged in a way that the pressure surface of every other blade was coated. Tables (12.1-12.4) list the coating thickness for each of the TBC systems. The coated turbines were then rebalanced, before being tested.

Table (12.5) lists the conditions under which these turbines were tested.

The results obtained for the 8%YPSZ TBC system are discussed in details. The results for the other systems are included for completeness.

All these systems consisted of 0.16 mm bond coat and a layer of over coat. The coated blades are numbered 1 to 6 and the sixth blade carries the thickest system.

Figure no. (12.6) shows the corrected surface temperature profile of blade no. (1) of turbine no. (1). This blade was coated with 0.125 mm of 8%YPSZ ceramic overcoat, and tested at turbine entry temperature of 973 K .

This profile can be subdivided into three parts. The first part closer to the blade tip, shows a slow decrease of surface temperature with radius ratio. The second part is longer than the first and steeper. This part is ended with a third part that includes the blade root .

These three parts of the profile can be understood by considering the blade geometry. Figure no. (10.1) shows the pyrometer scan line on the blade surface (chapter ten). The first part of the blade including the tip is thin and has a constant cross sectional area. Blade thickness then increases towards the root. The blade is ended with a part that joins it with the turbine wheel.

The overall tendency of the profile is that the tip is the hottest and the root is the coldest. As the hot gases expand and flow towards the root, the turbine extracts work and the gas temperature falls as the radius ratio (radius at the plane considered divided by the tip radius) decreases. The steady state blade metal temperature from tip to root falls in the same manner as the gas temperature falls. The rate of surface temperature fall is a function of the rate of area change towards the blade root.

Figure no. (12.7) is a plot of the corrected surface temperature profiles of the six coated blades and of one uncoated blade of turbine no. (1). These profiles were taken at turbine entry temperature of 973 K. This figure shows that the surface of blade no. (1) which was coated with 0.125 mm of 8%YPSZ was more

than 53 K hotter than the surface of the uncoated blade. The surface of the coated blade is then hotter the thicker is the coating. Blade no.2 was 58 K hotter, blade no.3 was 69 K hotter, blade no.4 was 78 K hotter and blades no.5 and 6 were 79 K hotter than the uncoated blade.

This is related to the relationship between coating thickness and surface spectral emissivity and the relationship between coating thickness and the conduction thermal resistivity. The surface spectral emissivity decreases with coating thickness increase up to a coating thickness of about 0.35 mm above which the surface spectral emissivity stays constant. The surface temperature increases with surface spectral emissivity decrease. Thermal resistivity which is equal to the coating thickness divided by the thermal conductivity increases with coating thickness for the same coating type (constant thermal conductivity). The amount of heat conducted is proportional to the inverse of thermal resistivity. Hence, the thicker is the coating the less heat is conducted and hence the higher is the surface temperature.

Because the RIT blade geometry is complex, the turbine wheel was fixed on the turntable for the purpose of applying the coatings (chapter eight). The turntable was rotated by (60) degrees intervals to bring each blade in line for coating. A robot was programmed to spray each blade with different number of passes, as each blade had different coating thickness applied on it. Because the plasma cone covers the entire blade height, the plasma cone was moved along the mid section of the blade surface and in a direction perpendicular to it. As a consequence it was easer to obtain uniform coating thickness in the mid section of the blade and the coating that resulted at the blade tip and root was less uniform.

Figure no. (12.7) also shows that the surfaces of the tips of blades no. (5) and no. (6) were at the gas temperature. These two blades have coating thickness of 0.535 mm and 0.595 mm respectively. So their surface emissivities were the same and hence their surface temperatures. Their tips were at the gas temperature because the thicker is the coating the lower is the surface spectral emissivity and the higher is the thermal resistivity hence, the higher is the surface temperature. So, as they were the blades with the thickest coating their temperature profiles were the highest. As the gas temperature is higher at the RIT entry the blade tip temperatures are higher. Combination of these effects namely, coating thickness, surface spectral emissivity, thermal resistivity, and gas temperature produced tip temperatures very close to the gas temperature.

Figure no. (12.9) is similar to figure no. (12.7) but at turbine entry temperature of 1073 K. This figure shows that as the turbine entry temperature was increased a larger proportion of the blade surface temperature reached the gas temperature. This figure also shows that the thicker the coating was the

larger the proportion of the surfaces that reached the gas temperature. Note that the surface of blade no. (1) was about 66 K hotter than the surface of the uncoated blade. The profiles of blades 3, 4, 5, and 6 show large parts at gas temperature. This figure also shows that blades 5, and 6 (with the thickest blade coating) have virtually the same surface temperature profiles .

Figure no. (12.11) shows the corrected surface temperature profiles of the blades of turbine no. (1) at turbine entry temperature of 1173 K. It shows that the surface of blade no. (1) was 80 K hotter than the surface of the uncoated blade. Again the surfaces were hotter the thicker were the coatings.

Figures 12.7, 12.9, and 12.11 show that as the coating thickness was increased the difference in blade surface temperatures between coated blades and the uncoated ones increased too. For the same coating thickness this difference was higher the higher was the TET. For a constant TET, the amount of heat transferred into the blade was constant, for constant heat removal the larger the coating thickness was (therefore the larger was the thermal resistivity) the higher was the surface temperature. As TET was increased the turbine rotational speed was increased (Table 12.5) and the gas velocity was increased therefore the forced convection heat transfer coefficient was increased. This increase in TET and forced convection heat transfer coefficient resulted in lower gas thermal resistivity and the amount of heat transferred into the blade was increased. However for the same conditions, the removal of heat which occurs at the blade roots does not increase at the same rate. As a consequence of this is that higher surface temperatures result as TET was increased.

Figures 12.12 to 12.17 show the corrected surface temperature profile of each of the six coated blades of turbine no. (1) at the three running conditions.

Figures (12.12-12.17) show :

1) similar general tendency of surface temperature variation with radius ratio .

2) the higher the turbine entry temperature the hotter is the blade surface .

3) the thicker is the coating the hotter is the surface at the respective turbine entry temperature .

4) some of the surfaces are at the gas temperatures , and

5) the higher is the turbine entry temperature , and the thicker is the coating the larger are the proportion of blade surfaces that are at gas temperature.

Figure no. (12.18) shows the corrected blade tip surface temperatures of the six coated blades and one uncoated blade of turbine no. (1) as function of the turbine entry temperature . It shows that the blade tip temperature increases linearly with turbine entry temperature. It can also be seen that the thicker was the coating the hotter was the blade tip surface. This figure shows that blades with the thickest coatings, namely blade no. (3, 4, 5, and 6) had their tip surfaces at the gas temperature.

Figure no. (12.19) shows the corrected blade tip surface temperature of turbine no. (1) as function of coating thickness for different turbine entry temperatures. It shows that the tip temperature increases with coating thickness before levelling out above coating thickness of about 0.35 mm.

Figure no. (12.20) shows the corrected blade root surface temperature as function of the turbine entry temperature. The blade root surface temperature was higher the higher was the turbine entry temperature and the thicker was the coating. It also shows a linear relationship between the surface temperature and the turbine entry temperature .

Figure no. (12.21) shows the corrected blade root surface temperature as function of the coating thickness for different turbine entry temperatures. It shows that the surface temperature increases with coating thickness before levelling out around 0.35 mm coating thickness .

Figures (12.22 to 12.34) show the results for turbine no. (2). Turbine no. (2) was coated with 0.16 mm bond coat of NiCrCoAl-Y2O3 and different thickness of the C-YPSZ ceramic overcoat. These figures are included for completeness and they show similar results to those presented in figures 12.6 to 12.21 for the first coating system.

Figures (12.35 to 12.47) show the measurements for the third turbine. This turbine was coated with 0.16 mm bond coat of NiCrCoAl-Y2O3 and different thickness of the 20%YPSZ ceramic overcoat.

Figures (12.48 to 12.60) show the measurements for turbine no. (4). This turbine was coated with 0.16 mm bond coat of NiCrCoAl-Y2O3 and different thickness of the 24%MPSZ ceramic

overcoat. Figures 12.35 to 12.60 are again included for completeness and they show similar results to those of figures 12.6 to 12.21 for turbine no. (1).

12.3 Comparison Between the Stabilized Zirconia TBC Systems

Four stabilized zirconia TBC systems were studied and these are :

1) 8%YPSZ

2) C-YPSZ

3) 20%YPSZ

4) 24%MPSZ

This section presents a discussion comparing between these types. Figure no. (12.61) shows a comparison between the corrected surface temperature profiles of blades coated with 0.325 mm of TBC system 2 (C-YPSZ) and system 3 (20%YPSZ). This figure shows that the blade coated with C-YPSZ was hotter than that coated with 20%YPSZ at the same turbine entry temperatures. It also shows that the higher was the turbine entry temperature the more was the difference. These temperature profiles are of blades which have the same coating thickness, and measurements (chapter nine) showed that the surface spectral emissivities of stabilized zirconia TBC systems of the same thickness were essentially the same. This difference in surface temperatures is therefore the result of the difference in the thermal conductivity of the two systems.

System no. (2), C-YPSZ, is a newly developed TBC system. It has a thermal conductivity of 0.9 W/m2 K. This makes it a better insulator. It has a better thermal shock resistance and a better adherence when compared with the other systems [Ref. 82]. Because the C-YPSZ is a resent development there is no known informations available about its spectral emissivity other than that contained in this thesis.

Figure no. (12.62) Shows the results of the measurements performed on systems 1 and 3. This figure shows that the 8%YPSZ out performs the 20%YPSZ by giving higher surface temperatures. The comparison of the coated blades was made with equal thickness and this suggests that system 1 is a better insulator than system 3. The thermal conductivity of system (1) (8%YPSZ) is 1.3 W/m2 K [Ref. 77].

Figure no. (12.63) shows a comparison between blades coated with 0.535 mm of 8%YPSZ and 0.515 mm of 24%MPSZ. This figure shows that the surface temperature profiles of system (1) were higher than those of system (4). This difference was higher the higher was the turbine entry temperature .

These two systems have the same surface spectral emissivities, but different thermal conductivities. The thermal conductivity for system 4 (24%MPSZ) is 1.5 W/m2 K which is greater than that for system 1. The thermal resistivity which is the thickness divided by the thermal conductivity was higher in this case for system 1 and hence the amount of heat conducted away was less for the case of system 1 which led to the surface temperature being higher.

Figure no. (12.64) shows a comparison between the corrected surface temperature profiles of blades coated with 0.185 mm of system 1 (8%YPSZ), and 0.235 mm of the newly developed C-YPSZ, (system 2). This figure shows that the second system gave higher surface profiles than the first one. This can be related to the facts that the C-YPSZ coating thickness was larger and both thermal conductivity and spectral emissivity were lower. The effect of these parameters produced higher surface temperatures for the blades coated with C-YPSZ from those coated with 8%YPSZ.

Figure no. (12.65) shows a comparison between three TBC systems. These are 0.325 mm of system 2 (C-YPSZ), 0.325 mm of system 3 (20%YPSZ) and 0.305 mm of system 4 (24%MPSZ). This figure shows that the blades coated with system 2 were hotter than those coated with system 3 which were hotter than those coated with system 4. This could be understood by considering that :

a) systems 2 and 3 had the same coating thickness , hence the same spectral emissivity which was lower than that for system 4.

b) system (4) had lower thermal resistivity than system (2) .

c) so, system (3) must have thermal resistivity that was lower than system (2) and higher than system (4).

12.4 Comparison Between the Experimental Results of The Grey and The White Alumina Systems

This section presents a comparison between the white alumina and the grey alumina TBC systems and between these two systems and the other four systems.

Figures (12.66 to 12.69) show comparative results of the six systems tested in this investigation. Figure no. (12.66) is a comparison between the corrected surface temperature profiles of blades coated with white alumina and with grey alumina. It shows that the white alumina gave hotter surfaces than the grey alumina at TETs of 973 K and 1173 K. These two systems had the same surface spectral emissivity. So, the white alumina was a better insulator.

Figure no. (12.67) is again similar to figure (12.66) but with different coating thickness. This figure again confirms the conclusion obtained from figure no. (12.66).

Figure no. (12.68) shows a comparison between the corrected surface temperature profiles of blades coated with white alumina with those coated with 20%YPSZ. It shows that white alumina gave hotter surfaces, so it was a better insulator.

Figure no. (12.69) shows a comparison between the corrected surface temperature profiles of blades coated with 0.485 mm of C-YPSZ ceramic TBC system and 0.455 mm of white alumina TBC system. This figure shows that both systems gave similar surface temperature profiles at the three conditions.

12.5 Observations

The development and testing of TBC systems is costly and lengthy process. Coating loss, if not detected can have costly implications.

The method employed for industrial, marine and to a less extent aero gas turbines for choosing a suitable TBC system is called the "rainbow test". In such tests, different coating systems are applied to various turbine blades belonging to the same turbine wheel. When the engine is run each blade, and therefore each coating system experiences the same environment and temperature history. After a number of running hours the coated parts are inspected. During this inspection the engine is stripped down, such that the condition of individual coated blades can be checked. As a result of this inspection a TBC system is chosen to be applied. This is usually the system that suffered minimum loss during the test .

The weakness in this test is that the decision is very much dependant on the end results. These results do not show which of the coating systems is best for example, at transient, high power operation, with contaminated fuel, etc. The results of the inspection are the results of the integrated operation over the entire test period. Therefore the coatings can not be properly chosen to suit the environmental and operating conditions for which they were chosen.

The use of an on line monitoring technique by employing a radiation pyrometer in such tests can cut both time and cost. It can also help to choose the right coating system for the particular power and environment in which the engine can be used.

This can be achieved by monitoring the coatings during different operational modes. It is not necessarily so that the system which survives continuous operation will perform best under for example cyclic testing. The more informed choice can be made by continuously monitoring the coatings through the different operational modes.

This view has yet to be developed further, but for instance the following sets of data reveal the possibility of this usage.

Figure no. (12.70) shows the pyrometer un-filtered signal of turbine no. (5) at turbine entry temperature of 973 K. This turbine has six of it's blades coated with grey alumina coating system. This figure shows that the coated blades (4, 6, 8, 10, and 12) are hotter than the adjacent blades (3, 5, 7, 9 and 11).

Figure no. (12.71) shows a similar signal at turbine entry temperature of 1073 K. It again shows that blades (4, 6, 8, 10, and 12) are hotter than blades (3, 5, 7, 9 and 11).

Figure no. (12.72) shows the signal at turbine entry temperature of 1123 K. In this figure, it is can be seen that blades (4, 6, and 8) are nearly as hot as the adjacent blades. This indicate that these blades have suffered coating degradation.

Figure no. (12.73) shows a similar signal at turbine entry temperature of 1173 K. This figure confirms that blades (4 , 6 , and 8) are nearly as hot as the adjacent uncoated blades. Which confirms that these blades have suffered coating loss .

Figures (12.74 and 12.75) show photographs of the turbines coated with 24%MPSZ, grey alumina and white alumina coating systems before and after testing, respectively. Figure no. (12.75) shows that turbine no. (5) which is coated with grey alumina has suffered coating loss on more than one blade. This coating loss was picked up by the pyrometer as shown in figures (12.72 and 12.73).

These observations open the prospect of employing the radiation pyrometer not only for producing more accurate blade temperatures but also for choosing the right coating system for the right engine task and to continuously monitor coating degradation during engine running.

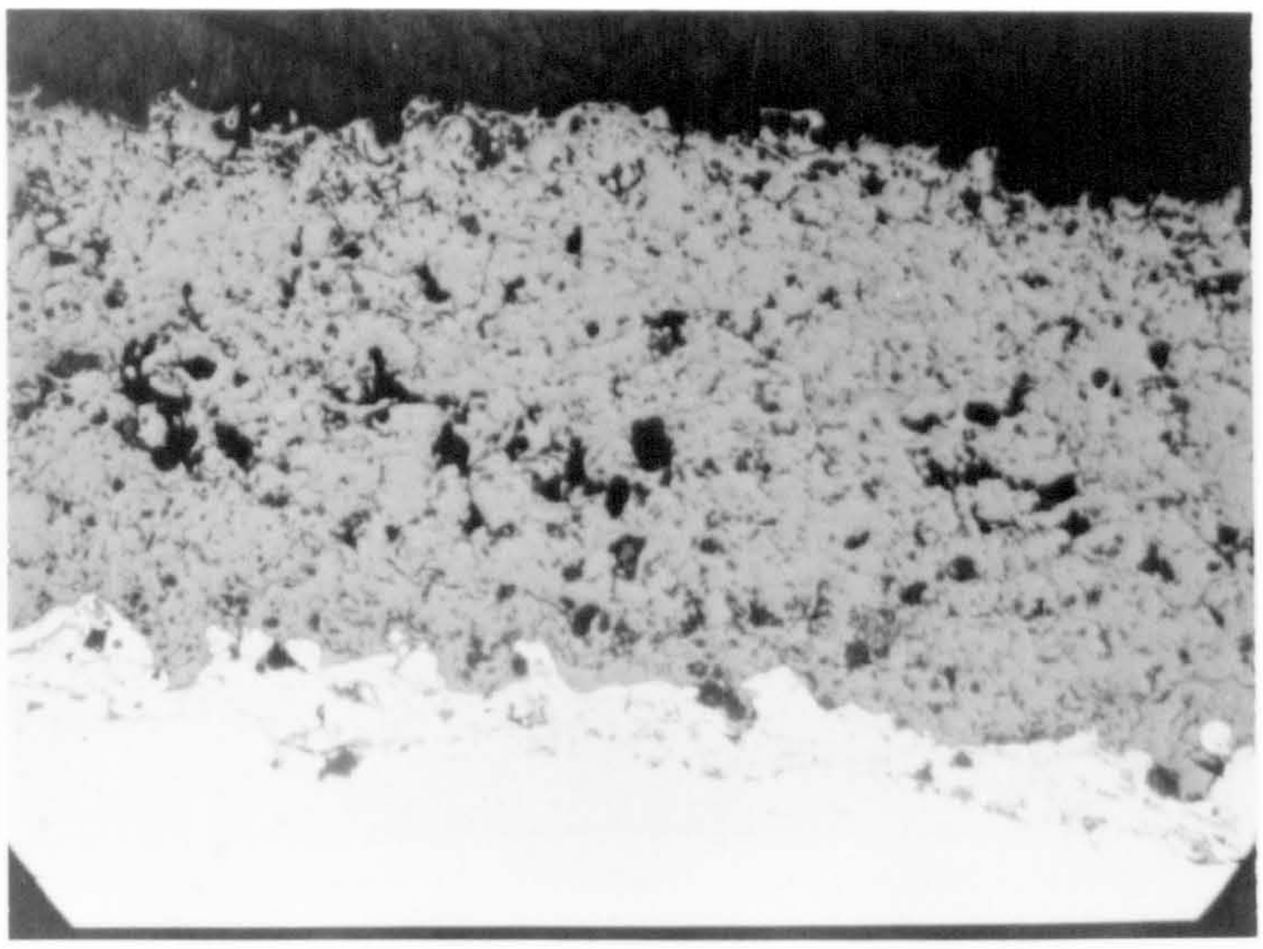

Fig.(12.1) Microstructure of 8%YPSZ TBC System (x125)

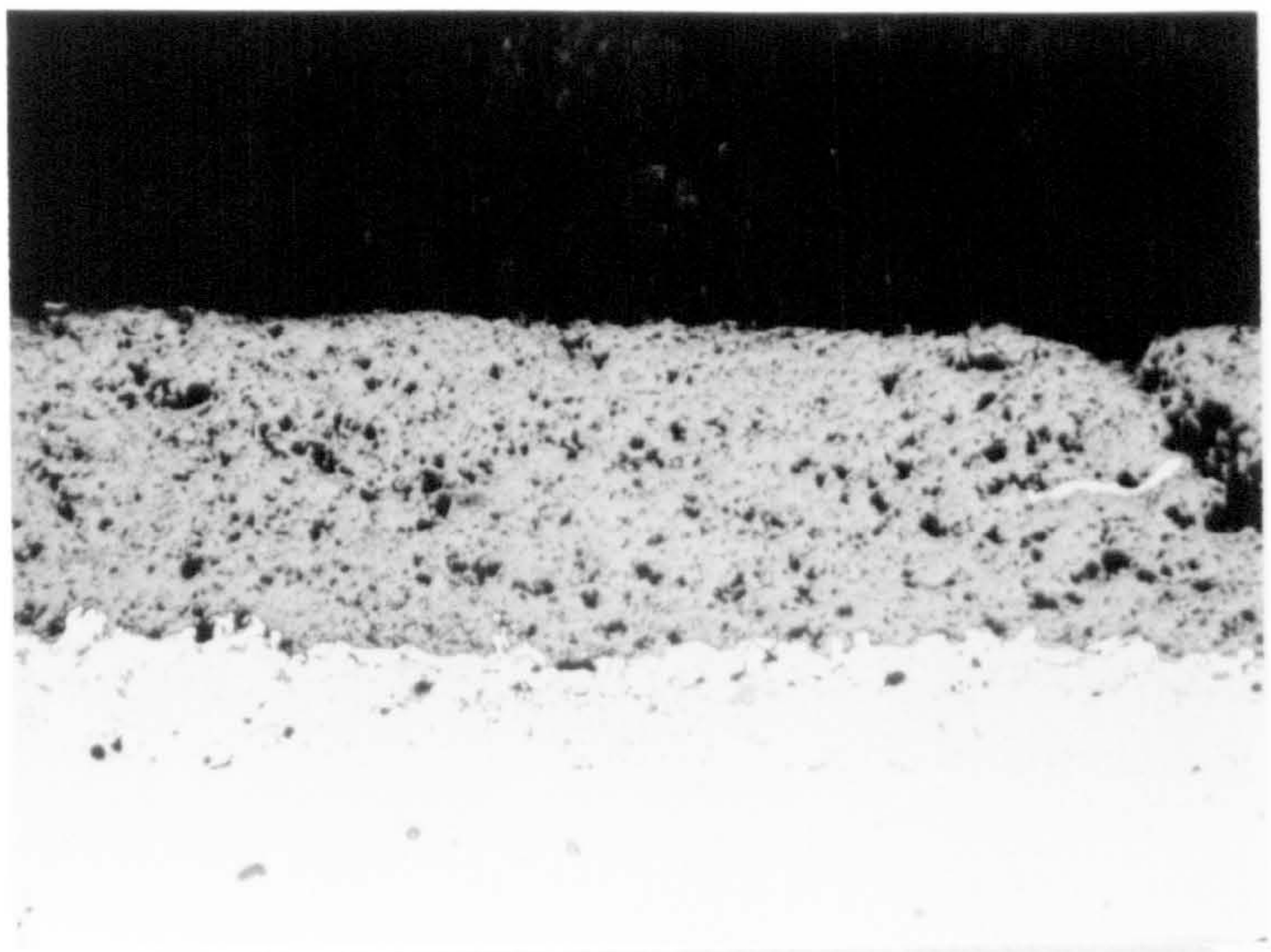

FIG no.(12.2) Microstructure of 20%YPSZ TBC System (x65)

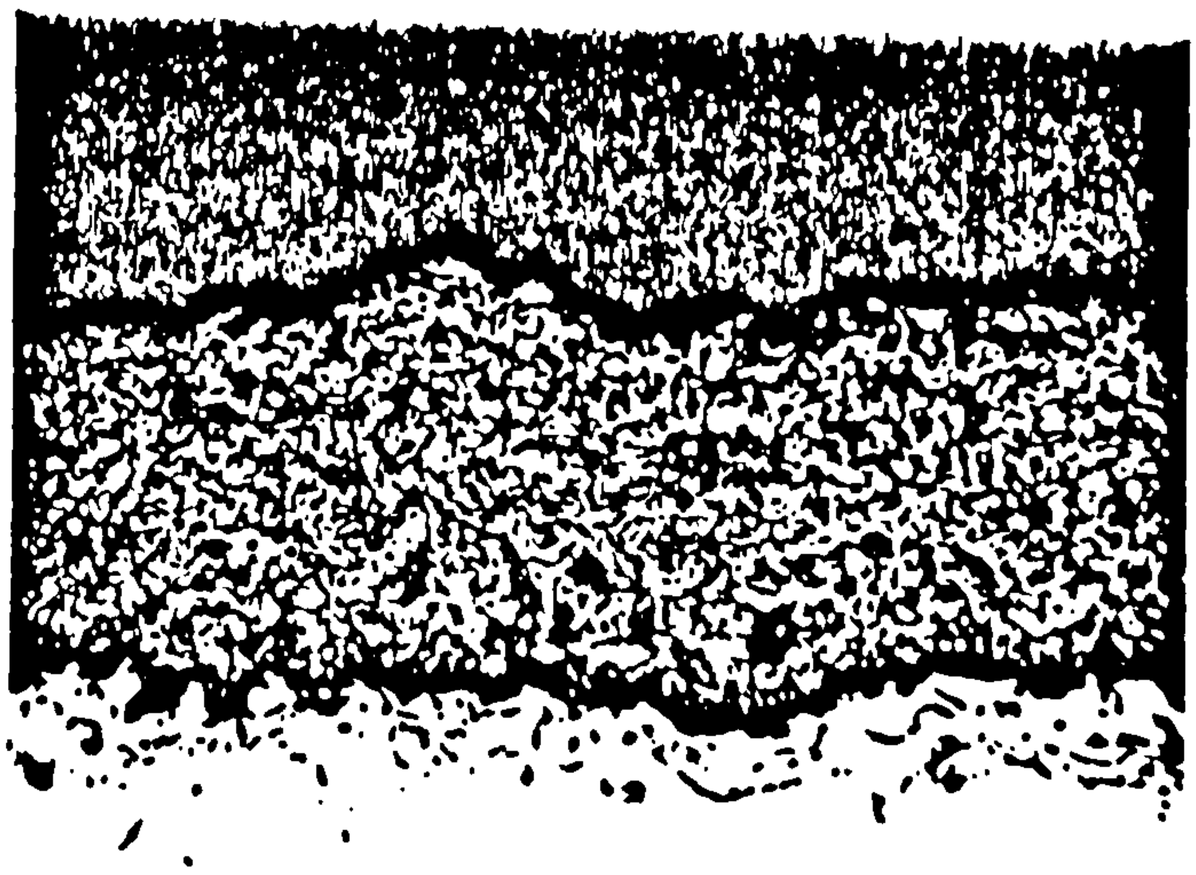

CROSS-SECTION OF TBC
WITH Ar/H, PARAMETERS
(100X)

CROSS-SECTION OF TBC
WITH N,/H, PARAMETERS
(100X)

FIG no.(12.3) Microstructure of C-YPSZ TBC System

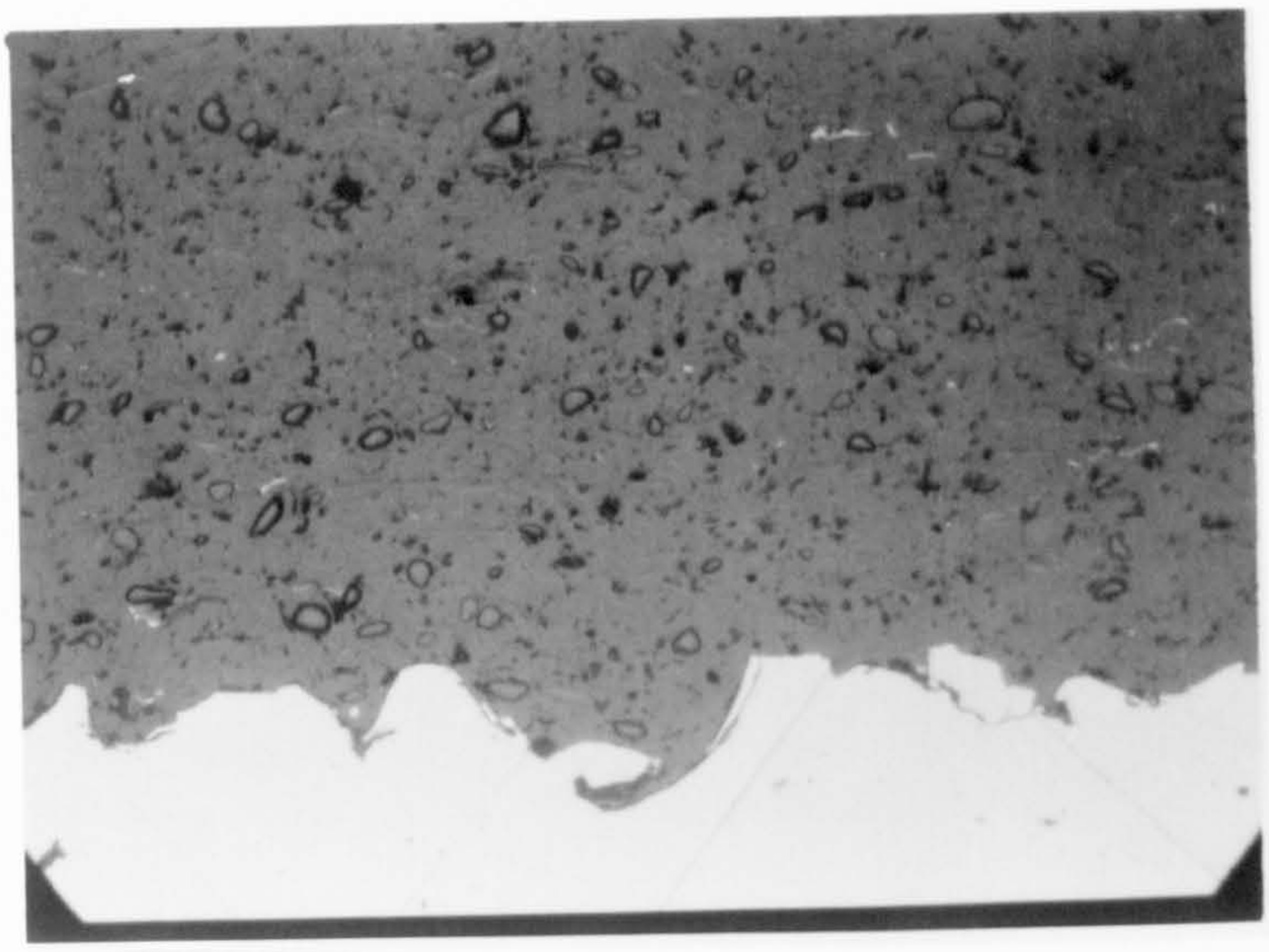

Fig.(12.4) Microstructure of
White Alumina (x125)

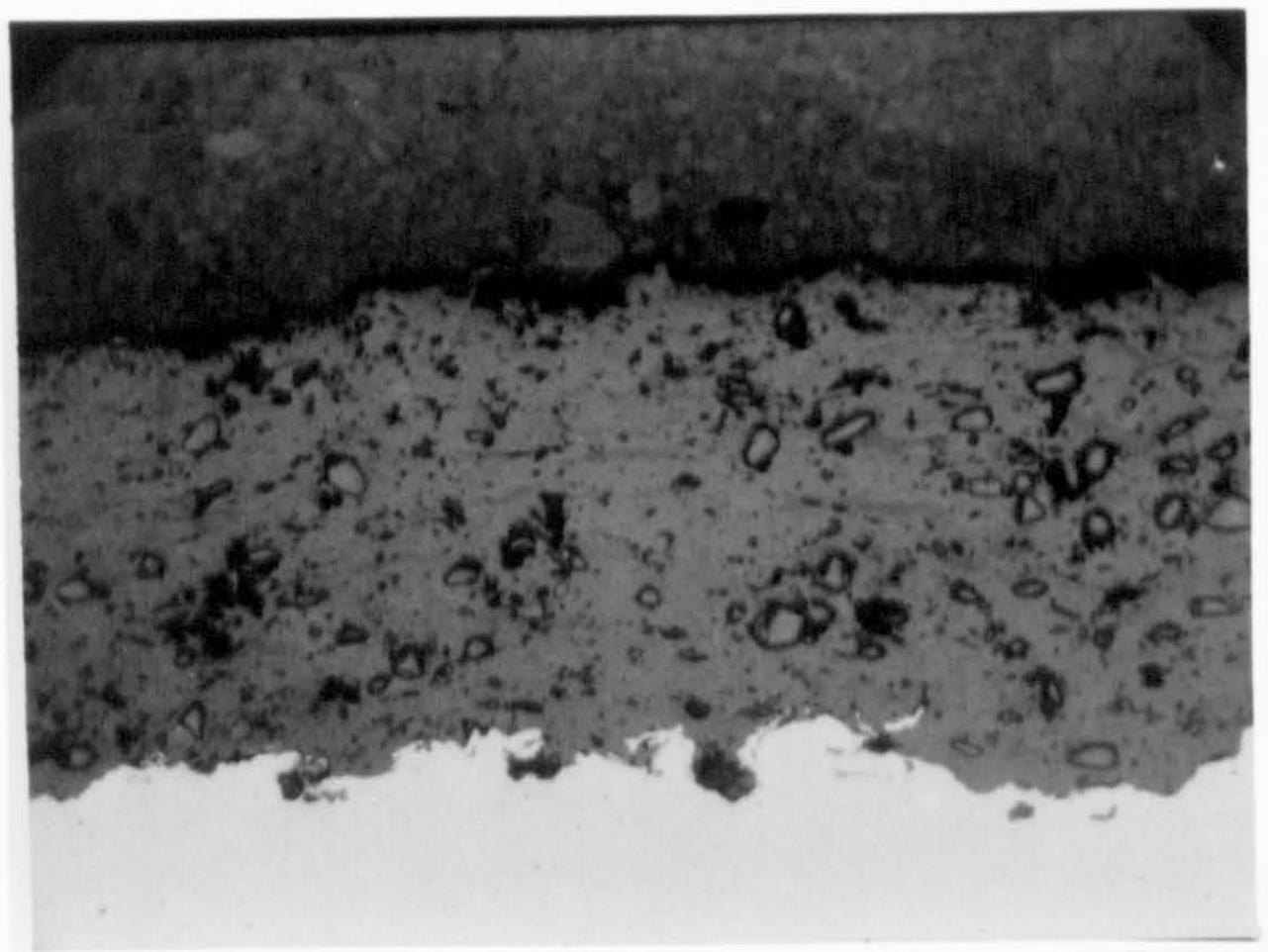

Fig.(12.5) Microstructure of Grey
Alumina System (x125)

TABLE 12.1 : Coating thickness and figure numbers for turbine 1 coated with (8%YPSZ) thermal barrier coating system

COATING THICKNESS [mm]	TURBINE ENTRY TEMPERATURE [K] 973	1073	1173
	Figure no 12.		
0.125	6,7,12	8,9,12	10,11,12
0.185	7,13	9,13	11,13
0.285	7,14	9,14	11,14
0.375	7,15	9,15	11,15
0.535	7,16	9,16	11,16
0.595	7,17	9,17	11,17

TABLE 12.2 : Coating thickness and figure numbers of turbine 2 coated with (C-YPSZ) thermal barrier coating system

COATING THICKNESS [mm]	TURBINE ENTRY TEMPERATURE [K] 973	1073	1173
	Figure no 12.		
0.035	24,27	25,27	26,27
0.235	24,28	25,28	26,28
0.325	24,29	25,29	26,29
0.365	24,30	25,30	26,30
0.365	24,31	25,31	26,31
0.485	24,32	25,32	25,32

TABLE 12.3 : Coating thickness and figure numbers of turbine 3 coated with (20%YPSZ) thermal barrier coating system

COATING THICKNESS [mm]	TURBINE ENTRY TEMPERATURE [K] 973	1073	1173
	Figure no 12.		
0.215	39,42	40,42	41,42
0.245	39,43	40,43	41,43
0.285	39,44	40,44	41,44
0.325	39,45	40,45	41,45
0.385	39,46	40,46	41,46
0.455	39,47	40,47	41,47

TABLE 12.4 : Coating thickness and figure numbers of turbine 4 coated with (24%MPSZ) thermal barrier coating system

COATING THICKNESS [mm]	TURBINE ENTRY TEMPERATURE [K] 973	1073	1173
	Figure no 12.		
0.165	54,57	55,57	56,57
0.305	54,58	55,58	56,58
0.415	54,59	55,59	56,59
0.515	54,60	55,60	56,60
0.655	54,61	55,61	56,61
0.750	54,62	55,62	56,62

TABLE 12.5 : Testing Conditions

TURBINE ENTRY TEMPERATURE [K]	ROTATIONAL SPEED [RPS]	TIP SPEED [m/s]	PYROMETER TIME CONST.[s] x10E-6
973	842	265	24.74
1073	883	277	23.59
1173	925	290	22.52

CHAPTER THIRTEEN

13 CONCLUSIONS AND RECOMMENDATIONS

13.1 Conclusions

An experimental rig for the assessment of gas turbine coatings was successfully designed, built and developed. This rig was based on a RIT. It was possible to run the rig at a typical blade passing frequency and metal temperature of current gas turbines. Six thermal barrier coating systems of current interest to gas turbines were tested. A radiation pyrometer was used for coating emissivity measurements and for surface temperature measurements. The radiation pyrometer system used was one that is of direct relevance to gas turbine application, and pyrometers of this type are actually in use in for example the RB199 gas turbine.

The following conclusions were formulated from this investigation.

The benefits attainable from coating systems can be evaluated based on their thermal barrier effect, which is a consequence of the low thermal conductivity that is typical of ceramics.

In the measurement of surface emissivities it was found that with both zirconia based and alumina based TBC systems the normal spectral emissivity was temperature invariant over the range 873 to 1023 K. It was also found that these emissivities were not a function of the stabilizing material .

For both coating systems the value of the emissivity drops with coating thickness then levels out at around a coating thickness of 0.35 mm. The normal spectral emissivity of alumina based TBCs was found to be higher than that of the zirconia based systems.

In the measurement of blade surface temperatures, it was found that the blade surface temperature increases with coating thickness for each of the six systems when TET was held constant.

The blade surface temperature was also found to increase with TET for a constant thickness of each of the coating systems. The blade tip surface temperature was found to increase linearly with TET. It also increases rapidly with coating thickness before levelling out at coating thickness of around 0.35 mm .

The blade root surface temperature was also found to increase linearly with TET. It increases with coating thickness then levels out at coating thickness of around 0.35 mm.

The newly developed C-YPSZ TBC system was found to adhere well to the blade surface. This coating outperforms the other systems in the thermal insulation it provides.

The turbine wheels coated with the two alumina systems suffered coating loss from more than one blade. The pyrometer was found to be able to pick up this coating loss as it occurs.

The indicated surface temperature profiles at TET of 973, 1073, 1123 and 1173 K for the uncoated blade was found to be within 10 K of those calculated .

Analysis shows that the metal temperature can be reduced by 310 K when coating the blades with 0.5 mm of C-YPSZ TBC system, 280 K with 8%YPSZ and 260 K with 24%MPSZ at TET of 1673 K. This metal temperature reduction increases linearly with TET and is higher the higher is the coating thickness. An 0.3 mm of C-YPSZ, 8%YPSZ and 24%MPSZ reduce the blade metal temperature by 270, 215 and 200 K, respectively.

Analysis also shows that the blade surface temperature increases linearly with TET and coating thickness. An 0.3 mm of C-YPSZ increases the blade surface temperature by about 250 K at TET of 1673 K.

An analysis showed the effect of varying lens transmissivity, for example due to lens contamination on the pyrometer temperature indication. If the lens transmissivity was reduced to 0.7 by contamination, the pyrometer error introduced is as high as 50 K, this error is 35 K for lens transmissivity of 0.8, and 15 K for lens transmissivity of 0.9. It was also found that the pyrometer error could be as high as 180 K for vane view factor of 0.4 and a flame view factor of 0.3.

This thesis also contain informations concerning the relative accuracy of obtaining blade metal temperature using radiation pyrometry or via calculation of the blade metal temperature from the EGT. Information also presented on the implication on engine life and performance because of the uncertainty that arise because of the inaccurate determination of the blade temperatures. For example, creep life can be improved by 25% by using radiation pyrometry in stead of thermocouples for the turbine blade determination for a low bypass engine assuming that the pyrometer is only 5 K more accurate. This improvement is 5% in thrust and 1.5% in SFC by using radiation pyrometry.

13.2 Recommendations

For future work in this field , the following would be recommended :

The investigation of more bond material types ,

Investigation of the effect of bond coating thickness ,

Testing of these systems on air cooled blades ,

Perform thermal shock and cycling testing of these TBC systems and of others ,

Correlate coating degradation with operation time ,

Develop a finite element computer package for calculating the blade metal temperature distribution of a radial inflow turbine blade and to compare the temperature profiles measured by employing a radiation pyrometer with those predicted by the package.

LIST OF REFERENCES

(1) M. Gell Et al , "Advanced superalloy air foils" , J. of Metals , July 1987

(2) R.J. Bratton , "Ceramic thermal barrier coatings for gas turbine engines" , ASME TRANS. 82-GT-265 , 1982

(3) C.H. Liebert and F.S. Stepka , "Potential use of ceramic coating as thermal insulation on cooled turbine hardware" , NASA TM-X-3352

(4) K.D. Sheffler and D.K. Gubta , " Current status and future trends in turbine application of thermal barrier coatings" , ASME paper no. 88-GT-286 , 1988

(5) K.R. Curwen , " Turbine blade radiation pyrometry system" , Aircraft engineering , V44 , PP. 16-21 , DEC. 1972

(6) Negretti Aviation , "Pyrometer transducer" , the airport , Southampton , Hants SO9 3FR , England

(7) Negretti and Land , "Turbine temperature transducer for continuous in flight monitoring and control of turbine exhaust gas and rotating blade temperature in gas turbines"

(8) D.A. Rohy and W.A. Compton , "Radiation pyrometry for gas turbine blades - final report" , Solar division Int. Harvester Co. , San Diego , Ca92138 , October 1973

(9) G.W. Meetham, "Limitations at high temperatures of present day engineering materials", New materials and application Warwick,22-25 Sept. 1987, U.K.

(10) J. Douglas , "Radiation pyrometry in gas turbine research and developments" , Rolls-Royce Ltd. , 1982

(11) Negretti Aviation, "Blade analysis and selection equipment" The airport, Southampton, Hants, England

(12) W.H. Atkinson and R.R. Strange , "pyrometer temperature measurements in the presence of reflected radiation " , ASME paper no. 76-HT-74 , August 1976

(13) W.H. Atkinson and R.R. Strange , "Turbine pyrometry for advanced engines", AIAA paper no. 87-2011 , July 1987

(14) J. Douglas , " High speed turbine blade pyrometry in extreme environment" , British J. of NDT , 1982 , PP. 335-343

(15) K.R. Curewn , "Turbine blade pyrometer system in the control of the Concorde engine", Inst. for air breathing engines , PP. 400-407 , 1972

(16) B.J. Berenblut and R.A. Mason , "No.2 radiation pyrometer for gas turbine engines - an introduction" , British J. of NDT , September 1982

(17) R.S. Sharpe , "Research techniques in ND testing" , Academic press , London and New York , PP. 443-478, 1970

(18) S. Stepka , " Two layer thermal barrier coating for turbine air foils-furnace and burner rig test results " , NASA TM-X-3425 , 1976

(19) R.L. Petritz , "Fundamentals of infrared detectors" , Proc. of the IRE , paper no. 3-3-1 , September 1959

(20) R. De Waard and E.M. Wormser , "Thermal radiation detectors" , Proc. of the IRE , paper no. 3-3-3 , September 1959

(21) M.J. Klein , "Max Planck and the beginning of the quantum theory" , Archive for history of exact sciences , V1 , PP. 459-479 , 1962

(22) Max Planck , "The theory of heat radiation", Authorised translation by Morton Masius , Dover publications , New York, 1959

(23) BDH , "Crytran crystals" , Advanced material division , Broom road , Pool , BH12 4NN , England , 1988

(24) D.A. Rohy and W.A. Compton , "Radiation pyrometry for gas turbine blades" , Final report for Dept. of the Navy Naval air system command , Washington , D.C.20360 , 1971

(25) F.G. Pollack , "Advances in turbine blade temperature measurements" , NASA TM X-71878 , 1976

(26) D.R. Buchele and D.J. Lesco , "Pyrometer for measurement of surface temperature distribution on a rotating turbine blade" , NASA TM X-68113 , 1972

(27) M.K.D. Smith , "The application of IR pyrometry to an industrial gas turbine for development and quality control purposes" , The transducer Tempcon , 1983

(28) T.G.R. Beynon , "Turbine pyrometry-an equipment manufacturers view" , ASME TRANS. , 81-GT-136 , 1981

(29) A. Barber , "A radiation pyrometer designed for in flight measurement of turbine blade temperature", SAE paper no. 690432 , 1969

(30) D.J. Arnold and O.E. Balje , "High temperature potential of uncooled radial turbines" , ASME TRANS. V100 PP.249-302 1978

(31) J. Pointer, "Radiation pyrometer",UK patent application GB 2158 575a, 1985

(32) W.G. Alwang , "Metal temperature measurement" , Advanced experimental techniques in turbo-machinery , PLS-1 , Japikse D. , Norwich Vermount 05055 USA , Library of Congress Card no. 86-70542 , 1986

(33) J. Pointer and R.A. Masom,"Radiation pyrometer", UK patent GB 2158 576A, 1985

(34) Negretti Aviation,"Operating instructions manual for type 12143 calibration furnace", The airport, Southampton, UK

(35) BS 1042 : Section 1.1 : 1981-Methods of measurement of fluid flow in closed circuits

(36) ISO 5168,"Measurement of fluid flow- estimation of uncertainty of a flow rate measurement", First edition, 1978-G7-15

(37) J.M. Hobbs , "Instrument science and technology - variable area and pressure difference flow-meters" , J. Phys. E. :Sci Instrum. 20 , 1987

(38) C.J. Etheridge , "BS1042,Section 1.1 : 1981-Methods of fluid flow in closed circuits", User guide

(39) B.C. Butler , "Private discussions with AK Husain" 21 April 1987

(40) A. Bennett , "Rolls Royce experience with thermal barrier coatings" , Proc. British ceramics , N34 , August 1984

(41) J.L. Pentecost ,"Coating materials and coating systems" , In : High temperature inorganic coatings , edited by J. Humink Jr.

(42) C.R. Wilkins ,"Ceramic / Metallic thermal barrier coatings for gas turbine engines" , 8th Intern. Thermal Spraying Conference . Miami , 1976

(43) M.P. Malik , "Plasma sprayed coatings in aircraft and engine components" , 7th. Int. Thermal Spraying Conf. paper no. 23 , London , 1973

(44) D.J. Stephenson ,"Erosion and related phenomenon" , in Engineering coatings seminars , School of Industrial Science , Cranfield Institute of Technology , 1987

(45) D.J. Stephenson , "Erosion by liquid and solid impact" Proc. 6th. Int. Conf. , P. 48.1 Cambridge , 1983

(46) D.G. Teer , "Wear process" , in Engineering coatings seminars , School of Industrial Science , Cranfield Institute of Technology , 1987

(47) R. Singh,"Liquid fuels for industrial gas turbines", Lecture note no. SME/2097/RS, Cranfield Inst. of Tech., Cranfield, Beds., MK43 OAL

(48) A.B. Hart and A.J.B. Cutler , "Deposition and corrosion in gas turbines" , Applied Science Pub. Ltd. , London , 1973

(49) T. Tamaru and Y. Kurosawa , "Evaluation of thermocouple and thermal radiation for measuring gas turbine combustor liner wall temperature" , Bull. JSME , V24 N233 paper no.83-0112 November 1984

(50) S.G. Burnay , "New materials and their applications" , Proc. of the Institute of Physics Conference , University of Warwick , 22-25 September 1987

(51) H.D. Stepka and H.A. Crostack , "Non-destructive testing of thermally sprayed coatings" , 9th. Int. Thermal Spraying Conf. , PP. 120-128 , Nederland , 1980

(52) A.J.A. Mom , "Overview of the AGARD SMP activities on turbine engine materials technology in 1972-1982 period"

(53) T.A. Cruse Et al , "Thermal barrier coating life prediction model development" , 1988 ASME Turbo Land Sea and Air , paper no. 88-GT-248 , 1988

(54) R.G. Stable and C.H. Liebert , "Aerodynamic performance of a ceramic coated core turbine vane tested with cold air in a 2-D cascade" , NASA TM X-3191 , 1975

(55) A.H. Sully Et al , "radiation suppressing coatings for metals at elevated temperatures" , Special report no.1

(56) A. Trsek , "The use of thermal sprayed coatings for extended life of aircraft jet engine parts" , 8th. Int. Thermal Spraying Conf. , 1976

(57) M.A. Levinstien and R.K. Betts , "Thermal spray coating in aircraft applications" , 6th. Int. Metal Spraying Conf. , Paris , September 1970

(58) M.P. Malik , "Application of plasma metal spraying in salvaging aircraft and engine components" , 6th. Int. Metal Spraying Conf. , Paris , September 1970

(59) C.H. Liebert Et al , "Durability of zirconia thermal barrier ceramic coatings on air cooled turbine blades in cyclic jet engine operation" , NASA TM X-3410 , September 1976

(60) H. Curt Et al , "Ceramic thermal barrier coating for cooled turbines" , AIAA N76-729 , AIAA / SAE 12th. propulsion Conference , Palo Alto , Calif. , July 1976

(61) H.D.Steffens and M. Malik ,"Application of sprayed coatings" AGARD LS106 , Material coating techniques , Section 9 , 1980

(62) C.C. Berndt , "Material property measurements on thermal barrier coatings" , ASME , 1988 Turbo Land and Air paper no. 88-GT-277 , 1988

(63) Dr Donald H. Boone ,"Overlay coatings for gas turbine air foils" , AGARD LS106 Materials coating techniques Section 8 , March 1980

(64) I. Zuidhof and G. England , "Private discussions with AK Husain" , Metco , Chobham , 6/1 , 23/5 , 30/5 , 1989

(65) R.C. Novak , "Processing aspects of plasma sprayed ceramic coatings" , 1988 ASME Turbo Expo Land Sea and Air , paper no. 88-GT-289 , Amesterdam , 1988

(66) M. Van Roode and Brad Beardsley , "Porosity determination of thermal barrier coatings" , 1988 ASME Turbo Expo Land Sea and Air , paper no. 88-GT-278 , Amesterdam , 1988

(67) J.C. Withers , "Methods for applying coatings" , High Temperature Inorganic Coatings , edited by J. Huminik

(68) G. Johner Et al , "How to achieve strain tolerant thermal barrier coatings by means of varying spray parameters" , 1988 ASME Turbo Expo Land Sea and Air , paper no. 88-GT-313 Amesterdam 1988

(69) Metco , "The guide to Metco coatings" , Metco Ltd. , Chobham Surrey , GU24 8RD , 1986

(70) Metco , "Metco plasma spray coating application" , Metco Ltd. , Chobham , Surrey , Gu24 8RD , 1985

(71) G.R. Blair , "Determination of spectral emissivity of ceramic bodies at elevated temperatures" , J. American Ceramic Soc. , V43 , PP. 197-203 , 1960

(72) R.V. Dunkle , "Thermal radiation characteristics of surfaces" , Theory and Fundamental Research in Heat transfer , J.A. Clark , Pergamon press , new York , 1963

(73) N.W. Snyder , "Radiation in metals" , ASME TRANS. N76 , PP. 541-548 , 1954

(74) H.E. Clark and D.G. Moore , "Method and equipment for measuring thermal emittance of ceramic oxides from 1200 to 1800 K" , Symposium on Thermal Radiation of Solids NASA SP-55 , 1965

(75) E.M. Sparrow and R.D. Cess , "Radiation heat transfer" , McGraw Hill Book Co. Augmented edition , 1978

(76) R.E. Rolling Et al , "Investigation of the effect of surface condition on the radiant properties of metals" , technical Report no. AFML-TR-64-363 , Lockhead missiles and Space Co. Palo Alto , Calif. , November 1964

(77) C.H. Liebert , "Emittance and absorbtance of NASA ceramic thermal barrier coating system" , NASA TP-1190 , 1978

(78) O.E. Balje , "Turbomachines , a guide to design , selection and theory" John Wiley and Sons , Inc. , 1981

(79) P.J. Kirby Et al , "Infrared thermometry for control and monitoring of industrial gas turbine" , ASME paper no. 86-GT-267 , New York , June 1986

(80) H. Herman , "Plasma sprayed coatings" , Scientific American V259 N3 PP. 78-83 , September 1988

(81) R.P. Taylor , "Surface roughness measurements on gas turbine blades" , paper no. 89-GT-285 , 1989

(82) Metco , "Prealloyed ceria-yttria stabilized zirconia powder for producing advanced ceramic thermal barrier coatings" Metco Ltd. , Chobham , Woking , Surrey , Gu24 8RD

(83) B. Haigh , "Private discussion with AK Husain" , Holset Eng. Co. , 7th July 1989

(84) D.K. Edwards and I.Catton , "Radiation characteristics of rough and oxidized metals" , Advances in Thermophysical properties at Extreme Temperatures and pressures , PP. 189-199 , ASME , New York , 1965

(85) P. Boch Et al,"Pre-standardization studies as a mean of helping the development of engineering ceramics", 2nd. European symposium on eng. ceramics, November, 1987

(86) G.S. Ubhi , "Emissivity measurement of gas turbine combustor coatings and its influence on combustor design" Ph.D Thesis , Cranfield Institute of Technology December 1986

(87) B.J. Wheatly , "Turbine blade pyrometry versus thermocouples effects on lifing and performance",MSc thesis, Cranfield Institute of Technology, 1989

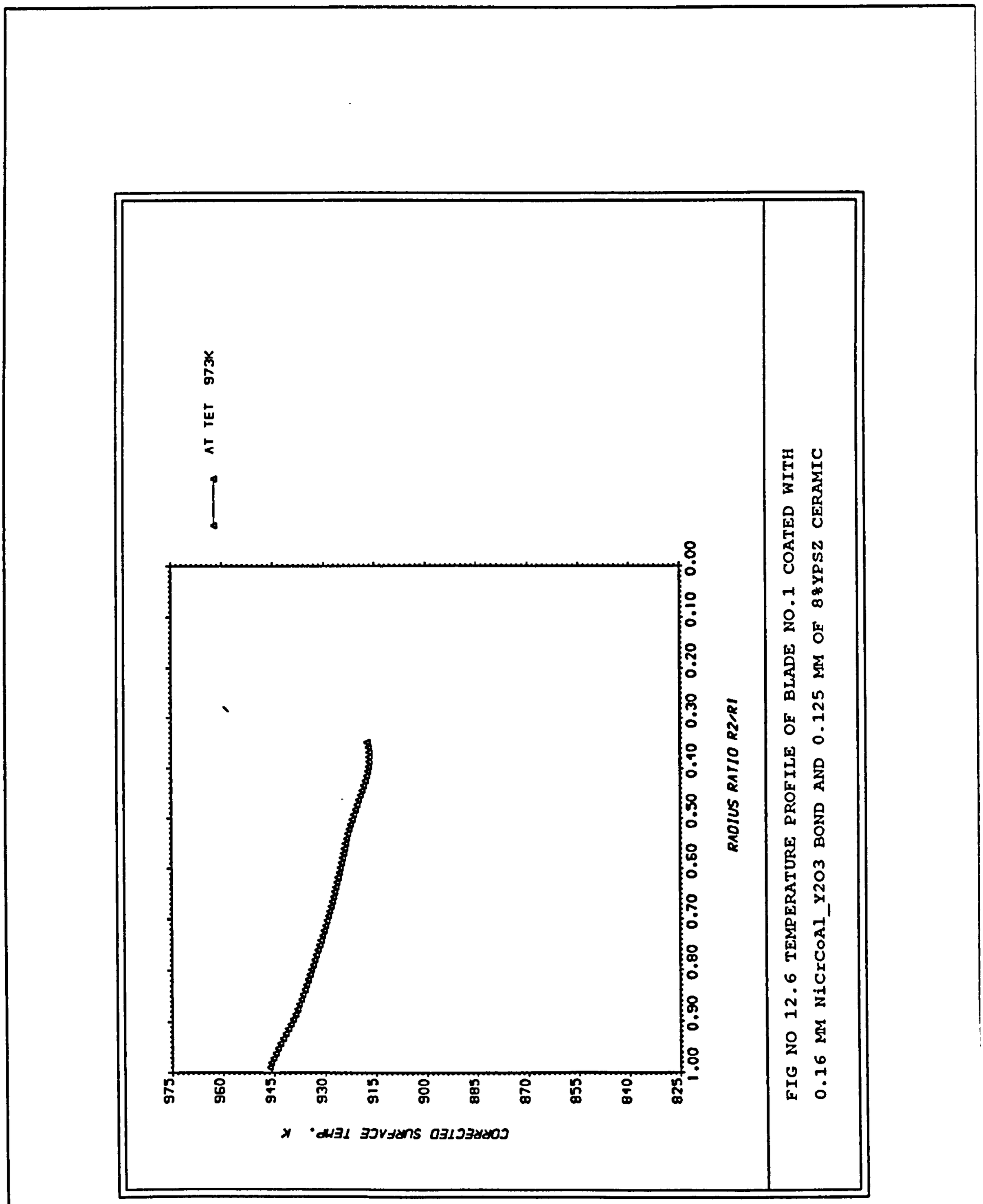

FIG NO 12.6 TEMPERATURE PROFILE OF BLADE NO.1 COATED WITH
0.16 MM NiCrCoAl_Y2O3 BOND AND 0.125 MM OF 8%YPSZ CERAMIC

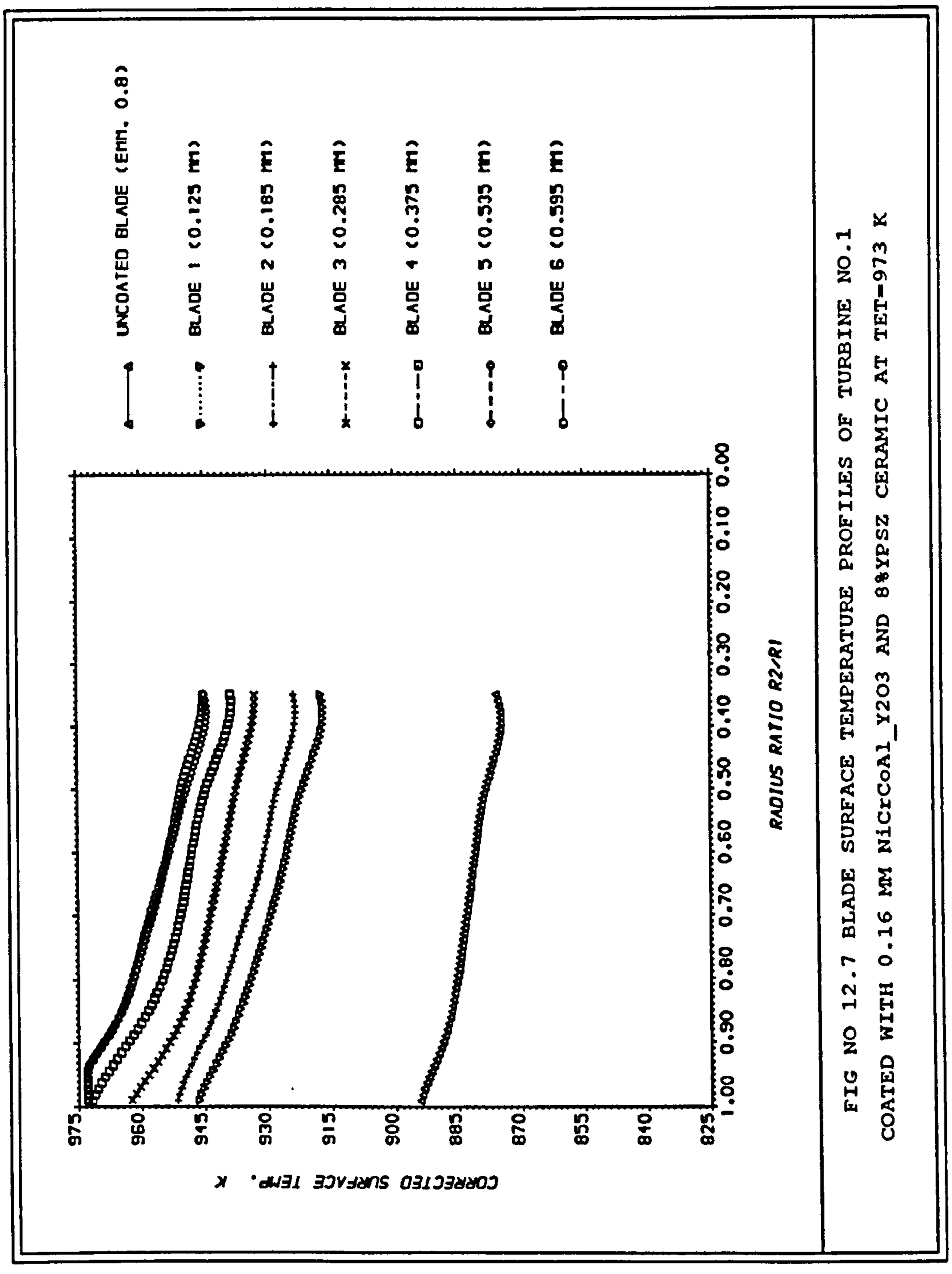

FIG NO 12.7 BLADE SURFACE TEMPERATURE PROFILES OF TURBINE NO.1
COATED WITH 0.16 MM NiCrCoAl_Y2O3 AND 8%YPSZ CERAMIC AT TET=973 K

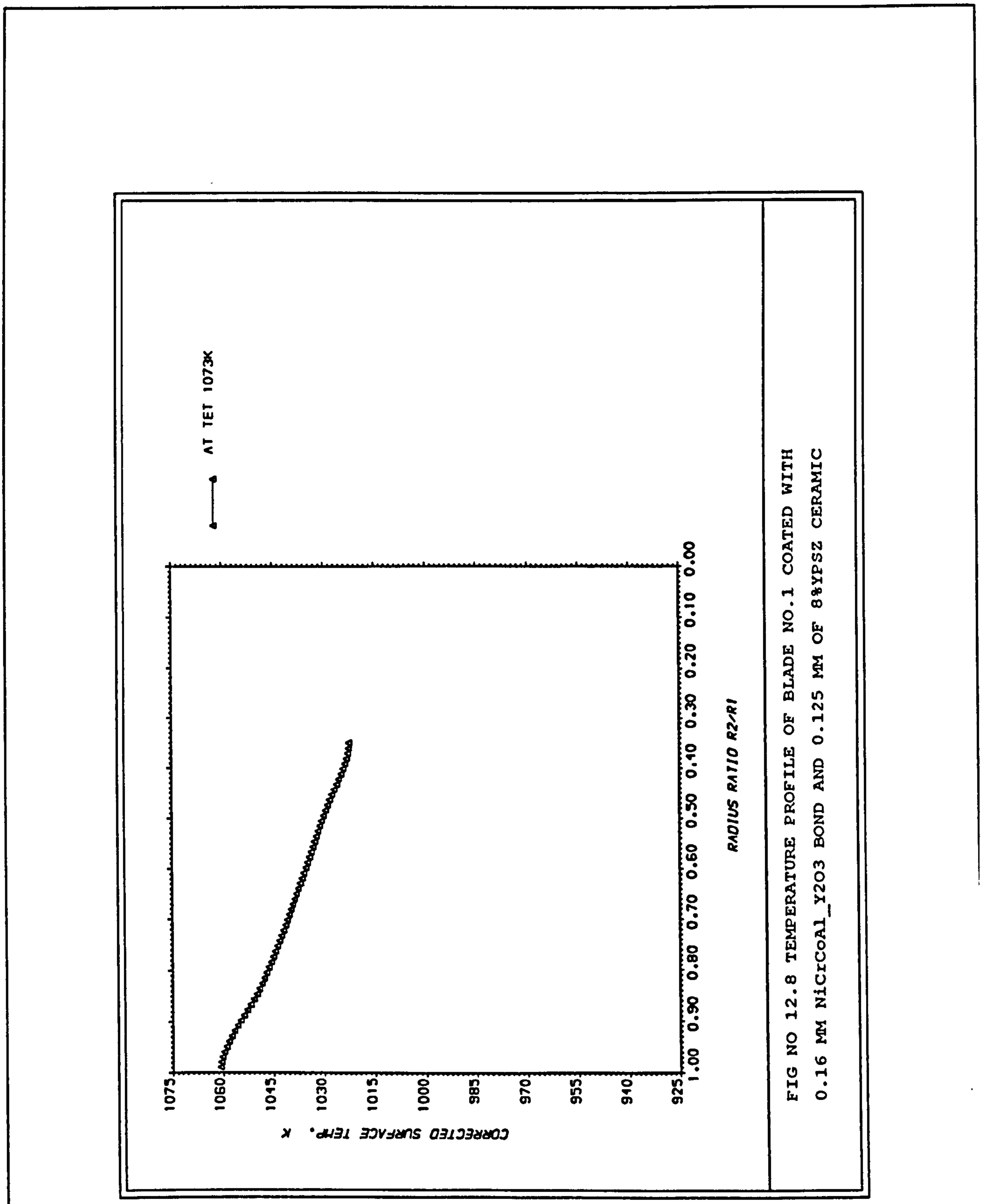

FIG NO 12.8 TEMPERATURE PROFILE OF BLADE NO.1 COATED WITH
0.16 MM NiCrCoAl_Y2O3 BOND AND 0.125 MM OF 8%YPSZ CERAMIC

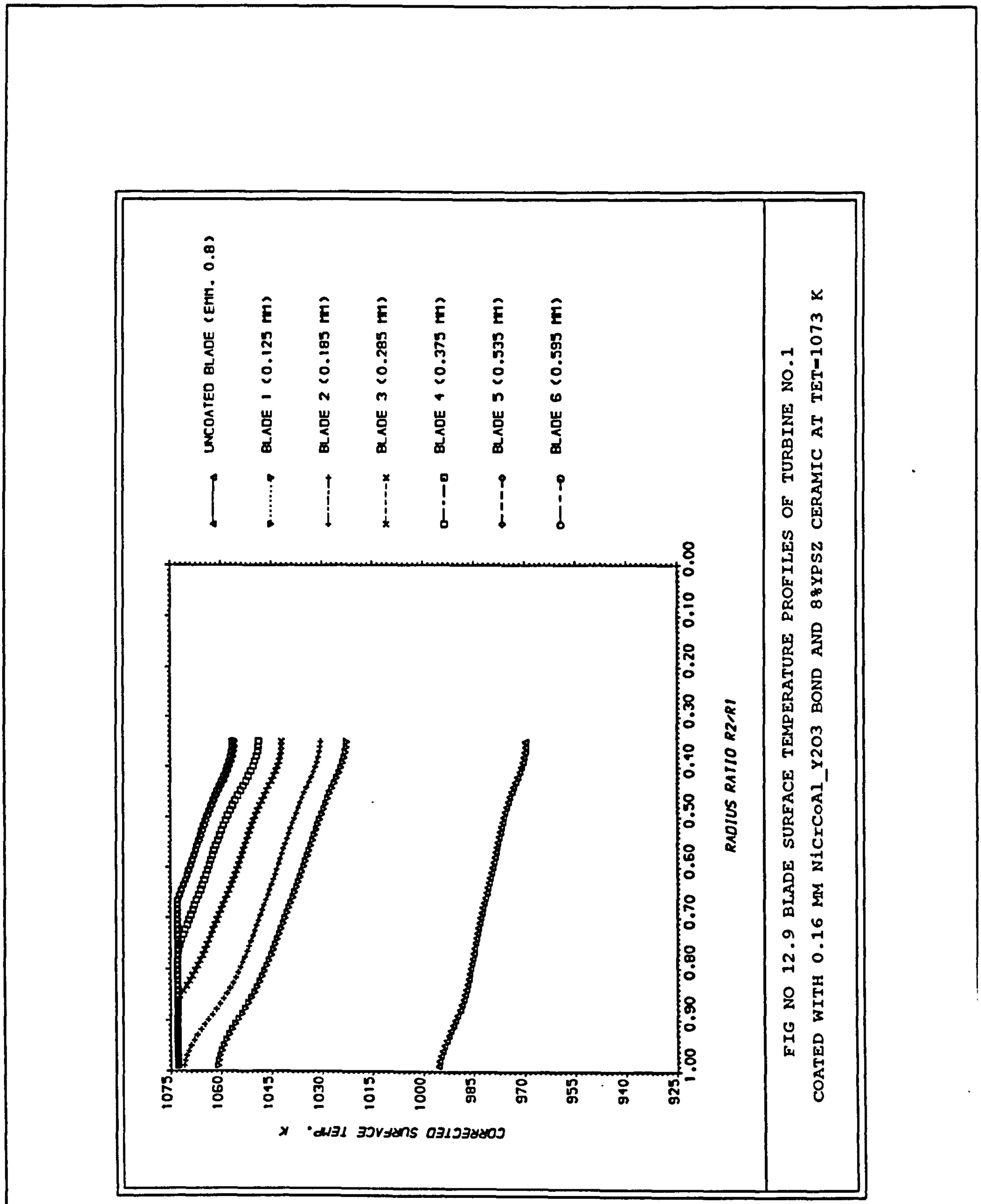

FIG NO 12.9 BLADE SURFACE TEMPERATURE PROFILES OF TURBINE NO.1
COATED WITH 0.16 MM NiCrCoAl_Y2O3 BOND AND 8%YPSZ CERAMIC AT TET=1073 K

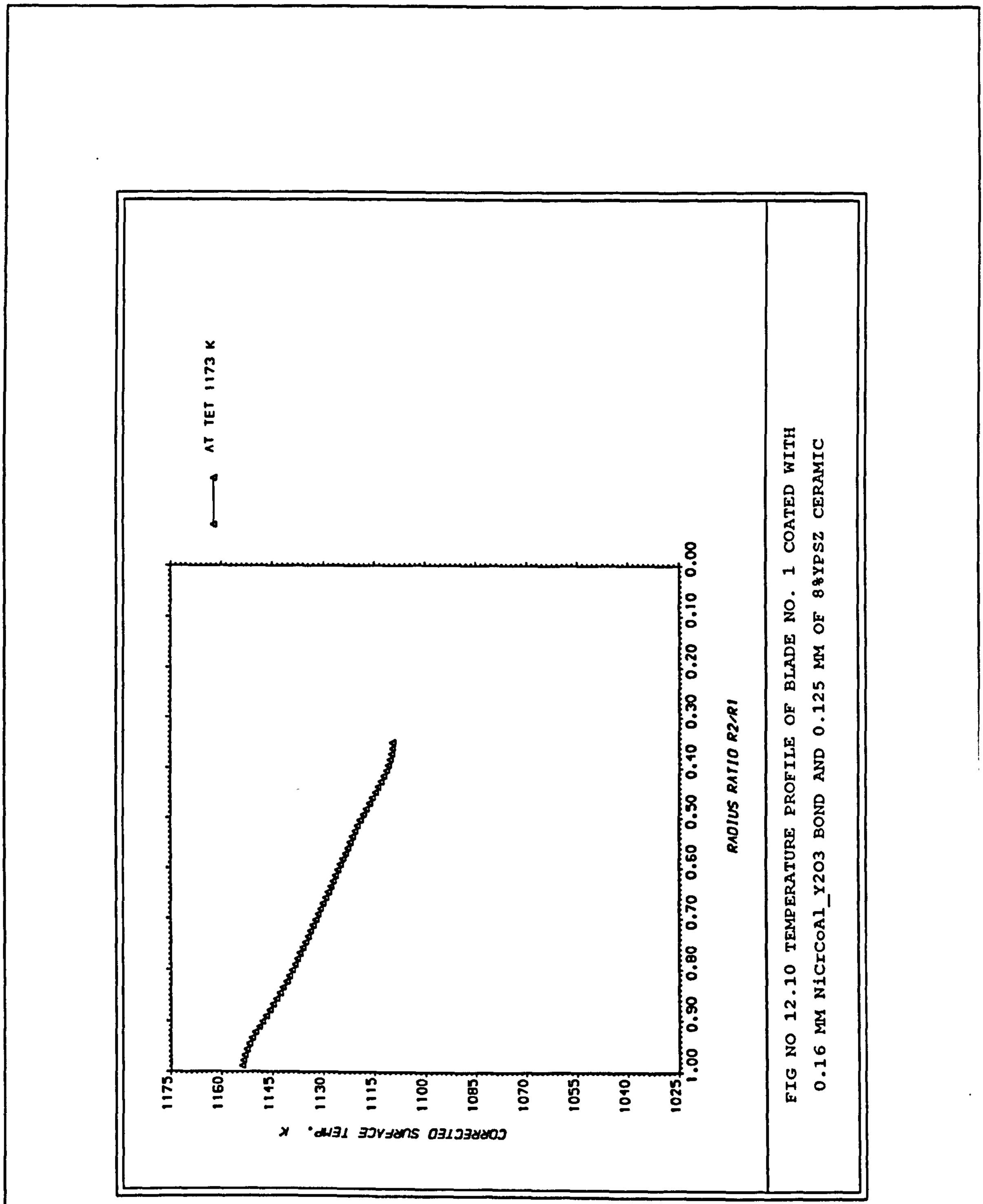

FIG NO 12.10 TEMPERATURE PROFILE OF BLADE NO. 1 COATED WITH
0.16 MM NiCrCoAl_Y2O3 BOND AND 0.125 MM OF 8%YPSZ CERAMIC

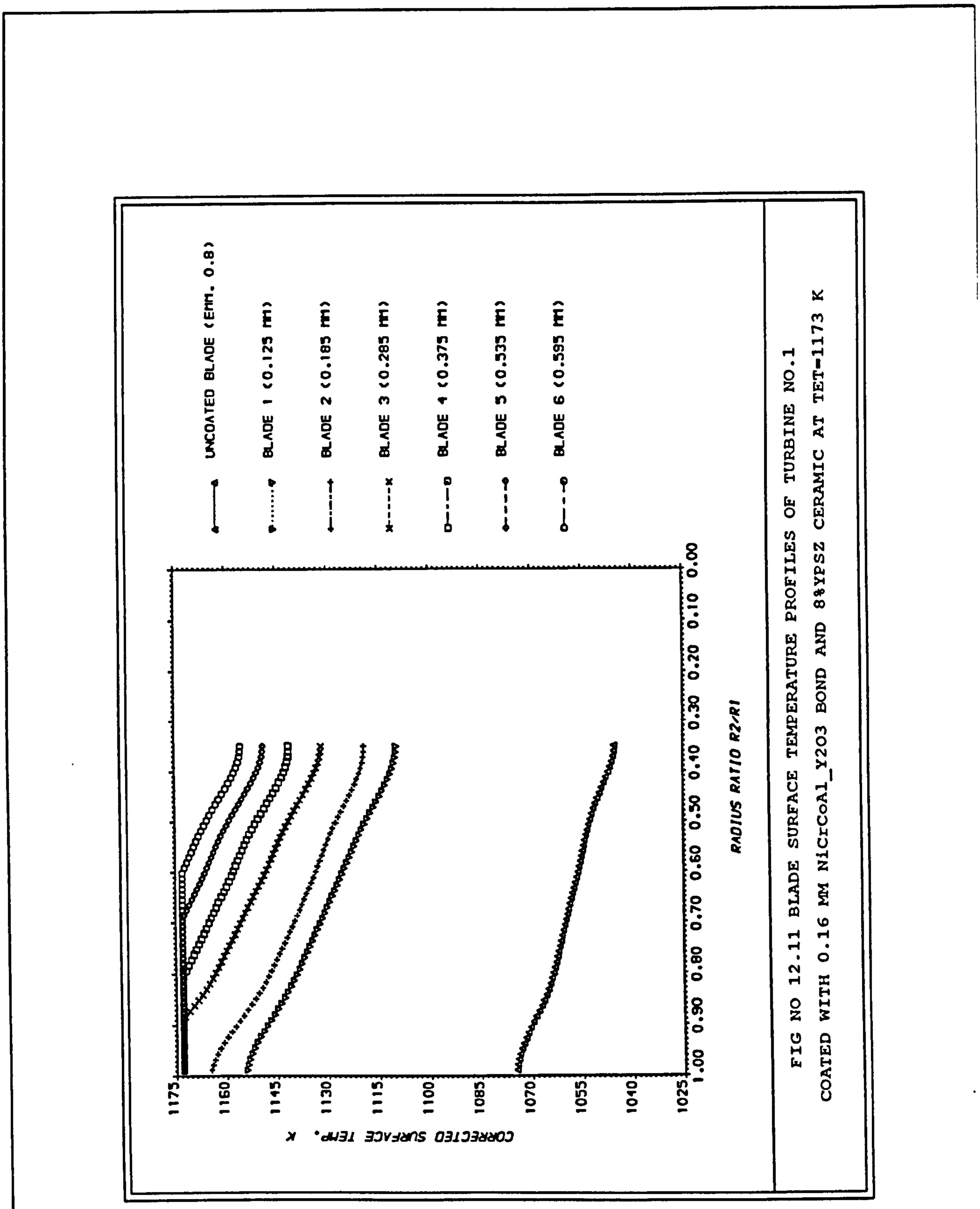

FIG NO 12.11 BLADE SURFACE TEMPERATURE PROFILES OF TURBINE NO.1
COATED WITH 0.16 MM NiCrCoAl_Y2O3 BOND AND 8%YPSZ CERAMIC AT TET=1173 K

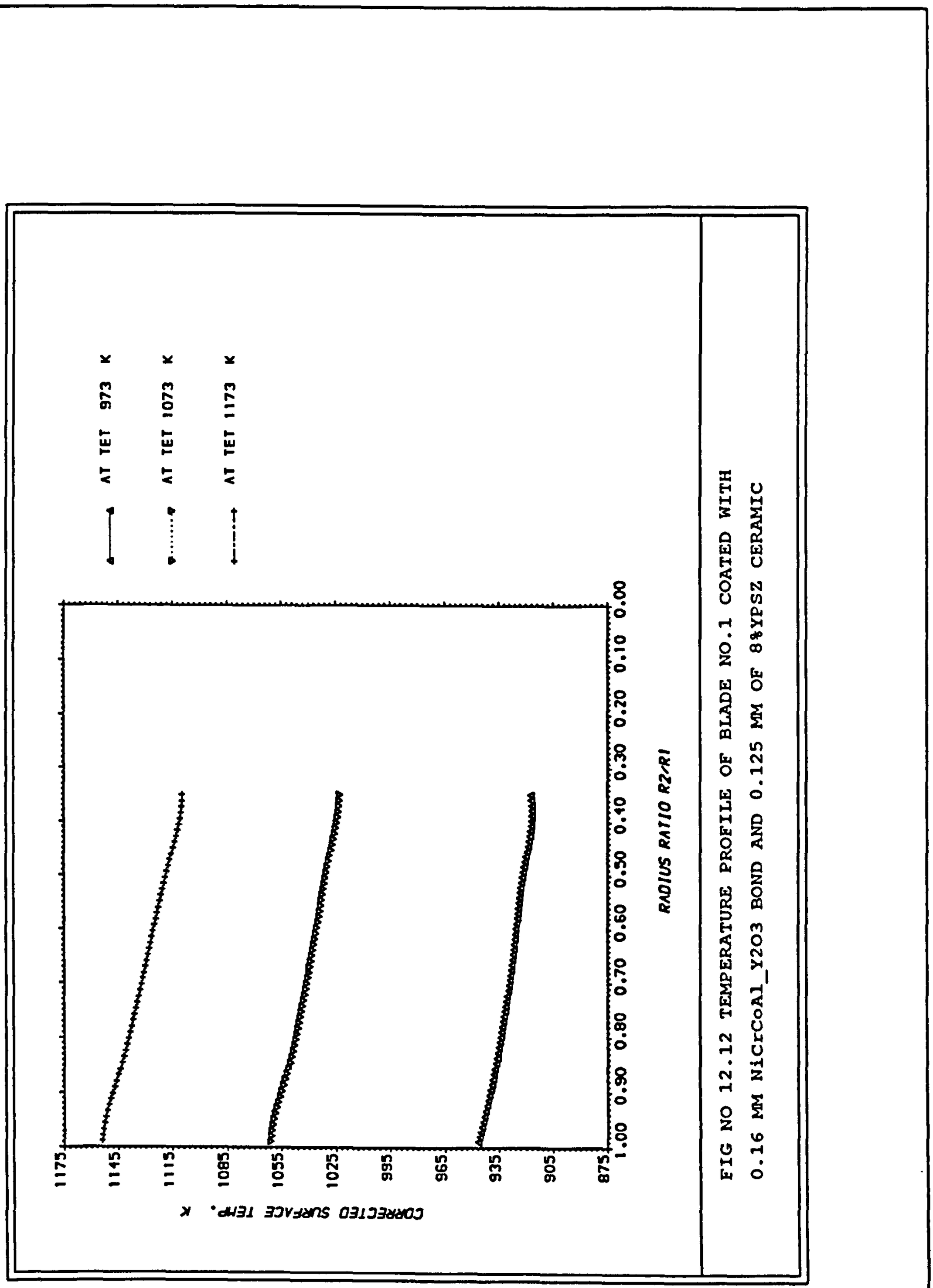

FIG NO 12.12 TEMPERATURE PROFILE OF BLADE NO.1 COATED WITH
0.16 MM NiCrCoAl_Y2O3 BOND AND 0.125 MM OF 8%YPSZ CERAMIC

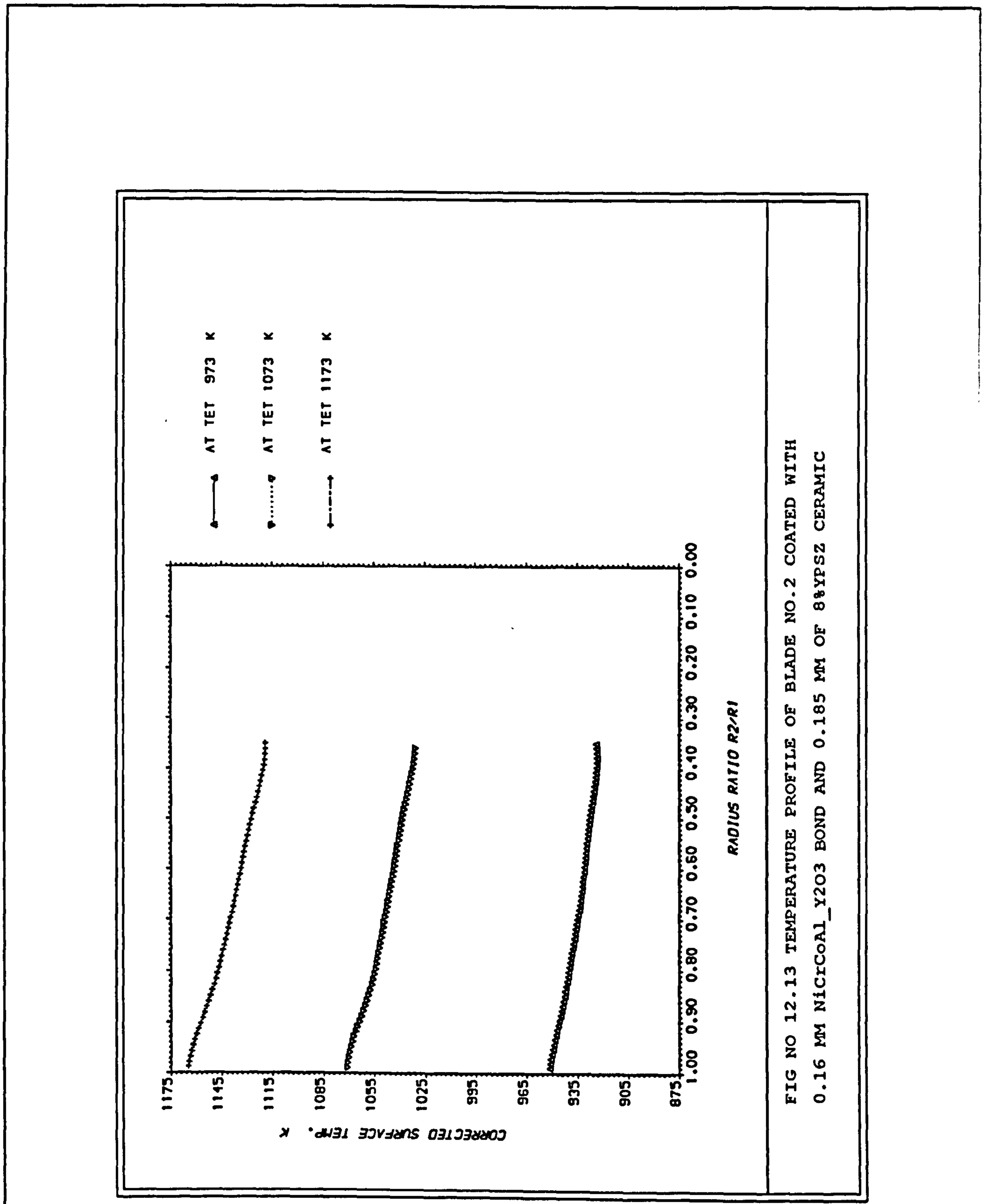

FIG NO 12.13 TEMPERATURE PROFILE OF BLADE NO.2 COATED WITH
0.16 MM NiCrCoAl_Y2O3 BOND AND 0.185 MM OF 8%YPSZ CERAMIC

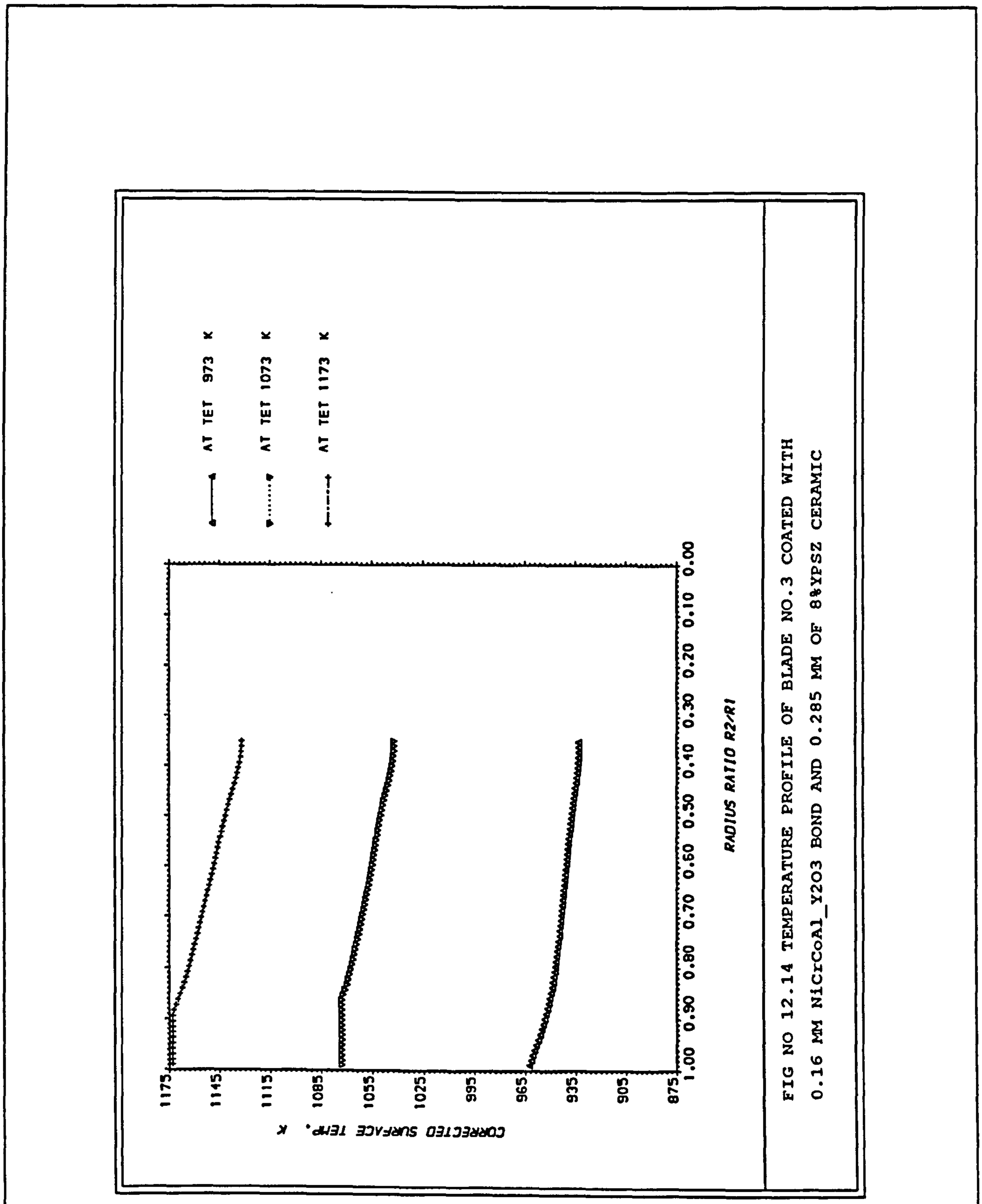

FIG NO 12.14 TEMPERATURE PROFILE OF BLADE NO.3 COATED WITH 0.16 MM NiCrCoAl_Y2O3 BOND AND 0.285 MM OF 8%YPSZ CERAMIC

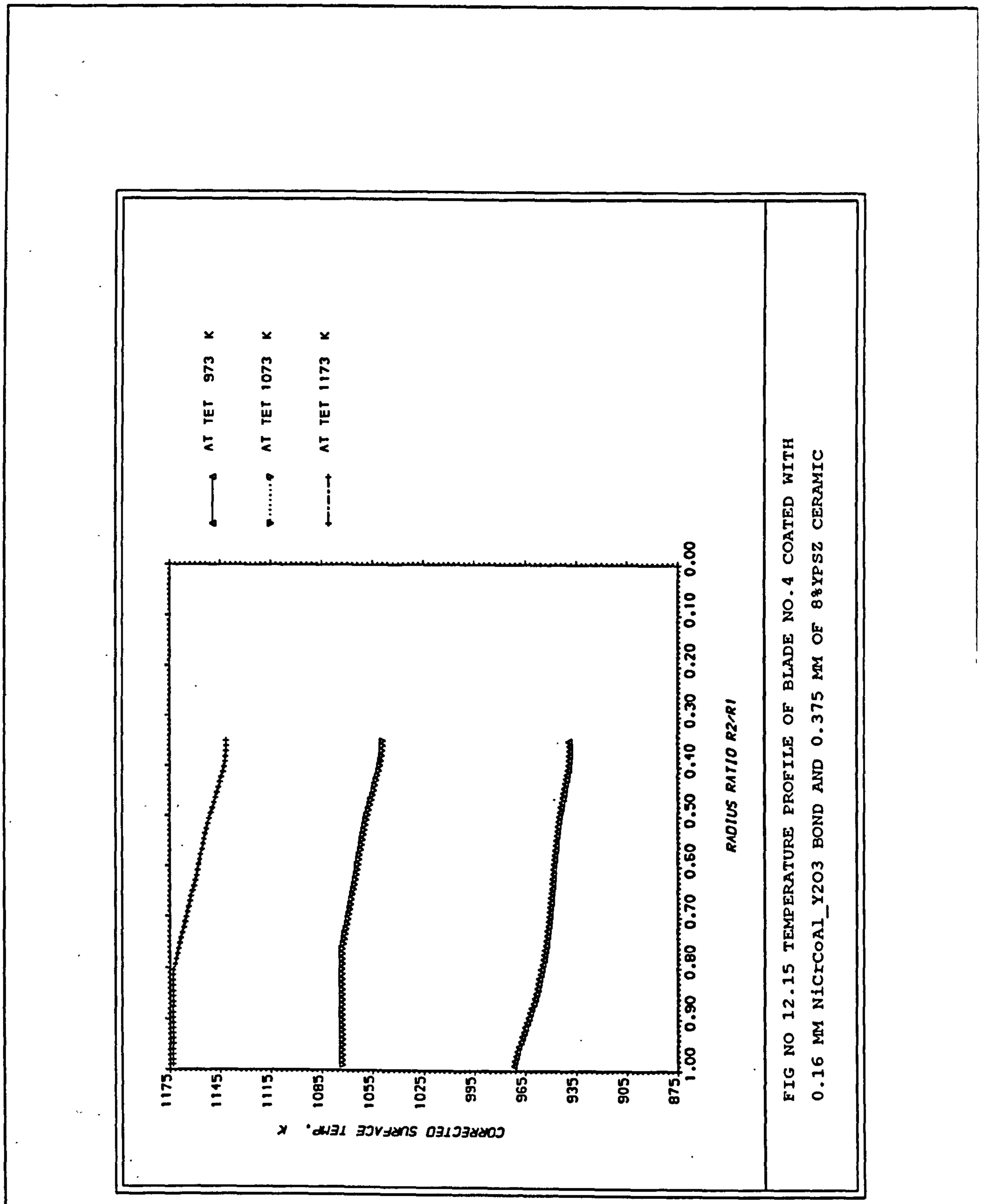

FIG NO 12.15 TEMPERATURE PROFILE OF BLADE NO.4 COATED WITH 0.16 MM NiCrCoAl_Y2O3 BOND AND 0.375 MM OF 8%YPSZ CERAMIC

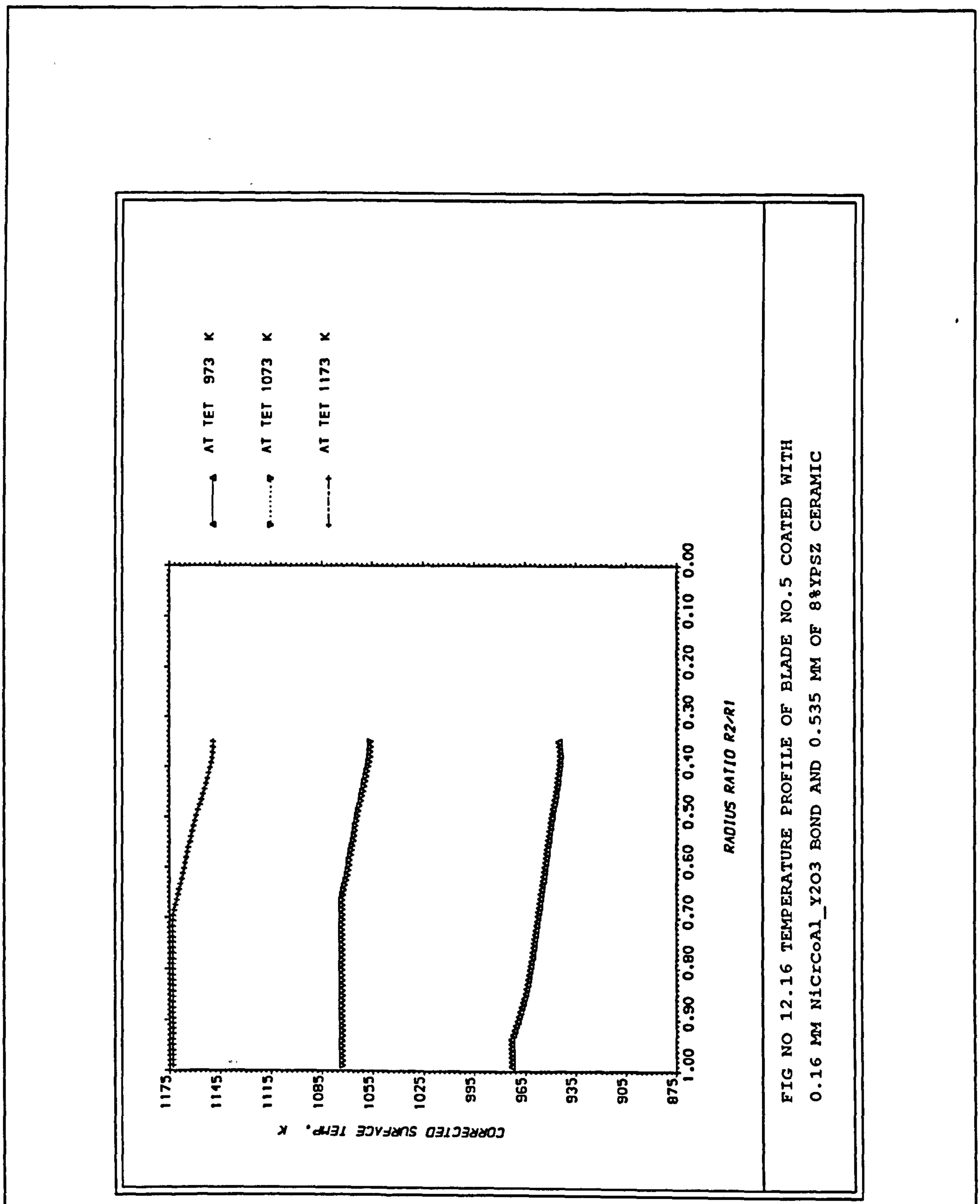

FIG NO 12.16 TEMPERATURE PROFILE OF BLADE NO.5 COATED WITH
0.16 MM NiCrCoAl_Y2O3 BOND AND 0.535 MM OF 8%YPSZ CERAMIC

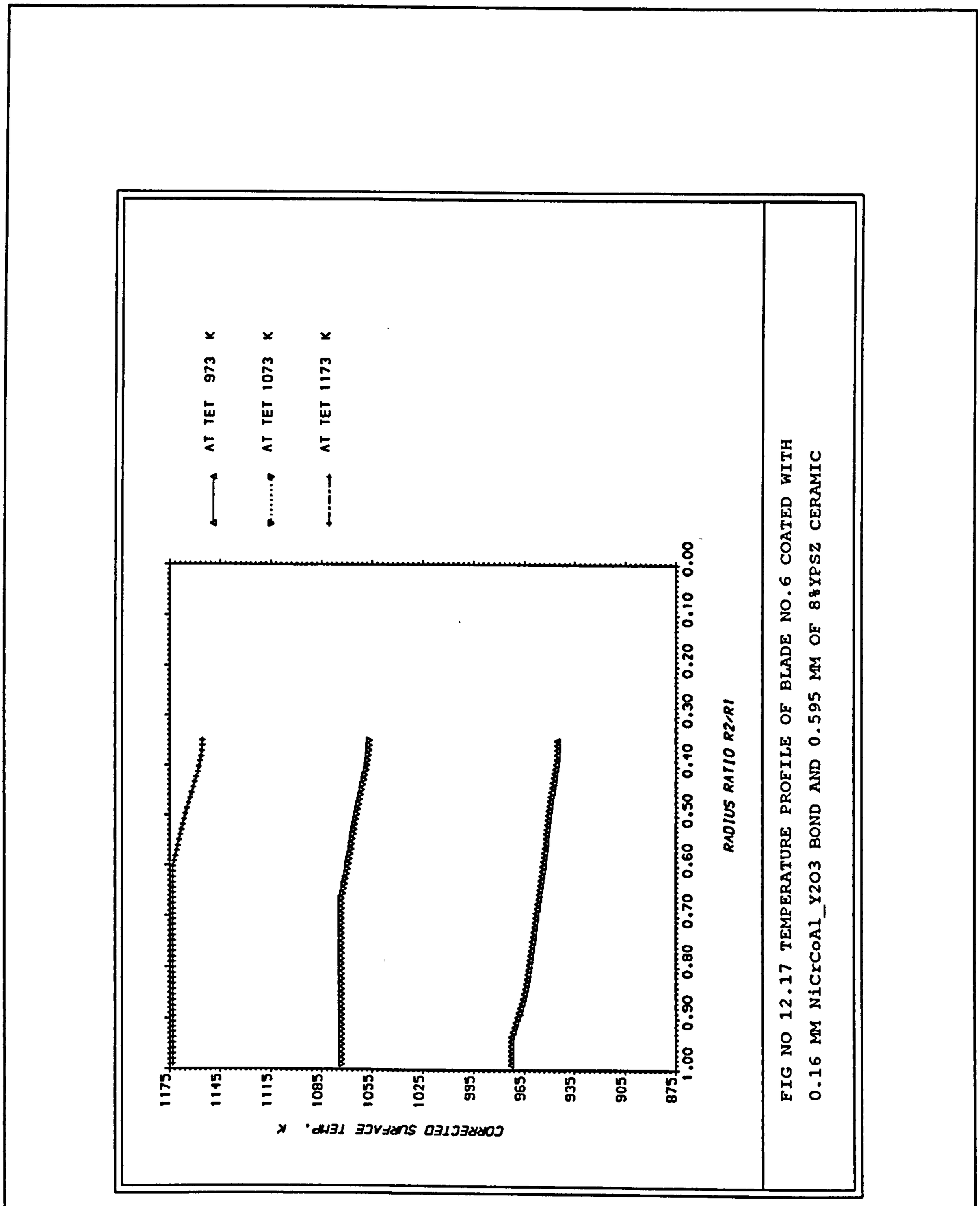

FIG NO 12.17 TEMPERATURE PROFILE OF BLADE NO.6 COATED WITH 0.16 MM NiCrCoAl_Y2O3 BOND AND 0.595 MM OF 8%YPSZ CERAMIC

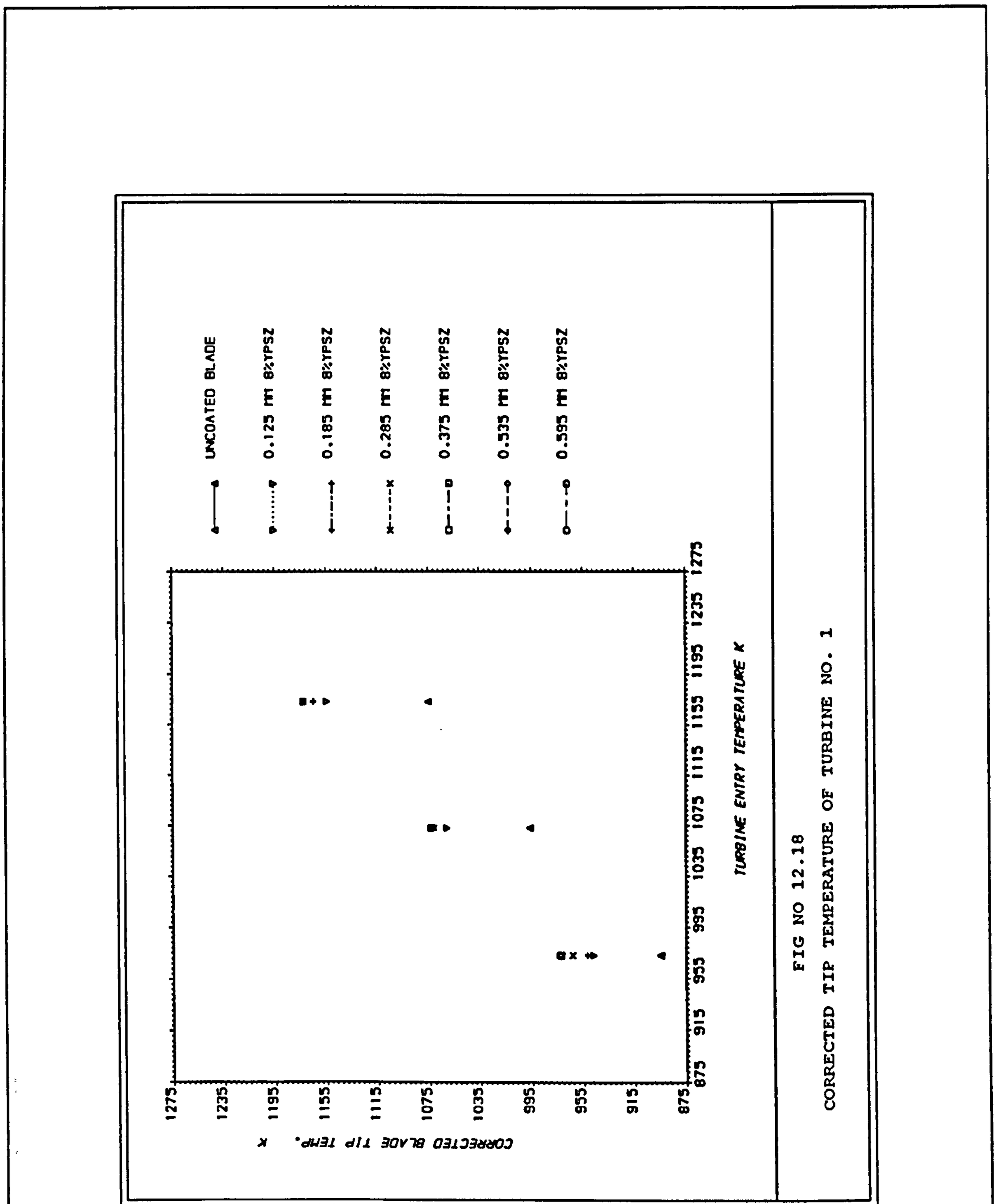
UNCOATED BLADE
0.125 MM 8%YPSZ
0.185 MM 8%YPSZ
0.285 MM 8%YPSZ
0.375 MM 8%YPSZ
0.535 MM 8%YPSZ
0.595 MM 8%YPSZ
CORRECTED BLADE TIP TEMP. K
1275
1235
1195
1155
1115
1075
1035
995
955
915
875
TURBINE ENTRY TEMPERATURE K
875
915
955
995
1035
1075
1115
1155
1195
1235
1275
CORRECTED TIP TEMPERATURE OF TURBINE NO. 1

FIG NO 12.18

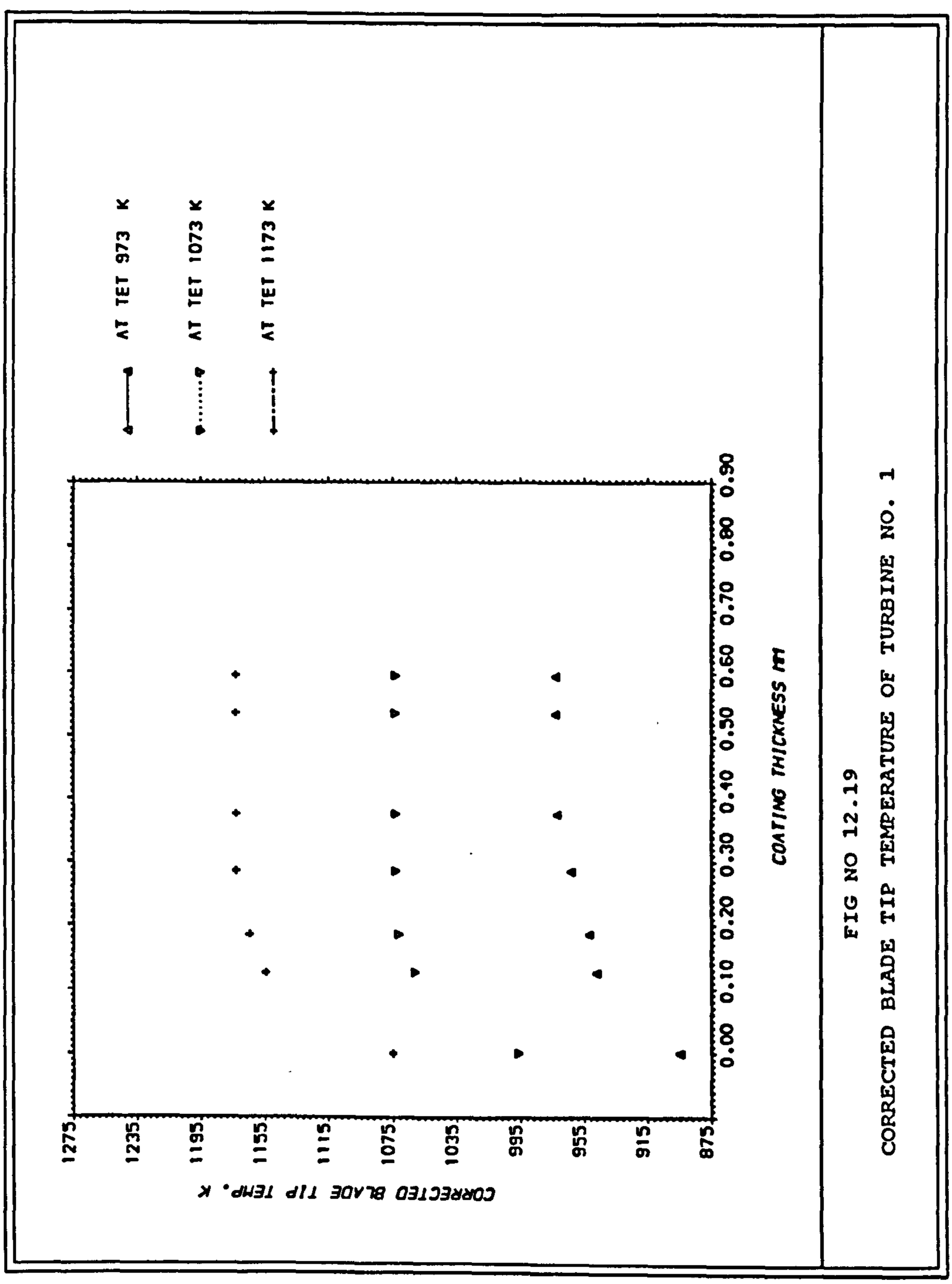

FIG NO 12.19

CORRECTED BLADE TIP TEMPERATURE OF TURBINE NO. 1

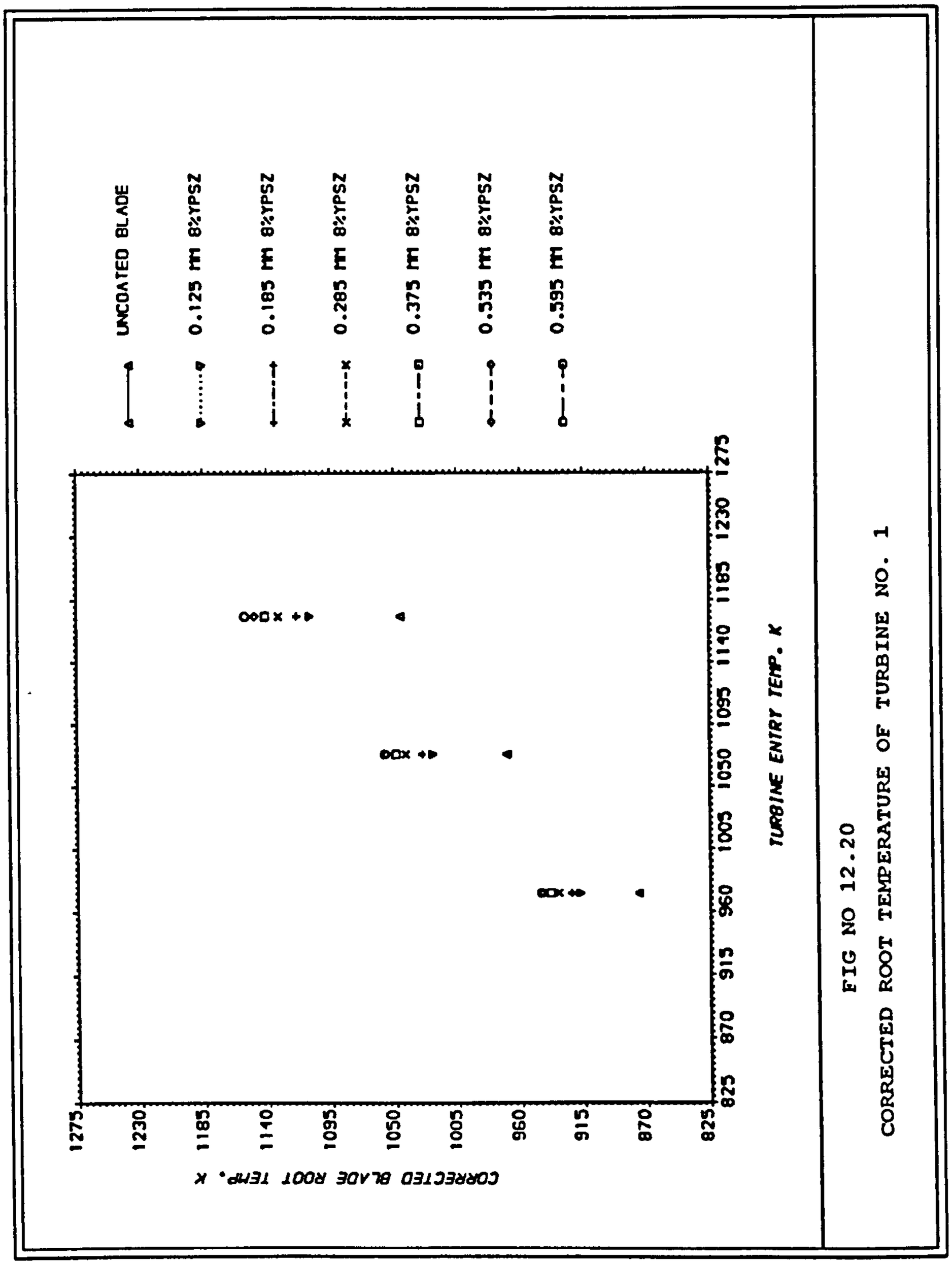

FIG NO 12.20

CORRECTED ROOT TEMPERATURE OF TURBINE NO. 1

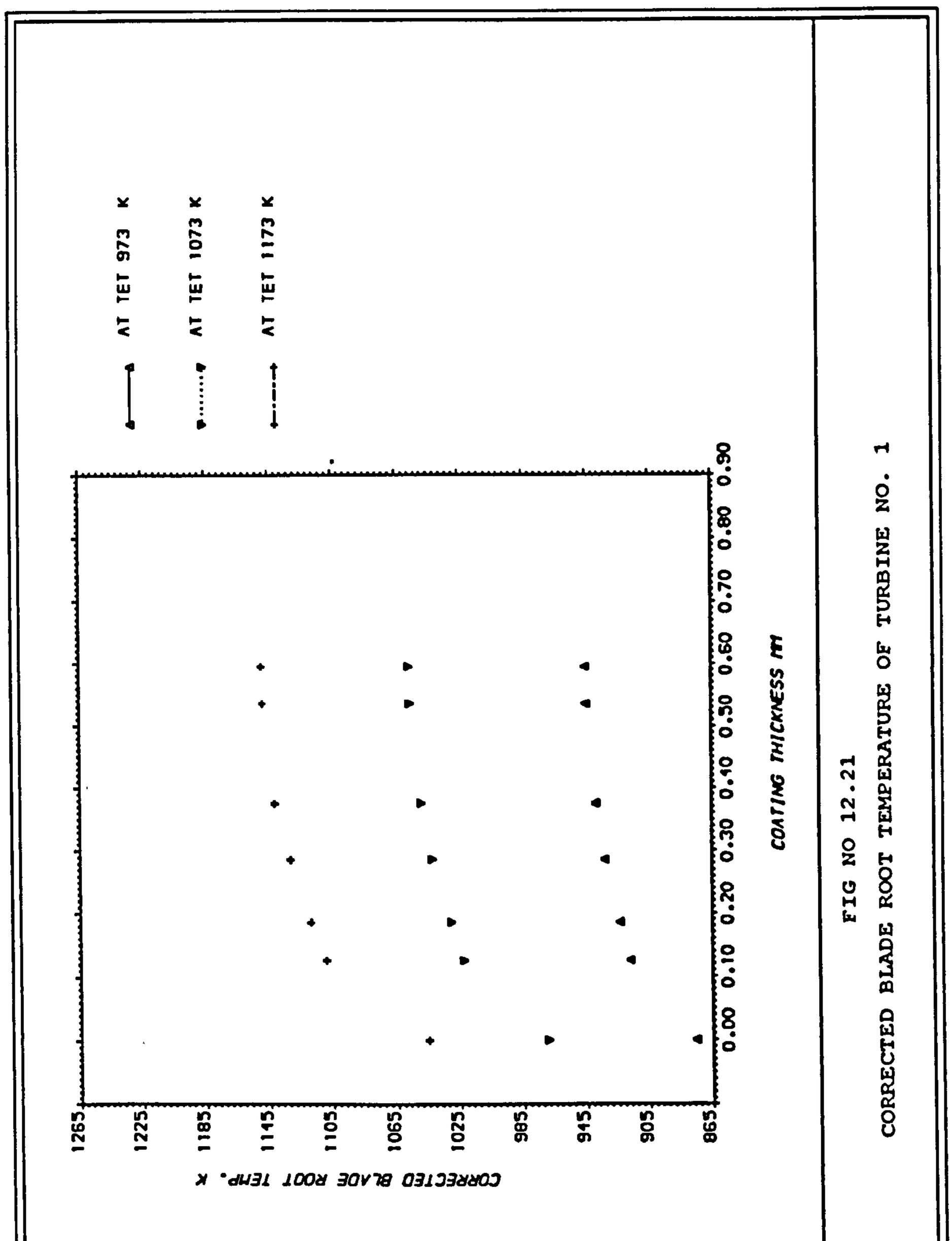

FIG NO 12.21

CORRECTED BLADE ROOT TEMPERATURE OF TURBINE NO. 1

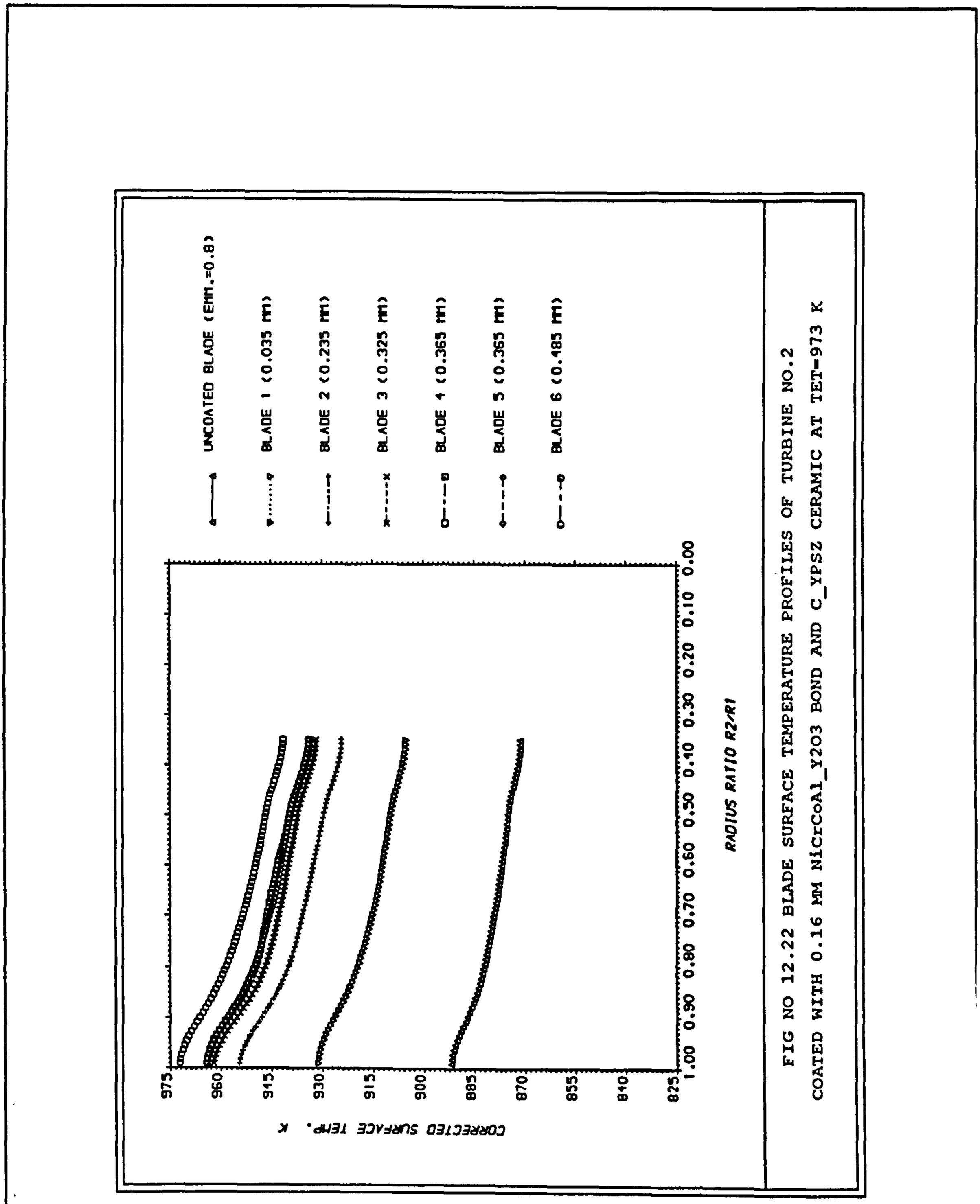

FIG NO 12.22 BLADE SURFACE TEMPERATURE PROFILES OF TURBINE NO.2
COATED WITH 0.16 MM NiCrCoAl_Y2O3 BOND AND C_YPSZ CERAMIC AT TET=973 K

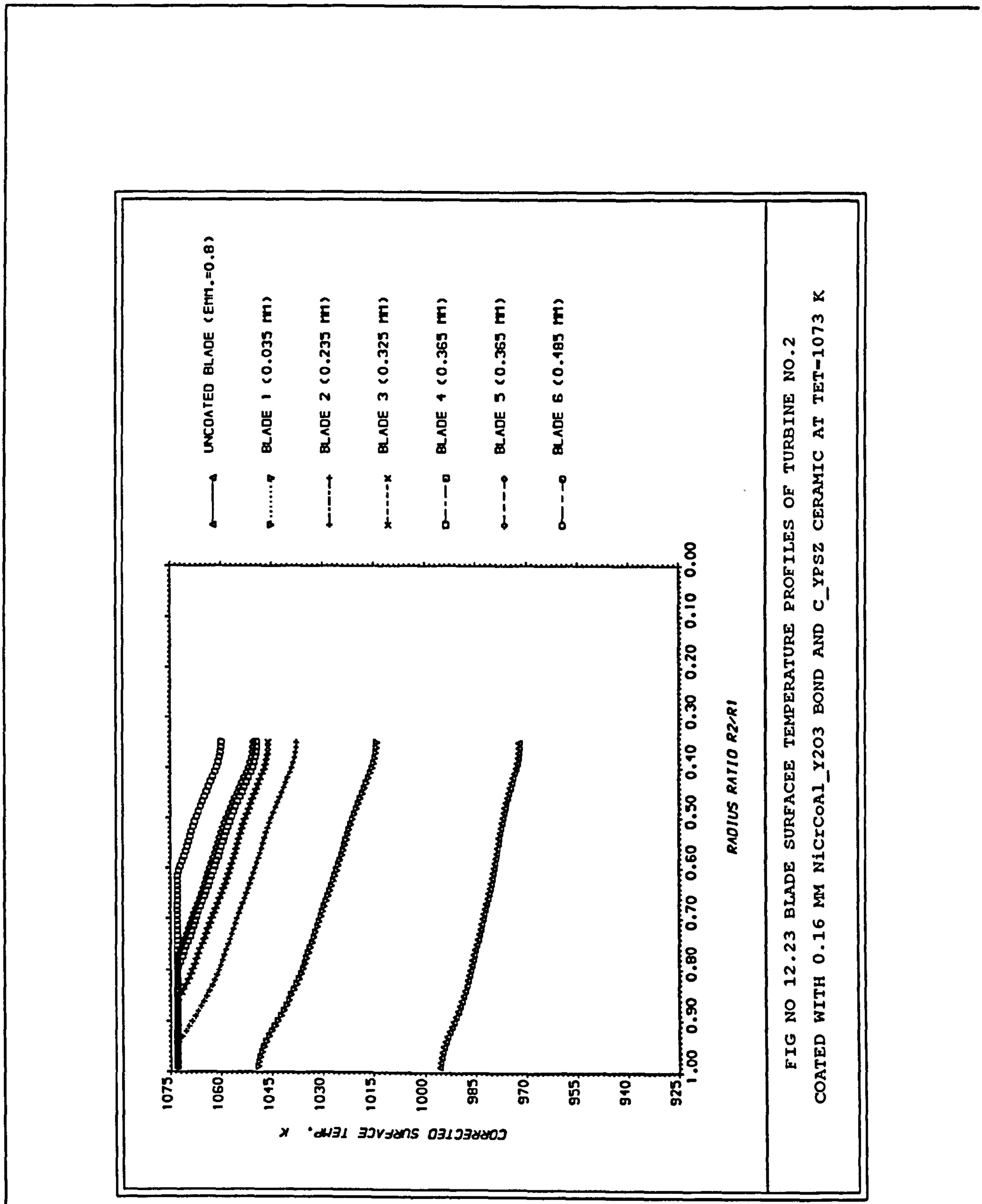

FIG NO 12.23 BLADE SURFACEE TEMPERATURE PROFILES OF TURBINE NO.2
COATED WITH 0.16 MM NiCrCoAl_Y2O3 BOND AND C_YPSZ CERAMIC AT TET=1073 K

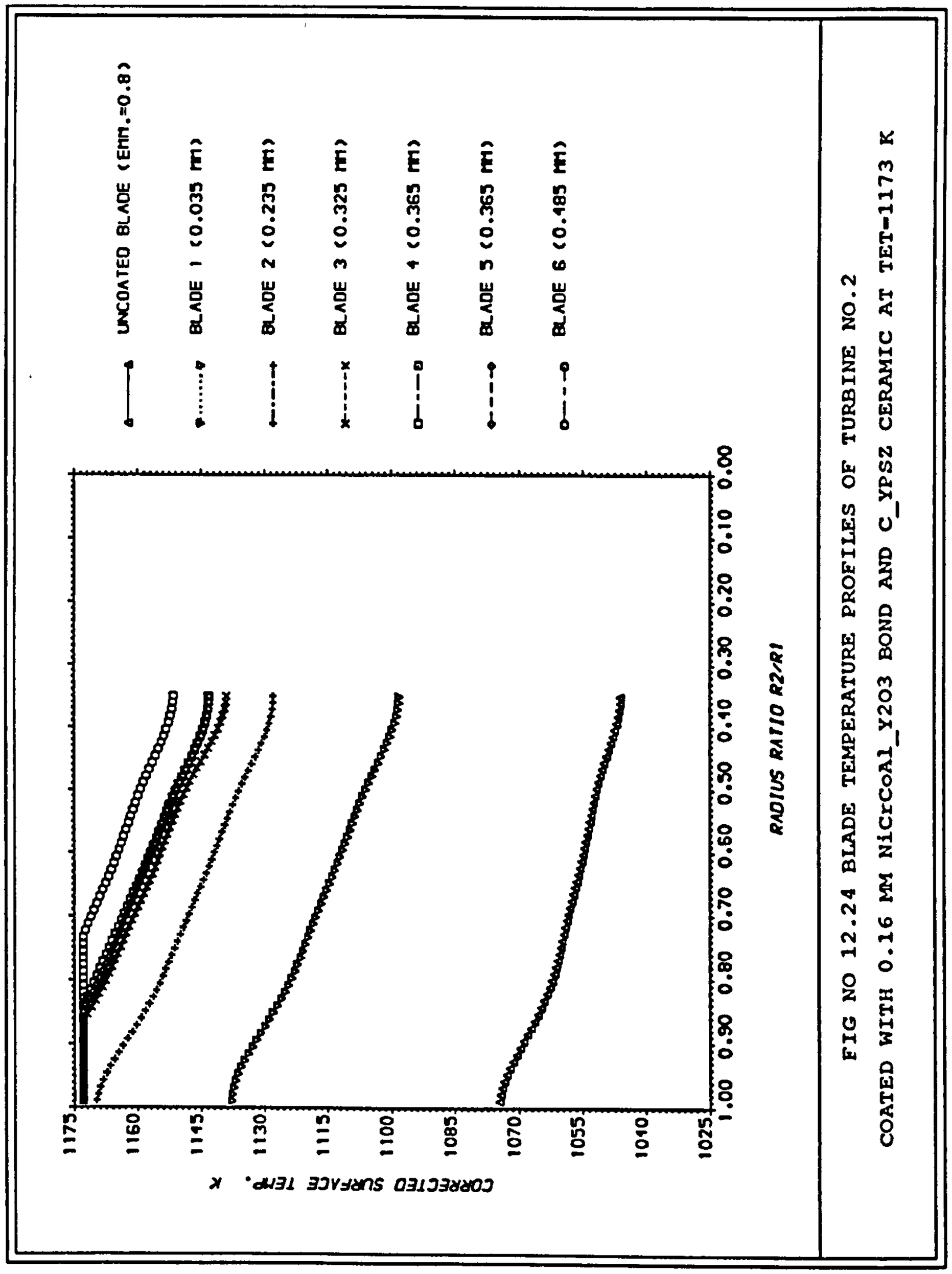

FIG NO 12.24 BLADE TEMPERATURE PROFILES OF TURBINE NO.2
COATED WITH 0.16 MM NiCrCoAl_Y2O3 BOND AND C_YPSZ CERAMIC AT TET-1173 K

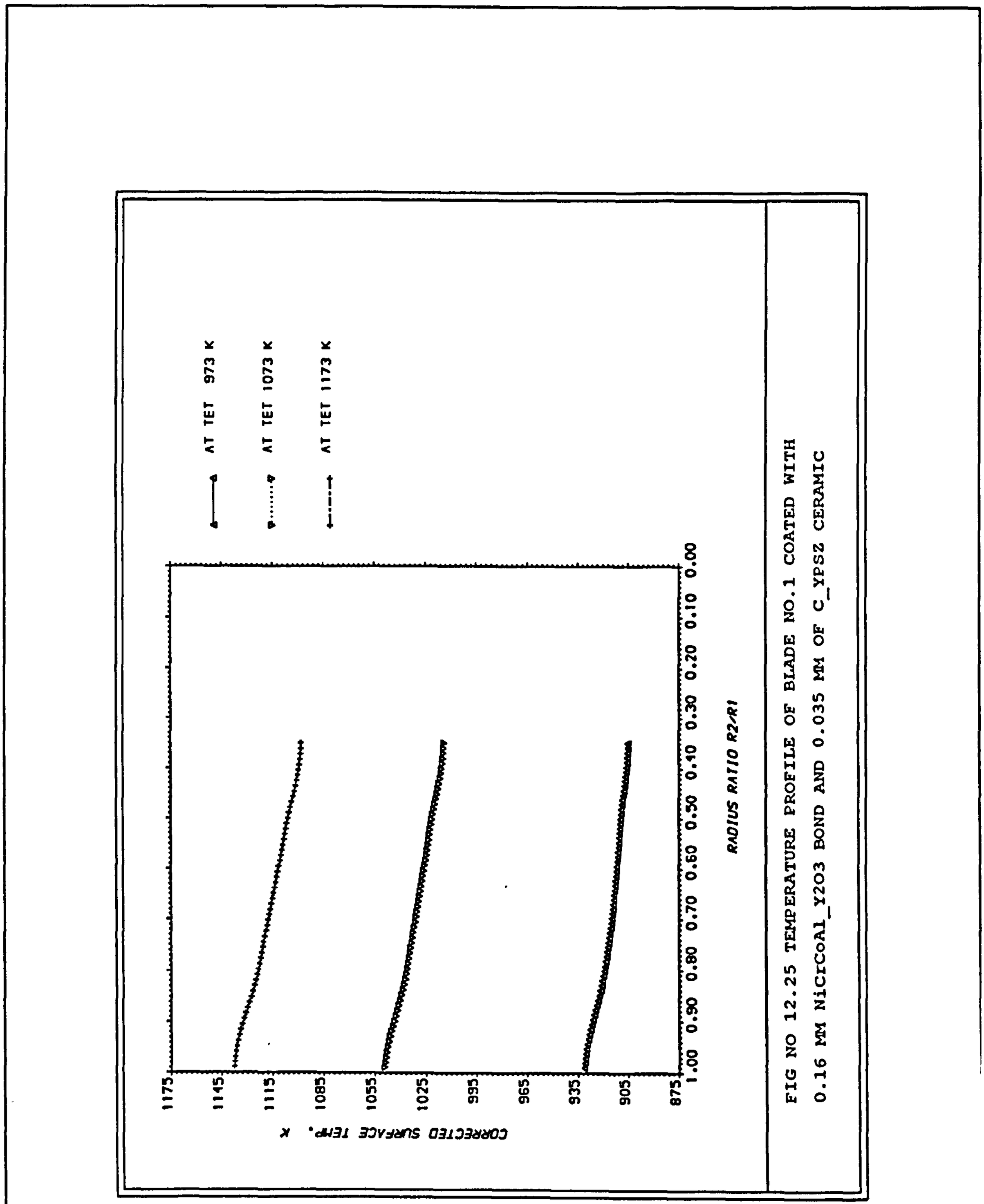

FIG NO 12.25 TEMPERATURE PROFILE OF BLADE NO.1 COATED WITH 0.16 MM NiCrCoAl_Y2O3 BOND AND 0.035 MM OF C_YPSZ CERAMIC

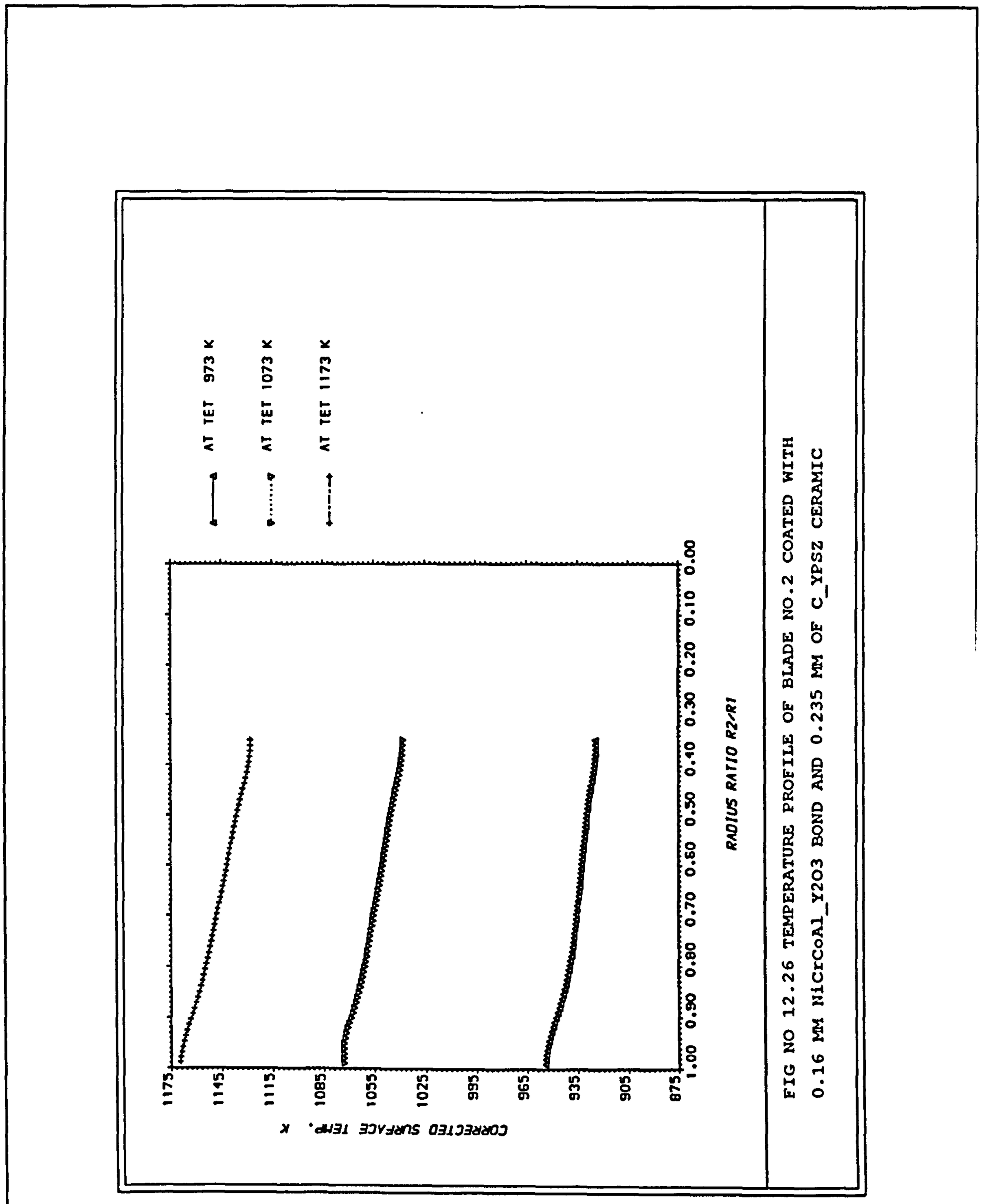

FIG NO 12.26 TEMPERATURE PROFILE OF BLADE NO.2 COATED WITH 0.16 MM NiCrCoAl_Y2O3 BOND AND 0.235 MM OF C_YPSZ CERAMIC

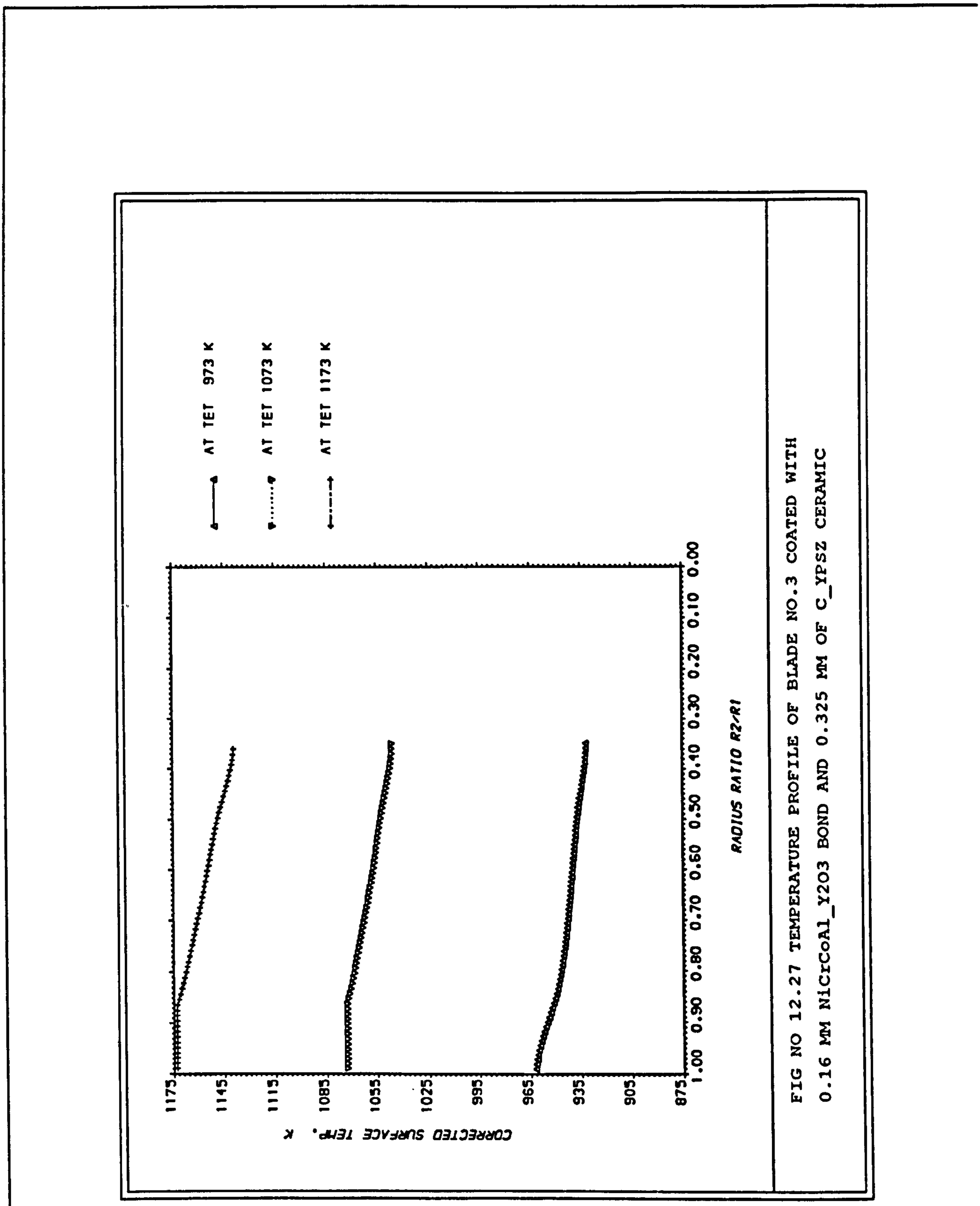

FIG NO 12.27 TEMPERATURE PROFILE OF BLADE NO.3 COATED WITH 0.16 MM NiCrCoAl_Y2O3 BOND AND 0.325 MM OF C_YPSZ CERAMIC

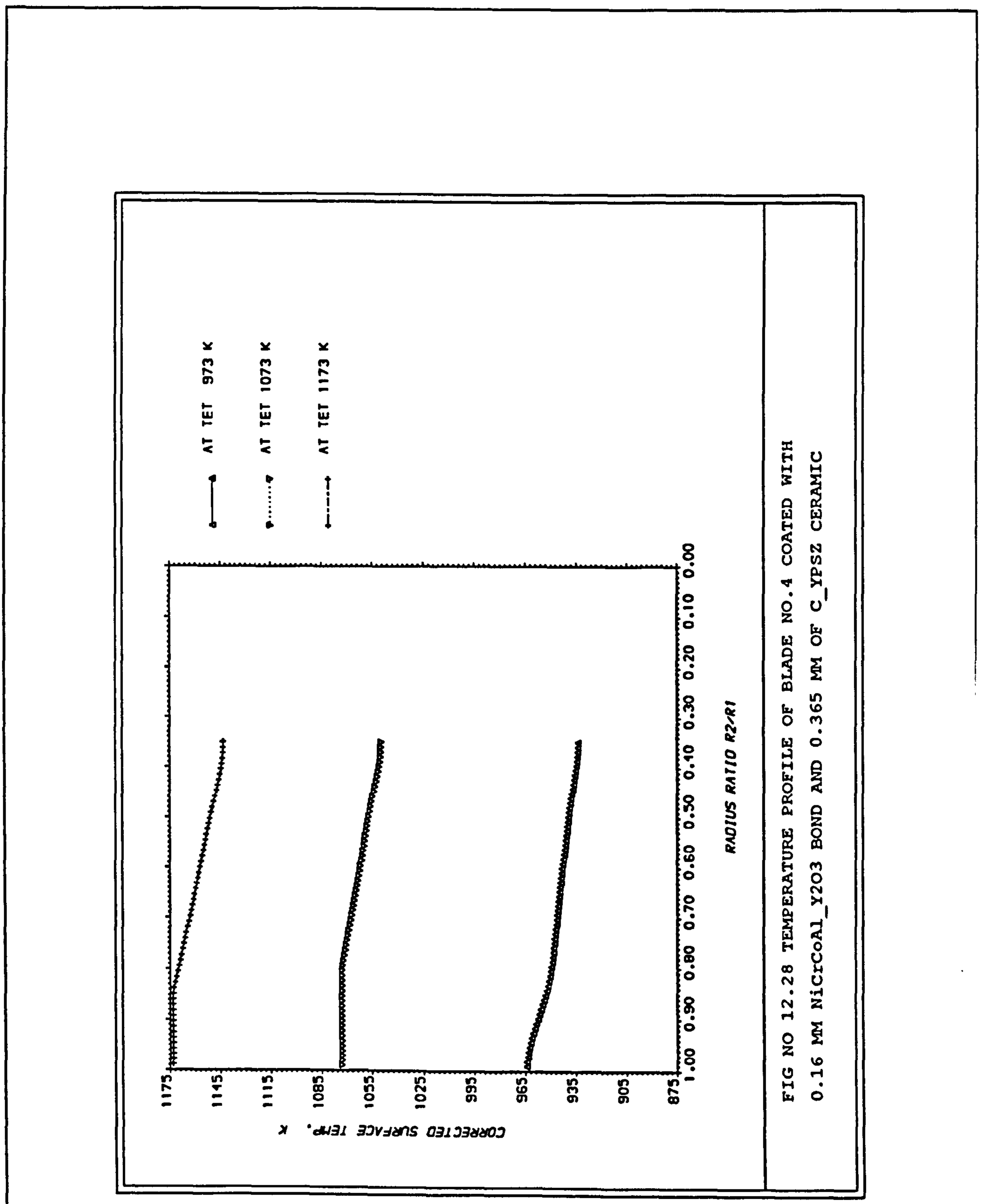

FIG NO 12.28 TEMPERATURE PROFILE OF BLADE NO.4 COATED WITH 0.16 MM NiCrCoAl_Y2O3 BOND AND 0.365 MM OF C_YPSZ CERAMIC

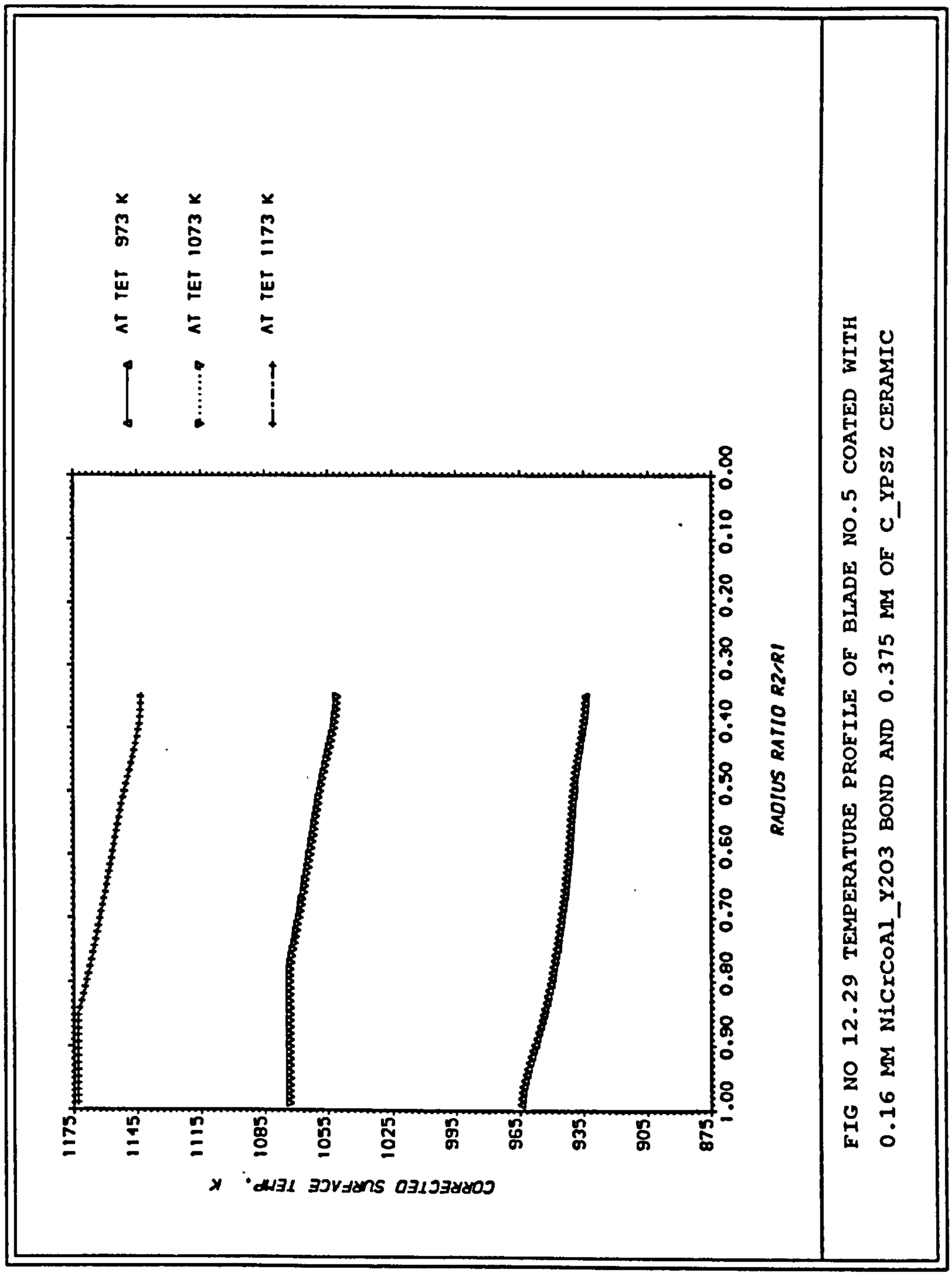

FIG NO 12.29 TEMPERATURE PROFILE OF BLADE NO.5 COATED WITH
0.16 MM NiCrCoAl_Y2O3 BOND AND 0.375 MM OF C_YPSZ CERAMIC

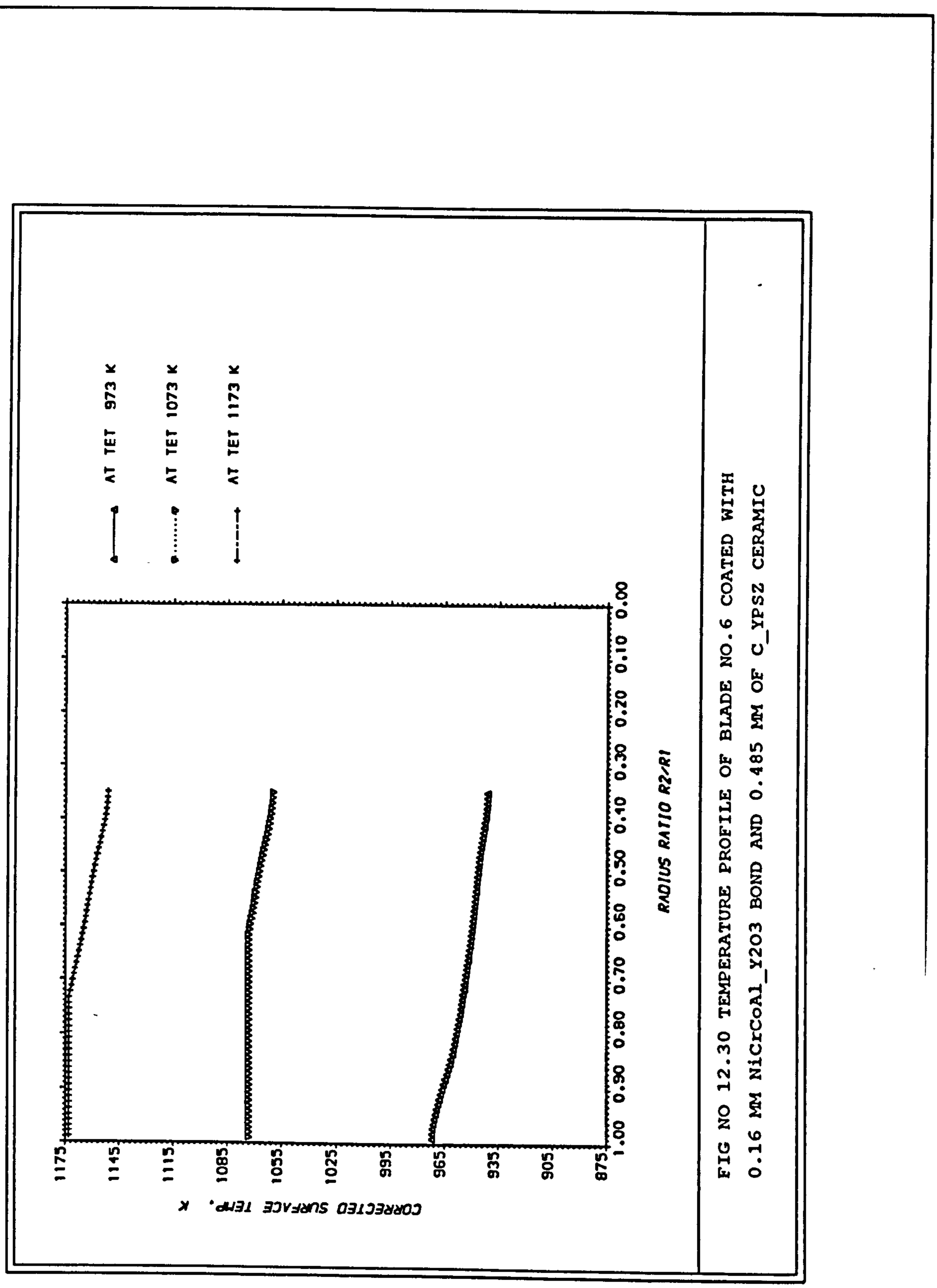

FIG NO 12.30 TEMPERATURE PROFILE OF BLADE NO.6 COATED WITH
0.16 MM NiCrCoAl_Y2O3 BOND AND 0.485 MM OF C_YPSZ CERAMIC

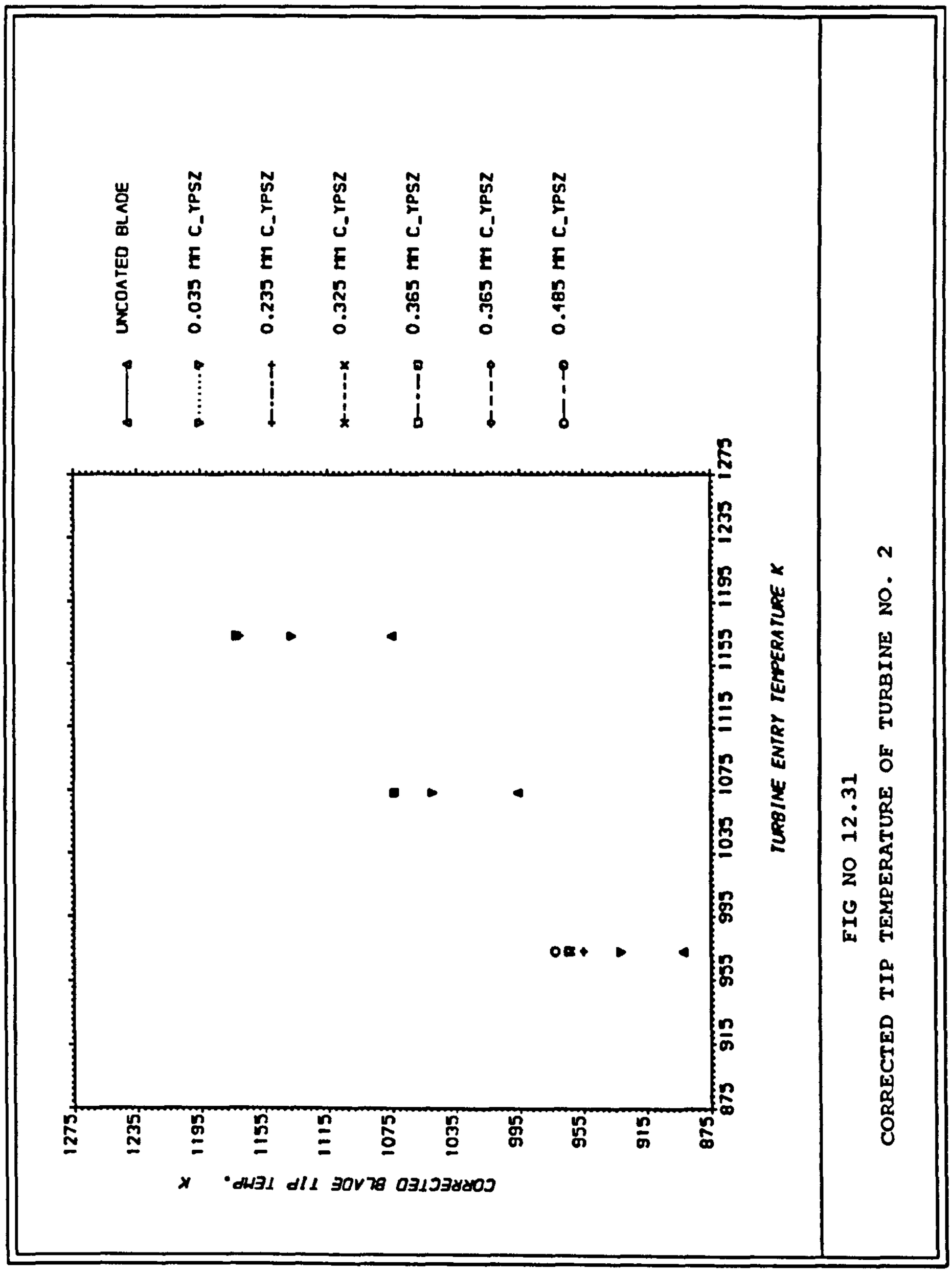

FIG NO 12.31

CORRECTED TIP TEMPERATURE OF TURBINE NO. 2

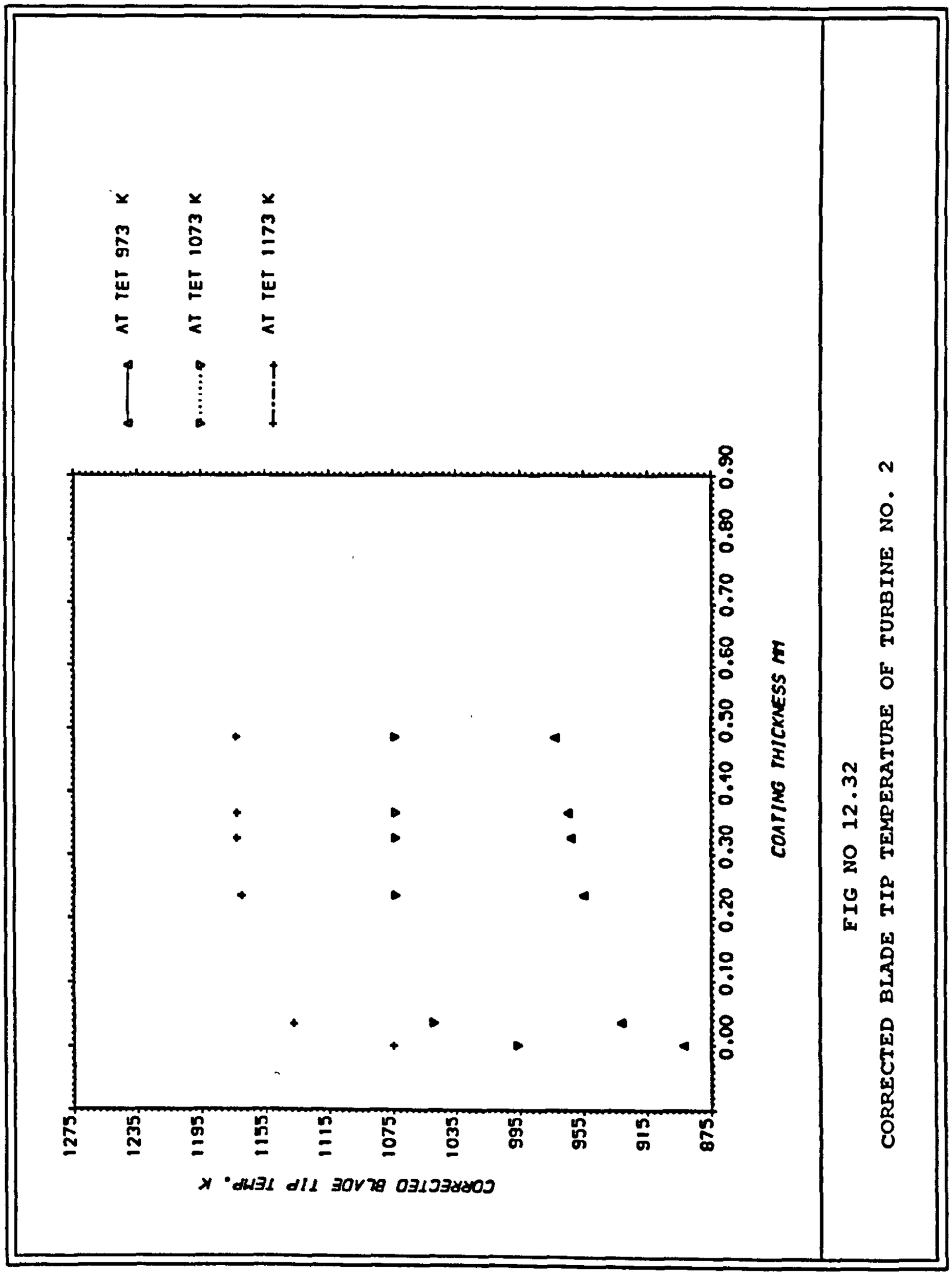

FIG NO 12.32

CORRECTED BLADE TIP TEMPERATURE OF TURBINE NO. 2

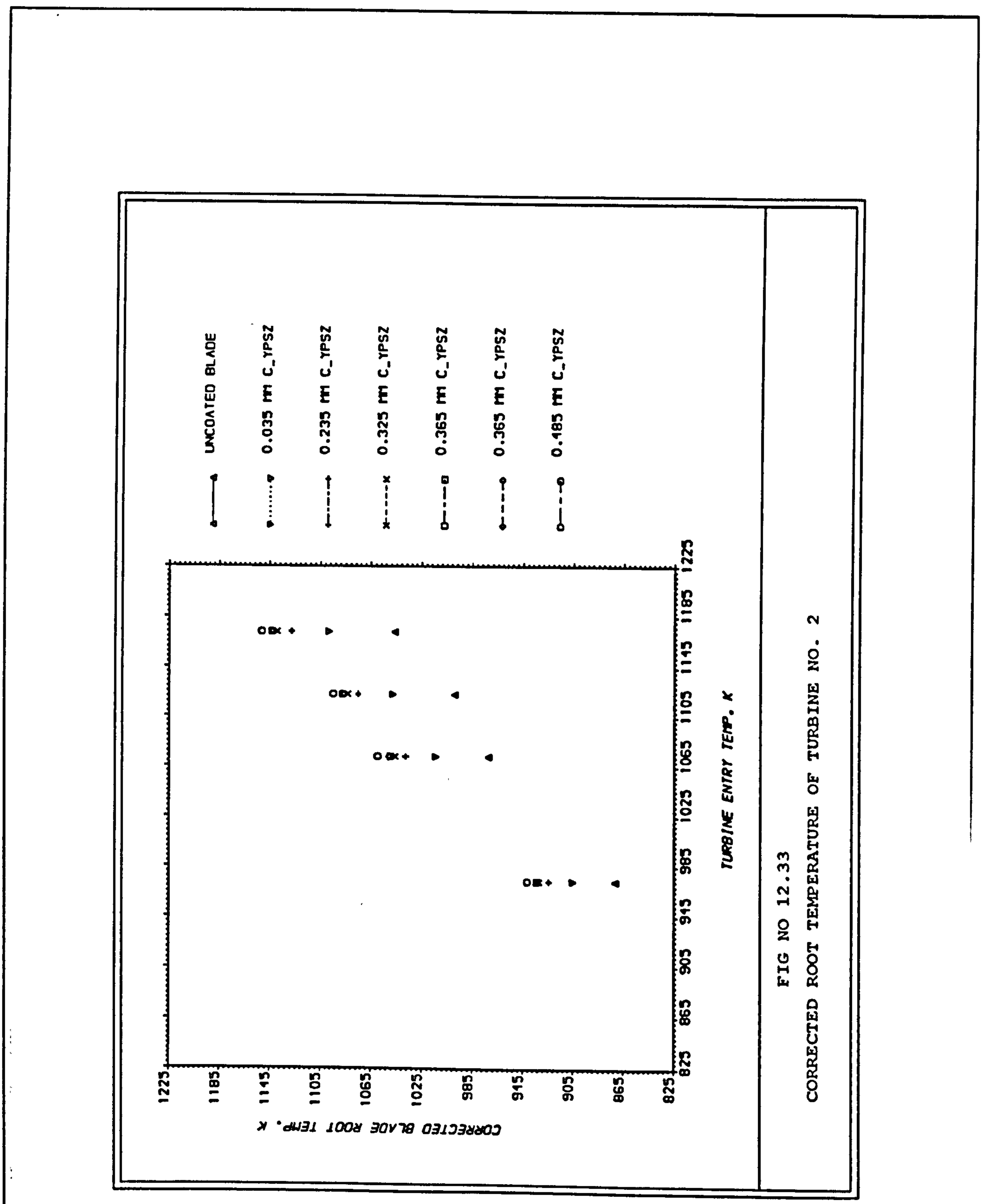

FIG NO 12.33

CORRECTED ROOT TEMPERATURE OF TURBINE NO. 2

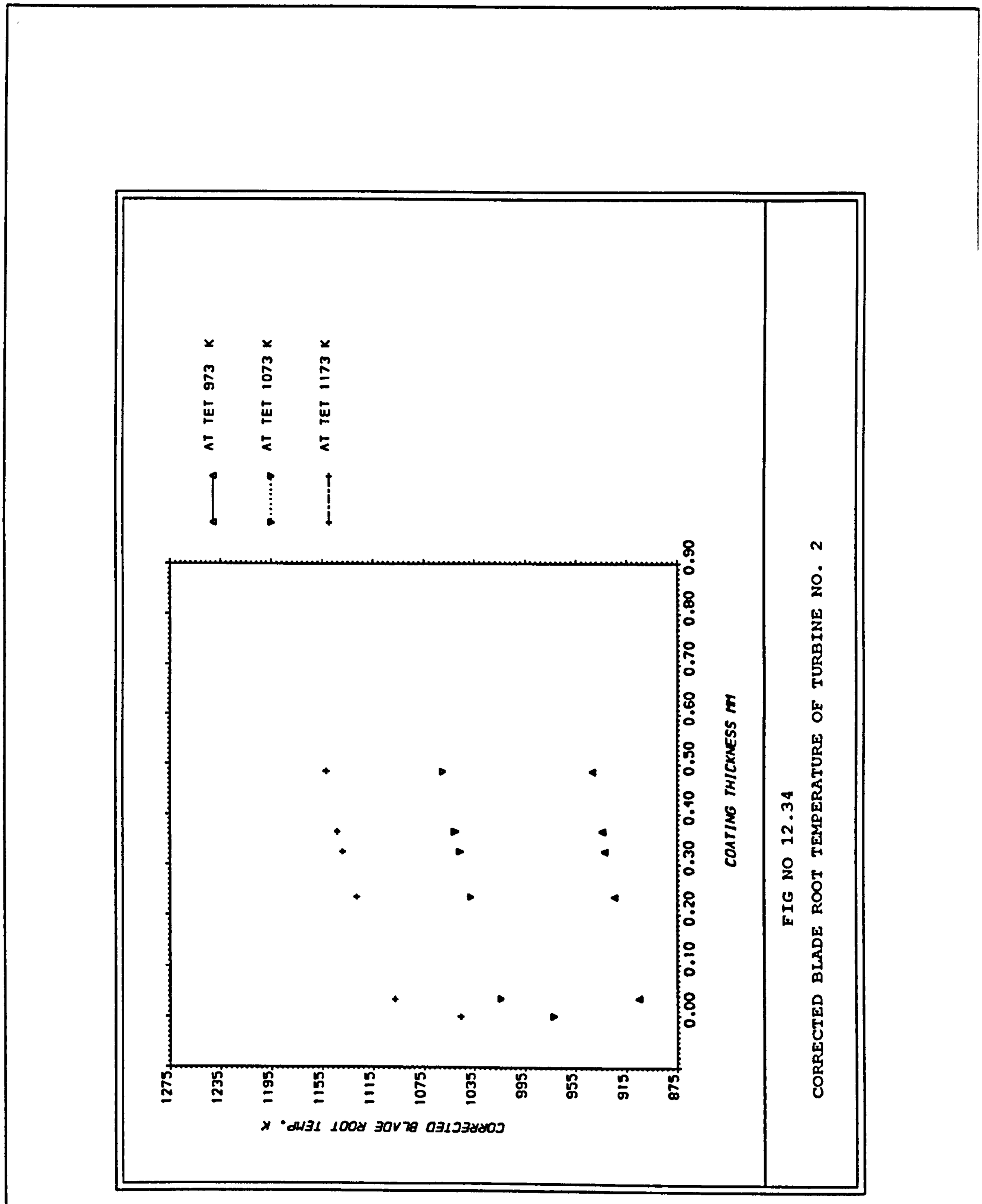

FIG NO 12.34

CORRECTED BLADE ROOT TEMPERATURE OF TURBINE NO. 2

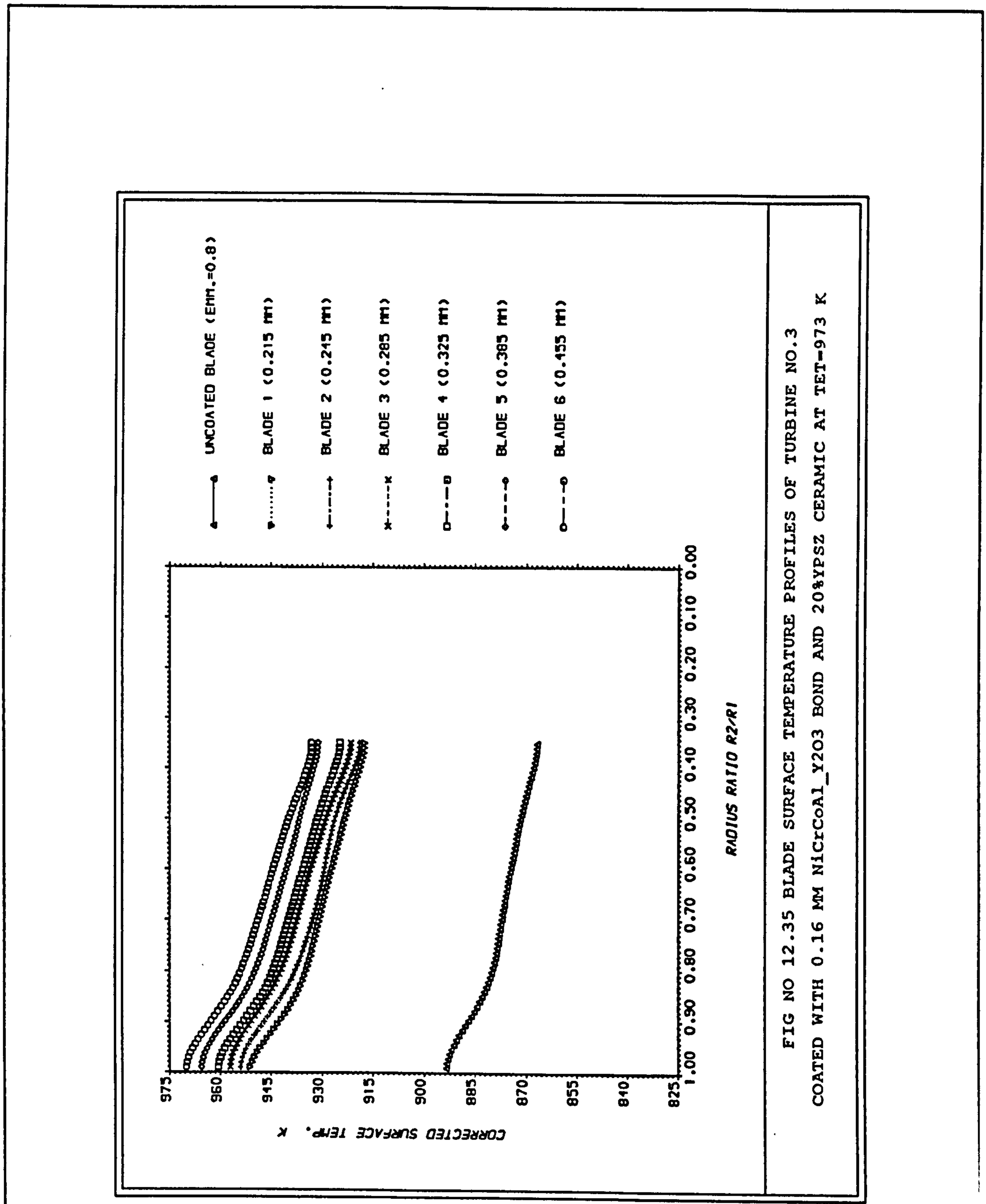

FIG NO 12.35 BLADE SURFACE TEMPERATURE PROFILES OF TURBINE NO.3
COATED WITH 0.16 MM NiCrCoAl_Y2O3 BOND AND 20%YPSZ CERAMIC AT TET=973 K

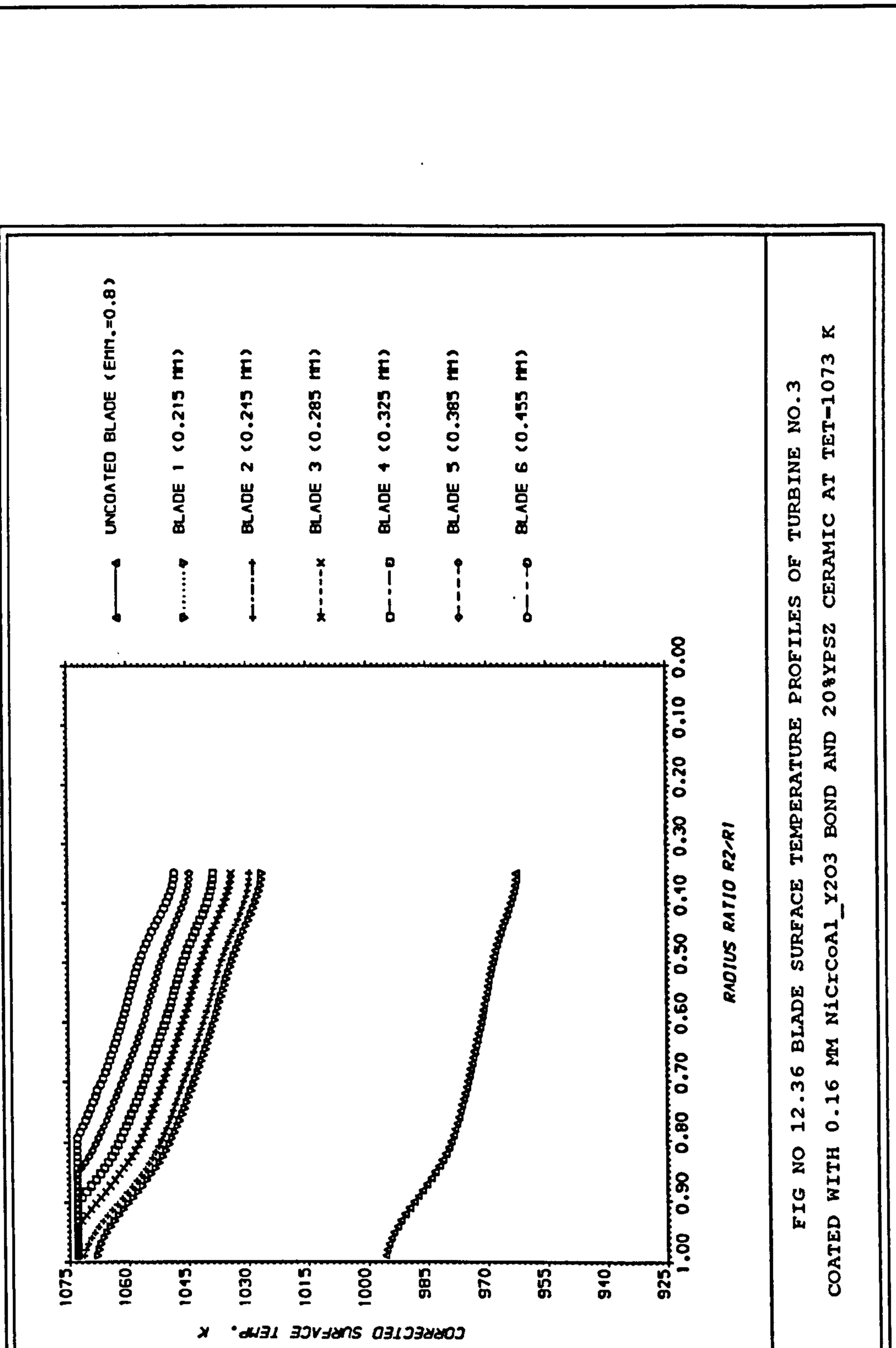

FIG NO 12.36 BLADE SURFACE TEMPERATURE PROFILES OF TURBINE NO.3
COATED WITH 0.16 MM NiCrCoAl_Y2O3 BOND AND 20%YPSZ CERAMIC AT TET=1073 K

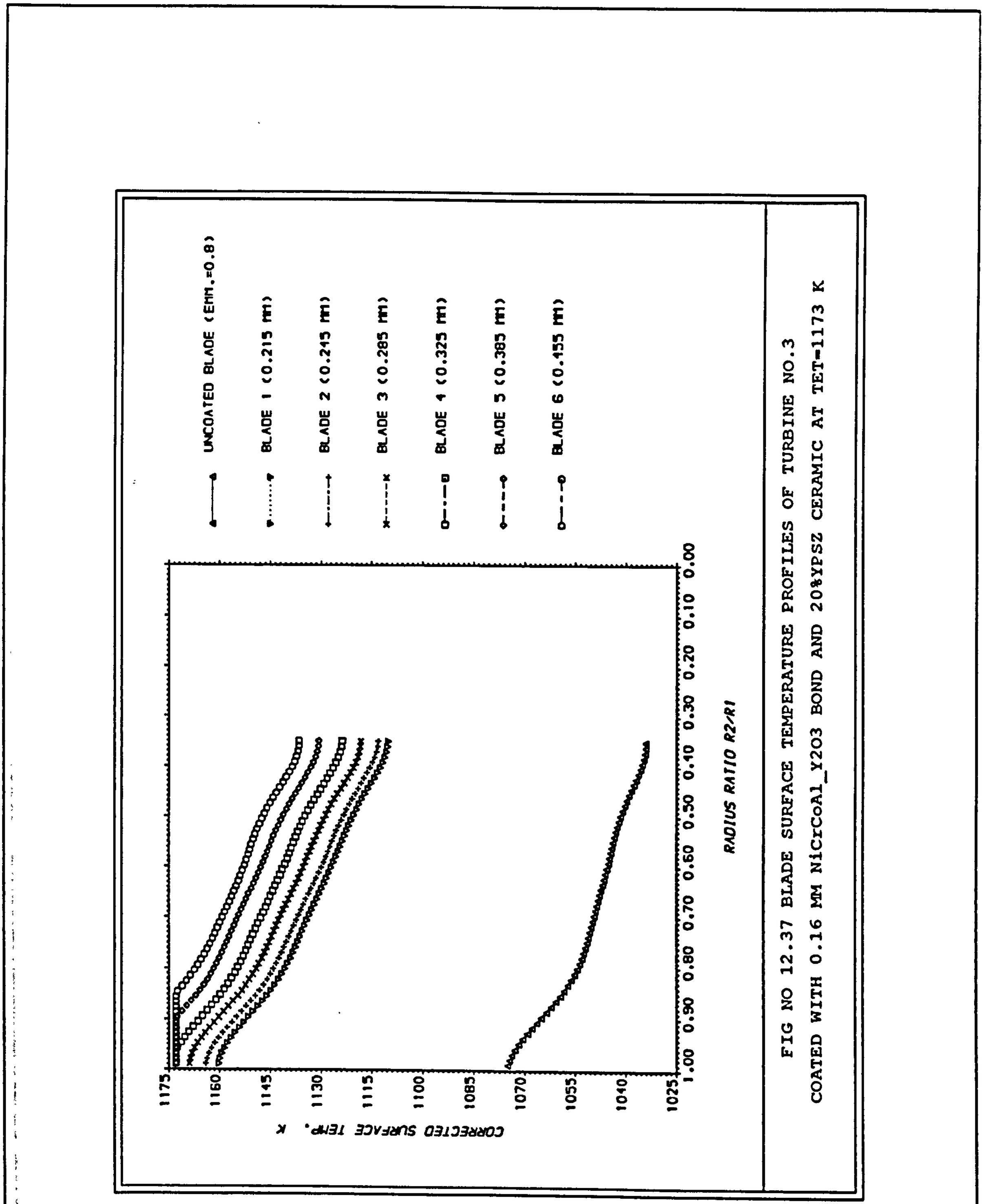

FIG NO 12.37 BLADE SURFACE TEMPERATURE PROFILES OF TURBINE NO.3
COATED WITH 0.16 MM NiCrCoAl_Y2O3 BOND AND 20%YPSZ CERAMIC AT TET=1173 K

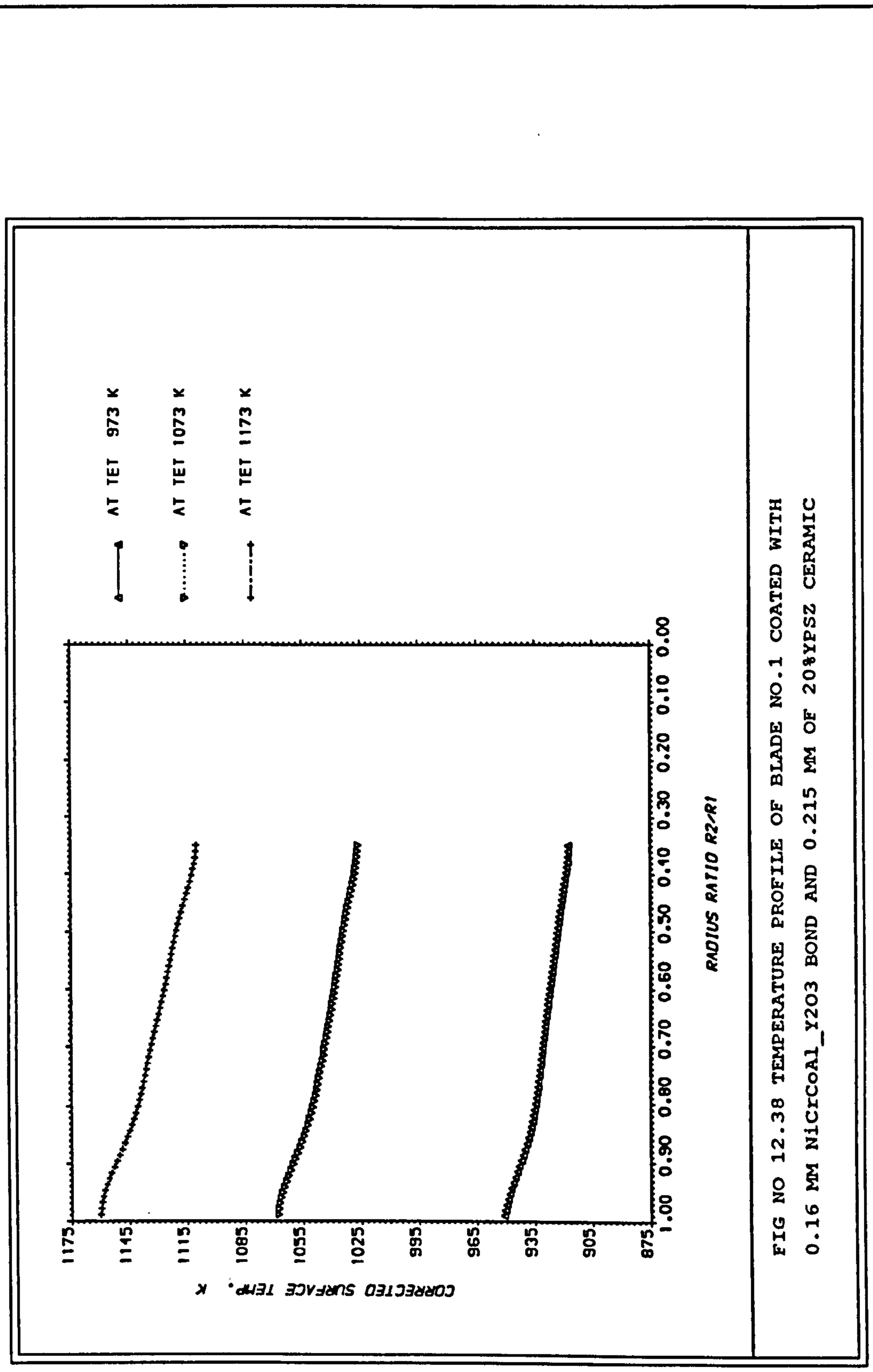

FIG NO 12.38 TEMPERATURE PROFILE OF BLADE NO.1 COATED WITH 0.16 MM NiCrCoAl_Y2O3 BOND AND 0.215 MM OF 20%YPSZ CERAMIC

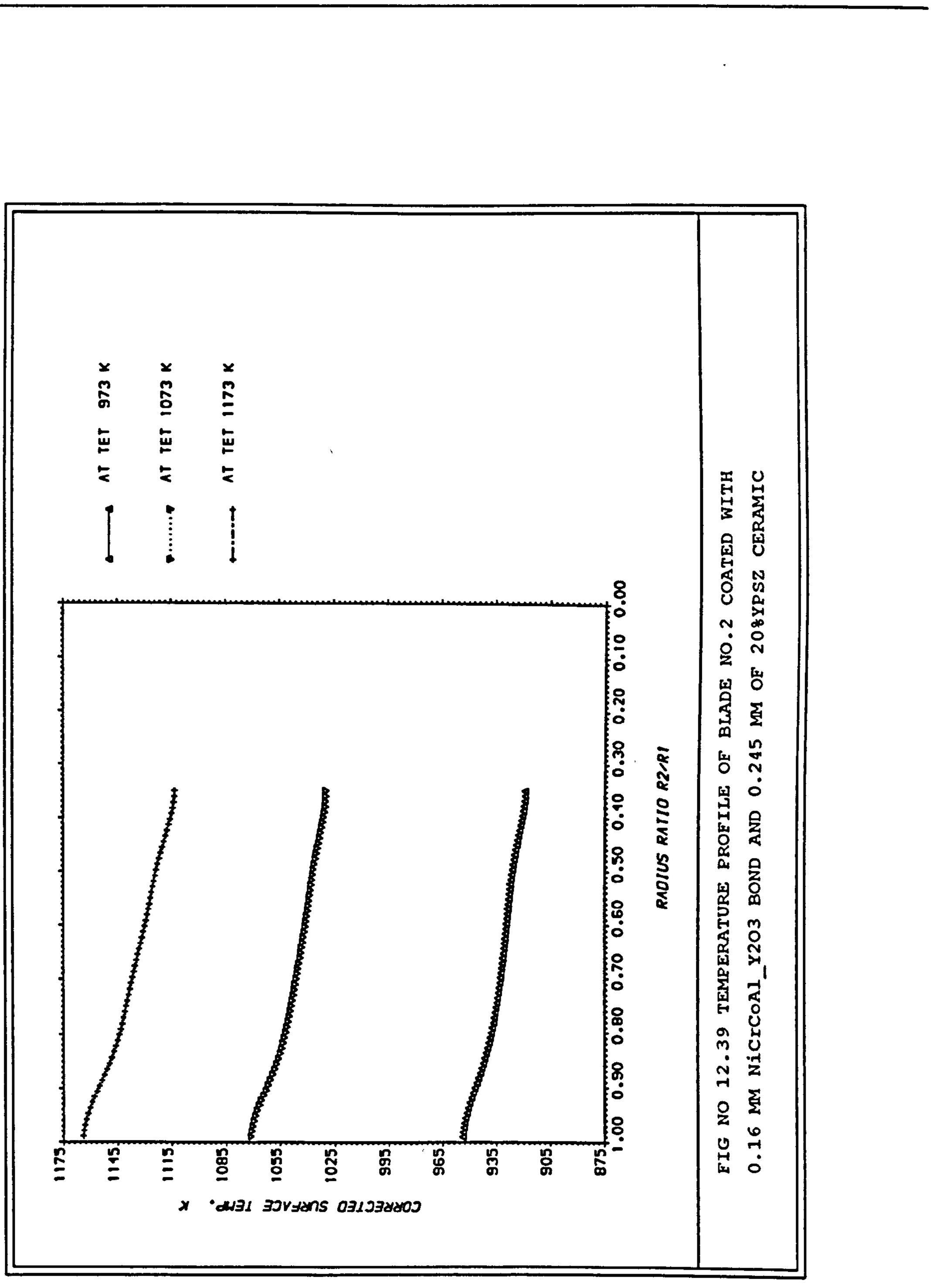

FIG NO 12.39 TEMPERATURE PROFILE OF BLADE NO.2 COATED WITH 0.16 MM NiCrCoAl_Y2O3 BOND AND 0.245 MM OF 20%YPSZ CERAMIC

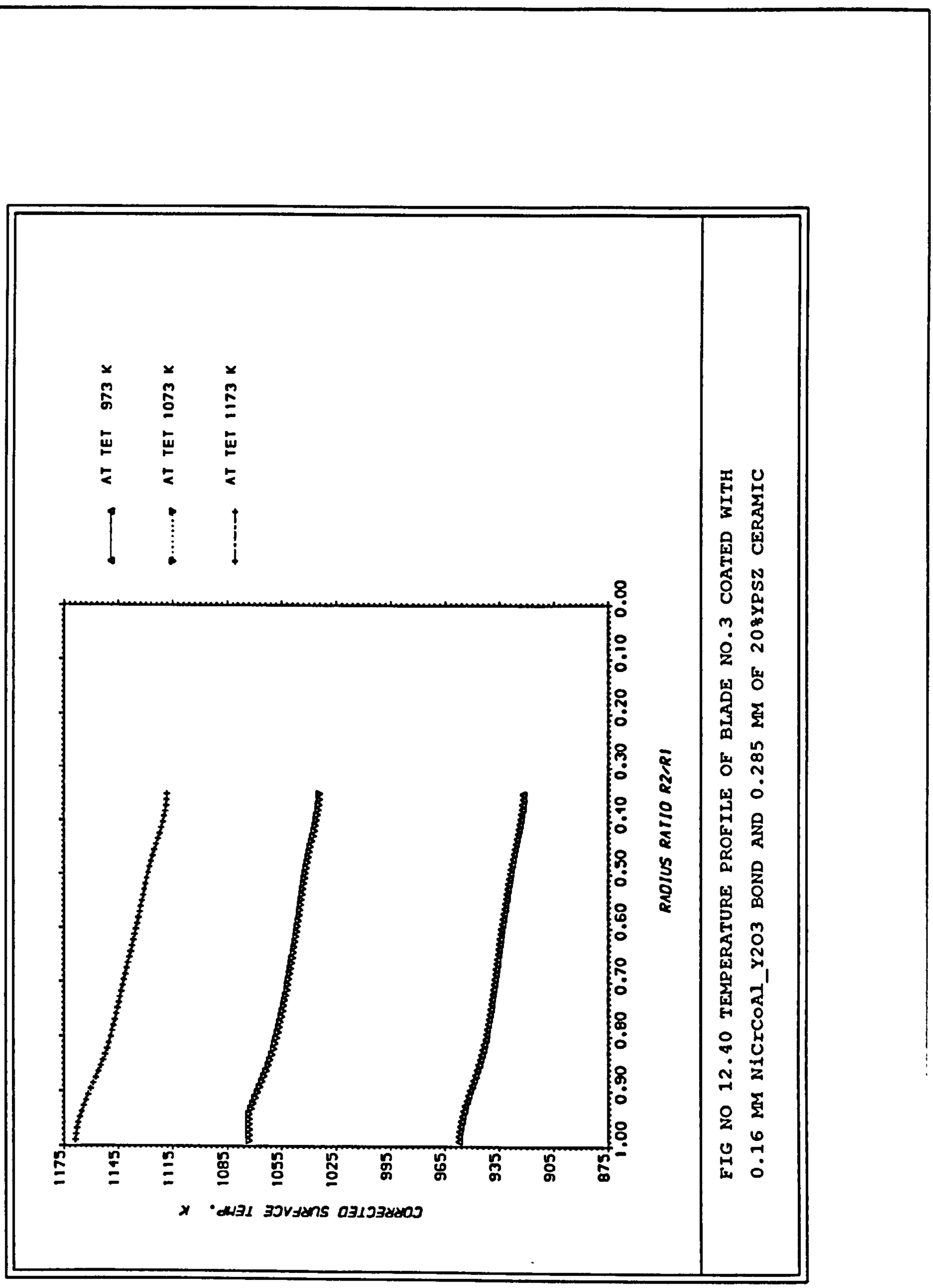

FIG NO 12.40 TEMPERATURE PROFILE OF BLADE NO.3 COATED WITH
0.16 MM NiCrCoAl_Y2O3 BOND AND 0.285 MM OF 20%YPSZ CERAMIC

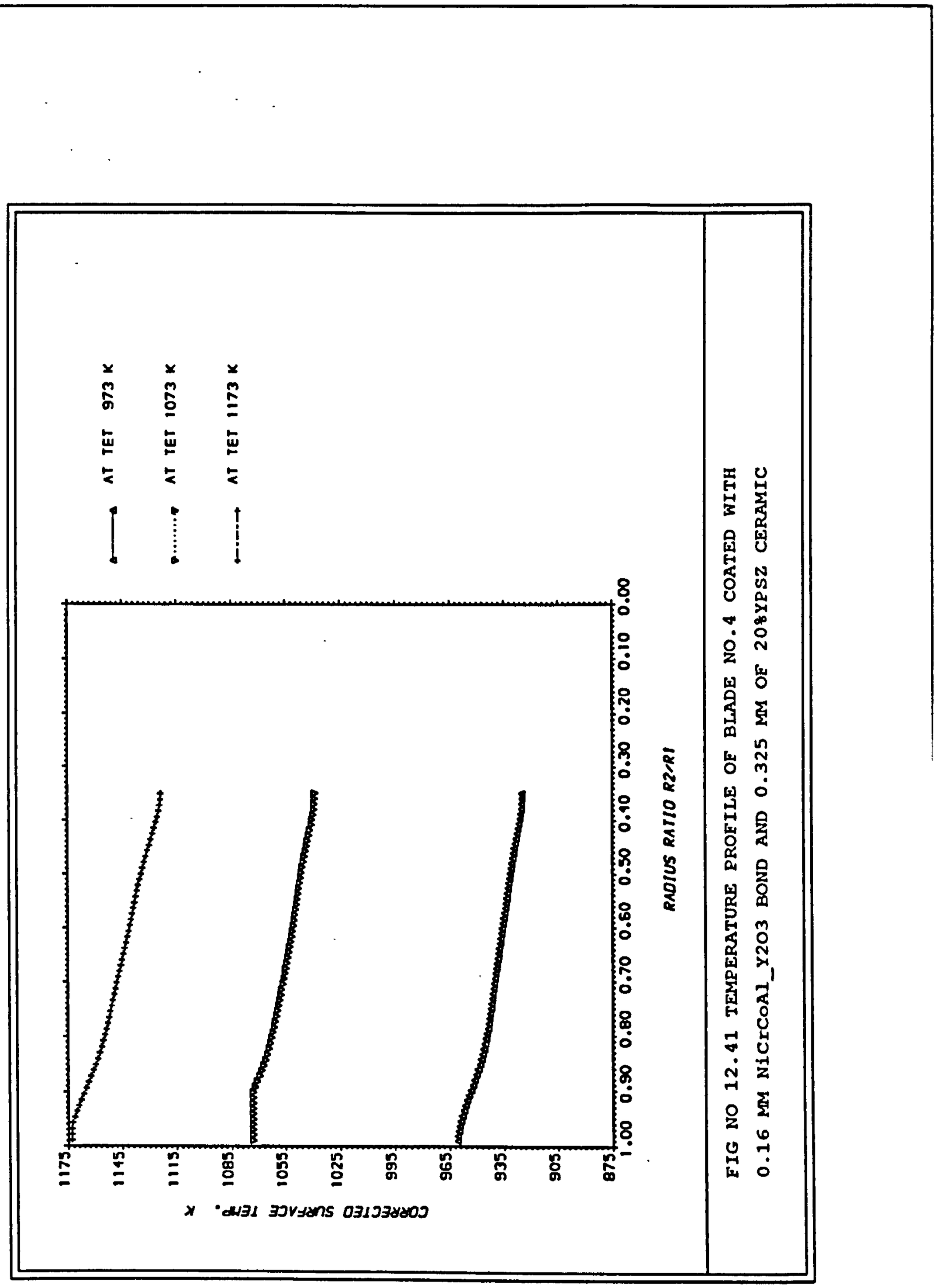

FIG NO 12.41 TEMPERATURE PROFILE OF BLADE NO.4 COATED WITH 0.16 MM NiCrCoAl_Y2O3 BOND AND 0.325 MM OF 20%YPSZ CERAMIC

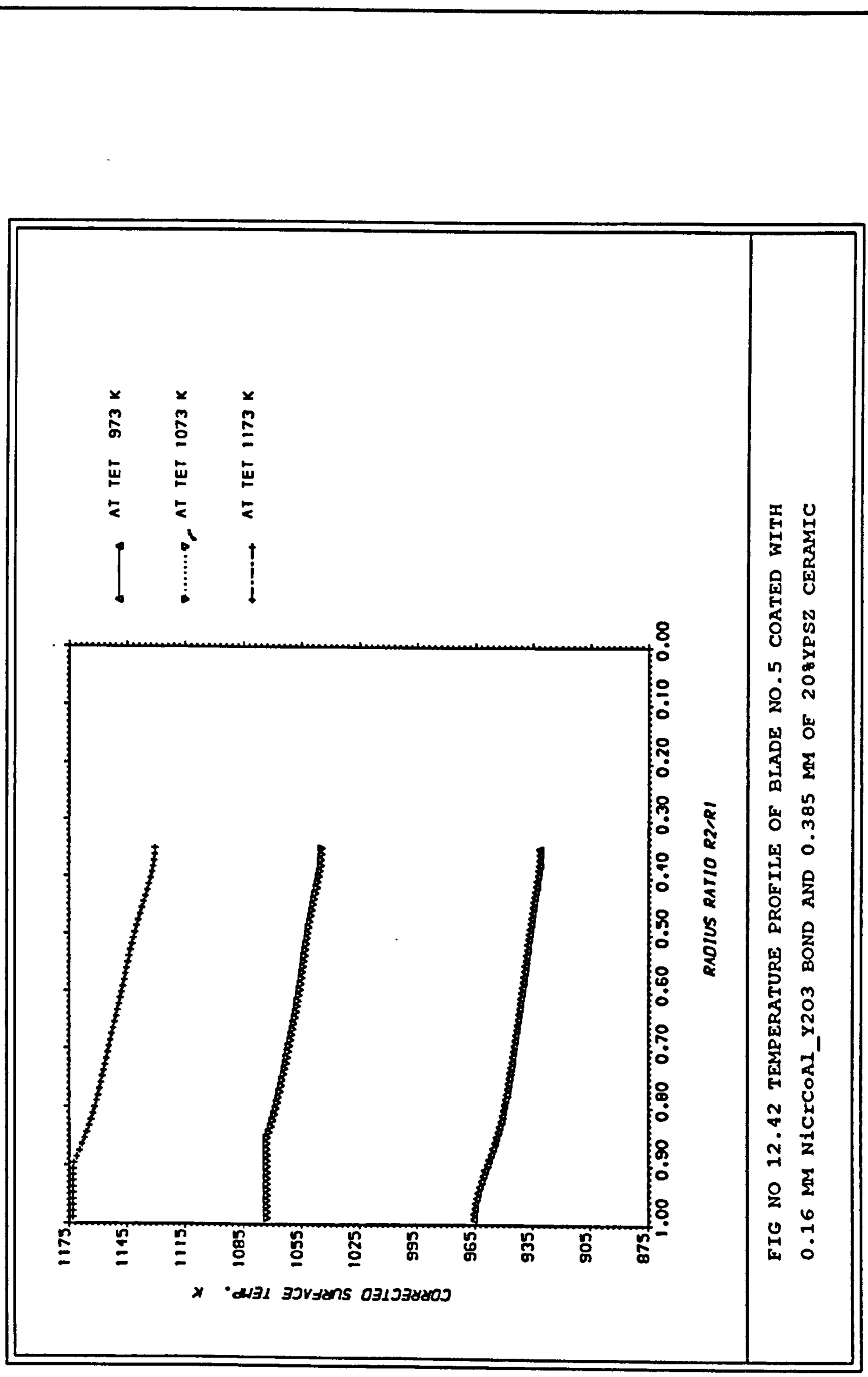

FIG NO 12.42 TEMPERATURE PROFILE OF BLADE NO.5 COATED WITH
0.16 MM NiCrCoAl_Y2O3 BOND AND 0.385 MM OF 20%YPSZ CERAMIC

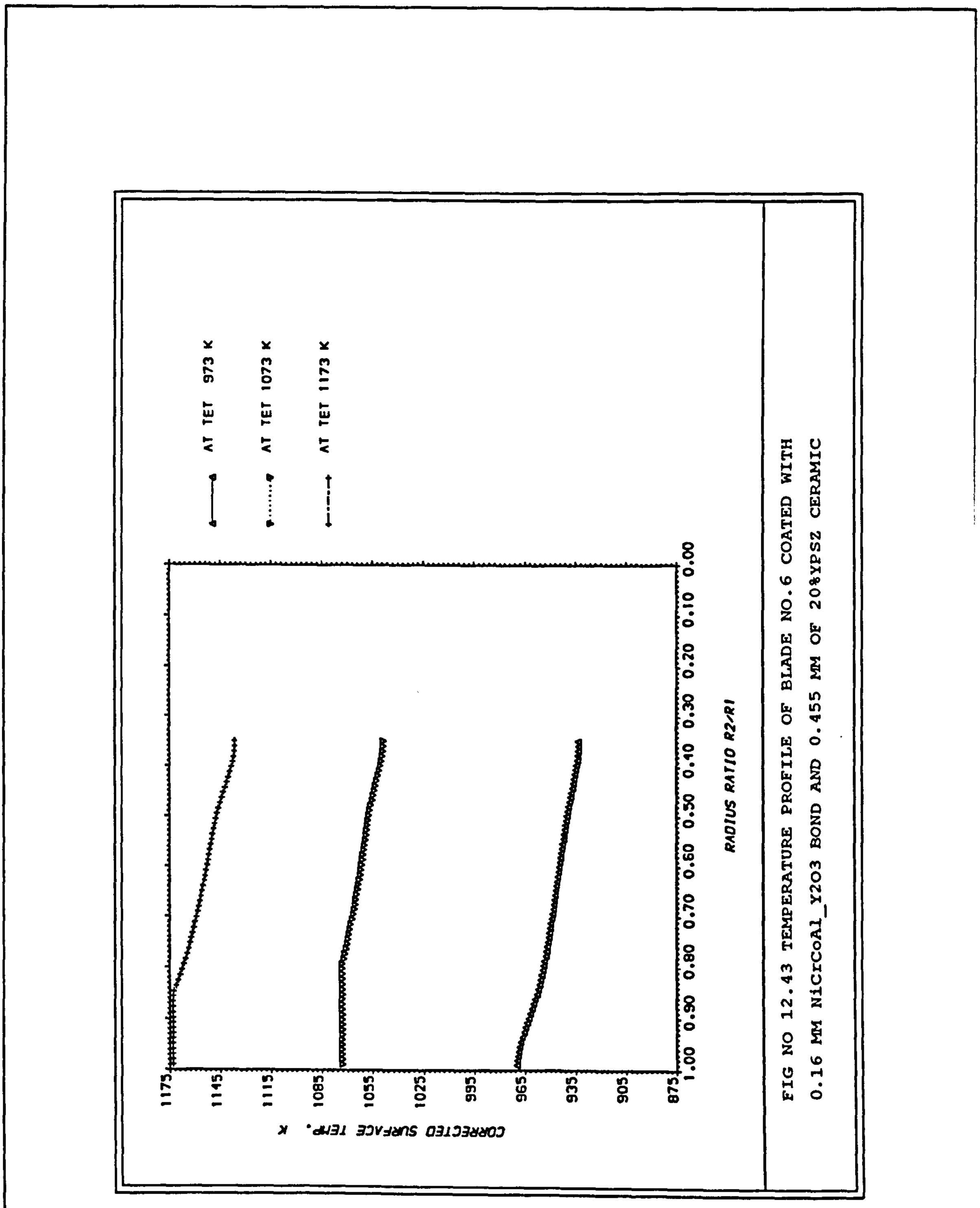

FIG NO 12.43 TEMPERATURE PROFILE OF BLADE NO.6 COATED WITH 0.16 MM NiCrCoAl_Y2O3 BOND AND 0.455 MM OF 20%YPSZ CERAMIC

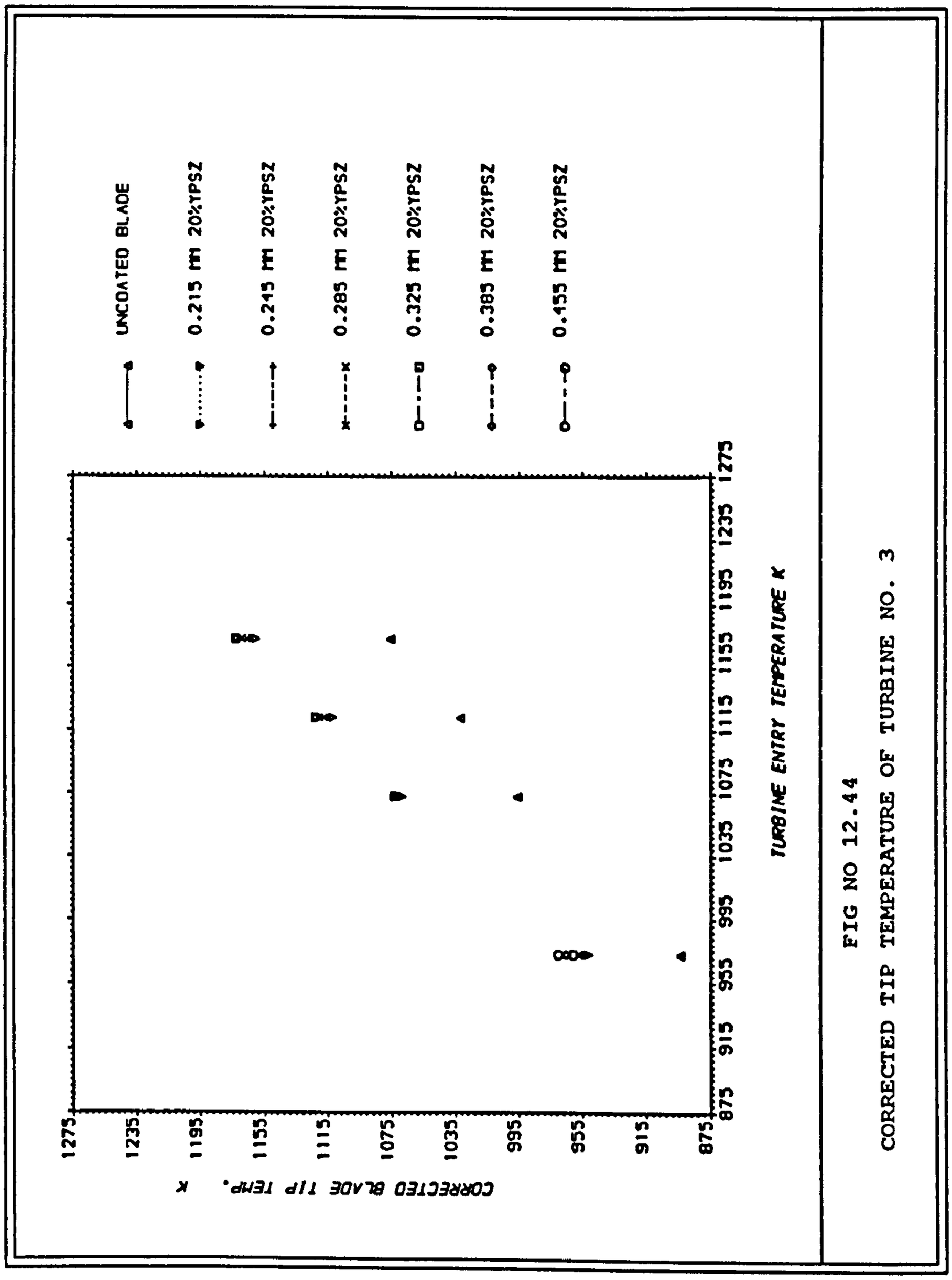

FIG NO 12.44

CORRECTED TIP TEMPERATURE OF TURBINE NO. 3

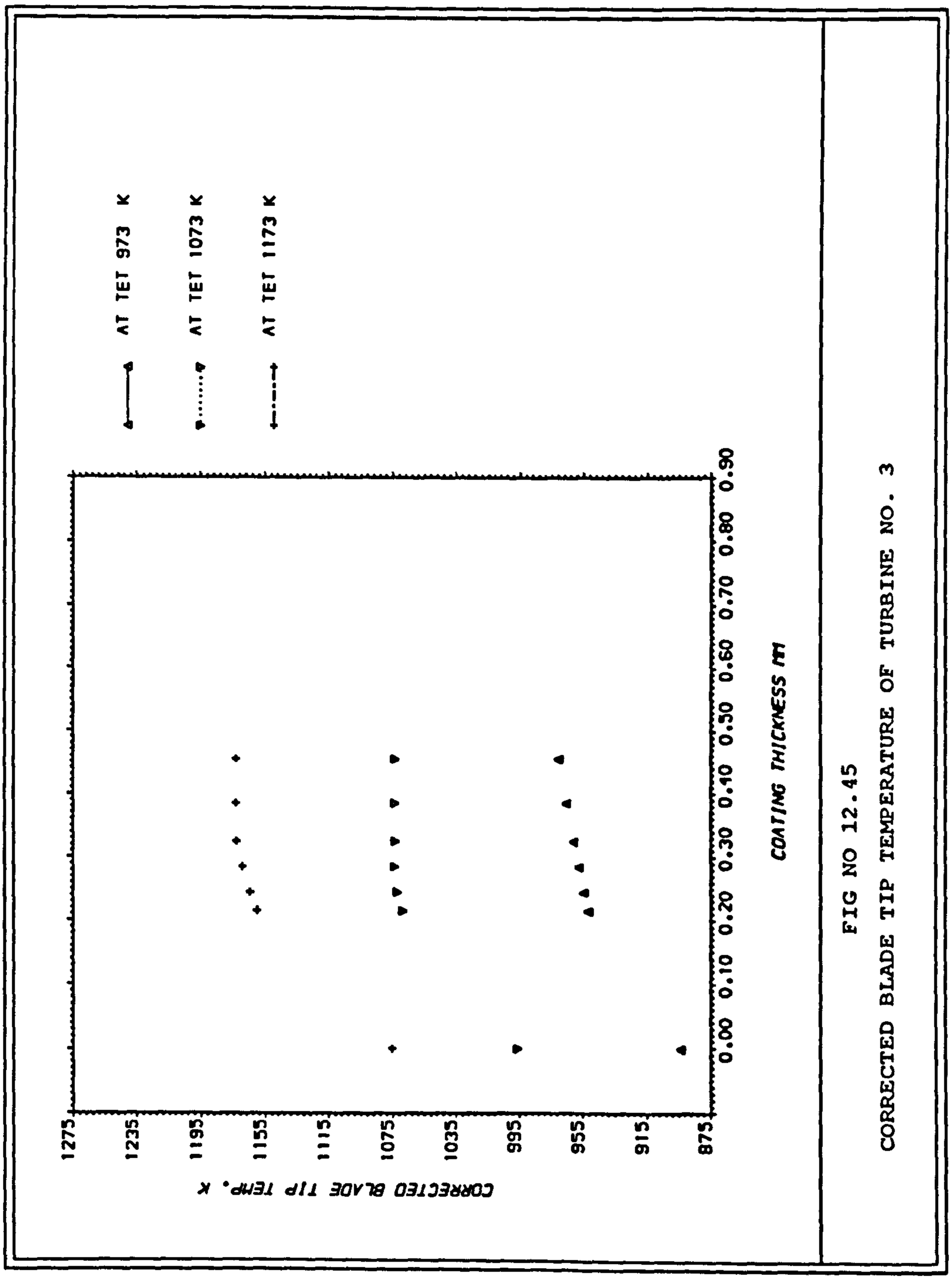

FIG NO 12.45

CORRECTED BLADE TIP TEMPERATURE OF TURBINE NO. 3

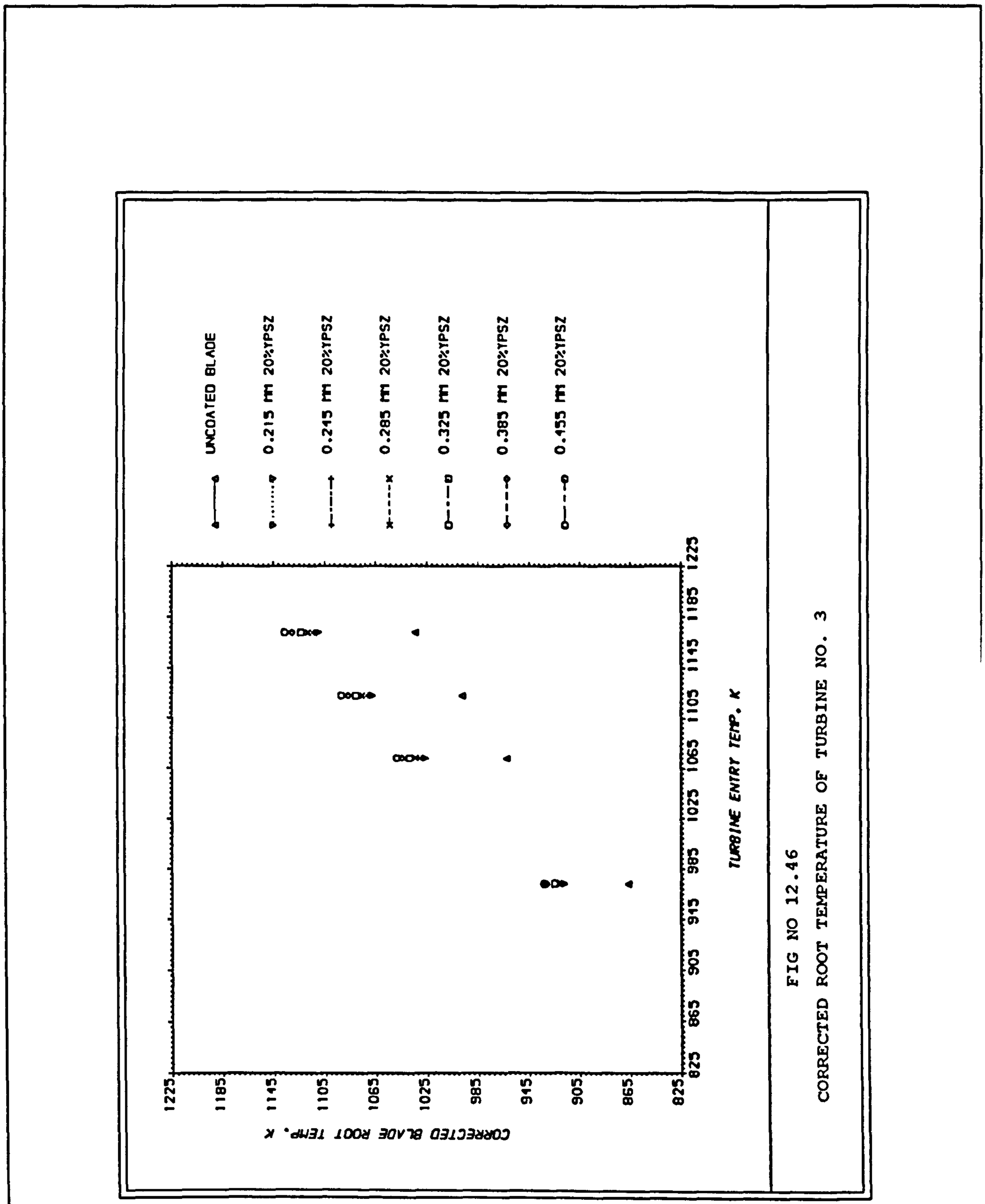

FIG NO 12.46

CORRECTED ROOT TEMPERATURE OF TURBINE NO. 3

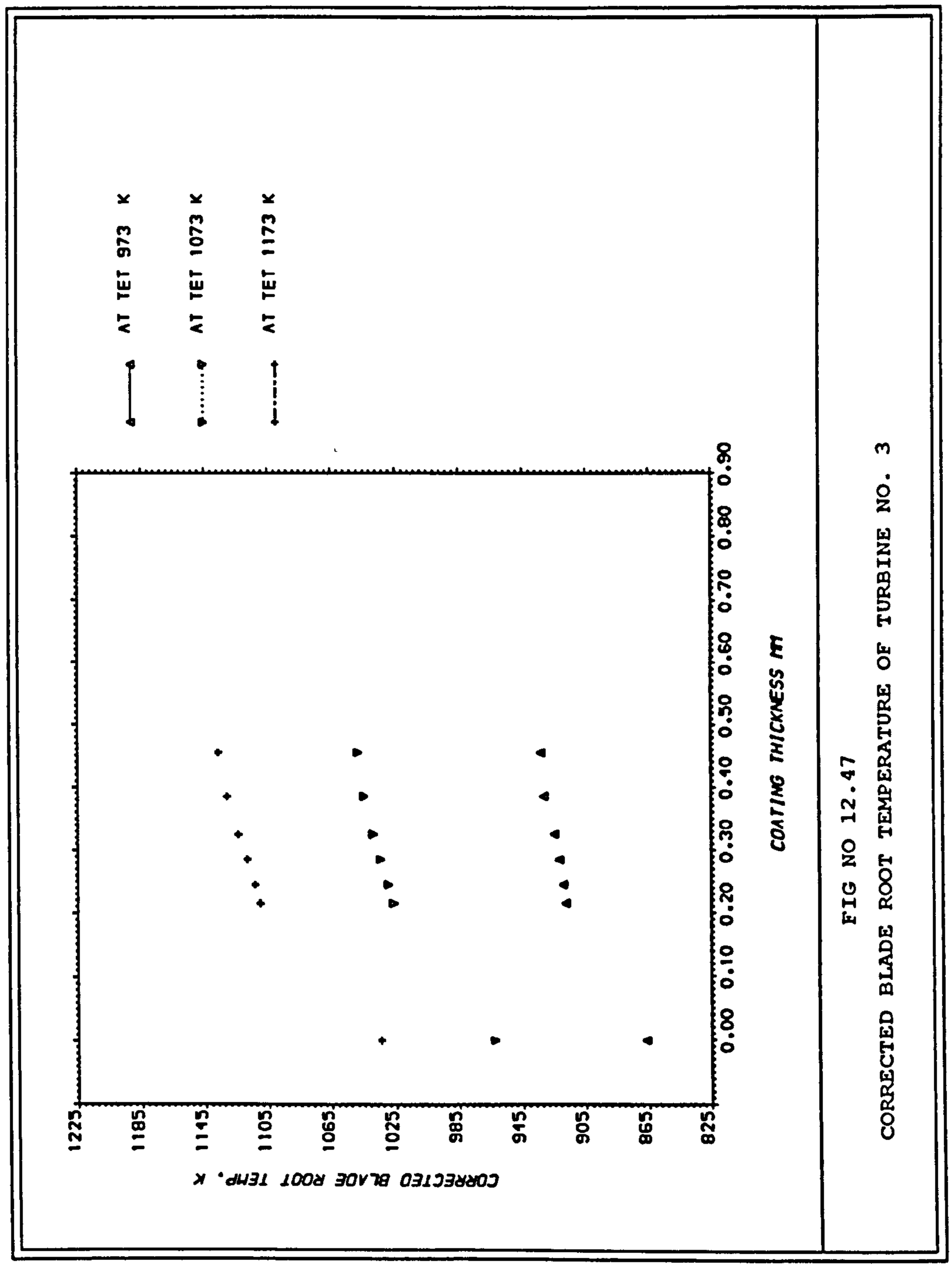

FIG NO 12.47

CORRECTED BLADE ROOT TEMPERATURE OF TURBINE NO. 3

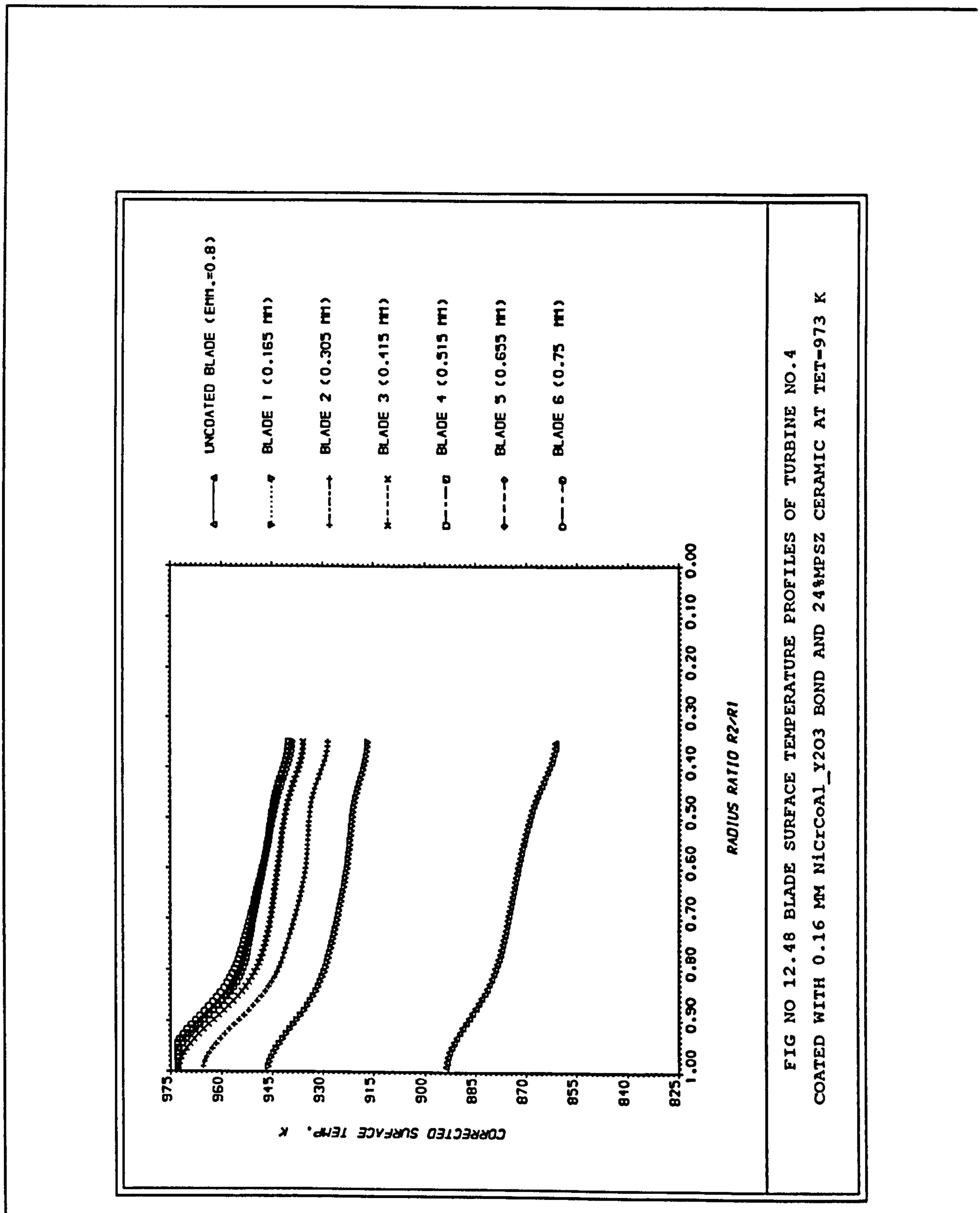

FIG NO 12.48 BLADE SURFACE TEMPERATURE PROFILES OF TURBINE NO.4
COATED WITH 0.16 MM NiCrCoAl_Y2O3 BOND AND 24%MPSZ CERAMIC AT TET=973 K

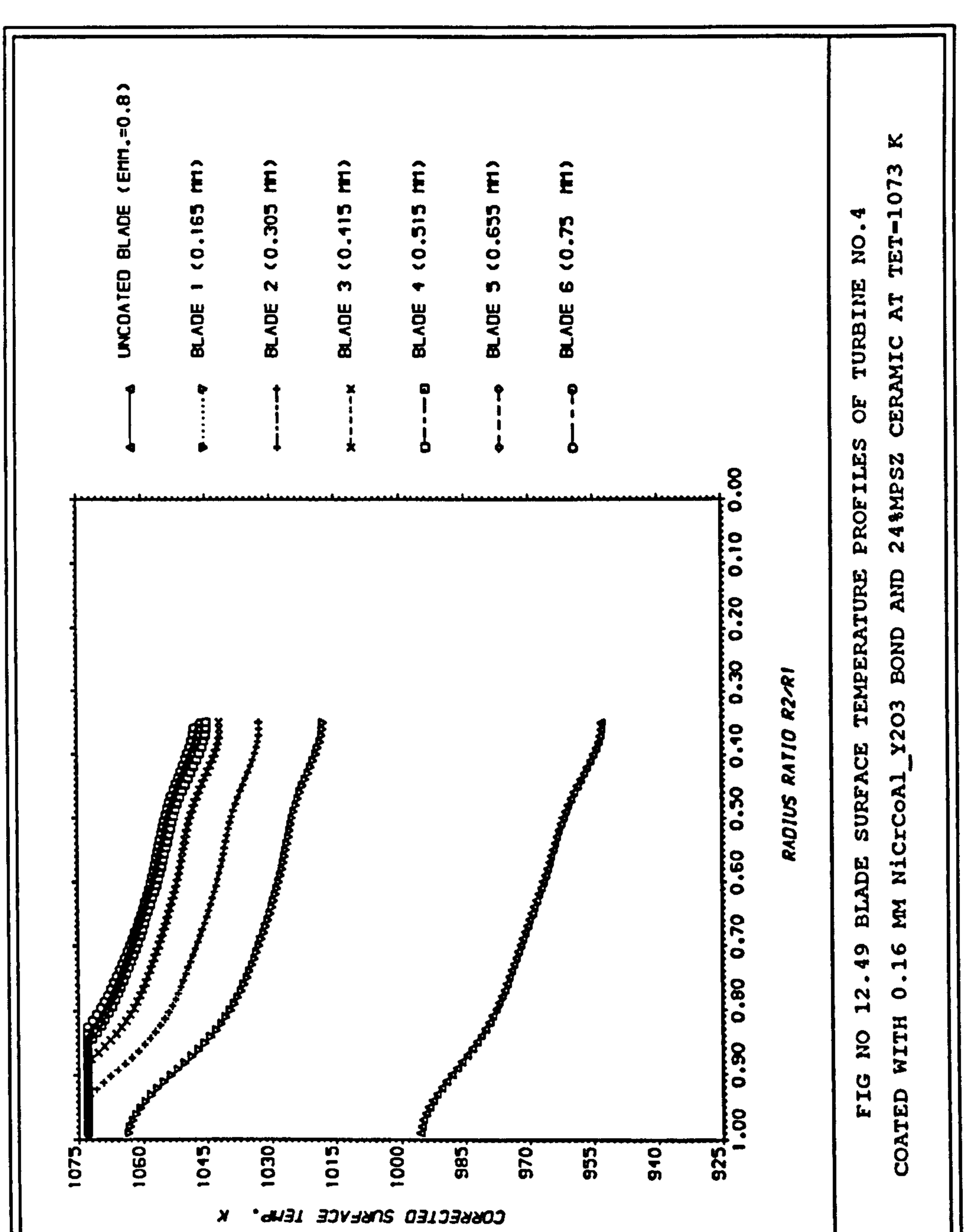

FIG NO 12.49 BLADE SURFACE TEMPERATURE PROFILES OF TURBINE NO.4
COATED WITH 0.16 MM NiCrCoAl_Y2O3 BOND AND 24%MPSZ CERAMIC AT TET=1073 K

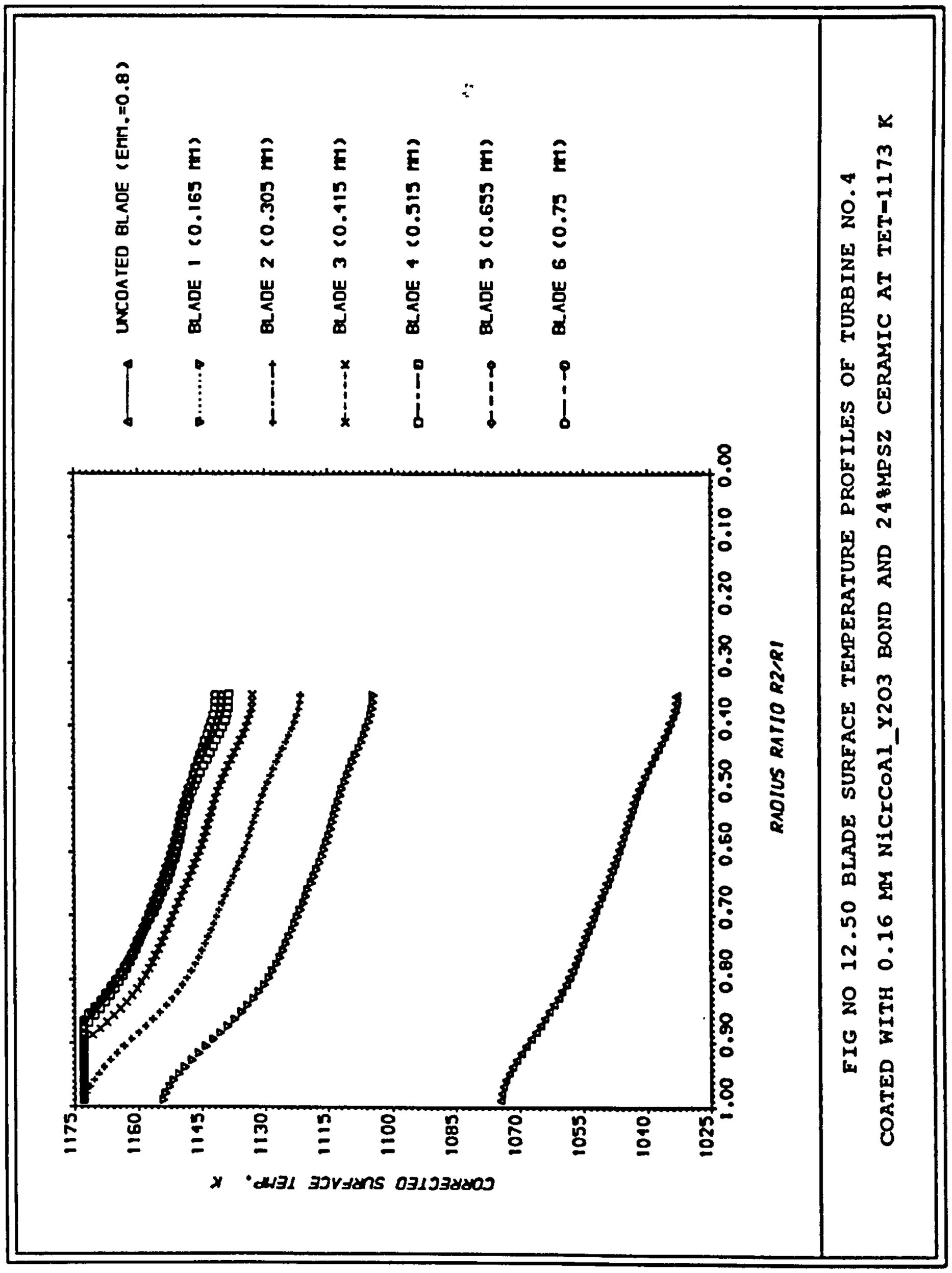

FIG NO 12.50 BLADE SURFACE TEMPERATURE PROFILES OF TURBINE NO.4
COATED WITH 0.16 MM NiCrCoAl_Y2O3 BOND AND 24%MPSZ CERAMIC AT TET=1173 K

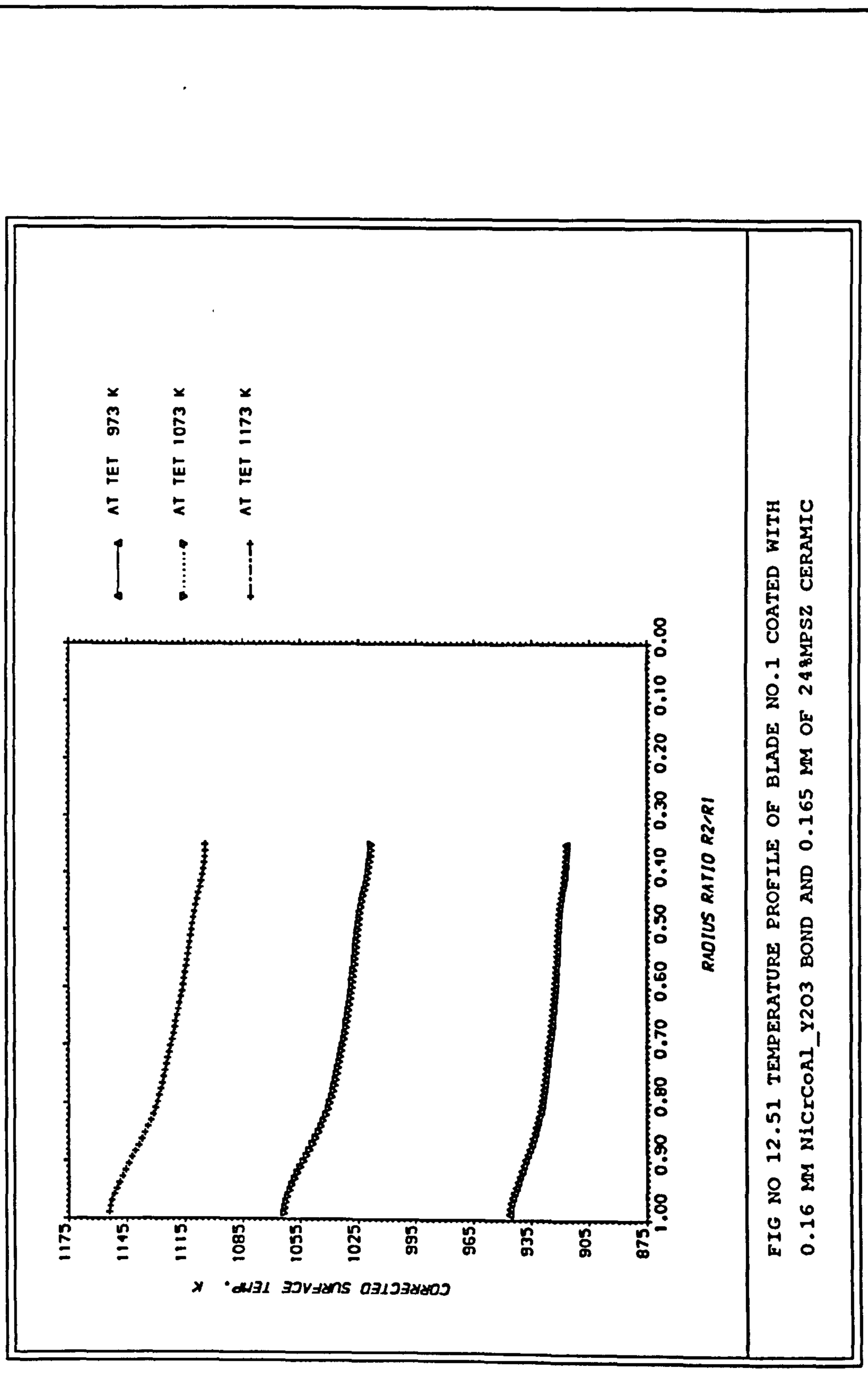

FIG NO 12.51 TEMPERATURE PROFILE OF BLADE NO.1 COATED WITH
0.16 MM NiCrCoAl_Y2O3 BOND AND 0.165 MM OF 24%MPSZ CERAMIC

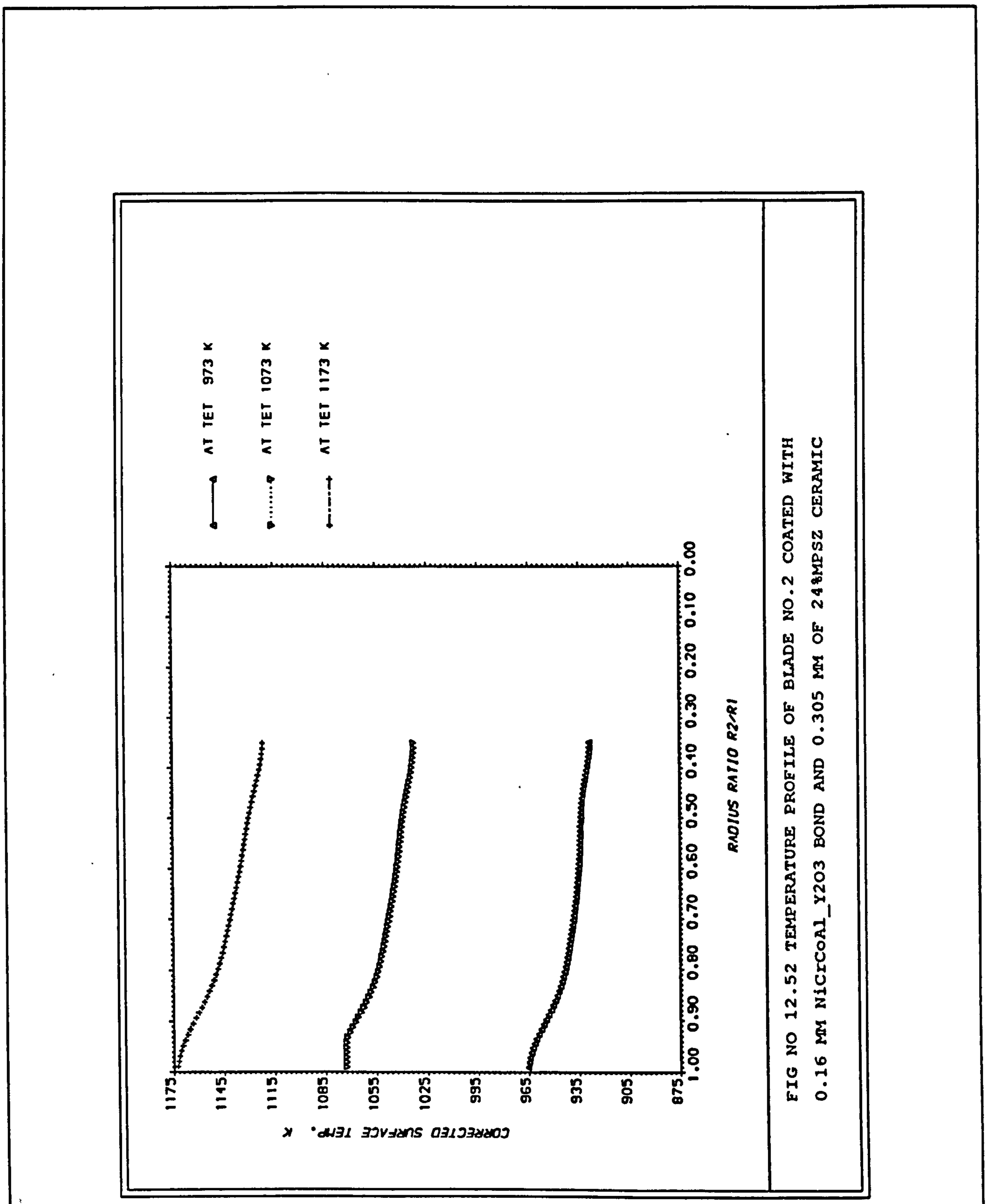

FIG NO 12.52 TEMPERATURE PROFILE OF BLADE NO.2 COATED WITH
0.16 MM NiCrCoAl_Y2O3 BOND AND 0.305 MM OF 24%MPSZ CERAMIC

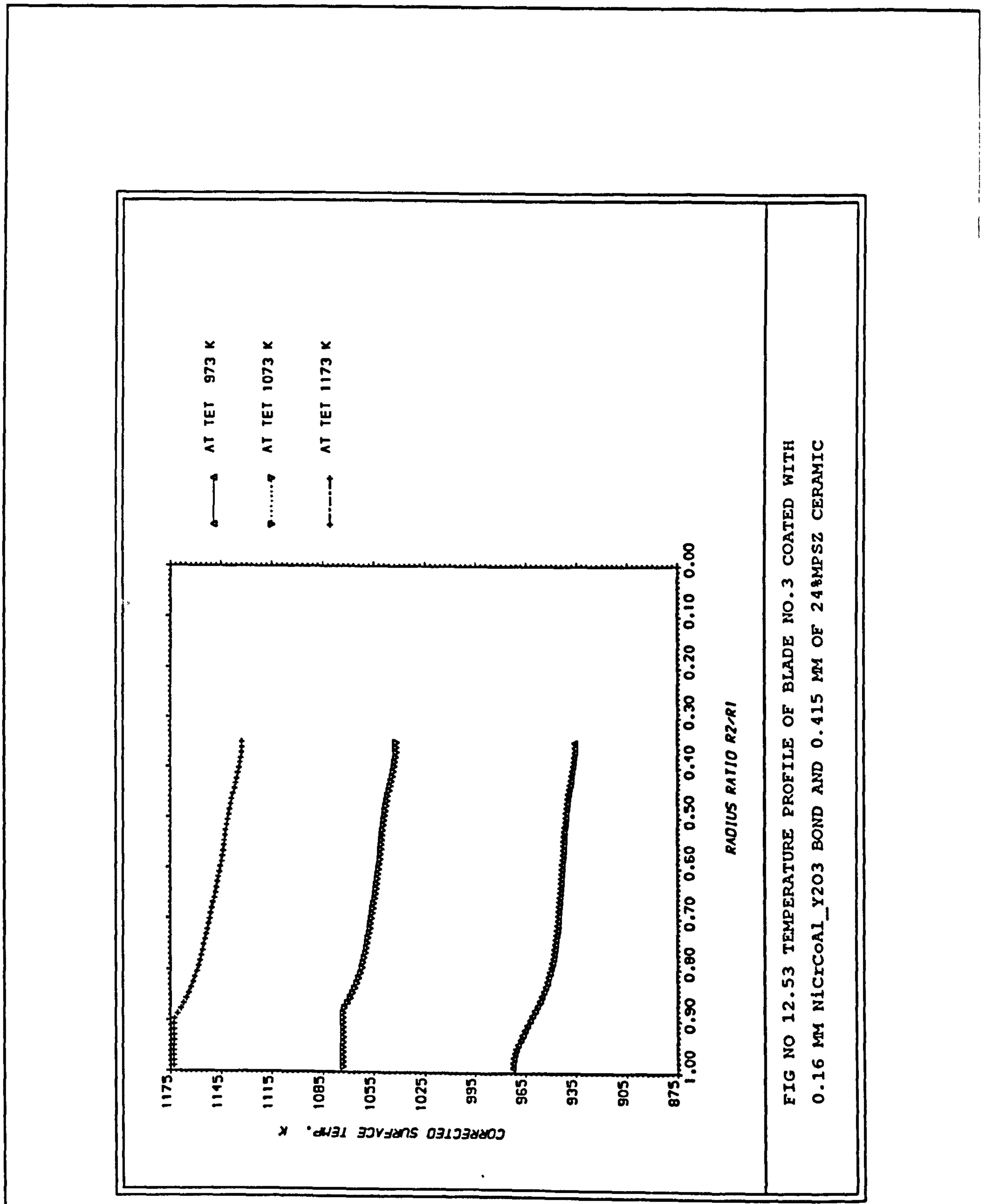

FIG NO 12.53 TEMPERATURE PROFILE OF BLADE NO.3 COATED WITH 0.16 MM NiCrCoAl_Y2O3 BOND AND 0.415 MM OF 24%MPSZ CERAMIC

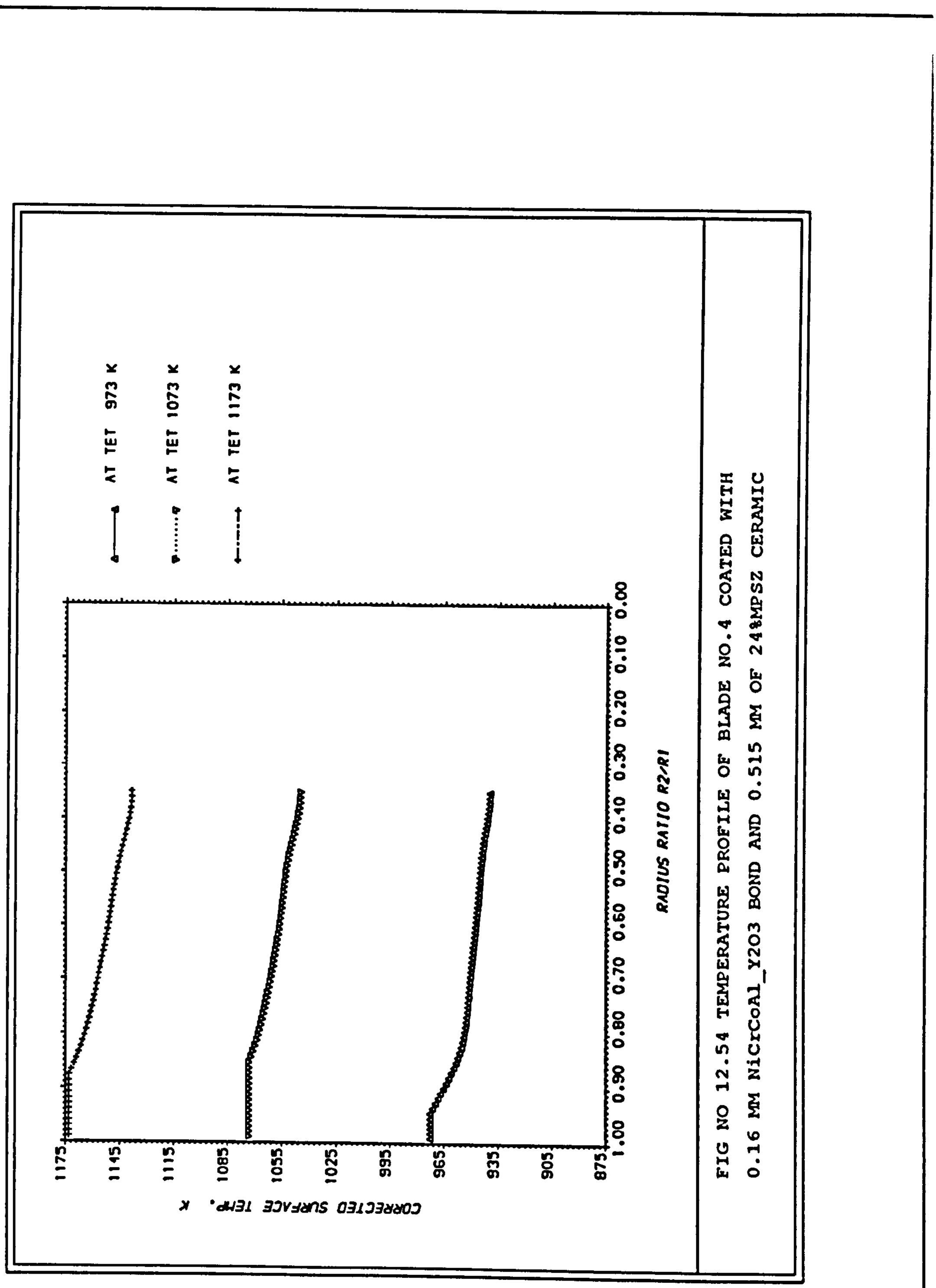

FIG NO 12.54 TEMPERATURE PROFILE OF BLADE NO.4 COATED WITH
0.16 MM NiCrCoAl_Y2O3 BOND AND 0.515 MM OF 24%MPSZ CERAMIC

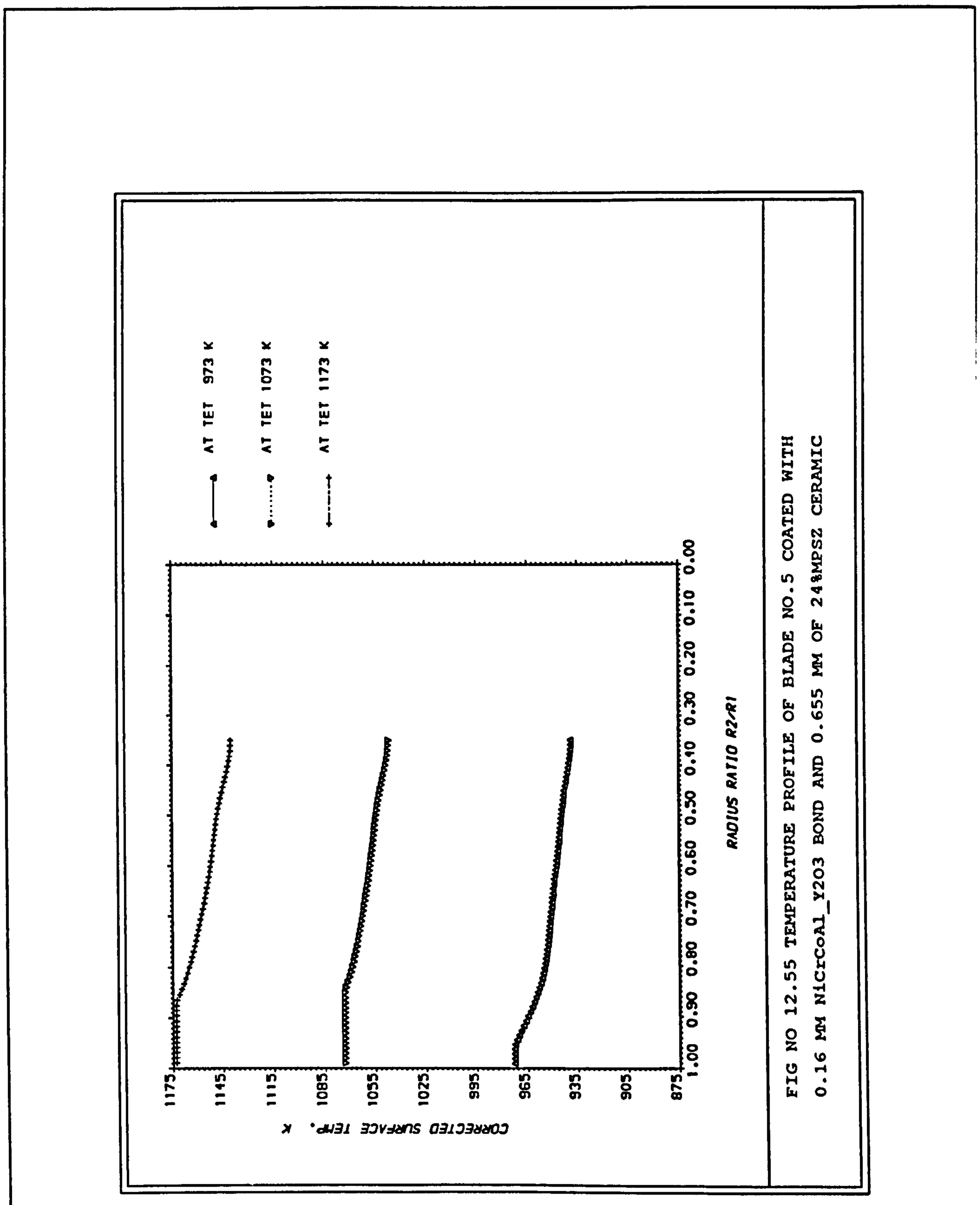

FIG NO 12.55 TEMPERATURE PROFILE OF BLADE NO.5 COATED WITH 0.16 MM NiCrCoAl_Y2O3 BOND AND 0.655 MM OF 24%MPSZ CERAMIC

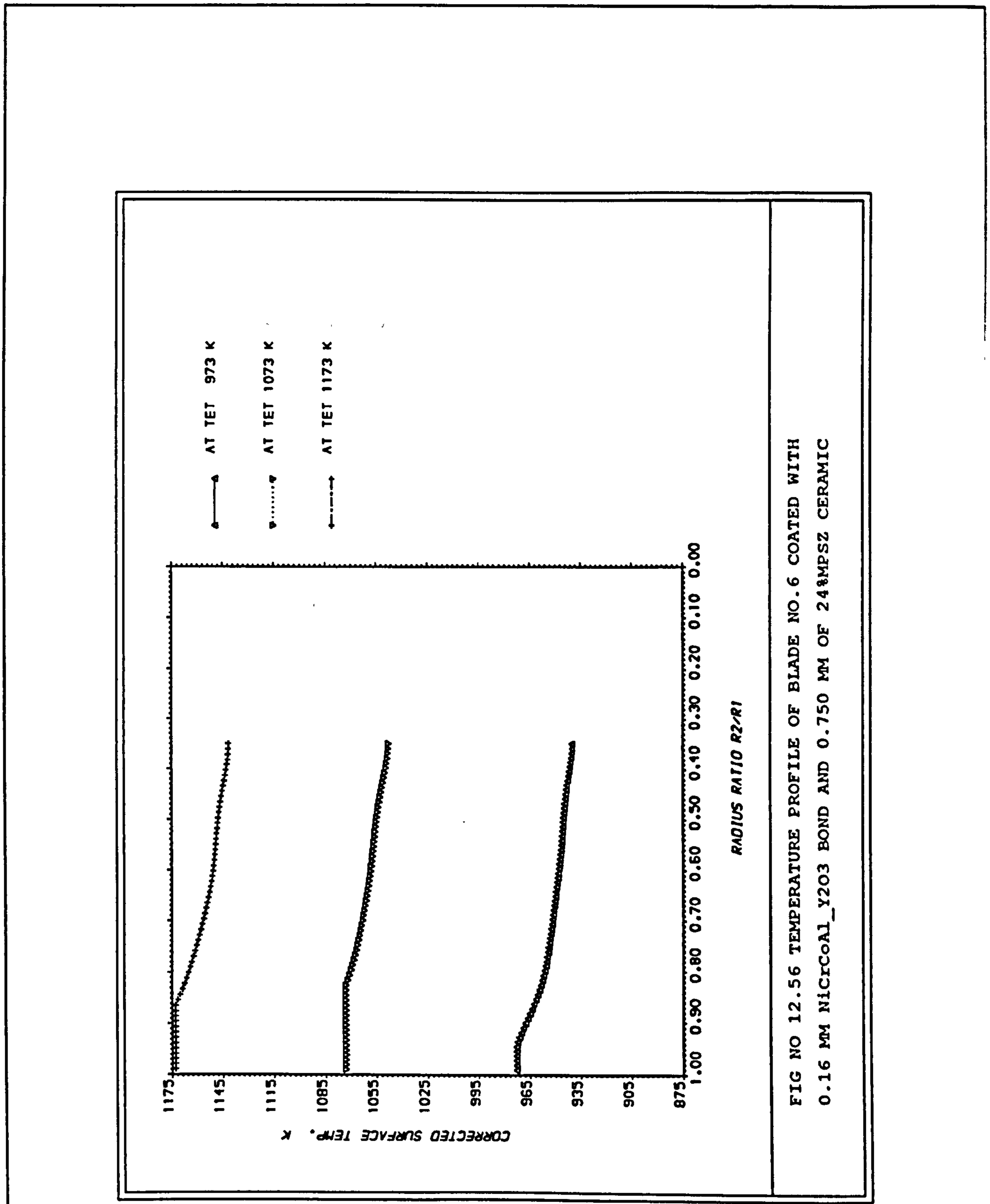

FIG NO 12.56 TEMPERATURE PROFILE OF BLADE NO.6 COATED WITH 0.16 MM NiCrCoAl_Y2O3 BOND AND 0.750 MM OF 24%MPSZ CERAMIC

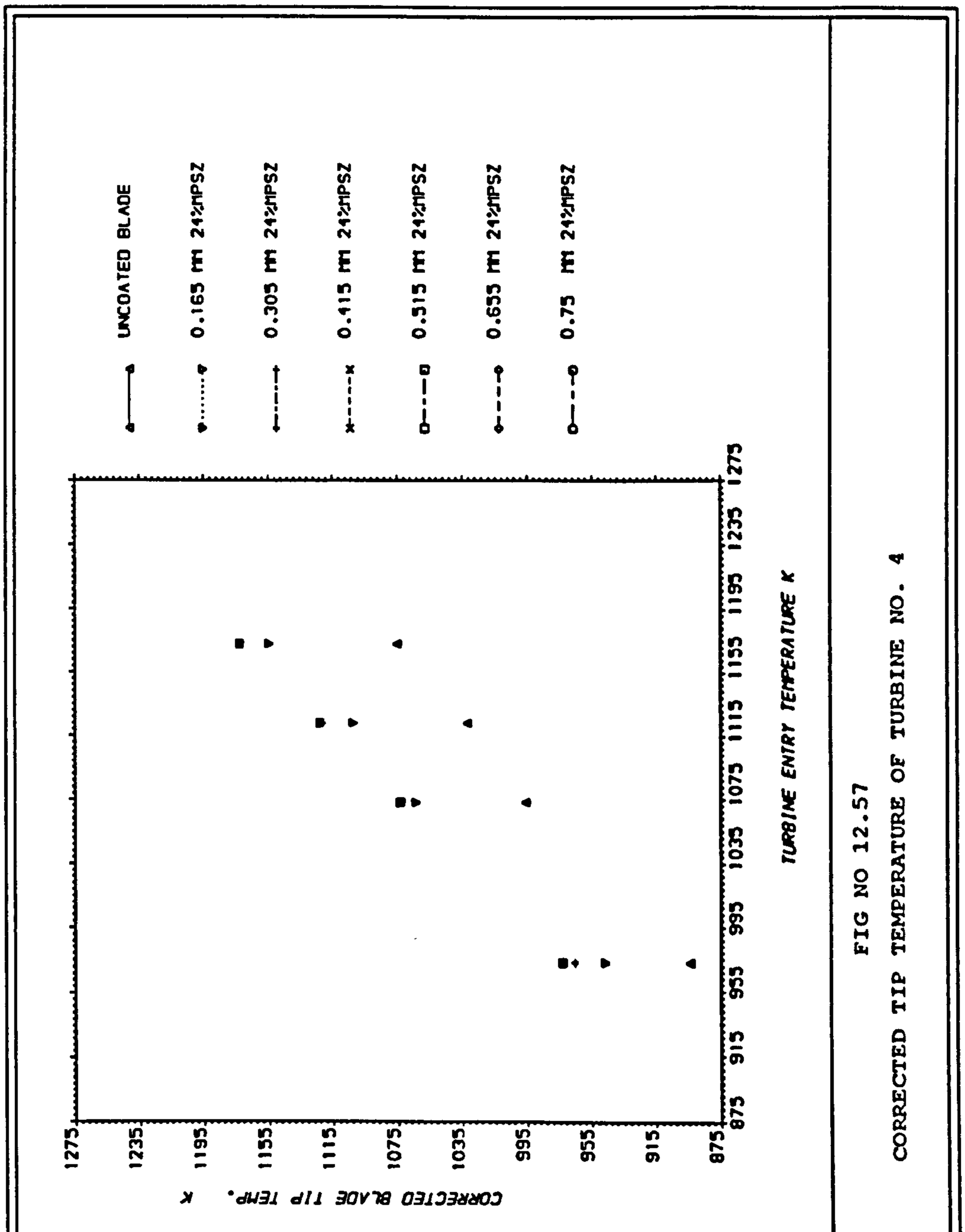

FIG NO 12.57

CORRECTED TIP TEMPERATURE OF TURBINE NO. 4

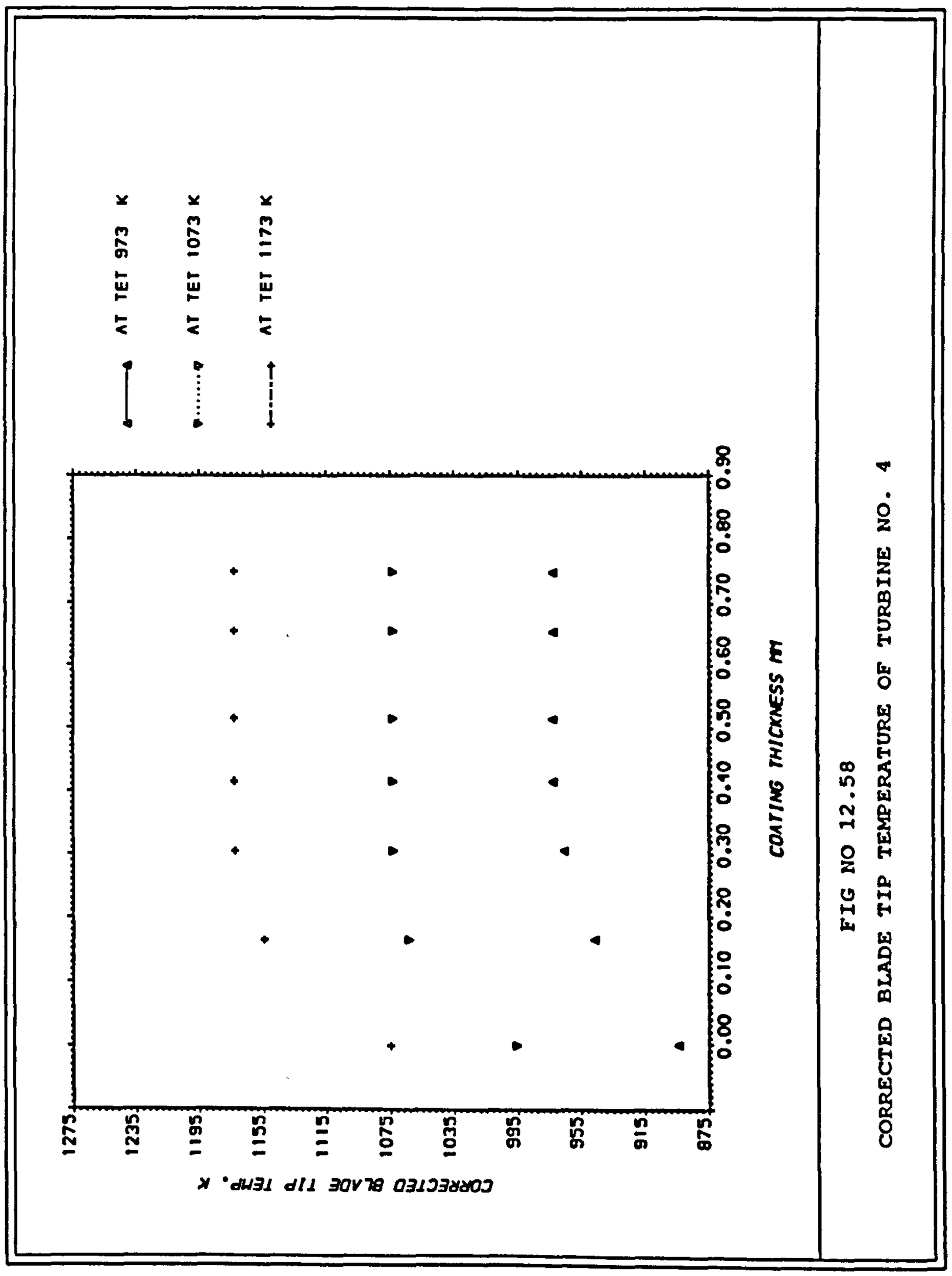

FIG NO 12.58

CORRECTED BLADE TIP TEMPERATURE OF TURBINE NO. 4

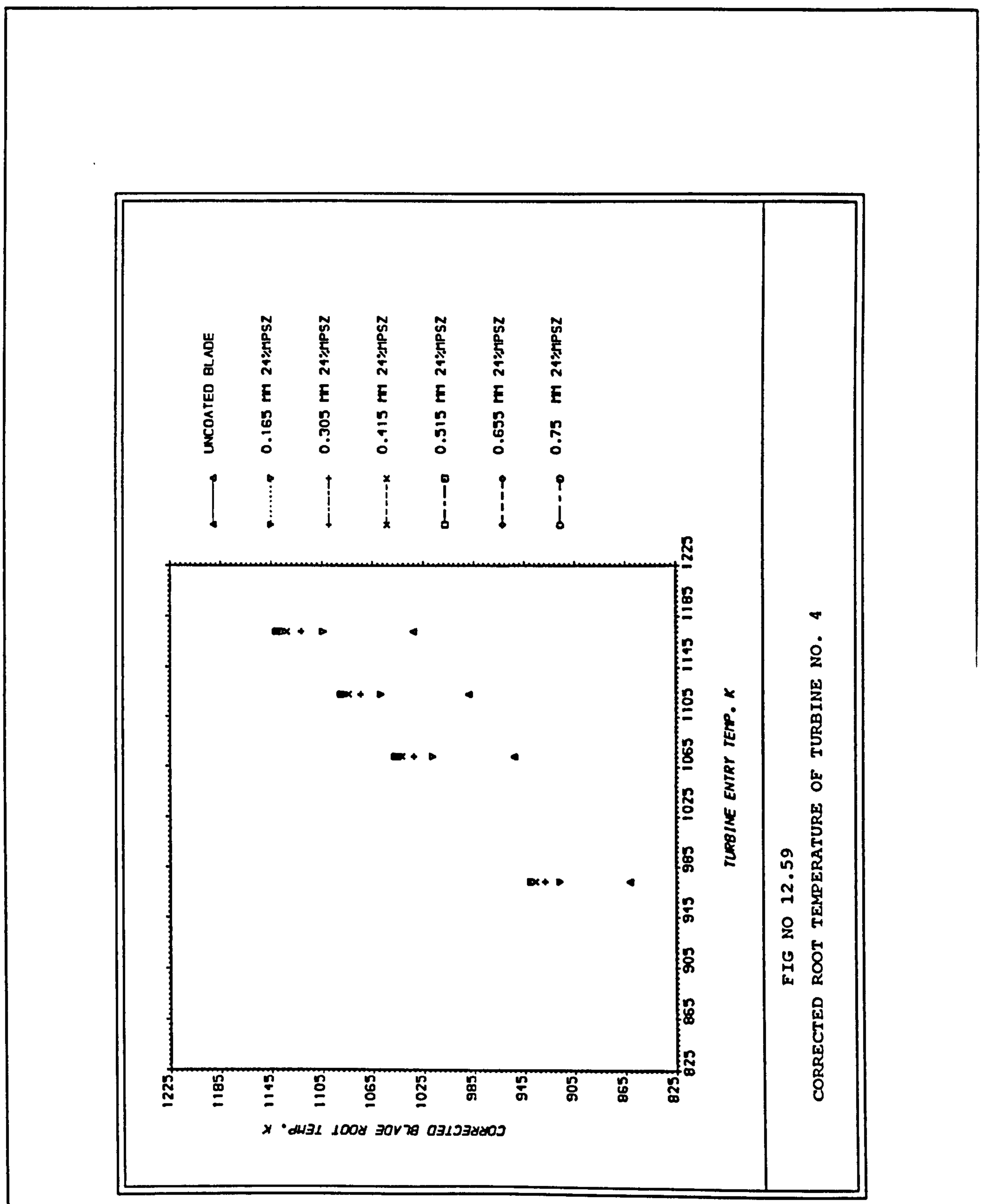

FIG NO 12.59

EFFECT OF CORRECTED ROOT TEMPERATURE OF TURBINE NO. 4

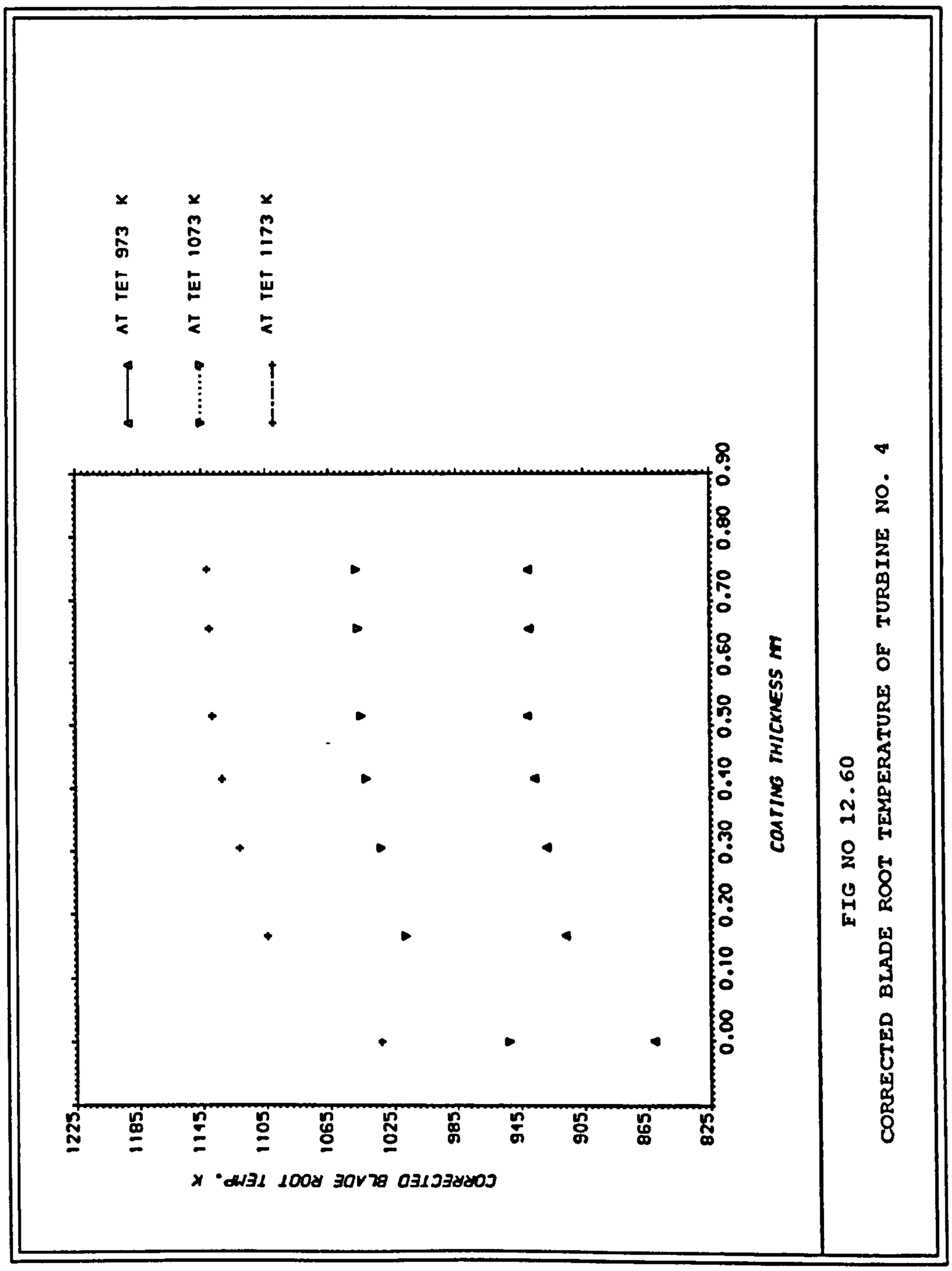

FIG NO 12.60

CORRECTED BLADE ROOT TEMPERATURE OF TURBINE NO. 4

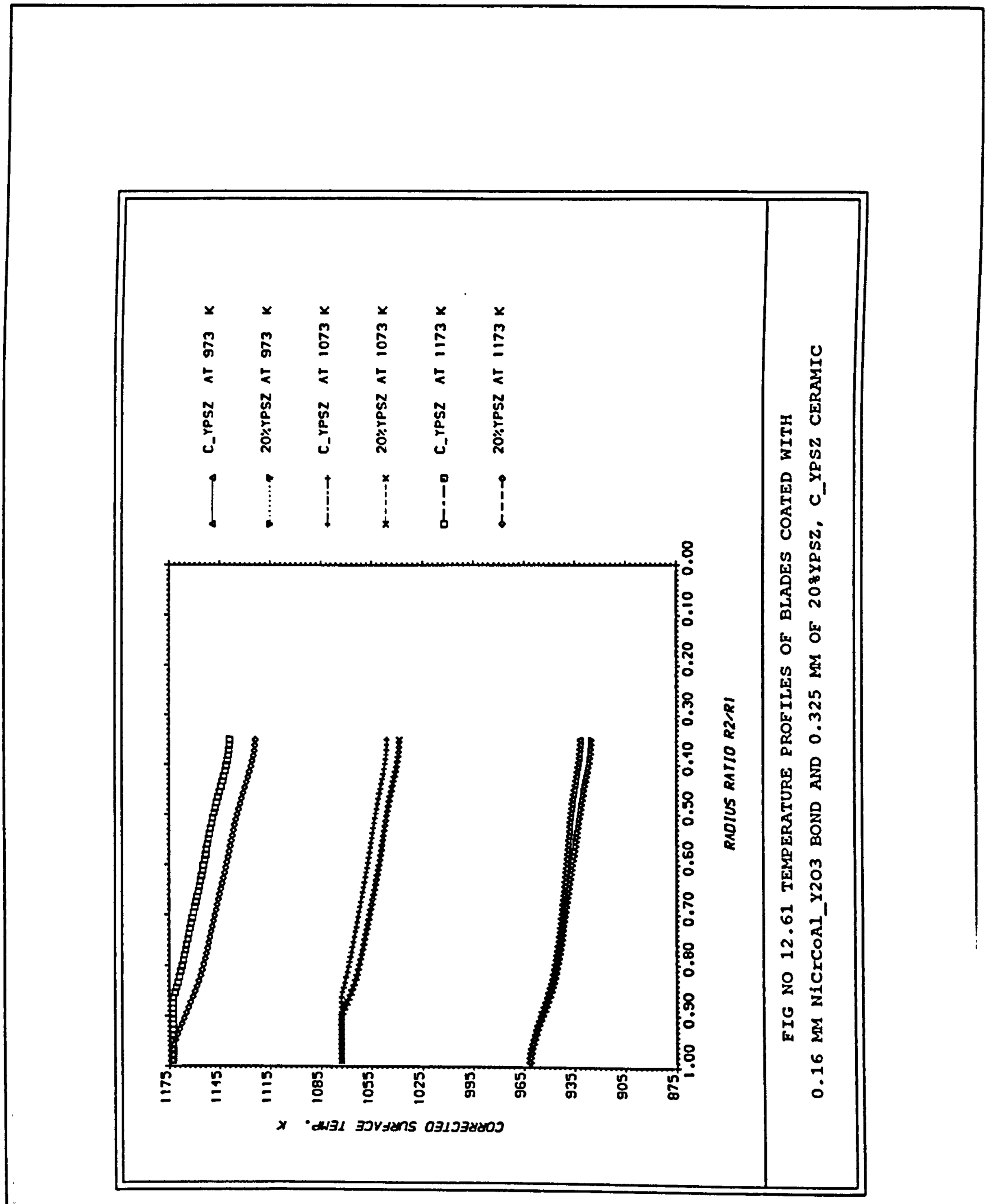

FIG NO 12.61 TEMPERATURE PROFILES OF BLADES COATED WITH
0.16 MM NiCrCoAl_Y2O3 BOND AND 0.325 MM OF 20%YPSZ, C_YPSZ CERAMIC

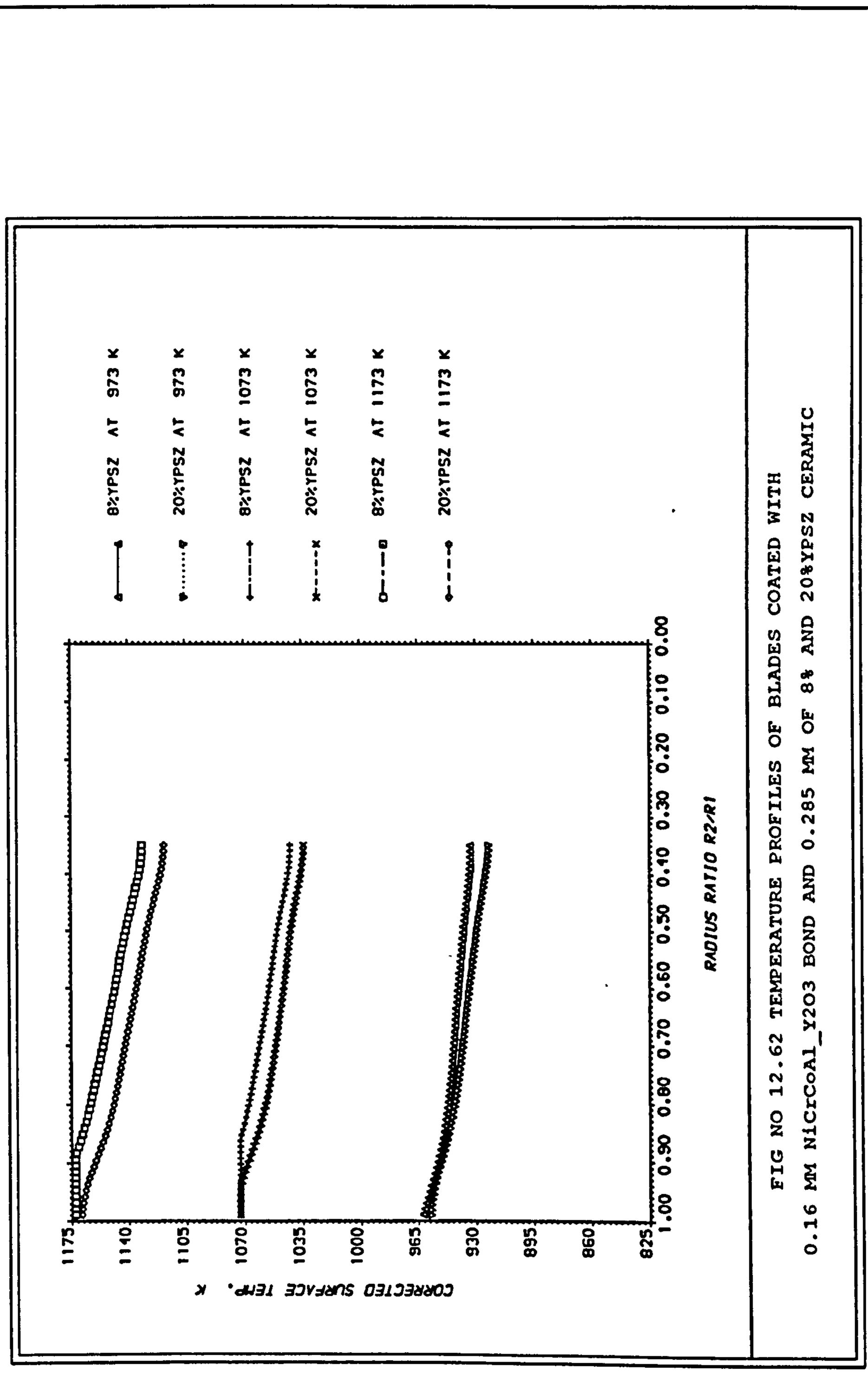

FIG NO 12.62 TEMPERATURE PROFILES OF BLADES COATED WITH
MM NiCrCoAl_Y2O3 BOND AND 0.285 MM OF 8% AND 20%YPSZ CERAMIC
0.16 MM

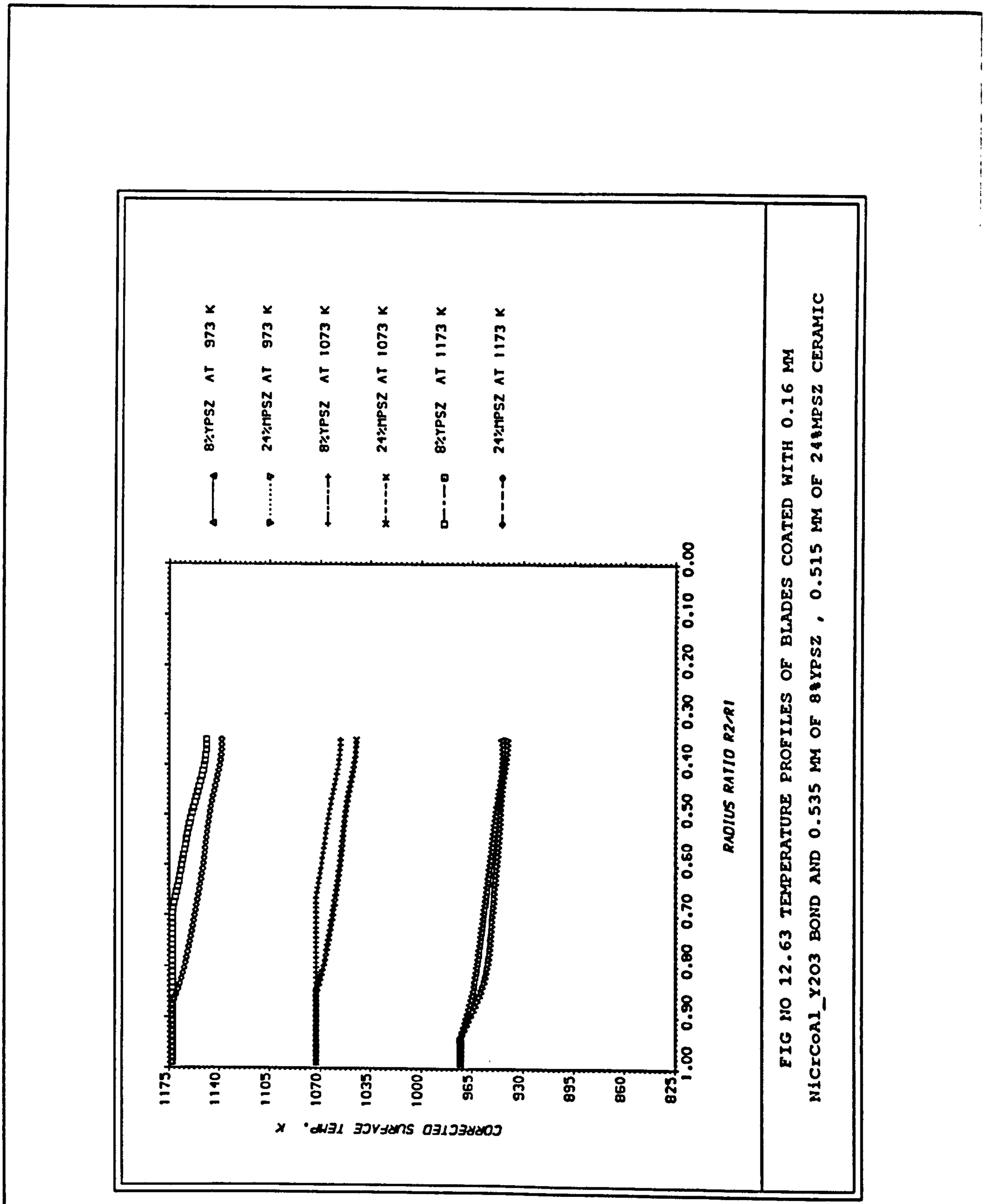

FIG NO 12.63 TEMPERATURE PROFILES OF BLADES COATED WITH 0.16 MM NiCrCoAl_Y2O3 BOND AND 0.535 MM OF 8%YPSZ , 0.515 MM OF 24%MPSZ CERAMIC

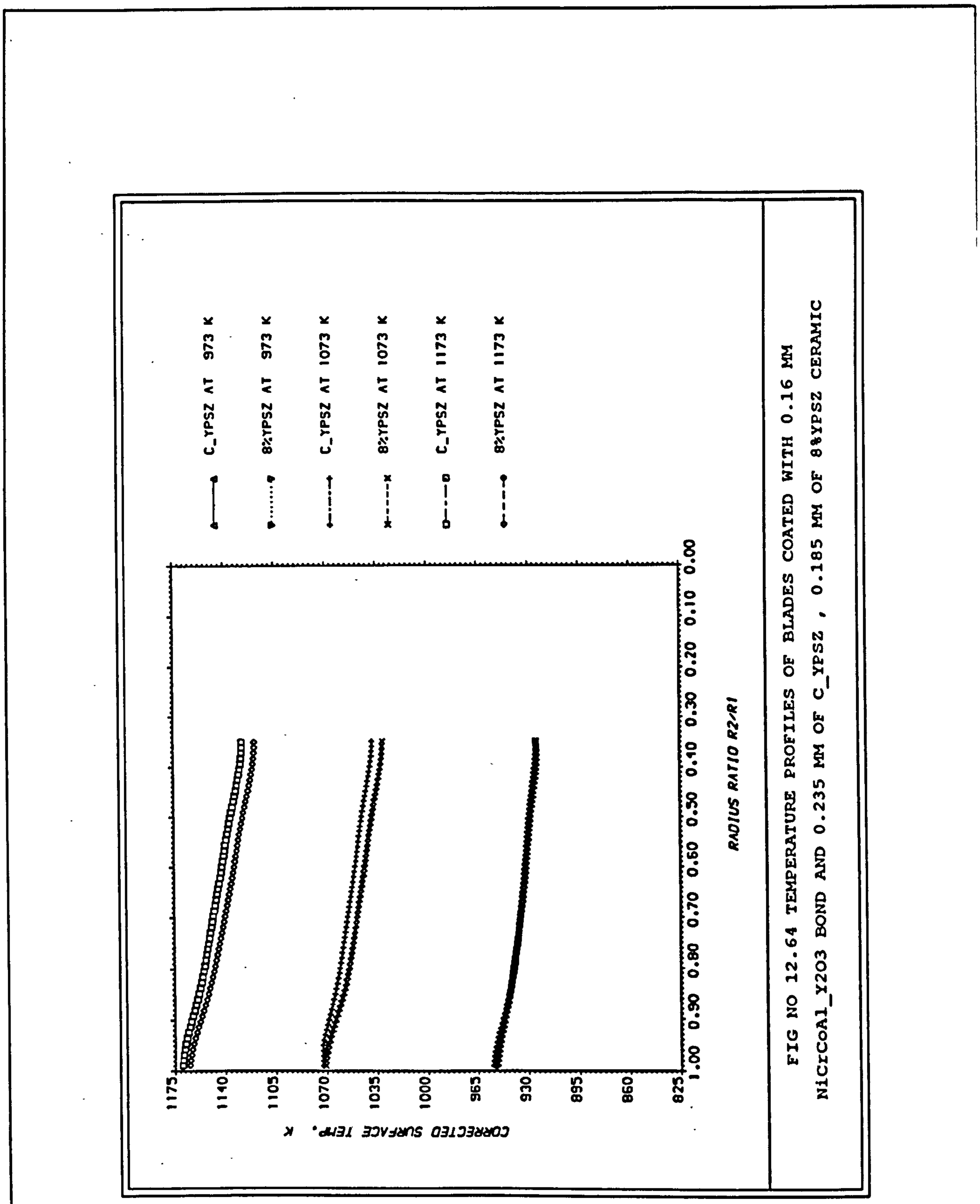

FIG NO 12.64 TEMPERATURE PROFILES OF BLADES COATED WITH 0.16 MM NiCrCoAl_Y2O3 BOND AND 0.235 MM OF C_YPSZ , 0.185 MM OF 8%YPSZ CERAMIC

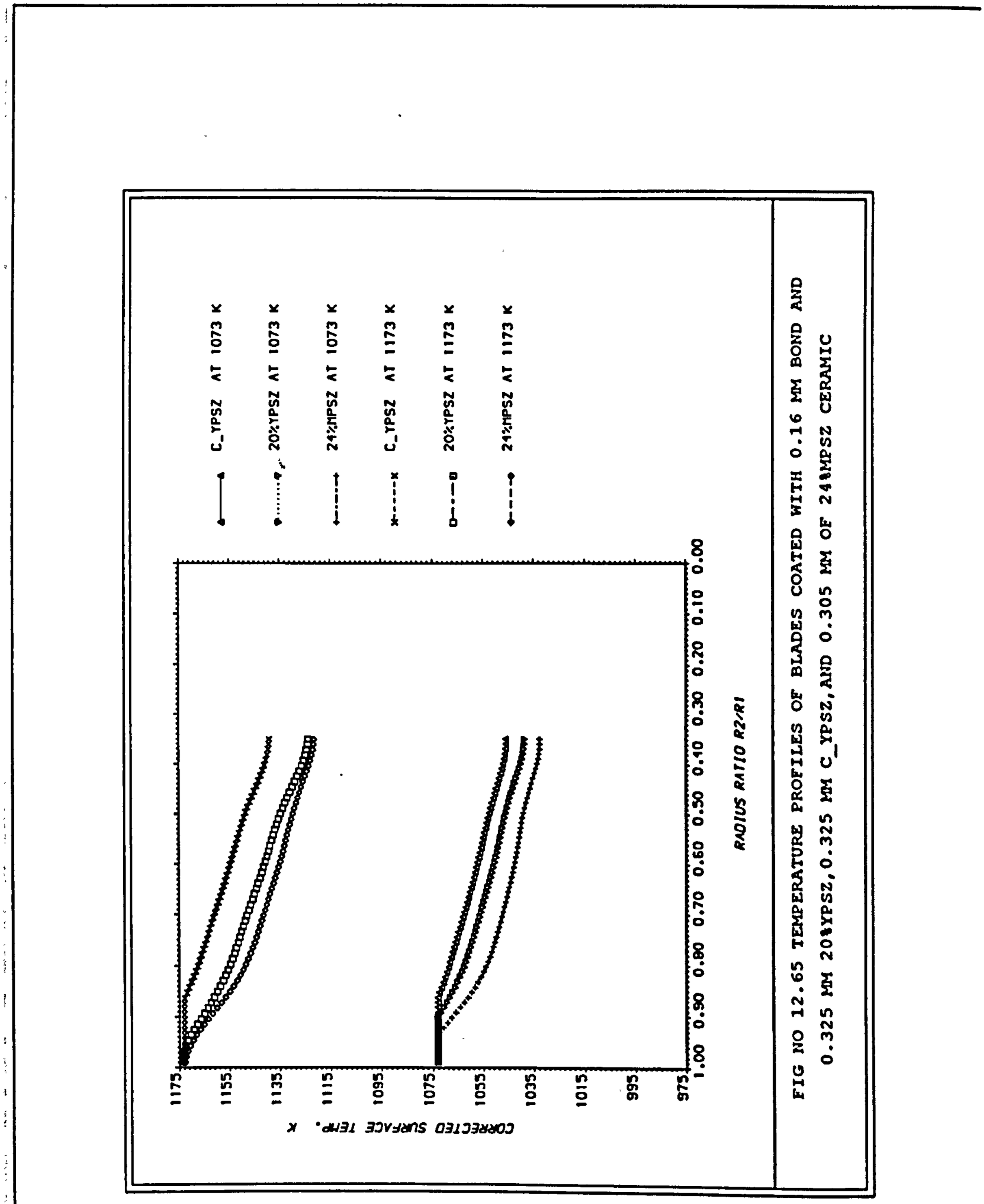

FIG NO 12.65 TEMPERATURE PROFILES OF BLADES COATED WITH 0.16 MM BOND AND 0.325 MM 20%YPSZ, 0.325 MM C_YPSZ, AND 0.305 MM OF 24%MPSZ CERAMIC

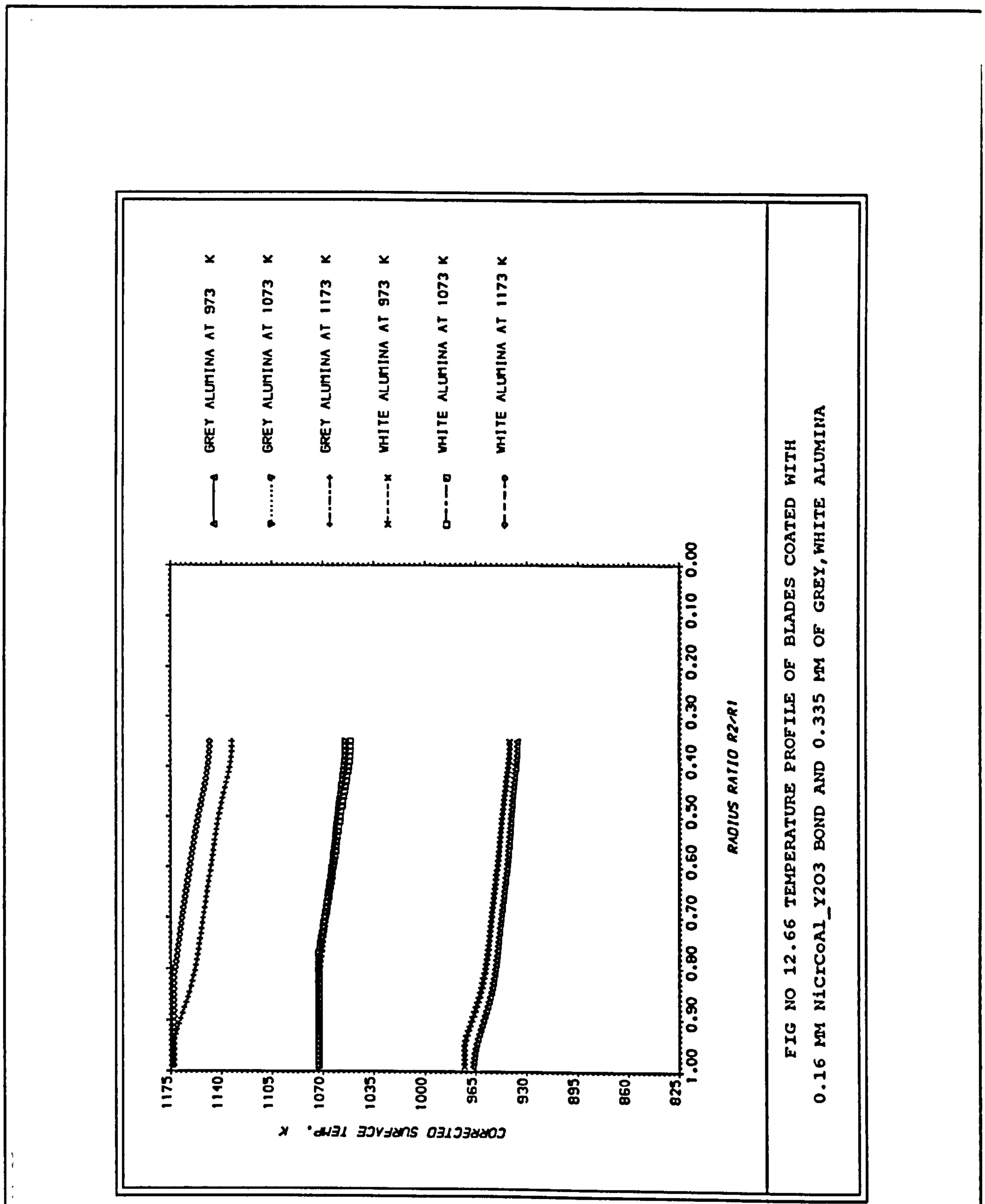

FIG NO 12.66 TEMPERATURE PROFILE OF BLADES COATED WITH
0.16 MM NiCrCoAl_Y2O3 BOND AND 0.335 MM OF GREY, WHITE ALUMINA

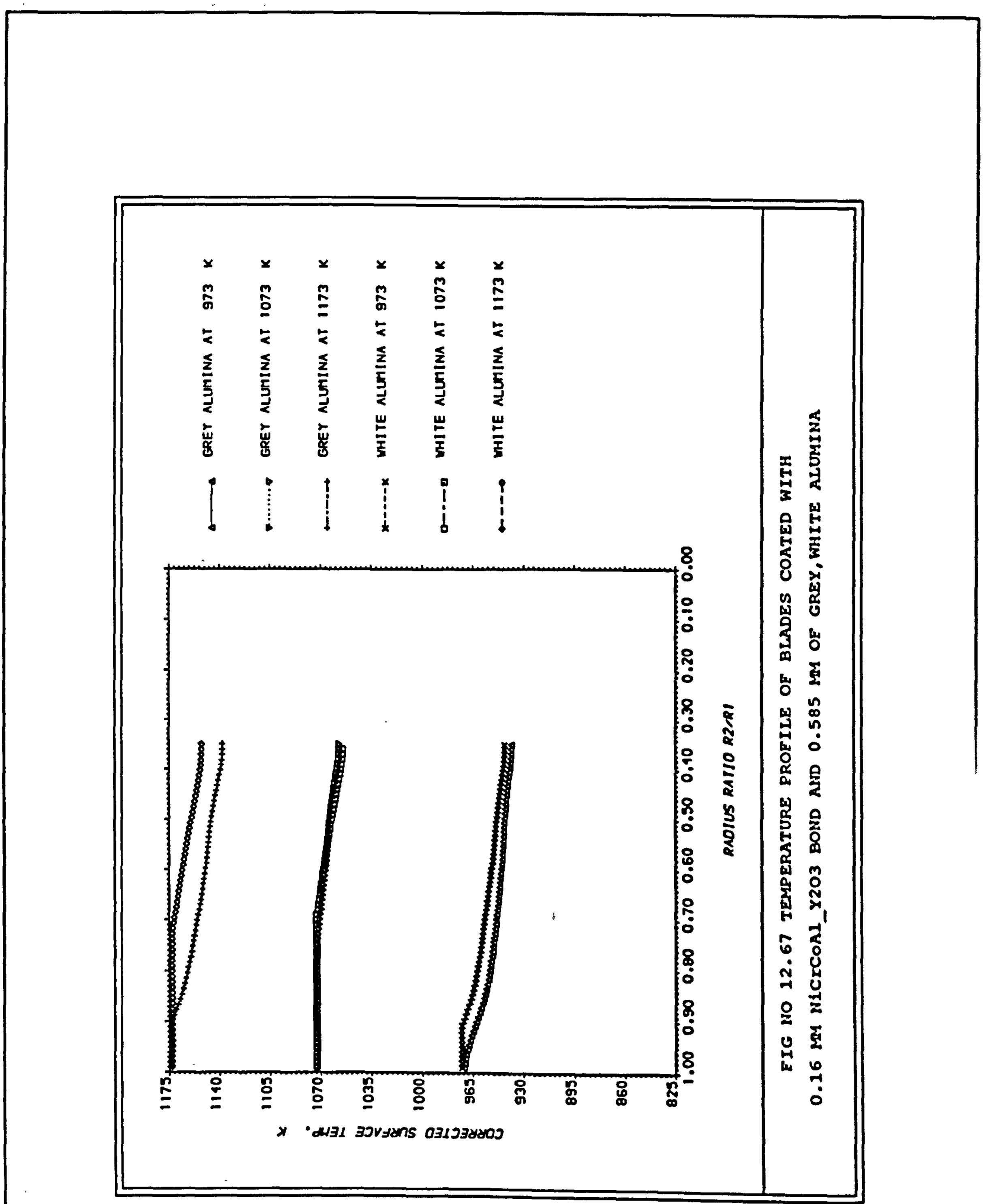

FIG NO 12.67 TEMPERATURE PROFILE OF BLADES COATED WITH
0.16 MM NiCrCoAl_Y2O3 BOND AND 0.585 MM OF GREY,WHITE ALUMINA

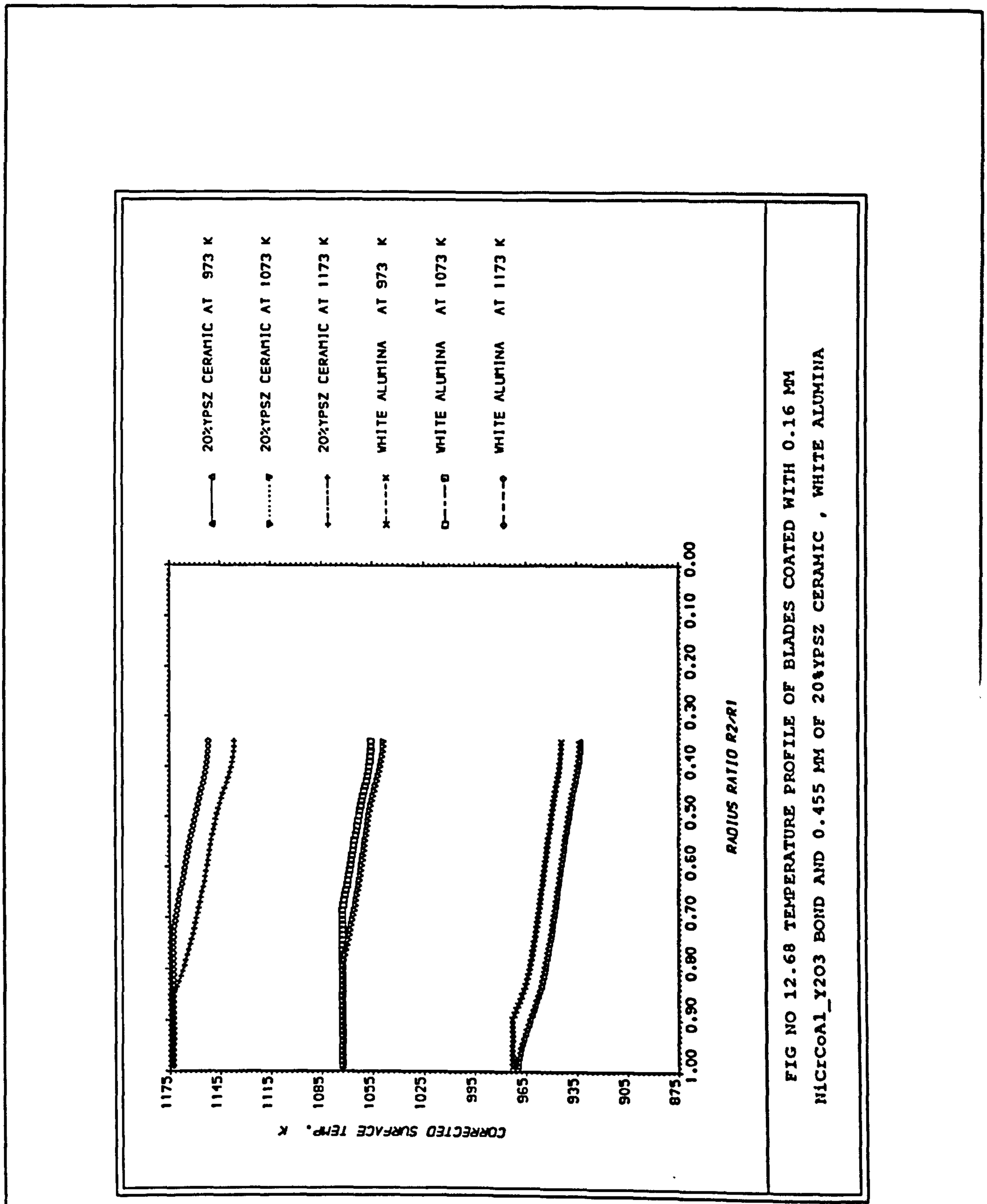
20%YPSZ CERAMIC AT 973 K
20%YPSZ CERAMIC AT 1073 K
20%YPSZ CERAMIC AT 1173 K
WHITE ALUMINA AT 973 K
WHITE ALUMINA AT 1073 K
WHITE ALUMINA AT 1173 K
RADIUS RATIO R2/RI
CORRECTED SURFACE TEMP. K
1.00 0.90 0.80 0.70 0.60 0.50 0.40 0.30 0.20 0.10 0.00
875 905 935 965 995 1025 1055 1085 1115 1145 1175
FIG NO 12.68 TEMPERATURE PROFILE OF BLADES COATED WITH 0.16 MM
NiCrCoAl_Y2O3 BOND AND 0.455 MM OF 20%YPSZ CERAMIC , WHITE ALUMINA

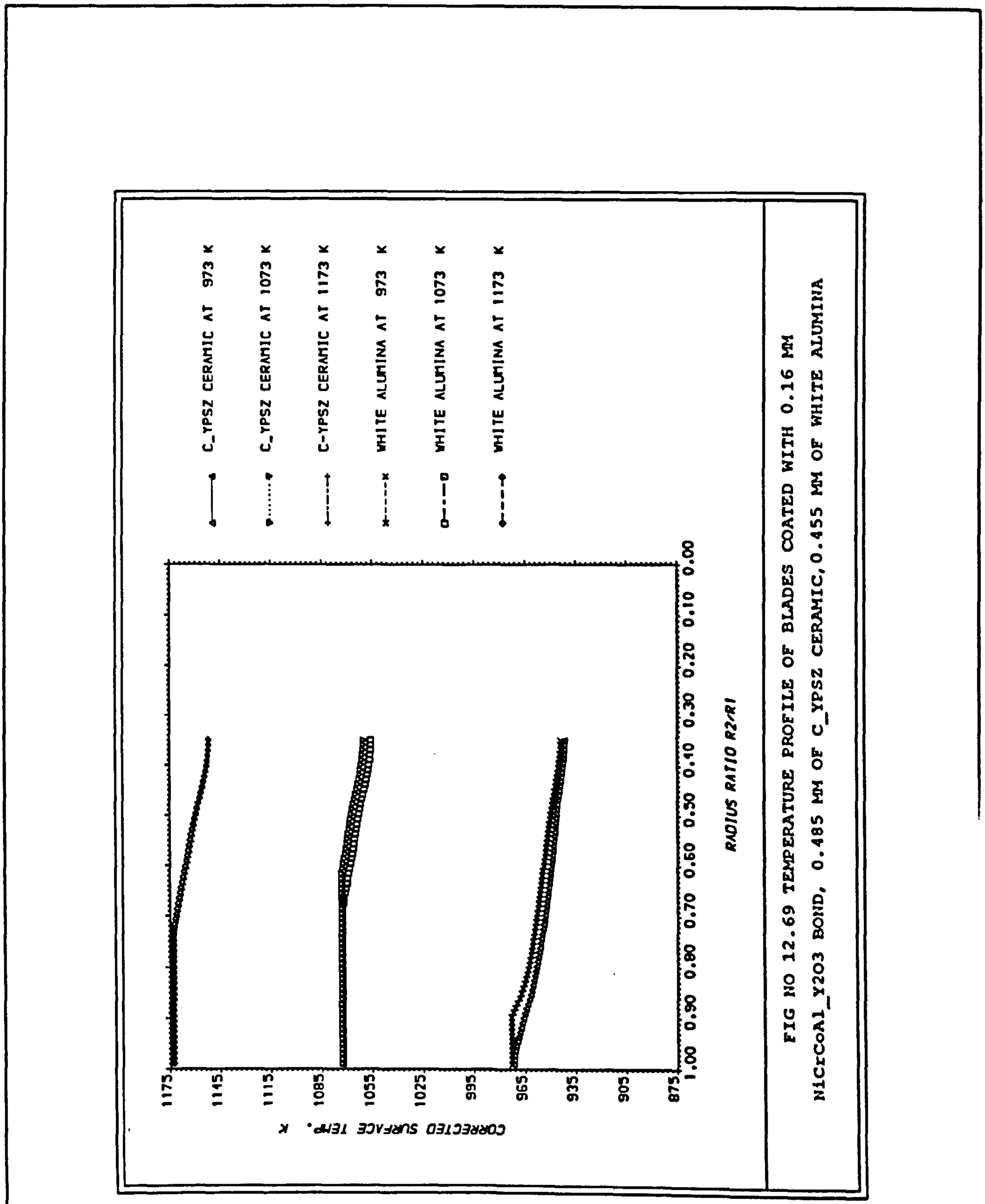

FIG NO 12.69 TEMPERATURE PROFILE OF BLADES COATED WITH 0.16 MM NiCrCoAl_Y2O3 BOND, 0.485 MM OF C_YPSZ CERAMIC, 0.455 MM OF WHITE ALUMINA

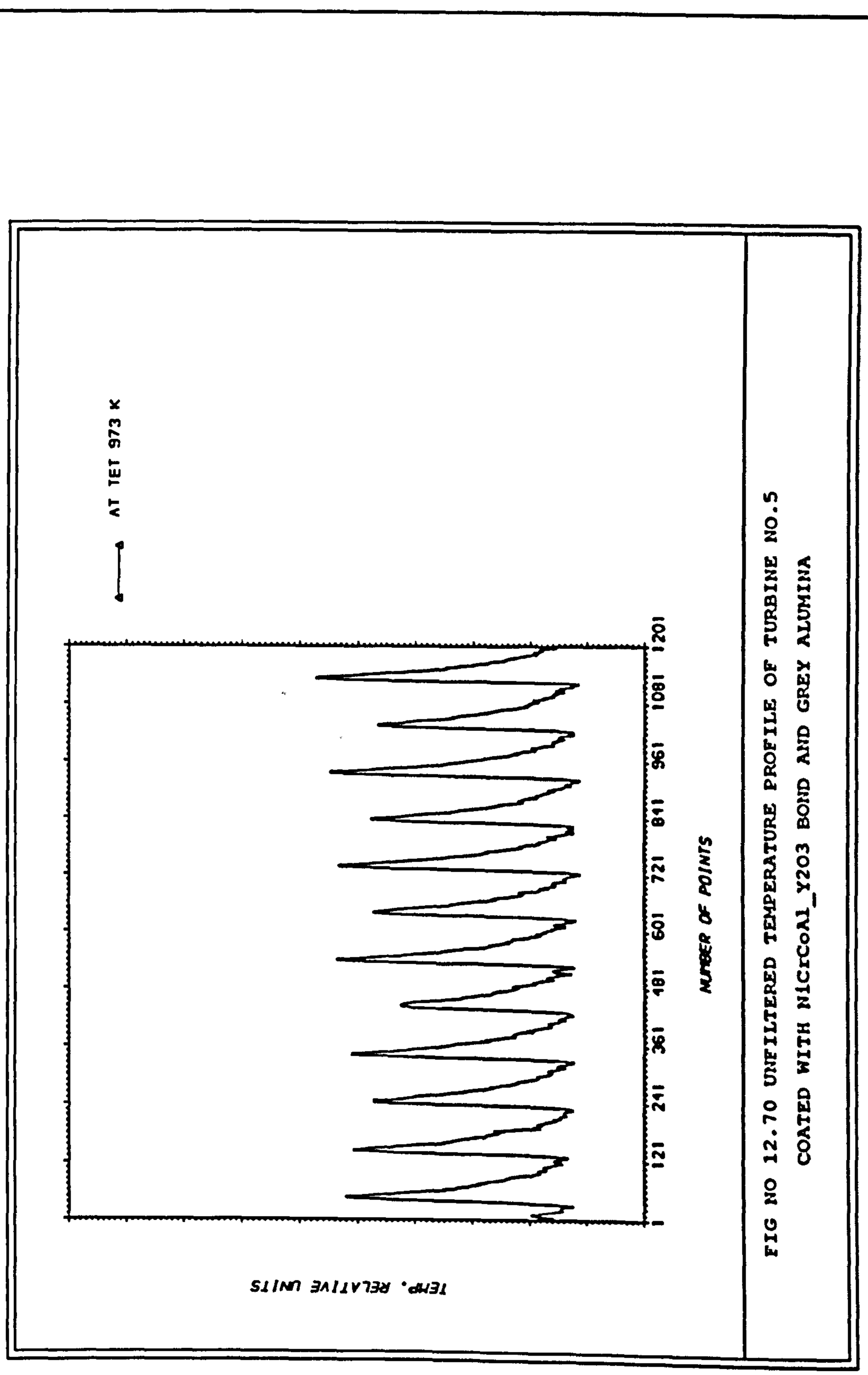

FIG NO 12.70 UNFILTERED TEMPERATURE PROFILE OF TURBINE NO.5
COATED WITH NiCrCoAl_Y2O3 BOND AND GREY ALUMINA

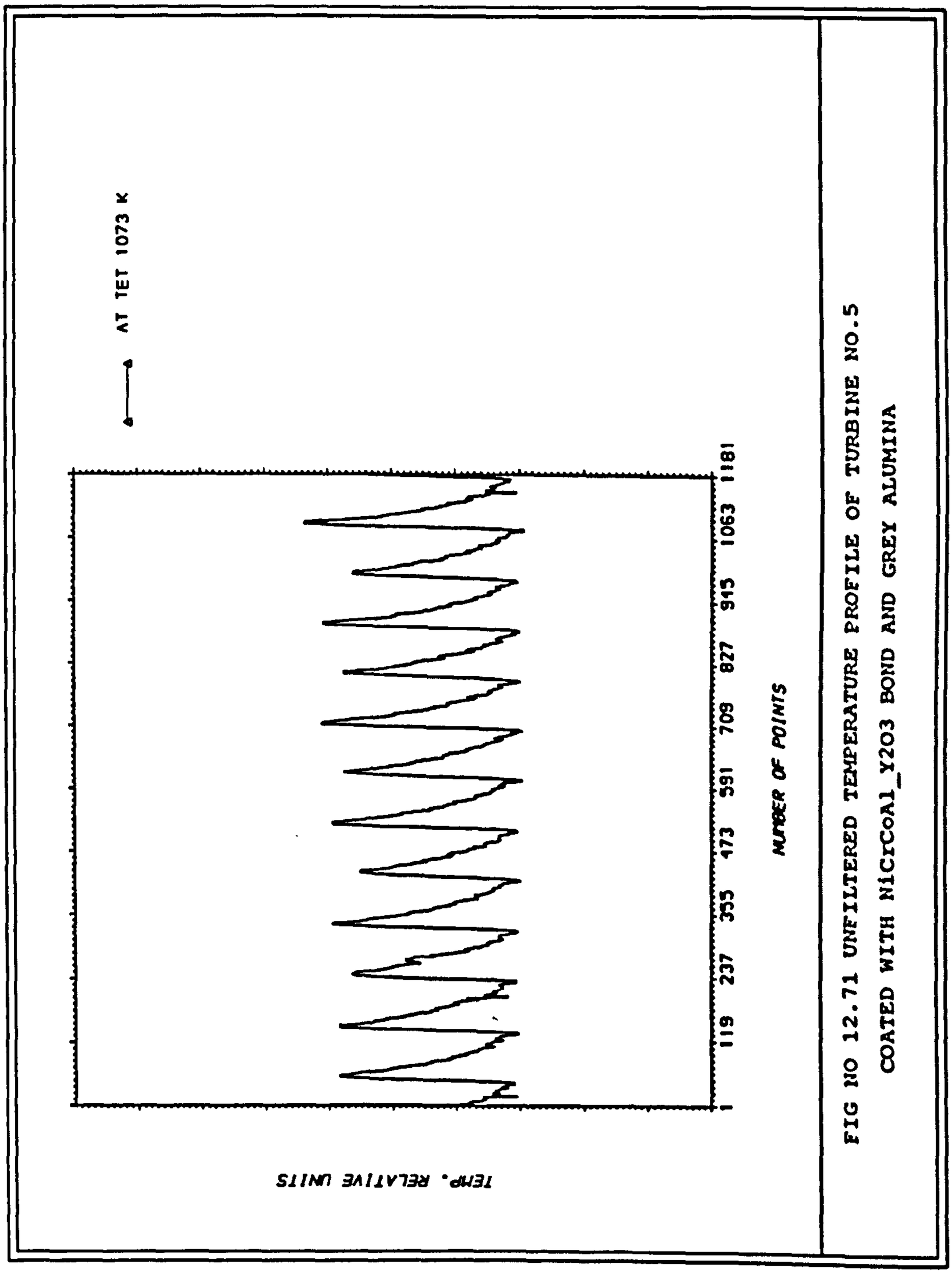

FIG NO 12.71 UNFILTERED TEMPERATURE PROFILE OF TURBINE NO.5
COATED WITH NiCrCoAl_Y2O3 BOND AND GREY ALUMINA

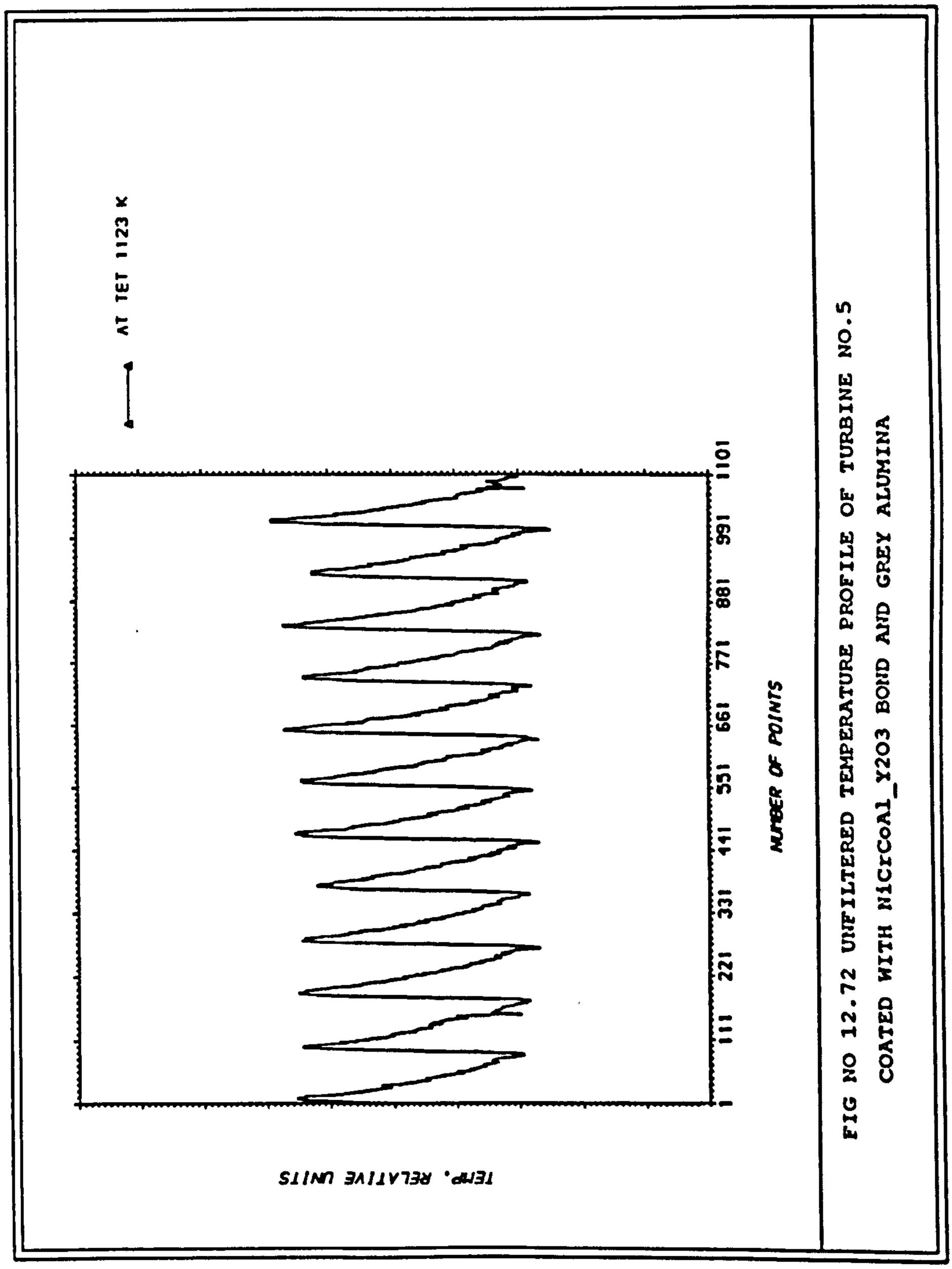

FIG NO 12.72 UNFILTERED TEMPERATURE PROFILE OF TURBINE NO.5
COATED WITH NiCrCoAl_Y2O3 BOND AND GREY ALUMINA

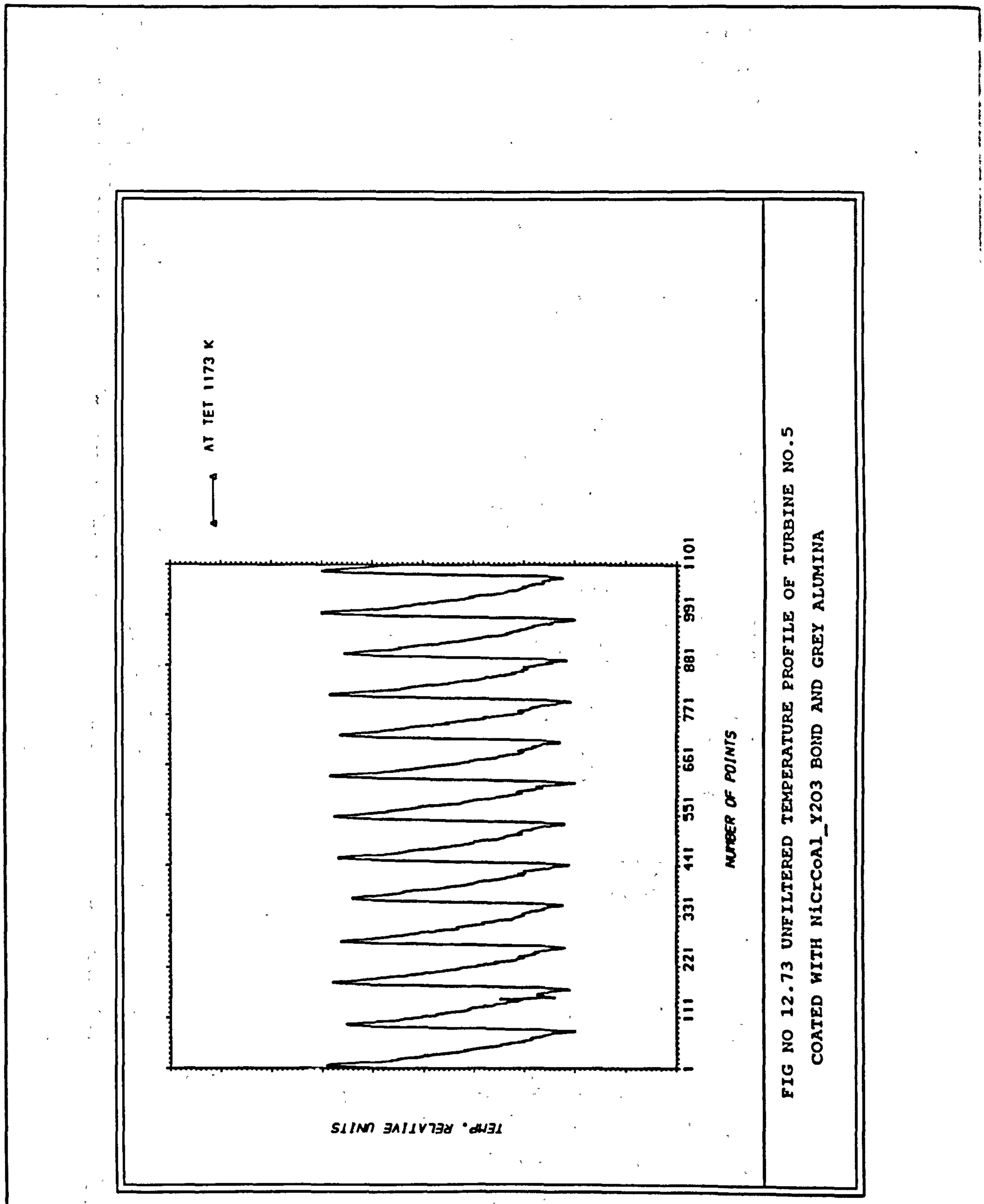

FIG NO 12.73 UNFILTERED TEMPERATURE PROFILE OF TURBINE NO.5
COATED WITH NiCrCoAl_Y2O3 BOND AND GREY ALUMINA

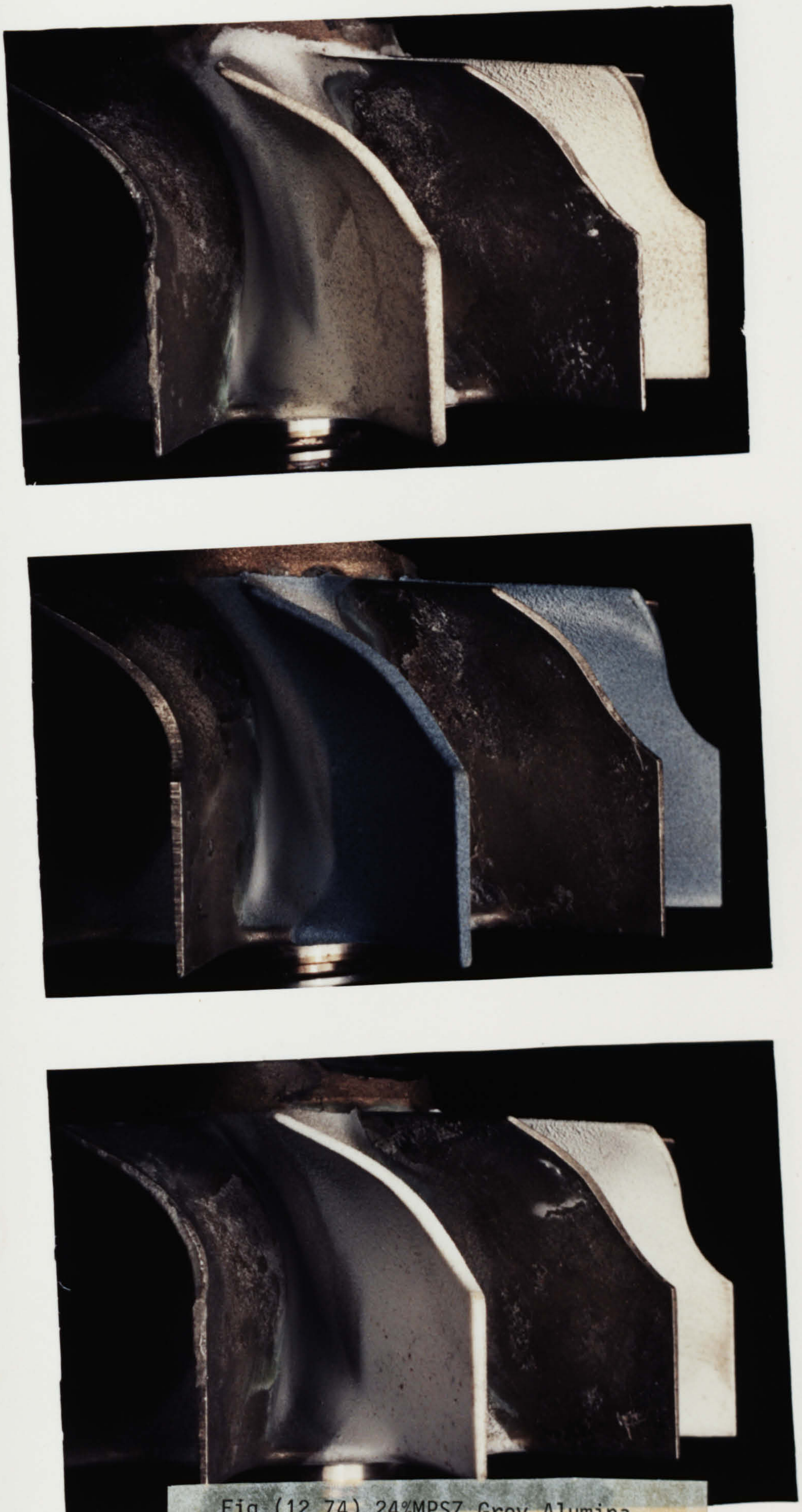

Fig.(12.74) 24%MPSZ,Grey Alumina and White Alumina Coated Turbine Before Testing

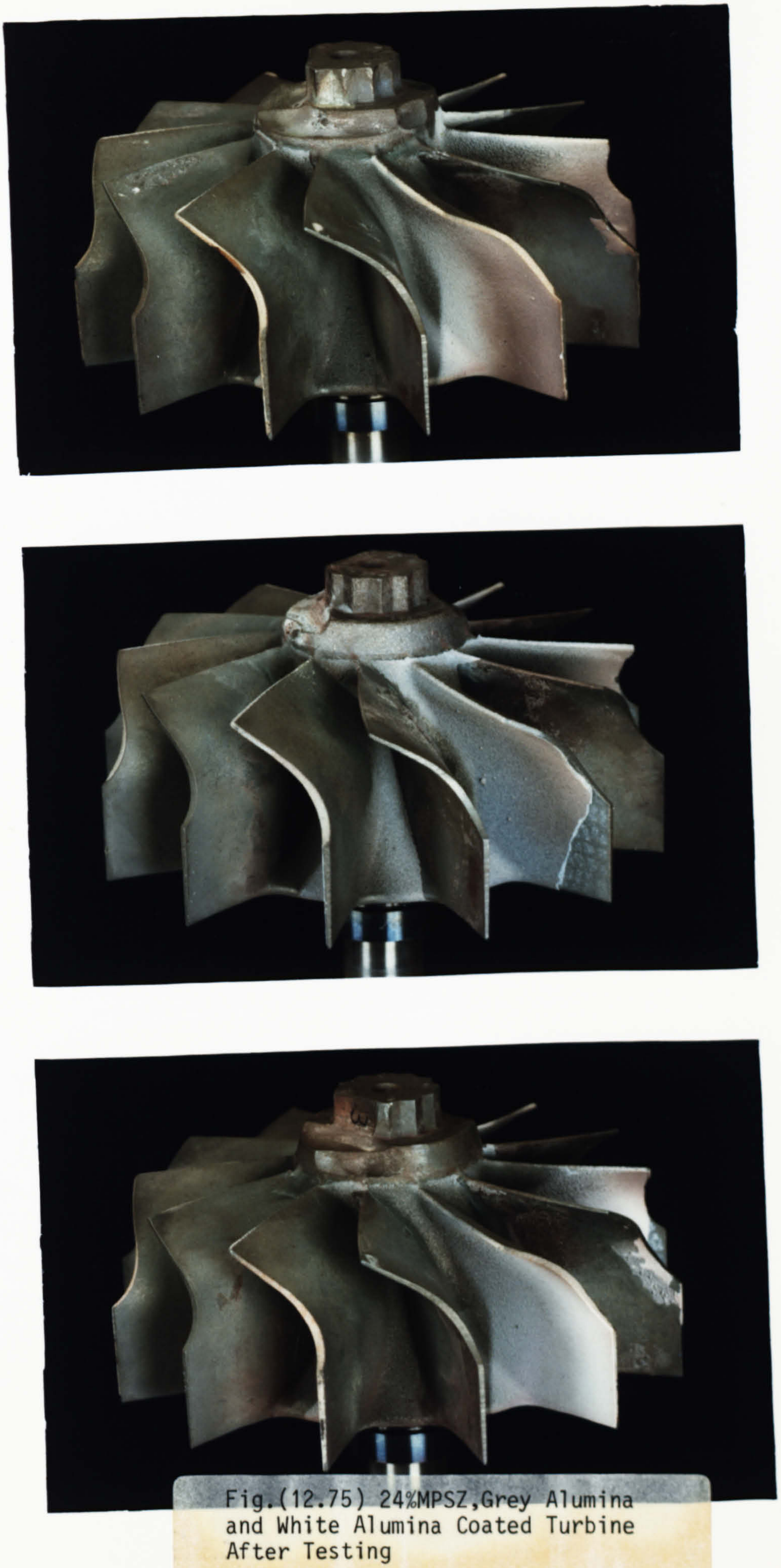

Fig.(12.75) 24%MPSZ,Grey Alumina and White Alumina Coated Turbine After Testing

APPENDIX (A)

EMISSIVITY MEASUREMENT OF ALUMINIUM ENAMEL COATING

by A. K. Husain
(Ph.D. student)
Cranfield Institute of Technology
Cranfield Bedford MK43 0AL

EMISSIVITY MEASUREMENT OF ALUMINIUM ENAMEL COATING

by A. K. Husain
(Ph.D. student)
Cranfield Institute of Technology
Cranfield Bedford MK43 0AL

SUMMARY

The School of Mechanical Engineering, Cranfield Institute of Technology, was contacted by Rolls-Royce plc, concerning the measurement of emissivity for Aluminium-Enamel coating.

This report describes the results of the measurement of emissivity within the range of 300 to 700 °C. Two Aluminium-Enamel coated plates were provided by the company. Plate no.1 was specially solid with engine contaminants. Plate no.2 was left as new. The emissivity of both plates is nearly constant (0.3 to 0.35) provided that, the plates were not heated beyond 550 °C. This report gives a brief description of the technique used, the data obtained and the calculated emissivity.

THE EXPERIMENTAL RIG

The experimental arrangement used in this investigation is based on the radiometric method. Fig.1 shows this arrangement together with the radiation flux path. The following is a brief description of its main elements :-

Black Body Furnace

The black body reference used is a Negretti Aviation calibration furnace type 12143. The furnace has a cylindical cavity, and is heated electrically by 220/240Volts A.C. main supply. The maximum power required is 1000 Watts, and the temperature control is via a closed loop. The furnace has been calibrated within 600 to 1200°C and has an emissivity of 0.9981, but still could be used below that without much loss of accuracy.

The Sample Furnace

The test plates are heated in an electrical furnace built at Cranfield Institute of Technology. The furnace has a cavity opening of 120 mm x 90 mm.

Three silicon carbide heating elements are used to heat the cavity. They are connected in series with a high amperage variable power supply.

The Infrared Detector

The detector used in this investigation is, a sensitive, fast response receiver, operating in a photovoltaic mode. The sensitive element is a semiconductor of p-n construction made from Indium Antimonide. The spectral range of the detector is 1.5 to 5.5 Microns. The working temperature of this semi-conductor is -169°C and this is accomplished by using liquid nitrogen as a coolant. To prevent the chip from 'frosting up' because of this very low temperature, the entire chip was suspended within a vacuum environment of (10 exp^{-5}) torr during this investigation.

The Optical System

Referring to Fig. 1, a plane surface two position gold plated mirror (M1) is used to steer the beam alternatively between the sample plate and the reference furnace.

Two calcium fluoride plano convex lenses (M2 and M3), are used to collect the radiant flux from a pre-selected target area and to delvier it as a focussed image into the detector.

The radiant flux is periodically chopped at 800 Hz, so as to produce an alternating signal at the output of the detector, to simplify the signal processing.

A circular limiting aperture stop is positioned close to the detector to eliminate any unwanted radiation from reaching the detector and to ensure that the focussed image is circular.

SURFACE TEMPERATURE MEASUREMENT

As the coating applied to the plates was very thin, it was assumed that the temperature of the coating is the same as the base metal temperature.

The temperature of the interface was measured by means of two thermocouples. These thermocouples were run into grooves machined in the plates back surface, then through holes into the interface as shown in Fig. 2.

A different technique would be necessary for thicker coatings where the temperature of the coating would be different to that of the interface.

A BRIEF DESCRIPTION OF THE EXPERIMENTAL PROCEDURE

First the apparatus is aligned and checked according to the layout shown in Fig. 1.

The alignment involved the use of a laser-beam and a tungsten inert gas lamp.

After alignment, the rig was used as follows:-

a) Both the reference furnace and the sample were set to a pre-determined temperature. The detector was evacuated and cooled. Then radiation from the reference furnace was measured at the detector.

b) The mirror M1 was steered towards the sample furnace and the radiation from the plate was measured.

c) In order to get the background radiation, the sight plate of the reference furnace was blocked by a black plate. The mirror M1 was steered towards it. The radiation from that black plate was measured at the detector.

d) These readings were repeated in the temperature range of interest.

e) The emissivity was then calculated as shown in Appendix B.

Initially the rig was used to measure the emissivity of a stainless steel plate. This test was performed in the range of 300 to 700°C. A second test was done identical to the first one. The results of both tests are shown in Table 1 and Fig. 3.

Four runs were carried out on each of the two coated plates. The first two runs were within 300 and 550°C surface temperature. The results of which are shown in Tables 2 and 3, and Figs. 4 and 5.

The second two runs were in the range of 300 to 700°C. Their results are shown in Tables 4 and 5, and Figs. 6 and 7.

Discussion of Results

Table No. 1 gives the data from the first and the second tests, which were carried out on an uncoated stainless steel plate. These results are shown plotted in Fig. 3. This shows an increase in the surface total emittance with surface temperatures. It also shows that after the surface temperature was raised up to 700°C, the surface properties were changed and gave higher values of emissivity in the second run.

The first run on each of Rolls Royce plates includes heating of the plates from 300 to 550°C. The results of which are presented in Table No.2, and shown plotted in Fig. 4. These show that the emissivity of the two plates were very similar.

The results of the second run which is essentially a repeat of the first run, are presented in Table No. 3 and shown plotted in Fig. 5. The results are very similar to that of the first run.

The third run includes heating of both plates within the range of 300 to 700°C. The results of which are presented in Table No.4 and shown plotted in Fig. 6. This shows that as the surface temperature was increased beyond 550°C, a rapid change in the surface properties takes place resulting in a considerable increase of emissivity with surface temperatures. This rapid increase is due to the spalling off of the coating at high temperatuers (higher than 550°C).

The data obtained from the fourth run (which is essentially a repeat of the third run), are presented in Table 5 and shown plotted in Fig. 7. Both of the plates have been overheated and the coating has spalled off, and the emissivity of the plates has been permanently affected.

Fig. 8 shows all the runs plotted on one graph. The photographs of both plates before and after the four runs are shown on photograph 1 and photograph 2. The two photographs show the damage in the coating resulted from heating the plates beyond 550°C.

REFERENCES

1. G.S. UBHI (Unpublished work)

TABLE NO. 1 Data for Stainless Steel (Uncoated) Plate

SURFACE TEMPERATURE °C	EMISSIVITY Run No. 1	Run No. 2
300	0.5206	0.5684
400	0.5270	0.5882
500	0.5708	0.6277
600	0.5903	0.6292
700	0.6338	0.6701

TABLE No.2 Data from Aluminium Enamel Coated Plates (The First Run)

SURFACE TEMPERATURE °C	TOTAL EMISSIVITY Plate No.1	Plate No.2
300	0.3565	0.3720
350	0.3459	0.3576
400	0.3385	0.3423
450	0.3272	0.3218
500	0.3214	0.3209
550	0.3152	0.3142

TABLE No.3 Data from Aluminium Enamel Coated Plates (The Second Run)

SURFACE TEMPERATURE °C	EMISSIVITY Plate No.1	Plate No.2
300	0.2987	0.3449
350	0.3045	0.3461
400	0.3128	0.3545
450	0.3191	0.3594
500	0.3190	0.3633
550	0.3189	0.3625

TABLE No.4 Data from Aluminium Enamel Coated Plates (The Third Run)

SURFACE TEMPERATURE °C	EMISSIVITY Plate No.1	Plate No.2
300	0.2937	0.3454
350	0.3014	0.3483
400	0.3108	0.3555
450	0.3167	0.3583
500	0.3149	0.3610
550	0.3165	0.3680
600	0.3403	0.3830
650	0.3885	0.4388
700	0.6888	0.6900

TABLE No.5 Data from Aluminium Enamel Coated Plates (The Fourth Run)

SURFACE TEMPERATURE °C	EMISSIVITY Plate No.1	Plate No.2
300	0.4787	0.7049
350	0.4967	0.7047
400	0.5091	0.7049
450	0.5081	0.7197
500	0.5105	0.7345
550	0.5360	0.7361
600	0.5843	0.7379
620	0.6001	———
650	Failed	0.7395
700	———	0.7771

PHOTOGRAPH NO. 1 ALUMINIUM ENAMEL COATED PLATE NO. 1
(solid with engine contaminants)

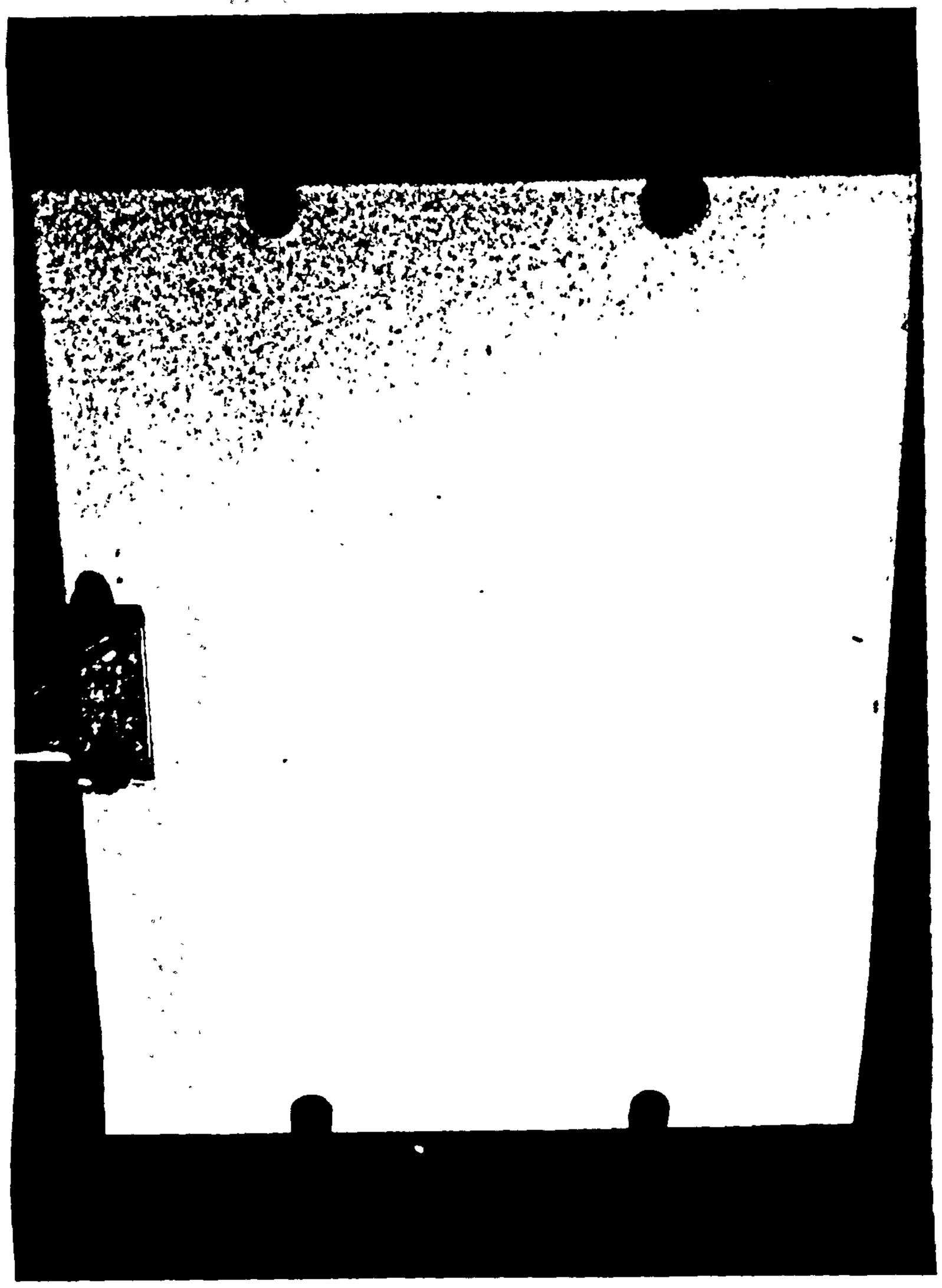

a - As received (new)

b - After the fourth run

PHOTOGRAPH NO. 2 : ALUMINIUM ENAMEL COATED PLATE NO. 2 (clean)

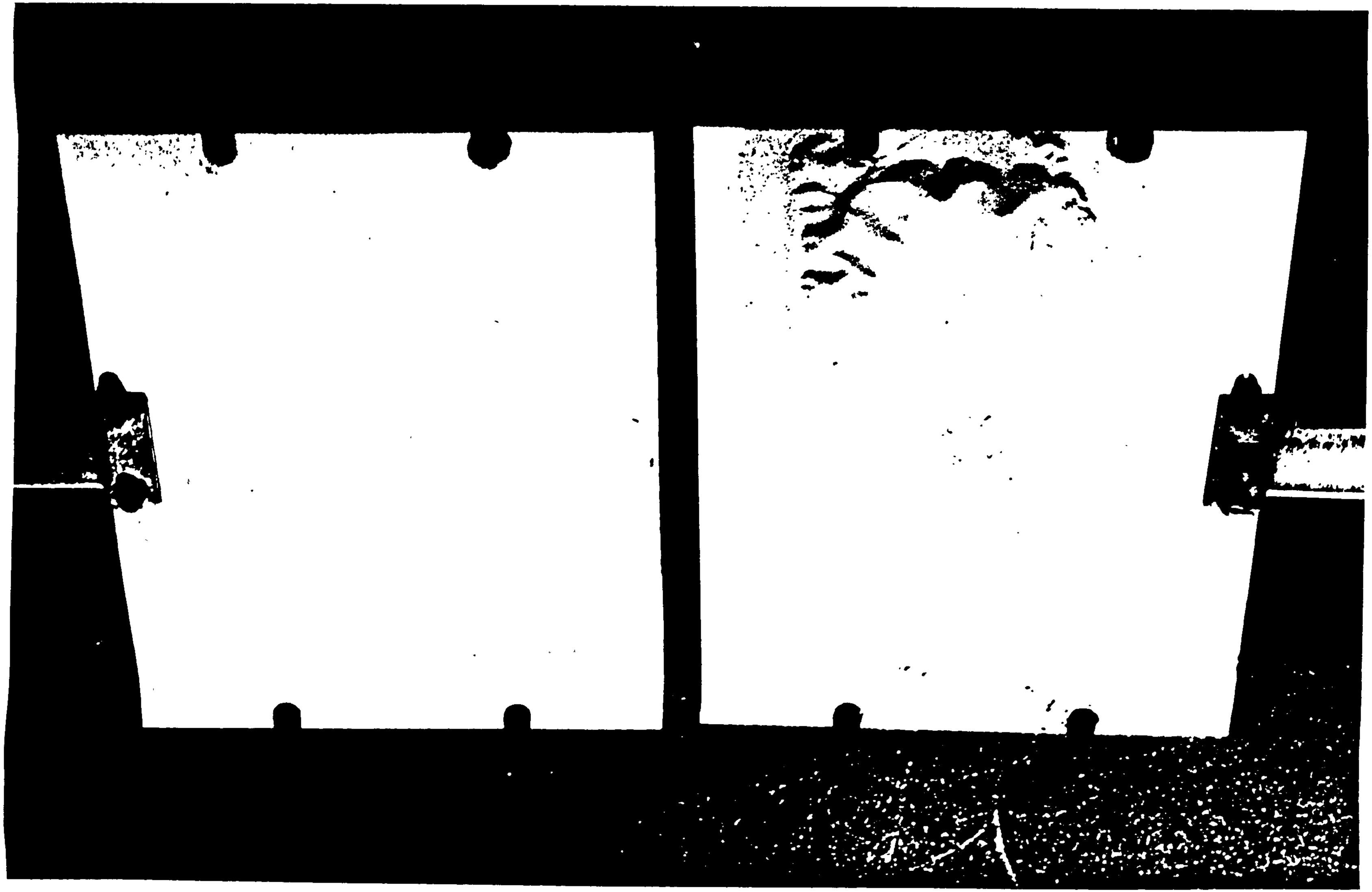

a - As received (new)

b - After the fourth run

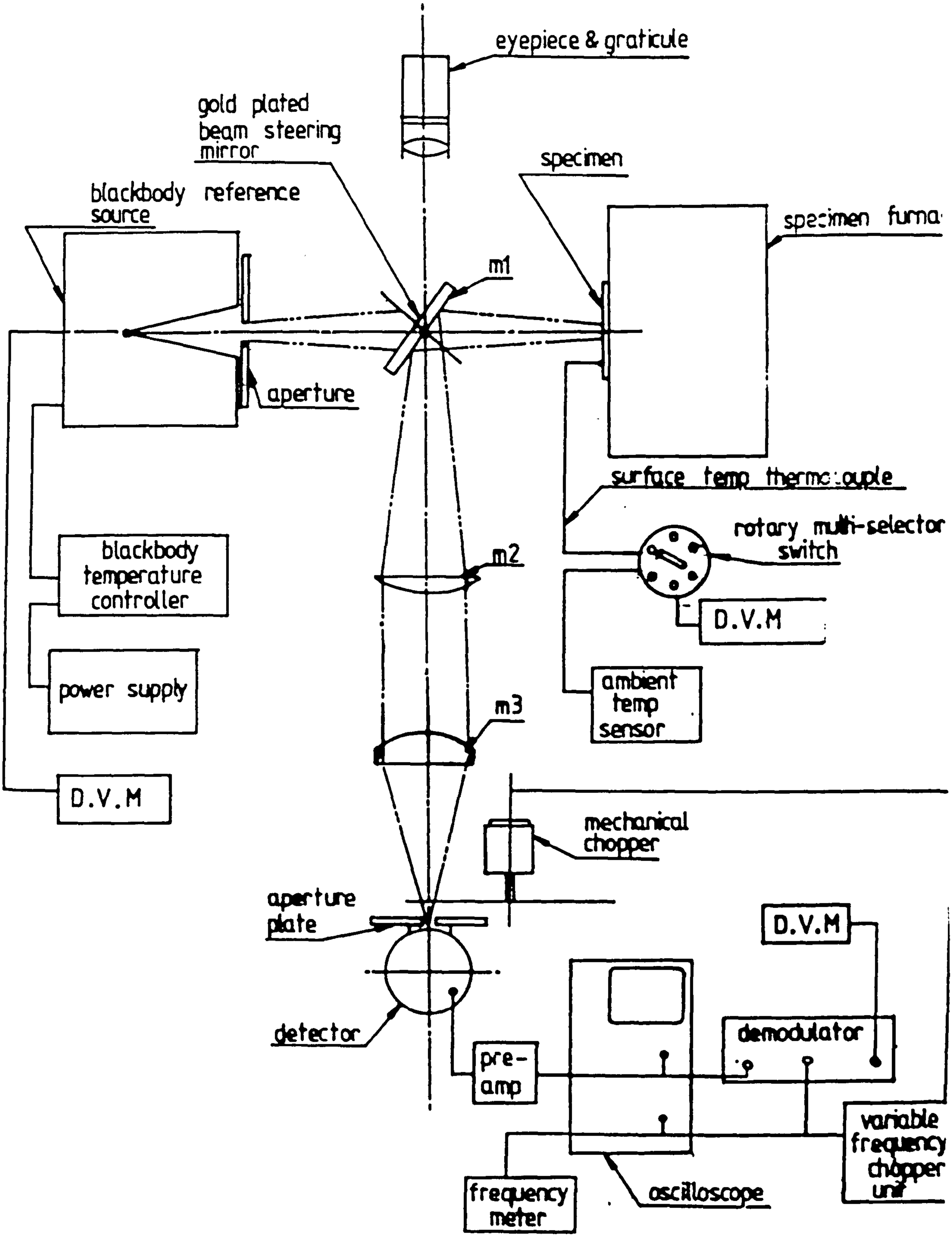

Figure 1 ; A schematic of the emissivity measuring experimental rig.(*ref.1*)

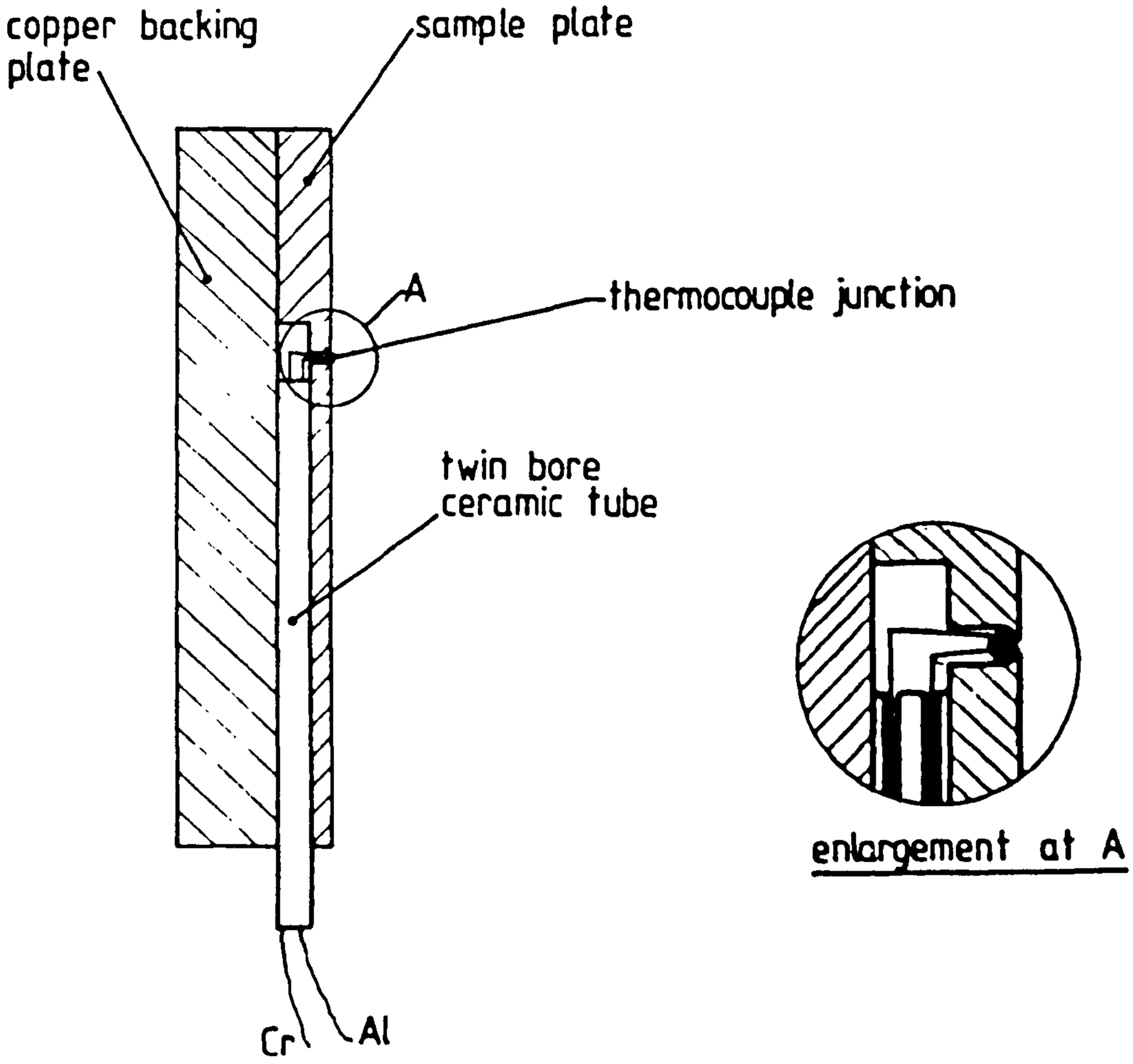

Figure 2 ; Method illustrating a technique for the measurement of surface temperature of a metal plate *(ref.1)*.

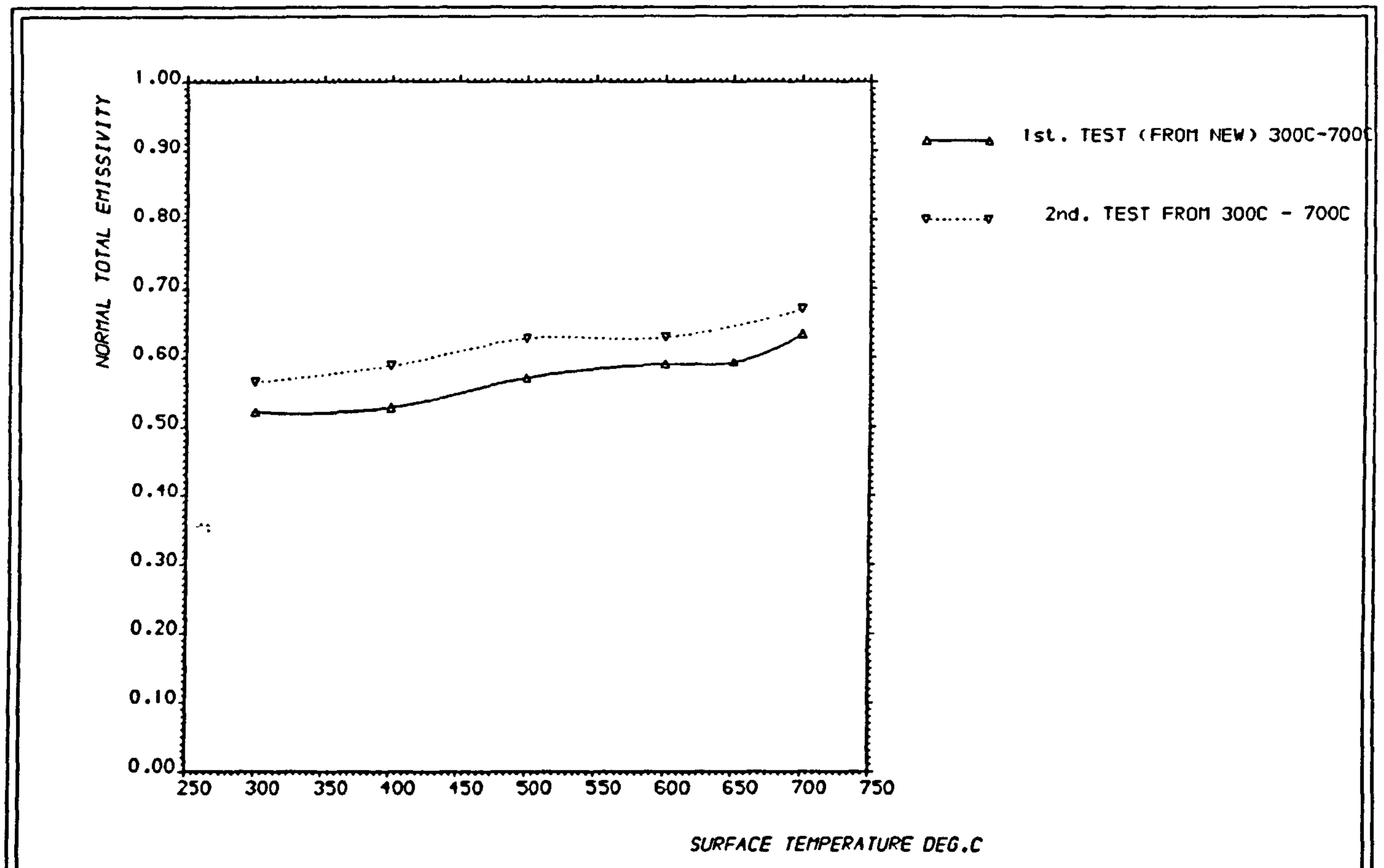

FIG.3 EMISSIVITY MEASUREMENT
OF STAINLESS STEEL PLATE

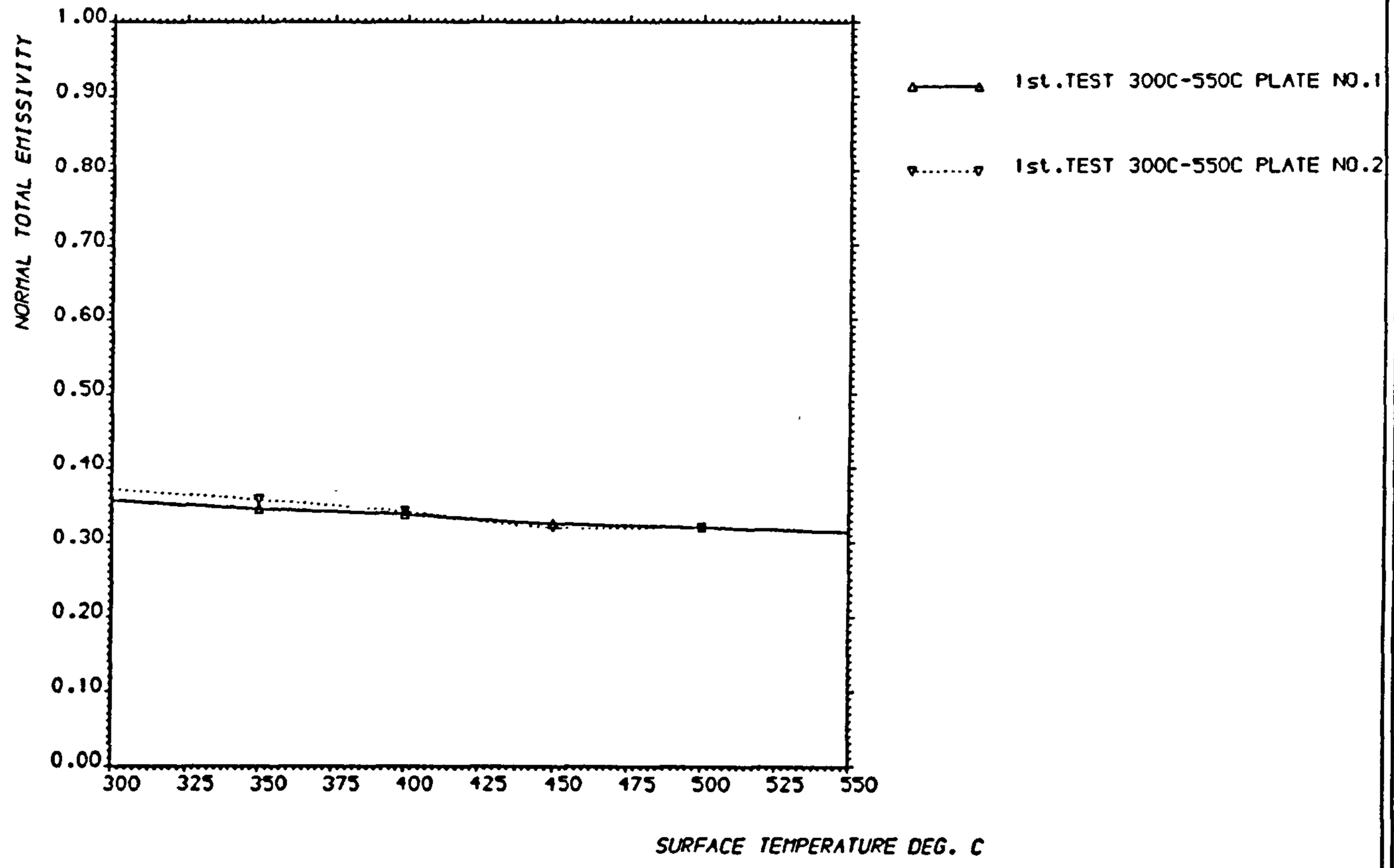

FIG.4 EMISSIVITY MEASUREMENT
OF POLLSROYCE PLATE NO.1 & 2

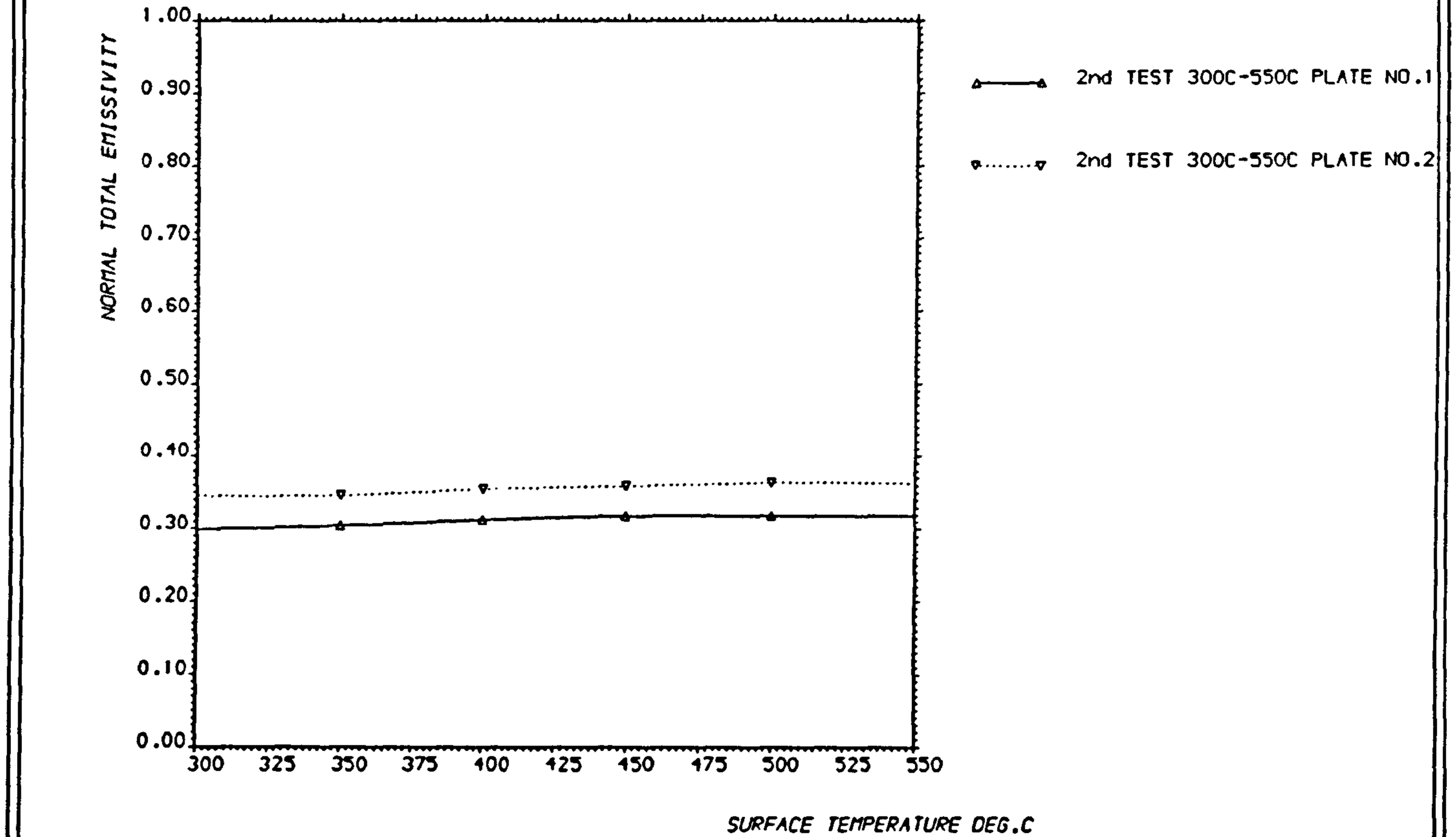

FIG.5 EMISSIVITY MEASUREMENT
OF POLLSROYCE PLATE NO.1 & 2

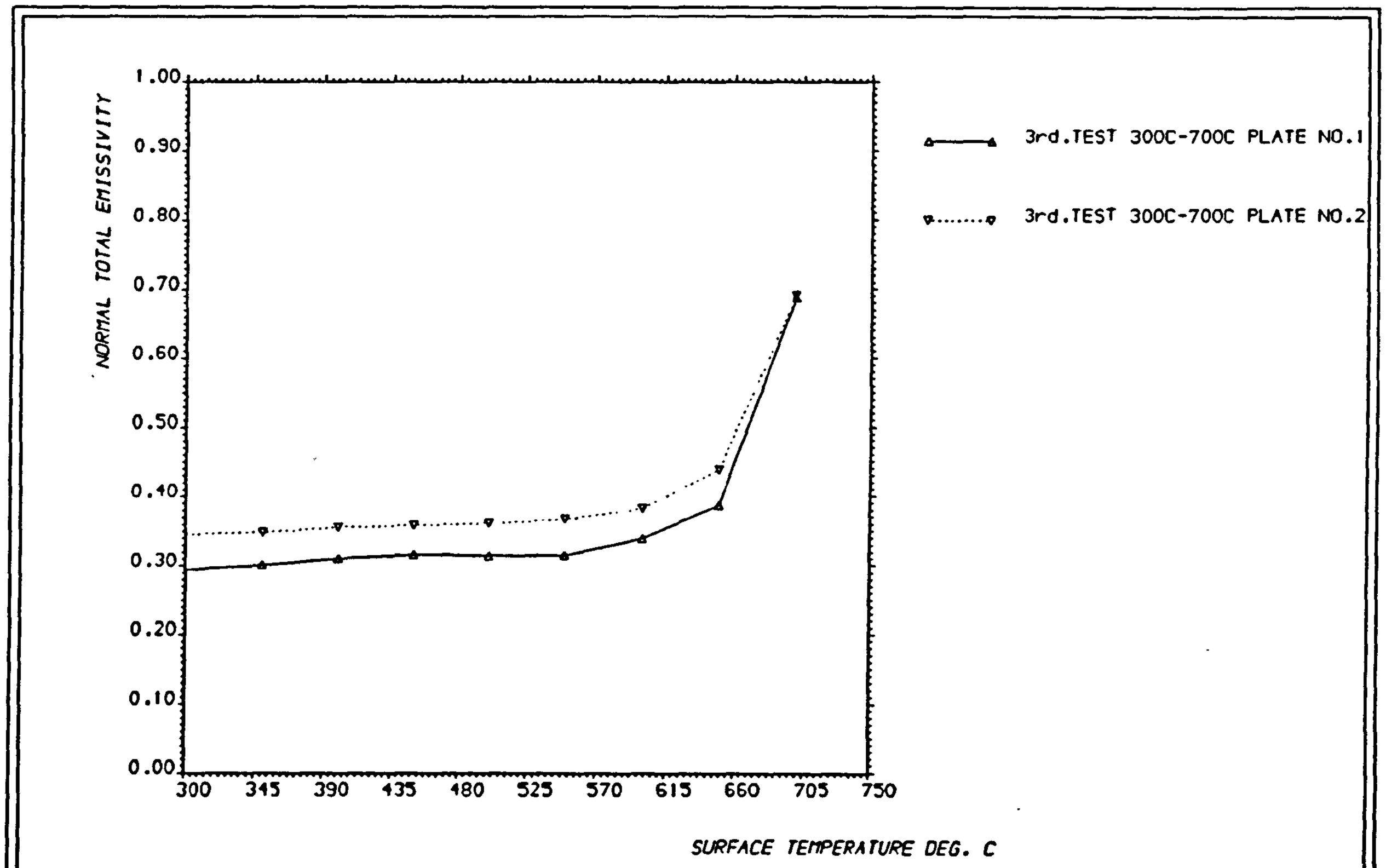

FIG.6 EMISSIVITY MEASUREMENT
OF ROLLSROYCE PLATE NO.1 & 2

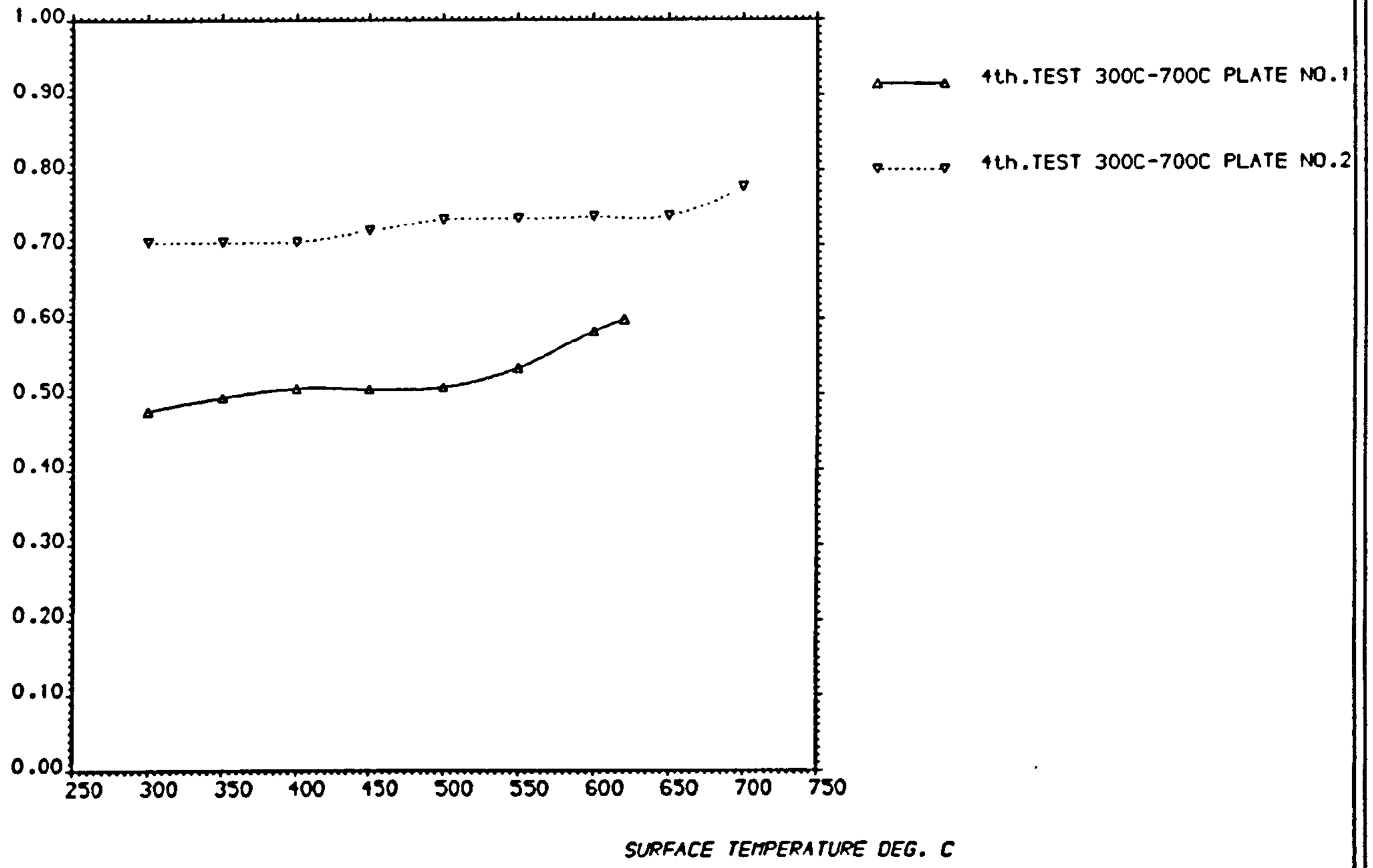

FIG.7 EMISSIVITY MEASUREMENT
OF ROLLSROYCE PLATE NO.1 & 2

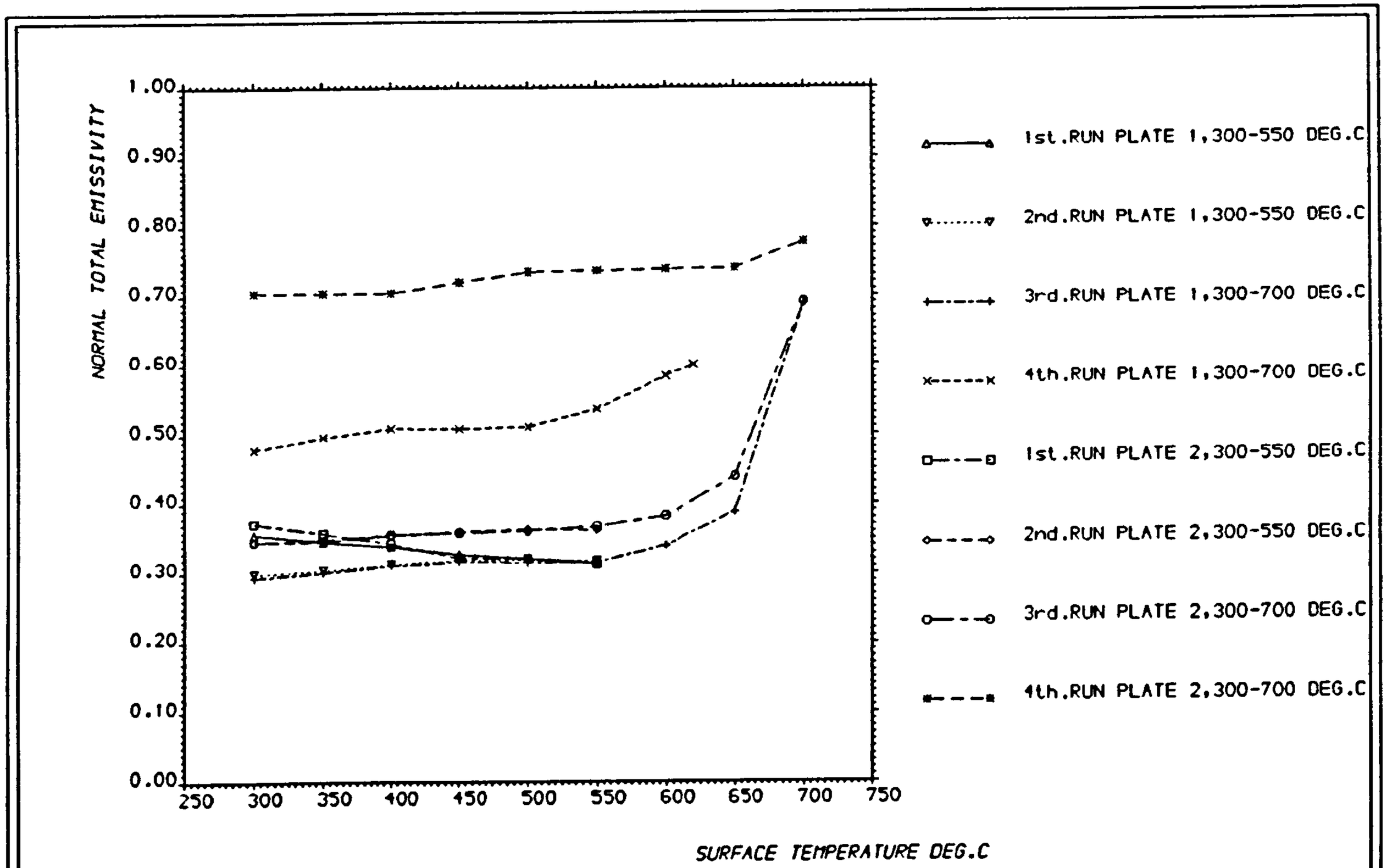

FIG.8 COMPARISON BETWEEN ALL
THE RUNS OF PLATES 1 AND 2

APPENDIX A DEFINITION

The ratio between radiance emitted from a material to that from a black body at the same temperature is termed the emissivity.

All matter emits energy to its surrounding as a function of its temperature, if that temperature is greater than absolute zero. Solids radiate at all wavelengths. The amount of power radiated at each wavelength is a function of temperature and surface conditions of that matter. A perfect emitter is called blackbody which also absorbs all radiation incident upon its surface. All real (gray) surfaces radiate a lesser amount of energy at all wavelengths.

Two methods are basically available for determining the emissivities of metals. They are the radiometric and caliometric methods.

The radiometric method is based on comparison of radiation emitted from the surface whose emissivity is required to that from a black body at the same temperature.

While the caliometric method is based on comparison of heat lost or gained by the material, to that calculated theoretically for a black body at the same temperature.

Another method is based on the calculation of the emissivity from the measurement of the reflectivity then subtracting that from unity.

APPENDIX B THEORY

The black body radiation 'NB' is given by Planck's function as :-

$$NB = (C1/L^5) / (EXP\ (C2/LT)-1) \qquad (1)$$

where :

T Black body temperature (DEG.K)

L Wavelength (CM)

C1 = 3.7413 exp -12 (WATT/CM2)

C2 = 1.4388 (CM x DEG.K)

Radiation from a real surface NS is given by Planck's function as:

$$NS = E\ (c1/L^5) / (EXP\ (C2/LT)-1) \qquad (2)$$

where E is the surface total emissivity.

Equation 2 is exactly equation 1 multiplied by the emissivity.

If equation 1 is integrated over the entire wavelength range we get :

$$NB = \sigma\ T^4 \qquad (3)$$

where σ is the Stefan-Boltsman constant.

So if NB and NS are known then E could be calculated.

$$E = NS/NB \qquad (4)$$

correcting equation 4 for the surrounding radiation it becomes :

$$E = (NS-NR) / (NB-NR) \qquad (5)$$

where NR is the surrounding radiation.

Due to the difficulties in obtaining both the surface of the real material and the black body reference at the same temperature another correction is used :

$$E = (NS-NR) / (NB-NR) * \frac{EXP(C2/LT_S)dL - EXP(C2/LT_B)dL}{EXP(C2/LT_S)dL - EXP(C2/LT_R)dL} * \frac{(EXP(C2/LT_R)-1)dL}{(EXP(C2/LT_B)-1)dL} \quad (6)$$

where :- TS, TB and TR are the surface, black body and surrounding temperatures in DEG.K.

Equation (6) enables us to carry out the test, even if the temperatures of the reference and the test plate are not exactly the same.

APPENDIX C TEST PLATES DIMENSIONS

The dimensions of the test plates shown in photograph 1 and photograph 2, are (89 x 117 x 2) MM. Plate no.1 is nickel steel alloy coated with aluminium enamel (PL101), and is specially solid with engine contaminants to simulate engine degradation, while plate no.2 is left clean after coating.